Metal Carbonyl Complexes and Porphyrin Macrocyles: Photochemistry and Potential Therapeutic Applications

This thesis is presented for the degree of

Doctor of Philosophy

By

Nivedita Das, MSc.

Under the Supervision of Dr. Mary T. Pryce

School of Chemical Sciences

Dublin City University

2014

Declaration

I hereby certify that this material, which I now submit for assessment on the programme of study leading to the award of PhD is entirely my own work, that I have exercised reasonable care to ensure that the work is original, and does not to the best of my knowledge breach any law of copyright, and has not been taken from the work of others save and to the extent that such work has been cited and acknowledged within the text of my work.

Signed: _____(Nivedita Das)

ID No.: _____

Date: _____

This thesis is dedicated to my husband Avi, parents and my brother

Acknowledgement

I am extremely grateful, thankful and extend my sincere gratitude to my supervisor Dr. Mary T. Pryce for her expert advice, encouragement, suggestions and motivation throughout my research work. I am truly indebted for giving me an opportunity to work in her research lab. It has been a great pleasure and privilege for me to have invaluable research experience and training under her supreme guidance.

I would express my heartiest thanks to Dr. Wesley Browne for giving me an opportunity to carry out my singlet oxygen studies in the University of Groningen, Netherlands and providing all the necessary help. I would also like to thank Prof. Wybren Buma for giving me an opportunity to work in his lab in the University of Amsterdam and Saeed for helping me carrying out time resolved infrared spectroscopic studies. I would also like to thank Prof. Conor Long for his invaluable advice and help in TRIR studies. I would also like to thank all my lab mates Avi, Nikki, Emma, Jen, Suzanne, Liam, Diego, Finn and Yvonne for their love, help and cooperation.

My heartfelt thanks go to my family for their unconditional support and affection to pursue my research interest. I feel deeply indebted to them for whatever I achieved so far. I express my special thanks to my husband Avi for all his continuous help and encouragement without whom it would not have been possible to carry out my research work with such an ease. Thanks a lot for always being there for me and supporting me in every difficult situation of my life.

I would also like to say huge thanks to my very good friend Mary McDonald, Lech and Krystina for make my stay in Dublin so comfortable. Thanks a lot for all your kind support and all the help.

I am also thankful to the technical team Veronica, John, Damien, Brendan, Ambrose, Vinnie, Niamh, Rob and Catherine for their support and smiling help.

Nivedita Das

Table of Contents

Chapter 1: Introduction

Chapter 2: Dipyrrins and their Re metal carbonyl complexes

Chapter 3: Synthesis, time resolved infrared studies electrochemistry and a thermal assessment of ruthenium(II), rhenium(I) and manganese(I) complexes for their ability to lose CO

Chapter 4: Singlet oxygen and CO release studies of pophyrin-based metal-carbonyl complexes

Chapter 5: Group VI metal carbonyls as CORMs

Chapter 6: Future Work

Abstract

Chapter 1 serves as an introduction to the concepts and methods used throughout this thesis. This chapter highlights how main group and transition metal carbonyl complexes have potential therapeutic applications. The latter part of this chapter focuses on photodynamic therapy specifically using porphyrins. This is followed by an overview on the time resolved infrared (TRIR) spectroscopy. Also discussed are the excited states, energy transfer and applications of time-resolved infrared spectroscopy.

Chapter 2 contains with a short literature review on the dipyrrins and metal coordinated dipyrrin compounds. It describes the luminescence and photophysical properties of various transition metal based dipyrrin complexes reported in literature. This chapter describes the synthesis and characterisation of novel dipyromethenes and their corresponding coordination to form tetra and tri carbonyl complexes of Re metal. Further in this chapter these complexes were accessed for their ability to act as CO releasing molecules (CORMs) using the myoglobin assay procedure both photochemically and thermally. Also presented are the results of time resolved infrared spectroscopy experiments, which show the existence of excited states based on *intra*-ligand charge transfer within the dipyrrin moiety.

Chapter 3 contains the study of Re and Mn based mononuclear as well as Ru-Re and Ru-Mn based heterodinuclear carbonyl complexes. This chapter begins with a literature survey on the photophysical properties and applications of the rhenium based mononuclear and ruthenium-rhenium based heterodinuclear systems. The synthesis and characterisation of mononuclear Re(I) and Mn(I) complexes as well as Ru(II)-Re(I) and Ru(II)-Mn(I) heterodinuclear complexes which contain 2,2'-bipyrine as a bridging ligand is given, followed by their photophysical and electrochemical properties. This chapter also includes TRIR and CO releasing properties of the above mentioned complexes both photochemically and thermally.

Chapter 4 covers a literature review on pyridyl porphyrins and related carbonyl complexes and their role in photodynamic therapy as well as CO releasing molecules. The synthesis and characterisation of the freebase, metalled monopyridyltriphenyl porphyrin and metal carbonyl derivatives using ^{1}H NMR, UV and IR spectroscopic tools are presented in this chapter. Further their ability to generate singlet oxygen has also been studied using two different sets of experiments involving toluene and dichloromethane as solvents. In addition, metal carbonyl tethered porphyrin were investigated for their ability to act as CO releasing molecules both thermally and photochemically using myoglobin assay.

Chapter 5 deals with the study of Group VI (Cr, Mo, W) metal carbonyl complexes attached to ligands such as anthracene, 2-methylthionaphthalene, mesitylene and bipyridine. In this chapter the synthesis and characterisation of metal carbonyl complexes using ^{1}H NMR, UV and IR spectroscopic techniques have been reported. The compounds were further assessed for their ability to act as CO releasing molecules both thermally and photochemically using myoglobin assays.

Chapter 6 outlines the future work for this thesis.

Abbreviations

Ag/AgCl	Silver/Silver chloride reference electrode
bpy	2,2’-bipyridine
bisbpy	2,2':5',3":6",2"'-quaterpyridine
5Brbpy	5-bromo-2,2’-bipyridine
CuI	Coper iodide
CORMs	Carbon Monoxide Releasing Molecules
^{13}C NMR	Carbon nuclear magnetic resonance
CO	Carbon monoxide
COSY	Correlation Spectroscopy
CT	Charge transfer
DCM	Dichloromethane
DDQ	2,3-Dichloro-5,6-dicyano-1,4-benzoquinone
DMF	N,N-dimethylformamide
DMSO	Dimethylsulphoxide
eV	Electron volt
E_{pa}	Anodic peak potential
E_{pc}	Cathodic peak potential
fac-	Facial
^{1}H NMR	Proton nuclear magnetic resonance
HOMO	Highest occupied molecular orbital
ILCT	Intra ligand charge transfer
IR	Infrared spectroscopy
ISC	Inter-system crossing
^{1}LC	Ligand centred singlet excited state
^{3}LC	Ligand centred triplet excited state
LUMO	Lowest unoccupied molecular orbital
mer-	Meridional
Mb-CO	Myoglobin bound carbon monoxide
mins	minutes
MLCT	Metal-ligand charge transfer
MPyTPP	Monopyridyltriphenylporphyrin

ns	nanoseconds
OD	Optical density
$^1O_2$	Singlet Oxygen
OLED	Organic light emitting device
PDT	Photo dynamic therapy
Ph	Phenyl
ps	Picosecond
Py	Pyridine
RT	Room temperature
$TBAPF_6$	Tetrabutylammonium hexafluorophosphate
TEA/Et_3N	Triethylamine
THF	Tetrahydrofuran
TLC	Thin layer chromatography
TRIR	Time Resolved Infrared Spectroscopy
TON	Turn over number
TPP	Tetraphenylporphyrin
tpphz	Tetrapyridylphenazine
UV-Vis	Ultra violet-Visible
λ_{max}	Maximum wavelength
ε	Extinction co-efficient
Φ	Fluoroscent quantum yield
τ	Luminescence lifetime
μs	Microsecond

Chapter 1

Introduction

Chapter 1 introduces the concepts discussed in the thesis. A comprehensive overview of how main group and transition metal carbonyl complexes can be used as CO releasing molecules and their therapeutic applications is discussed. The latter part of this chapter focuses on singlet oxygen and time resolved infrared studies.

1.1 General introduction to bio-organometallic chemistry

Photosynthesis by green plants, respiration by plants and animals, biosynthesis of such macromolecules as proteins, nucleic acids, carbohydrates, etc., utilization of metabolic energy, transfer of genetic information, all are mediated by specific enzymes, most of which require one or more biological metal ions for their activity and / or their structural integrity. Enzyme bound transition metal ions, by virtue of their unique coordination chemistry, may provide binding sites to substrates, and hence stabilize the appropriate conformation of the enzymes and may function as catalytic centres. Lability and inertness of metal-ligand bonds, stereochemistry, stability, magnetic and redox properties of metal-ligand complexes manifest themselves in all the reactions of metal ions in metallo-proteins and metallo-enzymes. In fact, biochemistry of metal ions is a reflection of the chemistry of transition metal ions in general and coordination chemistry in particular.

The earliest reports on the therapeutic use of transition metal complexes in cancer and leukemia date from the sixteenth century. In 1960 the anti-tumor activity of an inorganic complex *cis*-diammine-dichloroplatinum(II) (cisplatin) was discovered. Cisplatin has developed into one of the most frequently used and most effective cytostatic drugs for treatment of some carcinomas. Other complexes containing metals like gallium, germanium, tin, bismuth, titanium, ruthenium, rhodium, iridium, molybdenum, copper and gold were also found to be effective against tumors.[1]

Some of the therapeutic applications of transition metal complexes can be summarised as follows:[2-4]

1) Transition metal complexes of silver, zinc and manganese have been used for years as anti-microbial agents. Metal complexes of Pt(II) and Ru(II) with *o*-vanillin-(4- methyl thiosemicarbazone), and o-vinillin-(4-phenyl thiosemicarbazone) have been prepared, characterized by chemical methods and studied for antibacterial, antifungal activity and are proven anti-infective agents. Currently silver based materials e.g. silver sulfadiazine and silver dressings are used as biocidal agents in burn wound treatment and biomedical materials.

2) Transition metals have also been used as anti-inflammatory and anti-arthritic agents. For example, several injectable transition gold complexes like sodium aurothiomalate,

aurothioglucose and sodium aurothiopropanol are used clinically in the treatment of severe cases of rheumatoid arthritis.

3) There are a number of vanadium complexes that have been developed, many of which have insulin-mimetic properties.

4) Transition metal complexes are also used in the treatment of neurological disorders. Neuronal Zn(II) serves as an important, highly regulated signalling component responsible for the initiation of a neuroprotective pathway.

5) Sodium nitroprusside drug has potent vasodilating effects and successfully used as a treatment for severe pefrexia, myocardial infarcation, celebral vasospasm as a result of its breakdown to nitric oxide.

6) Cu(III) and Ga(III) based complexes are used as myocardial perfusion imaging in positron emitting radiopharmaceuticals.

Living systems routinely synthesize tetrapyrrolic macrocycles, either in their metal free forms (e.g., pheophorbide) or, more commonly, the corresponding metal complexes (e.g., chlorophyll, heme, coenzyme B_{12}, etc.). The resulting species have been called “the pigments of life” because they perform a variety of fundamental biological functions that lie at the very core of life as we understand it.[5,6]

Over the past three decades, the chemistry of expanded porphyrins have brought about remarkable synthetic advances and provided new insights into the fundamental features of aromaticity.[7] More recently, the scope of expanded porphyrin chemistry has grown to encompass the field of anion binding and transport. However, one of the main motivating forces behind the synthesis of expanded porphyrins are that they may extend the frontiers of “porphyrin-like” coordination chemistry.To date, some of this latter promise has been realized. For instance, porphyrins have been used to stabilize complexes containing typically large cations, including those of the lanthanide and actinide series. They have also allowed for the generation of complexes containing multiple cations. These synthetic findings, combined with a range of spectroscopic and physical properties, have prompted the study of expanded porphyrin metal complexes as photosensitizers in photodynamic therapy,[8] contrast agents in magnetic resonance imaging,[9] building blocks in nonlinear optical materials,[10] and enzyme models in bioinorganic chemistry.[11]

1.2. Carbon monoxide –releasing molecules (CORMs)

Carbon monoxide (CO) is considered an odourless, colourless and toxic gas with no biological relevance. For decades, scientists have neglected CO because of its bad reputation as a harmful and poisonous gas. This is due to the fact that affinity between CO and hemoglobin is approximately 220 times stronger than the affinity of hemoglobin for oxygen. Thus, it can significantly reduce the oxygen-carrying capacity of this protein, prevent mitochondrial respiration and form carbon-monoxy-haemoglobin (HbCO) which leads to CO poisoning in humans.[12, 13]

However the perception about the negative effects of exerting only CO is challenged by the studies corroborating cytoprotective and anti-oxidant activities of inducible heme oxygenase-1 (HO-1), the enzyme that produces CO in the body.[14] Studies indicate that the increase in the generation of endogenous CO in stressful conditions reflect a dynamic and active involvement of this by-product in the protective response.[15] In the majority of the experimental models where a beneficial participation of HO-1 has been demonstrated also dovetails with the fact that CO "at appropriate doses" exerts a comparable protective effect on its own, even when heme oxygenase activity is totally abolished.[16] The tissues of most mammals, including human beings generates CO locally as cells express both inducible (HO-1) and constitutive (HO-2) heme oxygenase isoforms.[17] These enzymes present in all tissues examined so far, with high abundance in the brain (HO-2), liver (HO-2 and HO-1), spleen (HO-1), vascular endothelial cells and smooth muscle tissues (HO-1 and HO-2), catalyze the conversion of heme to ferrous iron, CO and biliverdin.[18, 19] Heme is oxidized at the α-position of the protoporphyrin ring by heme oxygenase and participates in the reaction as both prosthetic group and substrate, while O_2 and NADPH are required as cofactors[20] (**Scheme 1.1**).

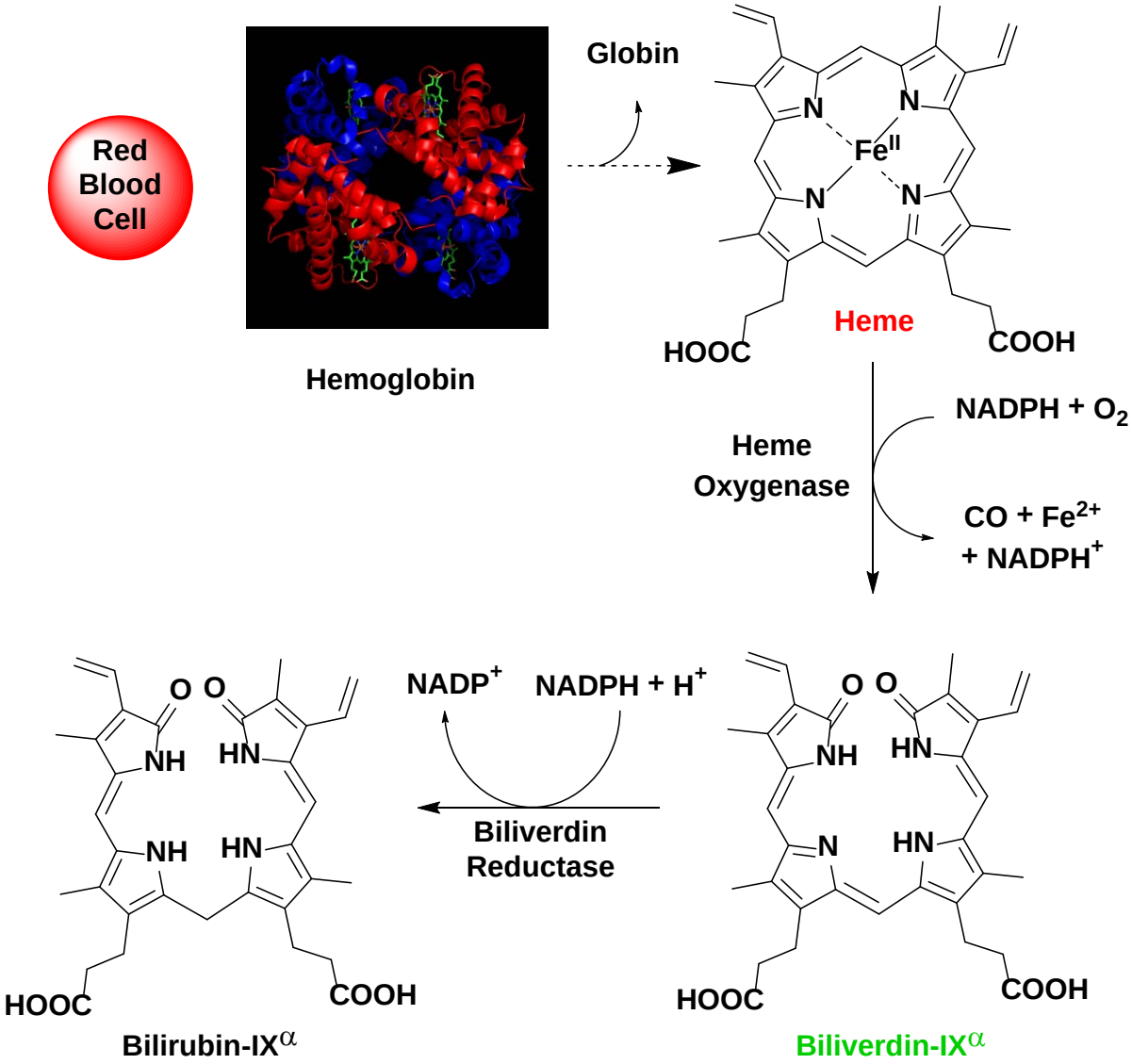

Scheme 1.1 *Mechanism of hemoglobin degradation of red blood cells with generation of CO by heme oxygenase (HO).*

The presence of different isoforms suggests that evolved cells control this enzymatic pathway to regulate the consumption of heme and production of CO, biliverdin and iron during physiological and pathophysiological situations.[21] Basal production of CO is estimated to be 6 μmol $kg^{-1}day^{-1}$.[21] This rate increases substantially in pathological states such as hemolytic

disease, asthma, cystic fibrosis and diabetes, suggesting that the response of the body to counteract stressful conditions leads to increased CO levels.

The biological effects mediated by endogenous CO can be simulated when this gas is applied exogenously; this approach revealed various beneficial actions by CO, including potent anti-inflammatory and anti-apoptotic effects,[22] suppression of atherosclerotic lesions following aortic transplantation, prevention of reperfusion-induced ventricular fibrillation in the myocardium and protection against ischemic lung injury.[16, 22-24] These interesting studies led scientists to the concept that CO could be used for therapeutic purposes.

Further, CO is emerging as an important and versatile mediator for physiological processes to the extent where the treatment of animals with exogenous CO gas can have beneficial effects in a range of vascular and inflammatory-related disease model.

The practical obstacles and problems associated with the systemic effects imposed by inhalation of CO gas on the oxygen transport and delivery, led to the discovery and development of molecules having the inherent property to liberate CO under appropriate conditions and function as CO-releasing molecules (CORMs) in biological systems.

Initially two carbonyl complexes, manganese decacarbonyl [$Mn_2(CO)_{10}$] and tricarbonyldichlororuthenium(II) dimer [$Ru(CO)_3Cl_2$] (termed as CORM-1 and CORM-2, respectively) emerged as first class CORMs and showed CO-releasing properties for the first time. Although these two compounds are soluble only in organic solvents and CORM-1 requires irradiation to induce CO loss, they both are pharmacologically active by exerting effects that are typical of CO gas, including vessel relaxation, attenuation of coronary vasoconstriction and suppression of acute hypertension.[25, 26]

1.2.1 Main group elements

The production of CO from main group compounds is not very promising since the “pro-CO” carbon is usually involved in two strong bonds which have to be broken homolytically. The reaction involving cleavage of these bonds is very unlikely at room temperature or at 37 ^{o}C (normal human body temperature range 36.5 – 37.2 ^{o}C) due to the high thermodynamic stability coupled with high activation energies. A more promising strategy is to bind CO

directly to a strong lewis acid in a potentially reversible equilibrium. The bonding of CO to main group elements can be described in an analogous manner to transition metals. The HOMO of CO is a slightly antibonding σ-orbital, localized on the carbon (**Figure 1.1**). **Figure 1.2** represents the metal-CO bonding interaction in the transition metal carbonyl complexes. The HOMO of CO donates electrons into empty metal orbital forming an σ bond. A bonding interaction (back bonding) is formed where metal donates its *d*-electrons to an empty anti-bonding orbital (LUMO) of CO (pπ*). Also, antibonding π* orbital of CO might take electrons by back bonding from filled p-orbitals from main group elements as well.[27] As an acceptor of electrons in orbitals with π-symmetry, CO is also known as π-acceptor or π-acid. Most importantly, a stronger σ-donation increases the electron density at the metal, therefore enhancing the π-back donation. This bonding scheme is favoured for metals with low oxidation states with high energy d-electrons. Increasing the positive charge on the metal ion decreases the energy of its d-electrons, forming an effective back-bonding, hence weakening and labilising of M-CO bond. This control can be finely tuned by manipulation of the electron density donated or removed by the ancillary ligands that share the coordination sphere of the metal. A striking example of the reactivity control provided by M-CO back donation is given by the binding characteristics of Hb to CO where heme is reduced to (Fe^{2+}) and releases it upon oxidation to methemoglogin (metHb) (Fe^{3+}).

In general group 13 elements, particularly boron compounds as very strong lewis acids are considered as a reasonable choice for binding with CO.

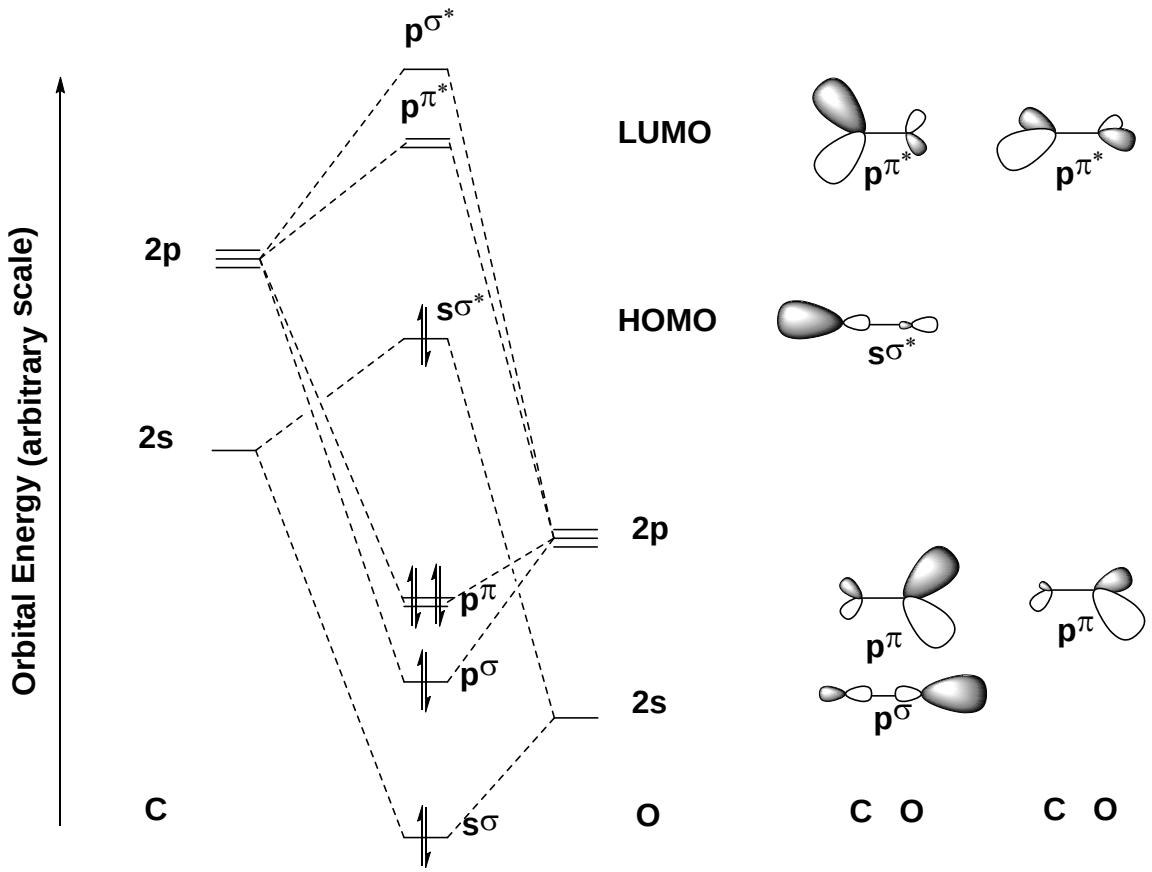

Figure 1.1 *Simplified MO diagram of CO with electronic occupancy in the ground state*

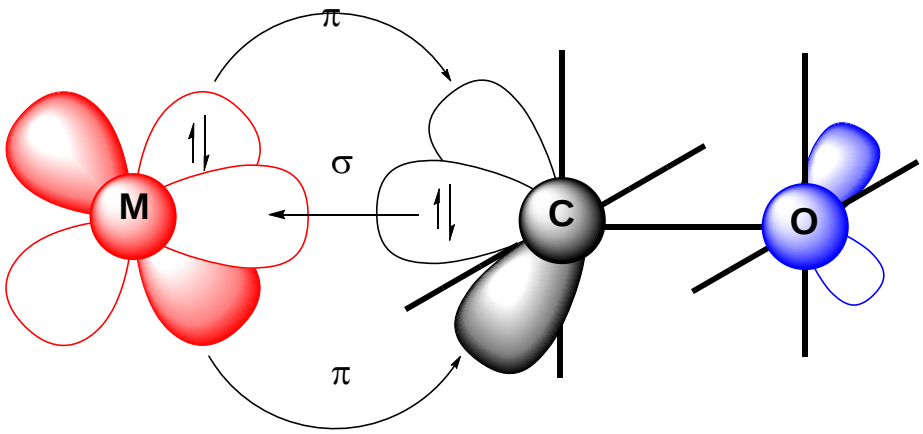

Figure 1.2: *Typical representation of M-CO bond*

Only boron is able to build stable adducts at room temperature with CO.[28] However, boranecarbonyl cannot act as a potential CORM because of its spontaneous reaction with air. Due to the high electrophilic nature of CO carbon bound to boron, in alkaline water it can form the stable boranocarbonate anion $[H_3BCO_2]^{2-}$ which can be isolated as an air and water stable salt with various counter-ions.[29] One of such compounds is $Na[H_3BCO_2H]$ which slowly releases CO at physiological pH and 37 ^oC with half lifetime of about 20 min for 48 µM of the complex (**Figure 1.3**).

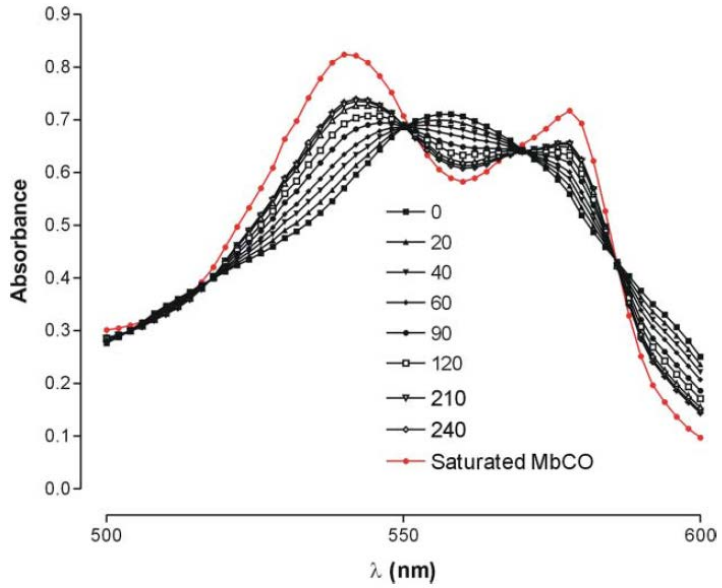

Figure 1.3 *Time dependent [min] formation of CO adduct of myoglobin (MbCO) after reaction with $Na[H_3BCO_2H]$. Legend shows the time passed in mins. The red line shows the typical spectrum of MbCO after reacting Mb with CO gas. Concentrations are Mb= 60 µM; $Na[H_3BCO_2H]$ = 48 µM.*[21]

At the same time, ester, amide and thioester derivatives of boroncarbonate are also capable of releasing CO under physiological conditions. But the introduction of any functional groups at

the boron atom leads to the loss of their CO releasing ability under physiological conditions. Therefore, very few boron containing compounds have been investigated as efficient CORMs.

1.2.2 Transition metal carbonyl complexes

An easier choice for CORMs is transition metal carbonyl complexes.

To qualify as potential CORMs, metal carbonyl complexes should have the following prerequisites for later in vivo applications

1) Reasonable water solubility (although insoluble complexes can be dealt with pharmacologically).
2) Controlled release of CO ligands with known follow up products
3) Non toxicity prior to and after decomposition

Generally, metal carbonyls with high CO stretching frequency are considered good CO releasing molecules as metal carbonyl stretching vibration at high wavenumbers indicates weak bonding between the metal and the CO ligand. Hence, it can easily dissociate thermally from the metal and be replaced by a water molecule. Another route for the generation of CO molecules is photochemical. The first reported CORMs, $[Mn_2(CO)_{10}]$ and $[Fe(CO)_5]$ complexes released CO upon irradiation.[30] But this approach has limited *in vivo* applications at the sites which are not exposed directly to the body's surface.

Another possible route for the promotion of CO can be the associatively supported substitution reaction which can take place in coordinating solvents such as water. Such reactions are not necessarily dependent on M-CO bond but on pH.

It is also necessary to consider that carbonyl metal complexes having very high CO stretching frequencies can also undergo the water-gas shift reaction and hence form a metallo-carboxylate complex followed by the formation of hydride and the release of carbon dioxide. This type of reaction can easily compete with the release of CO molecules.

The different possibilities and aspects are outlined in **Scheme 1.2**.

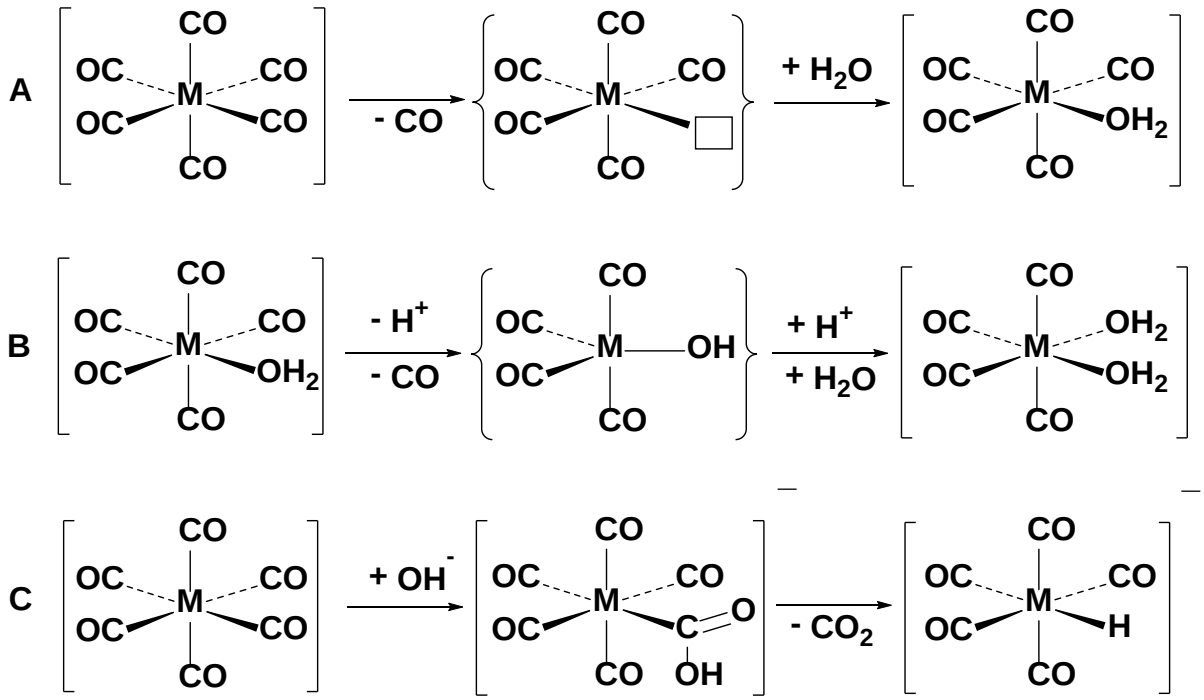

Scheme 1.2 *Different routes to CO release from metal carbonyl complexes.*[21] *(A) Dissociation of CO as a rate determining step; (B) base catalysed CO release; and (C) side reaction in which the conversion of CO with H_2O to CO_2 and a hydride may occur.*

As discussed previously, first transition metal carbonyl complexes namely $[Fe(CO)_5]$, dinuclear $[Mn_2(CO)_{10}]$ and $[\{Ru(CO)_3Cl_2\}_2]$ which were identified as CORMs, originated so as to mimic the CO releasing property of HO-1 enzyme in biological systems (see **Figure 1.4**).[30] In order to investigate the CO releasing property of the ruthenium complex, it was solubilized in DMSO due to its insolubility in water. This complex showed very good *in vivo* applications with low toxicity.[31, 32] In an attempt for the better control of solubility and release of CO, two of the coordinating sites of the complex $[\{Ru(CO)_3Cl_2\}_2]$ were replaced by the glycinato group. Studies on the new complex $[RuCl(gly)(CO)_3]$ showed that the release of CO not only depends on the strength of M-CO bond but also strongly on the pH of the medium in which the compound is studied.

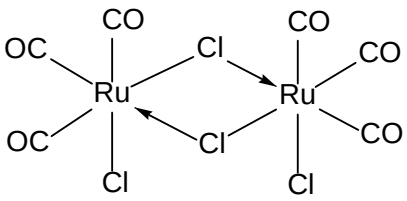

CORM-2

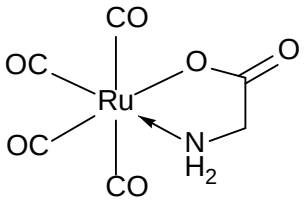

CORM-3

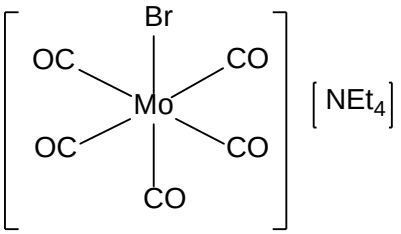

ALF062

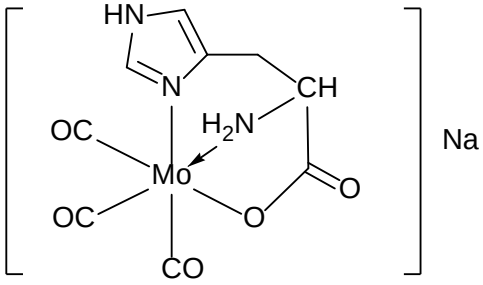

ALF186

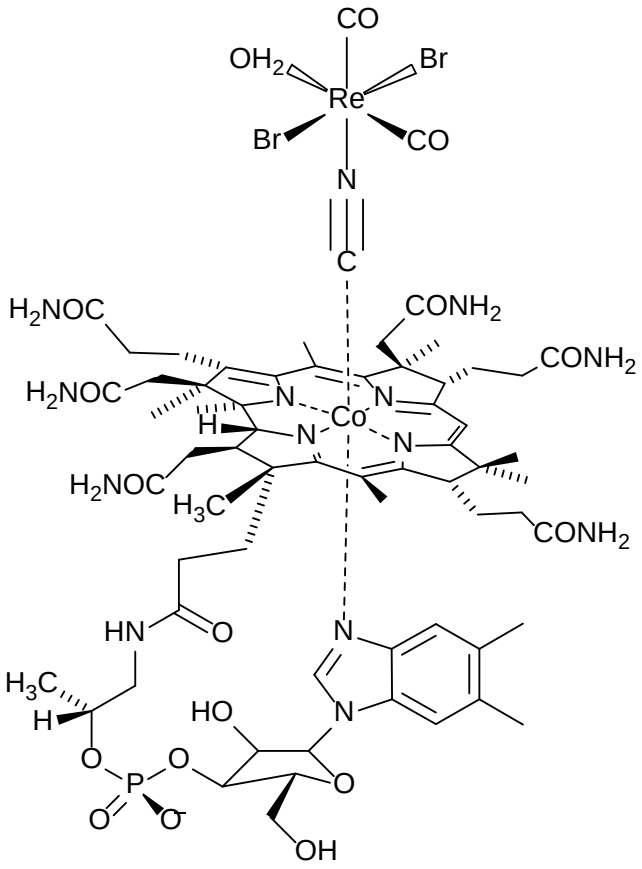

B_{12}-ReCORM-2

Figure 1.4 *Selection of CORMs from the literature.*[33, 34]

Another group of CORMs are η^4-pyrone Fe(0) complexes (**see Figure 1.5**). Motterlini and co-workers, investigated these complexes and found that electron withdrawing groups such as halides attached at the 4-position of 2-pyrone facilitated the release of CO. Furthermore, halogen attached at the 4-position together with a methyl group at the 6-position on the pyrone ring containing iron complexes led to lower cytotoxicity in these complexes compared to other CORMs.[35]

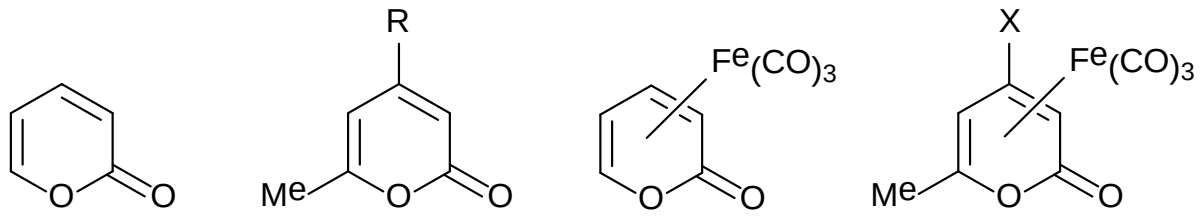

Figure 1.5 *η^4-pyrone and related Fe(0) complexes (X= H, Br; R=Aryl, alkenyl, alkynyl)*

Another η^4-pyrone molybdenum tricarbonyl complexes have been identified by Motterlini and co-workers as efficient CORMs (**Figure 1.6**).[36] CORM-F10 has been reported as a rapid CO releasing molecule. After 5 min, the total amount of CO released was quantified using a myoglobin assay was found to be 17 μM, which equates to a rate of MbCO formation to be 3.4 μM/min. Vasorelaxation and toxicity studies of this compound suggest its excellent therapeutic properties. The group further observed that the CO releasing ability of CORM-F4 and CORM-F10 was governed by one substituent on the η^1-pyrone ligand. Thus, it can be inferred that changes in the structure of the CORM may have a significant effect on its CO donating property.

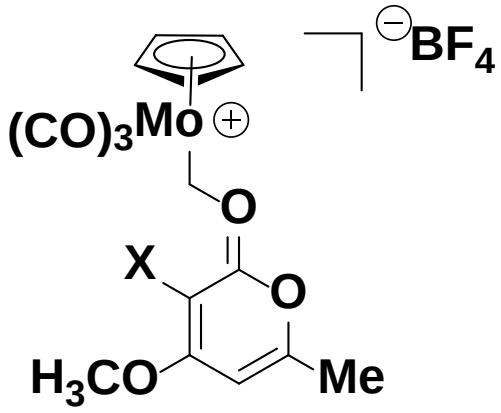

Figure 1.6 *Group 6 metal carbonyl complex is [Mo (CO)* $_3$ *(η^5-C_5H_5) (η^1-{O}-C {=O}-O-CMe=CH-COMe=CX)] BF_4 where X = Br, CORM-F10 and X = H, CORM-F4.*

A new family of compounds based on tetrachlorocarbonyliridate(III) $[IrCl_4(CO)L]^{n-}$ derivatives have been reported as potential CO releasing molecules. The rate of MbCO formation for these complexes was studied via myoglobin assays. The results showed that rate of MbCO formation depends on the nature of the sixth ligand, *trans* to CO and by changing the ligand a significant modulation on the rate of MbCO release can be modulated. For example the formation of of MbCO was accelerated by 20 folds when Cl^- *trans* to CO was replaced by DMApy (dimethylaminopyridine) ligand. The reported complexes are soluble in aqueous media and rate of CO release was found to be 0.03 – 0.58 μM/min in a 10 μM solution of myoglobin assay and 10 μM of the complexes (see **Figure 1.7**).[37]

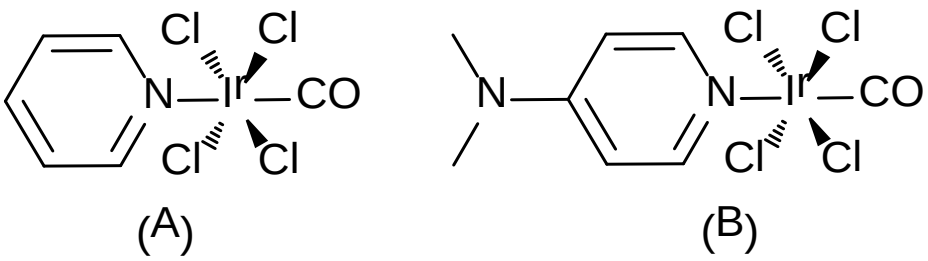

Figure 1.7 *Structure of $[IrCl_4(CO)(py)]^{n-}$ (A)and $[IrCl_4(CO)(DMApy)]^{n-}$ (B)*

Recently for better bio-availability, amino acids and amino ester groups were coordinated to group 6 metal carbonyl complexes. Fairlamb and co-workers reported that the loss of the amino ester organic group ($NH_2CH\{R\}CO_2R'$] which is bound to the $M(CO)_5$ metal framework (M=Cr, Mo, W) plays an important role in the rate determining step of the CO loss. They also noted that the release of CO is rapid when the $M(CO)_5$ is bound to this organic group compared to the absence of this group. A direct correlation between the electrophillic nature of the carbene carbon and rate of MbCO formation has been established for Fischer type carbene complexes. It was found that the electrophilicity of the carbene carbon depends on the R and X groups of the carbene complex $[Cr(CO)_5(=CRX)]$(R = Me, Ph-C≡CH;X = heteroatom group). Better π-donor groups, such as when X = amino or R = -C≡CH, makes the carbene less electrophilic when compared to the case when X = alkoxy and R = Me. As amino substituted carbene complexes exhibit far slower release than their alkoxy analogues (see **Figure 1.8**).[38]

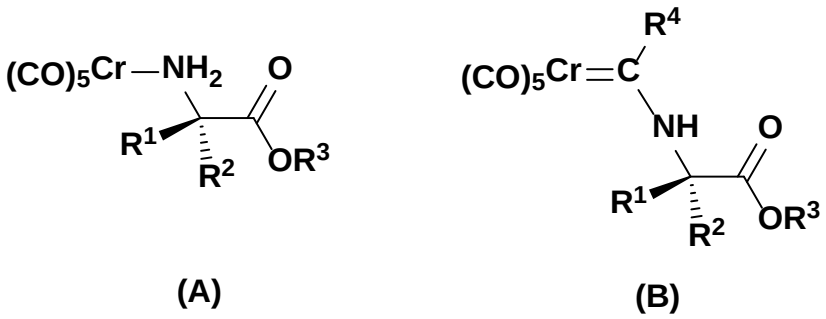

Figure 1.8 *Structure of* $[Cr(CO)_5(NH_2C\{R^1\}\{R^2\}CO_2R^3)]$ ***(A)*** *and carbene complex* $[Cr(CO)_5(=CRX)]$ ***(B)*** *(R = Me, Ph-C≡CH;X = heteroatom group).*

Fairlamb and co-workers also reported that μ_2-alkyne dicobalt(0) hexacarbonyl complexes as a new class of CORMs which exhibit cytotoxicity towards leukemia and tumour cells. Further they have specified that alkyne substituents play an important role in the rate of CO-release, cytotoxicity and cell viability (**see Figure 1.9**).[39, 40]

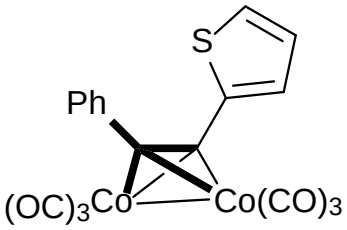

Figure 1.9 *Structure of μ_2-alkyne dicobalt(0) hexacarbonyl complexes*

Another example of biocompatible transition metal carbonyl complex which have CO releasing ability is 17 electron rhenium dicarbonyl complexes on a cobaltamin scaffold (see **Figure 1.10**).[33] Bogdanova *et al*. reported that B_{12}-Re^{II} $(CO)_2$ derivatives can act as efficient pharmaceutical CO releasing molecules as they exhibit a number of features such as effective stability in an aqueous aerobic medium, therapeutic protection against ischemia-reperfusion injury in cultured cardiomyocytes and after CO release in water under aerobic conditions, the rhenium complex is oxidized to ReO_4^- which is among the least toxic of all the rare inorganic compounds. The rate of MbCO formation from B_{12}-ReCORM-2 and B_{12}-ReCORM-4 was found to be same with $t_{1/2}$ life of 20 min.

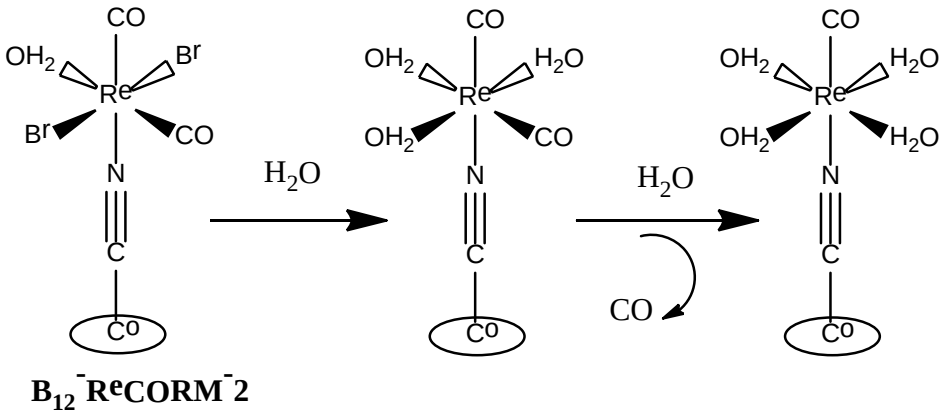

Figure 1.10 *Mechanism of CO release by B_{12}-ReCORM-2*

The above examples of CO releasing molecules provides an overview of the work that has been reported in recent years for the direct application of carbon monoxide as a therapeutic tool in the treatment of various human diseases.

1.2.3 Mechanism of CO release

It is essential to understand the factors which control the CO releasing property of CORMs under physiological conditions in order to know the activation and degradation pathways of these therapeutic agents. The general mechanism for the release of CO from metal carbonyl complexes was illustrated in **Scheme 1.3**.

Some of the key factors which control the rate of CO release in these molecules are described below:

1) water-solubility
2) electron density at the metal centre
3) oxidation state of the metal centre

Very few mechanistic studies on CORMs in the aqueous medium have been reported so far. However, one such study on $[NEt_4][MX(CO)_5]$ (M = Mo, W and X = Cl, Br, I) type complexes revealed the formation of an $[\{M(CO)_5\}_2(\mu\text{-}X)]^-$ intermediate and hydrolysis of the M-X bond controls the rate of CO release in aqueous systems.

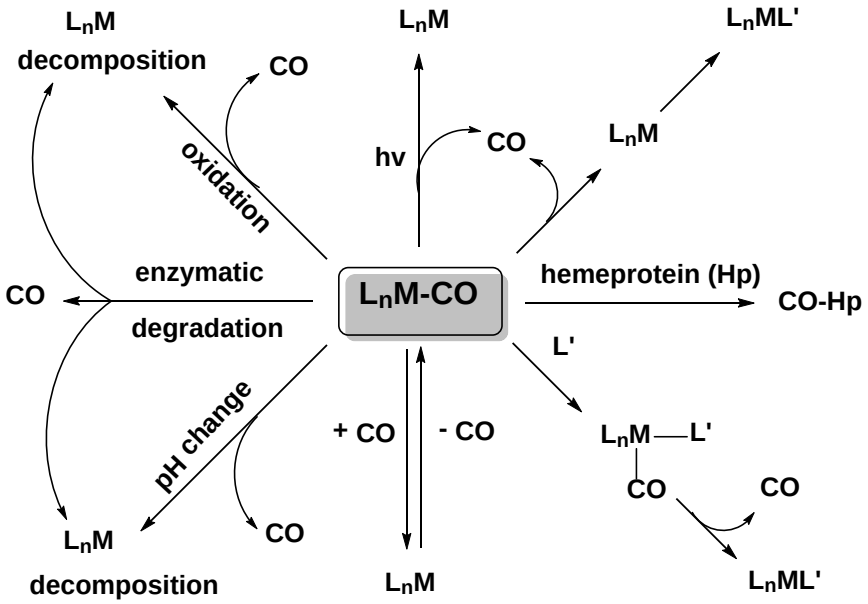

Scheme 1.3 *Mechanisms leading to CO release from a generalised metal carbonyl complex of formula L_nM-CO.*[41]

Another example of a CO-releasing molecule which has been investigated for mechanistic studies is illustrated below.

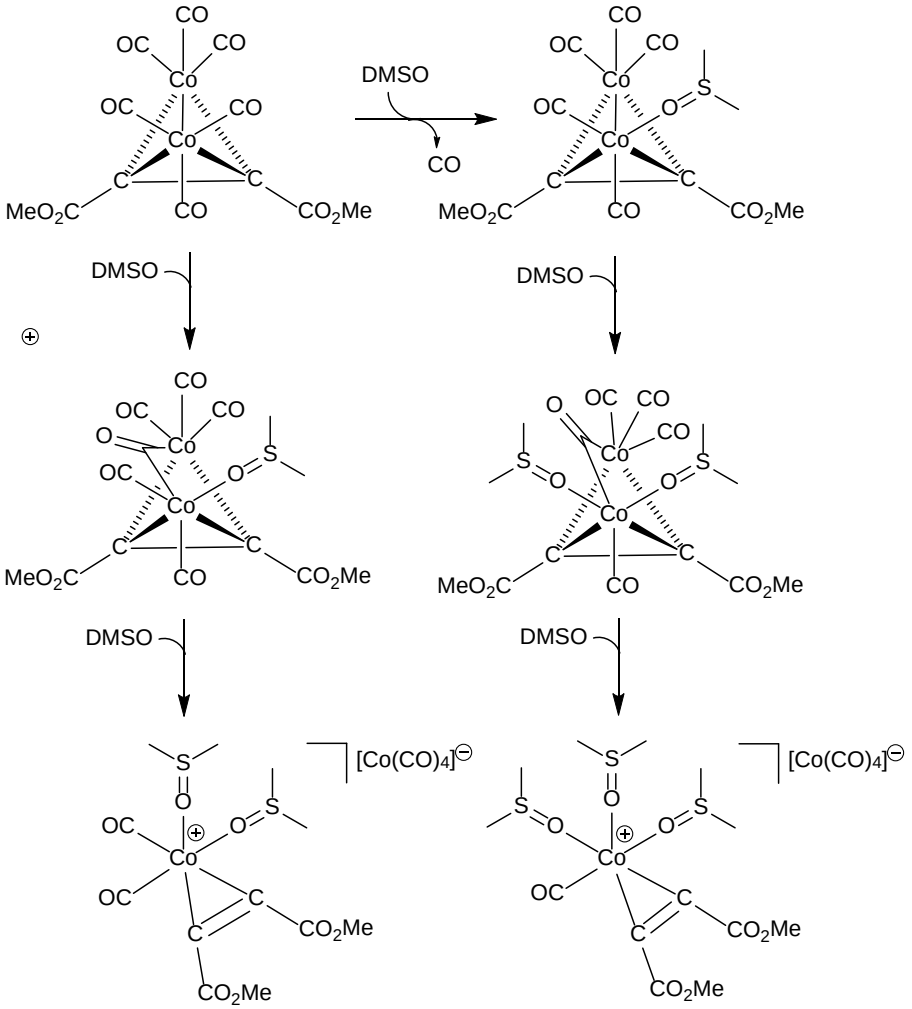

Scheme 1.4 *Proposed mechanism for DMSO activation of the CO-RM μ_2-alkyne dicobalt(0) hexacarbonyl complex*

From this mechanistic study it can be inferred that the release of CO occurs via the formation of the $[Co(CO)_4]^-$ anion (**Scheme 1.4**).[39] Also, the formed unstable cationic species can undergo substitution reaction by DMSO and water and formation of this anionic species is responsible for the faster release of CO.

1.2.4 Photo-CORMs

A more recent approach is based on photochemical strategies to aid the CO release. This area of research is extremely recent and known as photoactivable CO releasing molecules (Photo-CORMs).

Photo-CORMs would ideally use low energy photons (λ = 400-700 nm) for carbon monoxide release but to date various wavelengths have been employed. [29] [42] A drug delivery system must contain specificity and controlled release. To ensure the bioactive substance is delivered to the correct physiological location, the dosage and location must be closely regulated to maximise the effect. It is possible to control the timing of CO released by using a light source to initiate the release of CO.[43]

Experimental techniques such as FTIR analysis, gas chromatography analysis and analysis by flash photolysis can be used to measure the exact amount of CO that is released under certain physiological conditions.[44] Some examples of photo-CORMs are manganese decacarbonyl and iron pentacarbonyl, manganese tricarbonyl complexes of tris-(pyrazolyl)methane, manganese tri-carbonyl complexes of tris-(imidazolyl)phosphine, tungsten pentacarbonyl complexes of tris-(sulphonatophenyl)phosphine and di-carbonyl-bis-(cysteamine)iron(II) (see **Figure 1.11**).[46]

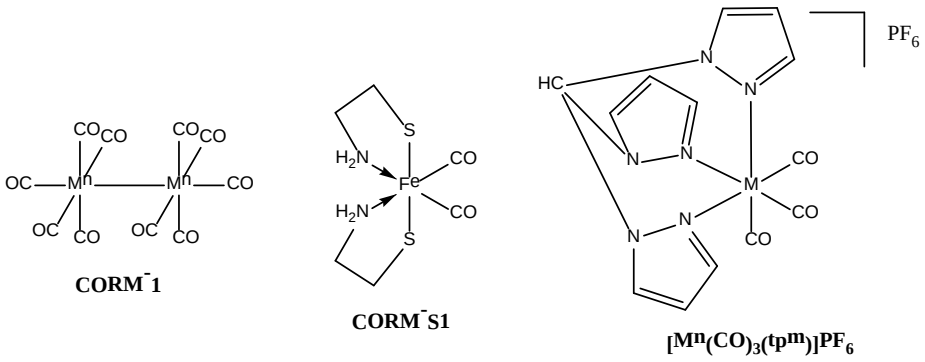

CORM⁻1 **CORM⁻S1** **$[M^n(CO)_3(tp^m)]PF_6$**

Figure 1.11 *Some examples of Photo-CORMs*

Photo CORMs are those molecules which can decompose under photo-excitation. $[Fe(CO)_5]$ was the first photo CORM that was irradiated to study its CO releasing properties. This complex is insoluble in aqueous environments and poses major threats as it is extremely toxic. CORMs soluble in aqueous solutions were developed in order to release CO under photochemical conditions. One such example based on iron, that can release CO photochemically has been developed; [*cis*, *trans*, *cis*-dicarbonyl-bis-(2-thiolato-κS-ethylamin-κN)iron(II)] which was termed CORM-S1.[45] This is an iron based CORM containing biogenic ligands (ligands produced from a living organism). It generates CO when irradiated with light at a wavelength greater than 400 nm. The biogenic ligand cysteamine is produced *in vivo* from the degradation of cysteine. It is comprised of two cysteamine ligands in a *trans* orientation and two carbonyl ligands in a *cis* co-ordination. The rate of MbCO formation from CORM-S1 when induced by light was quantified using a myoglobin assay and by spectrophotometric techniques. This iron complex is largely stable in the absence of light. However, when it is exposed to visible light, there is a rapid liberation of CO. *cis*-dicarbonyl-bis-(2-thiolato-κS-ethylamin-κN)iron(II) can be easily prepared from cysteamine and tri-irondecacarbonyl. The synthesis of CORM-S1 is shown in **Scheme 1.5**.

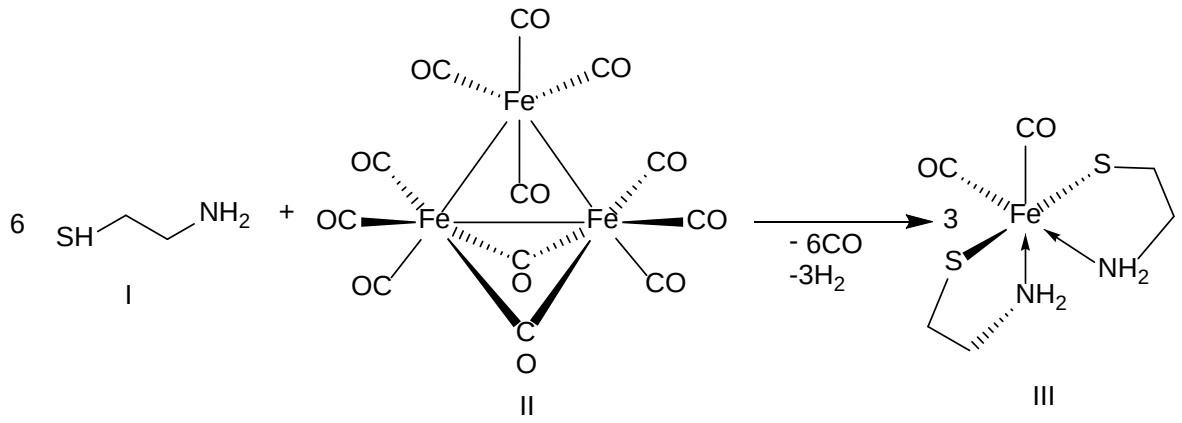

Scheme 1.5 *The synthesis of the iron complex CORM-S1, where I: cysteamine; II:triirondecacarbonyl; III: cis,trans,cis-dicarbonyl-bis-(2-thiolato-κS-ethylamin-κN)iron(II) as described by Kretschmer et al..*[46]

The synthesis and reactivity of molybdenum complexes containing functionalised alkynyl ligands have been analysed for potential CO releasing molecules. For example the reaction of $[MoCl(\eta^5\text{-}C_5H_5)(CO)_3]$ with propargyl alcohols such as ($HC{\equiv}CCR^1R^2OH$) in the presence of catalytic quantities of CuI, using $HNEt_2$ as a solvent resulted in formation of alkynyl complexes, $[Mo(C{\equiv}CCR^1R^2OH)(\eta^5\text{-}C_5H_5)(CO)_3]$. The ability of these complexes to liberate CO was demonstrated when a water soluble alkynyl complex which contained a β-D-fructopyranose group (a sugar-substituted complex) was exposed to UV light. The ability of the CO releasing properties of the complexes were assessed using an assay based on the conversion of deoxymyoglobin to carbomonoxymyoglobin (MbCO). This proves its application as a new type of photo CORM.[47] This is illustrated in **Scheme 1.6**.

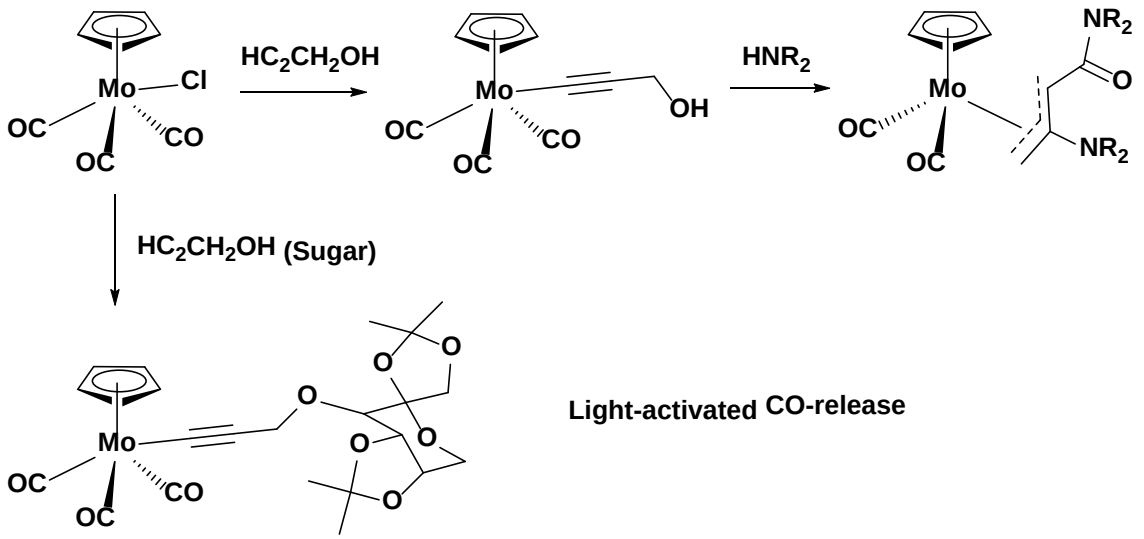

Scheme 1.6 *The alkynyl complex, $[Mo(C{\equiv}CCR^1R^2OH)(\eta^5\text{-}C_5H_5)(CO)_3]$ is formed from the reaction of $[MoCl(\eta^5\text{-}C_5H_5)(CO)_3]$ with propargyl alcohols ($HC{\equiv}CCR^1R^2OH$) using NEt_2H as a solvent, in the presence of catalytic quantities of Cu. Also a hydrophilic alkynyl complex that contains a β-D-fructopyranose group (a sugar-substituted complex) is observed above. Upon irradiation of UV light, this compound releases CO.*[47]

A series of tricarbonyl manganese(I) and rhenium(I) complexes of imidazole based phosphane ligands have been synthesised by Spingler and co-workers (**see Figure 1.12**). The

myoglobin assay, in accordance with UV/vis spectroscopic analysis, suggested that such complexes, upon irradiation with UV light, act as photo-inducible CORMs. In the absence of light, the complexes do not readily decompose and generate CO in solutions. When the manganese complexes were studied for CO release and it was found that substitution pattern of the imidazolylphosphane ligand determine the number of CO molecules released. Compounds 1 and 2 with imidazol-2-ylphosphane ligands are better CO releasers than those with imidazol-4-ylphosphane attached (3-5) as studies revealed that the former released twice as many moles of carbon monoxide per mole of complex compared to the latter.[48] The rhenium complexes do not show any significant absorption above 320 nm and thus were not studied as photo CORMs.

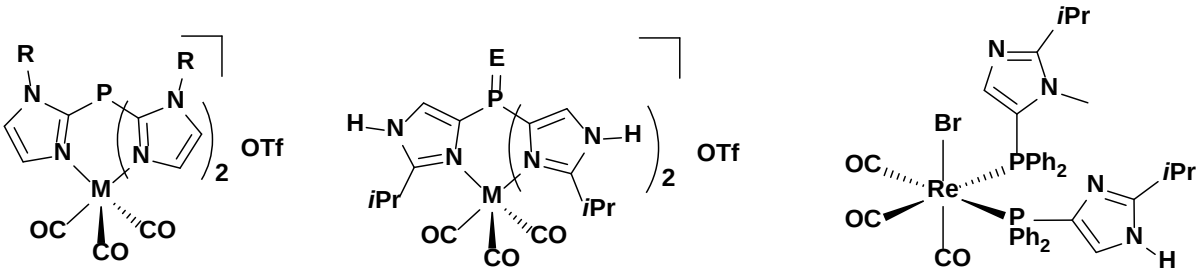

1	**M=Re**	**R=H**
2	**M=Mn**	**R=H**
3	**M=Re**	**R=CH_3**
4	**M=Mn**	**R=CH_3**

5	**M=Re**	**E=-**
6	**M=Mn**	**E=-**
7	**M=Re**	**E=O**
8	**M=Mn**	**E=O**
9	**M=Re**	**E=S**
10	**M=Mn**	**E=S**

11

Figure 1.12 *Tricarbonyl manganese(I) and rhenium(I) complexes of imidazol-based phosphane ligands as CORMs*

For highly selective transportation, certain photo-CORMs require the attachment of a targeting moiety. [42]A linked molecule can assist the delivery of CO in conjunction with "nanoCORMS" or "polyCORMs" which are nanometre in size. The main idea is to attach them to copolymers (polyCORMs or nanoCORMs). Therefore the compounds can be transported to the specific target sites and cause vasorelaxation and inhibit the inflammatory

response. [43] Thus, polymers containing metal carbonyls were also investigated for their ability to release CO using myoglobin assays. Photochemical CO releasing properties was assessed for the $[Mn(CO)_3tpm]^+$ {tpm = tris(pyrazolyl)methane}complex covalently linked to a silicon dioxide nanoparticle containing azido functional groups using myoglobin assays. During the analysis it was observed that the CORM functionalised nanoparticle released two moles of CO for every mole of the molecule following irradiation at 365 nm (see **Figure 1.13**). A controlled experiment was also undertaken which showed that the photo-CORM functionalised nanoparticles were stable in the absence of light.[43, 49]

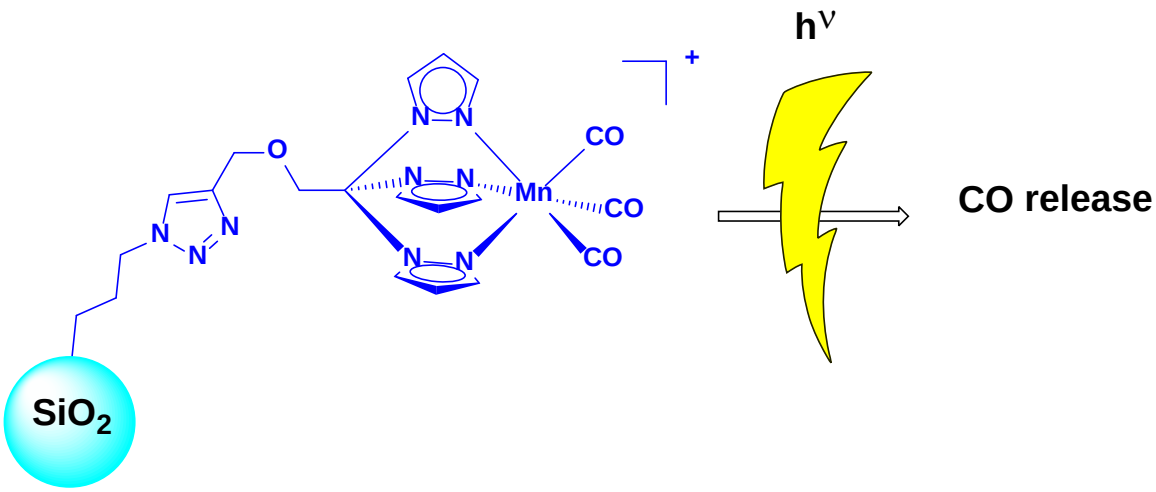

Figure 1.13 *Silicon dioxide nanoparticles containing azido groups, prepared by emulsion copolymerisation may be used as carriers for photo-CORMs.*[49]

The above developments on the area of photo CORMs demonstrate great prospects in the future for the pharmaceutical and physiological applications of such molecules.

1.2.5 Therapeutic applications of CORMs

Recently CO releasing transition metal carbonyls have gained significant attention due to their therapeutic applications. Based on the physiological behaviour of CO, efficient delivery of therapeutic amounts of CO through inhalation in a safe manner is rather challenging because the Hb of red blood cells constitutes a barrier that prevents CO from reaching the diseased tissue from the lungs. **Figure 1.14** illustrates graphically the alternative

administration of CO by intravenous injection or oral administration. The first two metal carbonyl complexes $[Mn_2(CO)_{10}]$ CORM-1 and $[\{Ru(CO)_3Cl_2\}_2]$ CORM-2 exhibited a decrease in blood pressure when administrated into the isolated heart of rats under *in vivo* conditions. This experimental study led to the development of different metal carbonyl compounds as a source of CO for various pharmacological effects. Now many experimental investigations have been carried out to synthesise different CORMs and assess their biological applications.

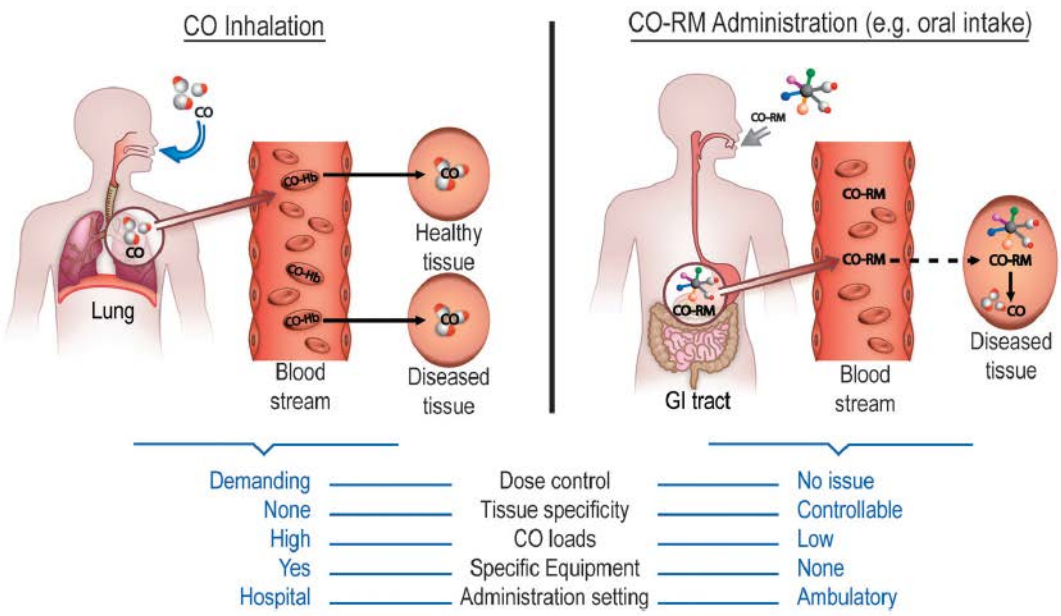

Figure 1.14 *Alternative pathways for the therapeutic delivery of CO to diseased tissues with their main advantages and disadvantages*

One of the early CORMs $[RuCl(gly)(CO)_3]$ CORM-3 and sodium boranocarbonate CORM-A1 which are soluble in water showed an enhanced renal function and protection against renal failure of the cells (see **Figure 1.15**).

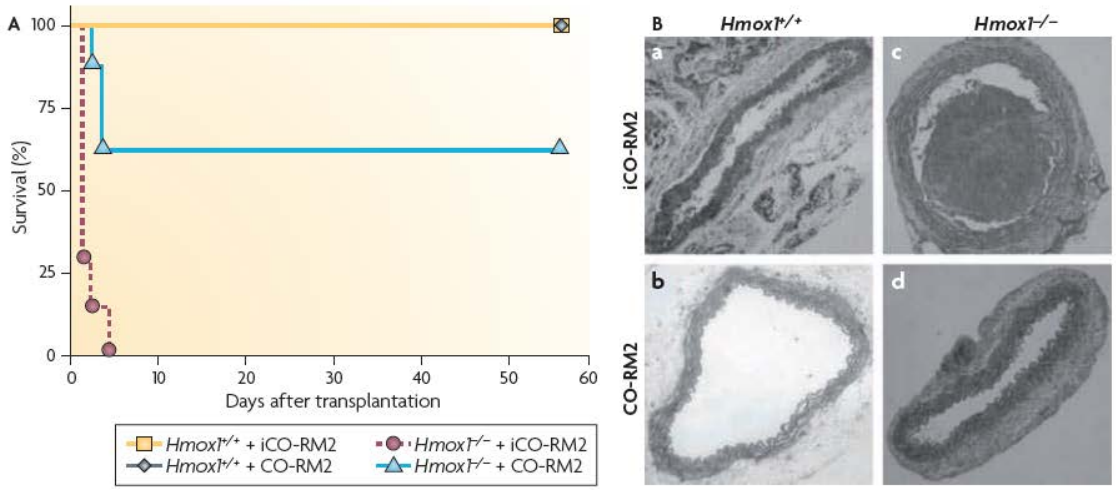

Figure 1.15 *describes the effect of CORM2 after aortic transplantation. A recent report showed that aortic transplantation in HO1-deficient mice results in 100% mortality within 4 days owing to severe arterial thrombosis.(Hmox cells are isolated aortic ring cells). Notably, treatment of HO1 deficient mice with CORM2 improved survival (62% survival at > 56 days).*[50]

In summary the many beneficial actions of CORMs include;

1) Cardio protection against ischemia and myocardial infarction[31, 51]
2) Prevention of cardiac graft rejection and positive inotropic effects on the heart[31, 51]
3) Suppression of the inflammatory response[25, 26]
4) Inhibition of platelet aggression[52]
5) Attenuation of endotoxin mediated vascular dysfunction[32]
6) Improved kidney function[53]
7) Protection against cisplatin-induced nephrotoxicity[53]

Furthermore, CORMs play an important role in the assessment of the contribution of CO to anti-inflammatory, anti-apoptotic, anti-proliferative and cytotoxic effects. Recently iron containing CORMs has shown prominent vasodilatory, cardio active and anti-inflammatory[54] effects in isolated aortic rings of RAW264.7 macrophages stimulated with endotoxin in a

dose dependent manner. Thus, growing scientific evidence supports that compounds capable of carrying and delivering CO can be administrated in the treatment of various medical ailments. In this regard, CORMs can be considered as effective pharmaceutical compounds whose chemical properties can be tuned for the delivery of CO safely in human cells.

1.3 Singlet Oxygen

Molecular oxygen has triplet multiplicity in its ground state, $^3\Sigma_g^-$. On excitation rearrangements of the electron spins within the degenerate orbitals occurs, resulting in two possible singlet states, $^1\Delta_g$ and $^1\Sigma_g^+$, above the triplet state. The only difference of these excited states is their electronic configuration in the π-antibonding orbitals (**see Figure 1.16**). The transition from the first excited state to the ground state $^1O_2$ ($^1\Delta_g$) → $^1O_2$ ($^3\Sigma_g^-$) is spin forbidden, thus the $^1\Delta_g$ O_2 is a relatively long lived species. Due to spin allowed transition, the decay of the second excited state, $^1O_2$ ($^1\Sigma_g^+$) → $^1O_2$ ($^1\Delta_g$) is short lived and occurs with almost unit efficiency. The meta-stability of $^1\Delta_g$ state, the $^1\Delta_g \leftrightarrow {}^3\Sigma_g^-$ transitions are observed in absorption and emission spectra is directly observed despite being spin and symmetry forbidden.

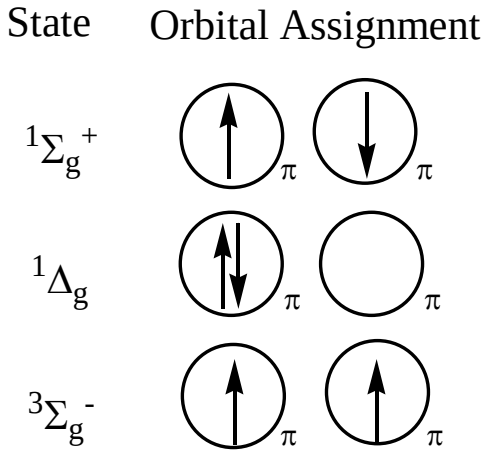

Figure 1.16 *Basic representations of molecular oxygen lowest triplet and singlet states*

Dioxygen in its singlet oxygen excited state can be deactivated by other species to return to its ground state in two ways:

1) Physical quenching where interaction leads to deactivation of the excited singlet state oxygen without oxygen consumption or product formation (see **Reaction 1**)
2) Chemical quenching where the "quencher" reacts with the singlet oxygen and new products are formed (see **Reaction 2**).

The singlet excited state oxygen is more oxidising than ground state oxygen and therefore is more electrophilic, reacting rapidly with unsaturated carbon carbon bonds as well as with anions. The chemistry of $^1O_2$ has been extensively studied due to its high reactivity with substrates. Typical reactions include oxidations of alkenes (ene-type reactions, [2+2] cycloadditions), 1,3-dienes ([4+2] cycloadditions), aromatic compounds and heterocycles.[55]

Reaction 1 $^1O_2 + A \rightarrow {}^3O_2 + A$

Reaction 2 $^1O_2 + Q \rightarrow P$

Where A = atoms or molecules that encounter singlet oxygen, Q = quencher and P = product

The main process for the formation of $^1O_2$ is by photosensitisation methods of generation, the requirements for which are oxygen, light of appropriate wavelength and a photosensitiser capable of absorbing and using that energy to excite oxygen to its singlet state. The sensitiser excitation is generally achieved *via* a one photon transition from the ground state (S_0), to a singlet state (S_n), followed by relaxation to the lowest excited singlet state (S_1), with subsequent intersystem crossing to generate the sensitiser triplet excited state (T_1). Due to the longer lifetime (in μs) of the triplet state compared to the lifetime (in ns) of the singlet state, it allows the triplet excited state of the photosensitiser to react with molecular oxygen. According to the nature of the quenching, the process occurs in two pathways; defined as Type I and Type II (see **Figure 1.17**).

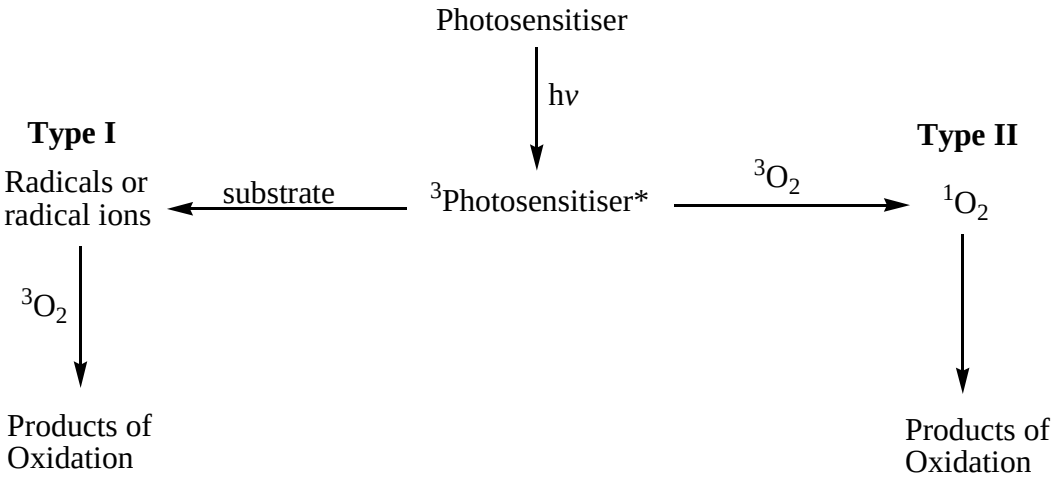

Figure 1.17 *Two pathways (Type I and Type II) of molecular oxygen sensitisation*

Type I involves hydrogen-atom abstraction or electron transfer between the excited sensitiser and a substrate, yielding free radicals. These radicals can react with oxygen to form an active oxygen species, i.e. superoxide radical anion (see **Figure. 1.18** and **Reaction 3**).

In type II singlet oxygen is generated via energy transfer during a collision from the excited sensitiser with the triplet oxygen (see **Figure 1.18** and **Reaction 4**).

Generally a photosensitiser can produce $10^3 - 10^5$ molecules of $^1O_2$ before being degraded through photobleaching by $^1O_2$. Photodegradation refers to the process in which singlet oxygen reacts with a substrate resulting in its degeneration, while photobleaching refers specifically to the degradation of the photosensitiser by singlet oxygen. The quantum yield of singlet oxygen formation, Φ_Δ, is dependent on the quantum yield of the triplet state of the sensitiser, Φ_T, though competing reactions must be considered (see **Figure 1.18** and **Reaction 5**). The competing reactions include monomolecular radiative and non-radiative processes (see **Figure 1.18**, **Reaction 6** and **7**) and bimolecular reactions such as physical deactivation by molecular oxygen or electron transfer (see **Figure 1.18**, **Reaction 8** and **9**). The excited state photosensitiser is quenched by molecular oxygen through electron transfer processes which yields the superoxide radical anion (Type I quenching).[55]

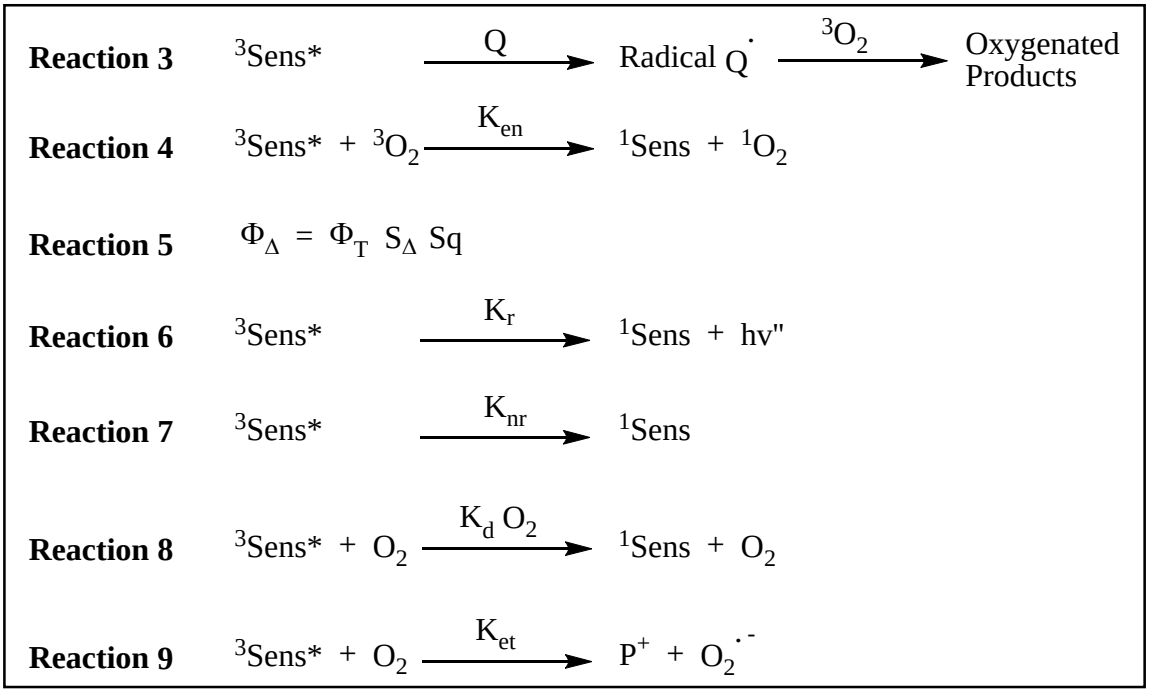

Figure 1.18 *Singlet oxygen production and processes affecting yield and efficiency, where Sens = sensitiser, Q = quencher, K_{en} = rate of energy transfer, S_Δ = fraction of triplet molecules quenched by oxygen and yielding singlet oxygen, S_q = fraction of oxygen dependant triplet deactivations, K_r = rate of radiative decay, K_{nr} = rate of nonradiative decay, K_dO_2 = rate of deactivation by O_2 and K_{et} = rate of electron transfer*

The following properties determine the efficiency of the photosensitisers for the generation of the singlet oxygen:

1. High extinction coefficients in the spectral region of excitation.

2. A triplet state with appropriate energy to allow efficient energy transfer to ground state oxygen.

3. High quantum yield of triplet excited state ($\Phi_T > 0.4$) and long lived triplet state lifetimes ($\tau_T > 1$ μs) .

4. High photostability of the singlet oxygen.

Generally, photosensitisers can be divided into three categories: organic dyes and aromatic hydrocarbons, porphyrins, pthalocyanines and transition metal complexes. The ability of the porphyrins and their derivatives to absorb several wavelengths in the UV-vis spectrum and their high quantum yield for long lived triplet excited state make them desirable candidates to act as photosensitiser for generation of singlet oxygen. The photophysical properties of porphyrins can be tuned by substitution around the macrocycle, coordination of metal ions at its centre and axial ligation of the central metal ion. Aggregation of the photosensitiser is not desirable as photodynamic efficiency decreases due to the decreased sensitising ability of dimers and higher aggregates. Aggregation can be overcome by bulky substituents on the periphery of the porphyrin macrocycle.

Singlet oxygen has found many applications in areas such as waste water treatment[56] and fine chemical synthesis[57] and in photodynamic processes. The photodynamic effect is the damage caused to living tissue by the combination of a photosensitiser, light and oxygen. Direct spectroscopic evidence of singlet oxygen in photodynamic therapy (PDT) is difficult to observe due to the rapid reaction of singlet oxygen with biomolecules. It is generally accepted the $^1O_2$ ($^1\Delta_g$) is the major participant.[58]

PDT is used for blood sterilisation, more specifically, for the decontamination of freshly frozen plasma units of the blood samples.[59] Methylene blue is non toxic to humans and is an effective photosensitiser in destroying extracellulary-enveloped viruses. Silicon-based phthalocyanines are also under investigation for sterilisation of blood components.[60]

PDT is a relatively new type of cancer treatment. In PDT, a photosensitiser, visible light and oxygen are combined to produce lethal agents which destroy or inactivate tumour cells. It is widely agreed that singlet oxygen is the primary cytotoxic agent responsible for the photobiological activity. PDT is highly selective due to the preferential accumulation of the photosensitiser in diseased tissue and the ability to confine activation of the photosensitiser by illumination of the tumour region only. This allows for tumour destruction without affecting normal healthy tissue. The majority of the photosensitisers investigated to date are of porphyrinoid structure.[61]

First generation photosensitisers included haematoporphyrin derivative (HpD) and analogues such as Photofrin and Photoheme, which were the first compounds to be authorised for clinical use.[62] These PDT agents were a mixture of about ten components. The major

component is haematoporphyrin diacetate (**2**). The solid is treated with aqueous base and then neutralised to form HpD at stage 2. This regenerates haematoporphyrin and produces 3-hydroxylethyl-8-vinyldeuteroporphyrin (**3a**) or 3-vinyl-8-hydroxylethyl-deuteroporphyrin (**3b**) and protoporphyrin (**4**). However these monomer compounds are not responsible for the photonecrotic behaviour of HpD at stage 2 (see **Figure 1.19**). Instead, a mixture of porphyrin dimers and oligomers consisting of ether, ester and carbon-carbon interporphyrin linkages serve as active components to localise within certain tissues. For example protofrin is a mixture of dimers and oligomers ranging from two to nine porphyrins units connected by mostly ether bonds. These first generation photosensitisers have been studied extensively and have been use in clinical work. However this type of photosensitisers is complex mixture and it has not been able to isolate a single active component which make is difficult to synthesise and difficult to reproduce its biological activity. Also, poor selectivity and long retention times meant a second generation of photosensitisers was required.

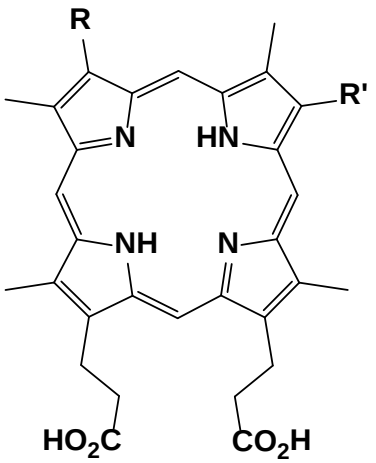

1 R=R'=CH(OH)Me
2 R=R'=CH(OAc)Me
3 a) R=CH(OH)Me; R'=CH=CH$_2$
b) R=CH=CH$_2$; R'=CH(OH)Me
4 R=R'=CH=CH$_2$

Figure 1.19 *Structure of haematoporphyrin diacetate (**2**), 3-hydroxylethyl-8-vinyldeuteroporphyrin (**3a**) or 3-vinyl-8-hydroxylethyl-deuteroporphyrin (**3b**) and protoporphyrin (**4**)*

This second generation of PDT sensitisers were structurally distinct compounds with long wavelength absorption. Absorption in the range of 675-800 nm is desired, because it would

allow for light penetration of up to 2-3 cm. A great deal of research has been focused on the discovery and testing of the second generation of PDT sensitisers.

Porphyrins: For example a series of asymmetric amide protoporphyrin derivatives were found to be efficient sensitizers of singlet oxygen with quantum yields of 0.01 – 0.64.[63] Tetrakismethoxyphenyl porphyrins have favourable photophysical properties such as high triplet quantum yield (0.63 – 0.84 depending on the number and position of the MeO groups) and can produce singlet oxygen quantum yield of 0.7.[64] Tetra and octa-glycogenated tetraphenyl chlorines and porphyrins have been synthesised and studied extensively by Mikata *et al*. All the derivatives were found to show comparable singlet oxygen producing ability, thus differences in photocytotoxicity reflected the extent of incorporation of the photosensitisers in the cell.[65] The octa-glycosated derivative showed little phototoxicity due to its excessive hydrophilicity. The tetra-glycosated porphyrin derivative was the most effective photosensitiser due to its membrane permeating ability. Halogenated chlorines such as TDFPC = 5, 10,15, 20-tetrakis(2,6-difluorophenyl)chlorin, ToCPC = 5,10,15,20 tetrakis(2-chlorophenyl)chlorine have been investigated as potential new PDT agents. The quantum yields of these complexes when excited at 655 or 660 nm are considerable: TDFPP = 0.88, ToCPC = 0.89.[66] A particular advantage of these chlorines is that their absorptivities are 10 times larger than those of related porphyrins.

Meso-tetraphenylporphryin and chlorine derivatives have been studied as potential photosensitisers for PDT. Study of photophysical properties of the amide linked dimers showed moderate absorption coefficients in the red portion of visible spectrum and high quantum yields of singlet oxygen formation ranging from 0.67 to 0.73.[67]

Phthalocyanines and Naphthalocyanines: complexes of phthalocyanine (Pc) and napthalocyanine (NPc) produce singlet oxygen with high quantum yields (Zn(II)Pc) = 0.56; (Zn(II)NPc) = 0.45 and show strong photobiological activity against tumors.[68] It is thought that tumour localisation and selectivity in phthalocyanines can be improved by adding polar groups such as carboxylic acids, hydroxyls to the hydrophobic macrocycle skeleton to improve its amphiphilicity.

Other macrocyclic systems: Texaphyrins have strong absorption in the 600 – 900 nm regions whose energy can be tuned via substitution and have high quantum yields. Lanthum and lutecium complexes with R = CH_2OH show photobiological activity *in vivo*.[69] In general second generation systems have improved photophysical properties and address some of the problems associated with the first generation dyes.

Third generation photosensitisers use second generation photosensitisers bound to carriers for a higher selective accumulation in the tumour.[55]

Photosensitisers of this generation have been developed for their selective delivery to the tumor tissue. This occurs through conjugation to biomolecules such as monoclonal antibodies (mAB). It is known that tumor cells have cell surface antigens that are different from those of normal cells. If the maB bound photosensitisers will bind specifically to the tumor tissue, this would allow selective photodamage without affecting normal tissue.[70] For example the properties of the avidin-biotin system have been used for the delivery of a photosensitiser onto specifically labelled tumor cells.[71] Metallated phthalocyanines have been covalently linked to adenovirus Type 2 capsid proteins, known to bind with great affinity and high selectivity to integrin receptors expressed by several types of cancer cells.[72]

In a similar manner the toxic effects of singlet oxygen can be used in photodynamic herbicides and insecticides to destroy unwanted plants or pests. Photodynamic herbicides cause the accumulation of chlorophyll and heme metabolic intermediates (tetrapyrroles) in green plants.[73] On irradiation these accumulated tetrapyrroles, act as photosensitisers for the production of singlet oxygen which kills the treated plants through oxidation of their tissues. δ-Aminolevulinic acid, (ALA), is the main component in these tetrapyrrole-dependant photodynamic herbicides (TDPH) as well as the main precursor of all tetrapyrroles in plant and animal cells. The insecticidal effects of photosensitisers have also been studied.[74, 75] For this purpose the organic dyes, such as xanthenes, were extensively examined. They can act as efficient photosensitisers and their lack of photostability can in fact be advantageous. Persistence of conventional insecticides in the environment is a serious issue but is eliminated by the facile decomposition of xanthene dyes. These compounds can be photosensitised by a range of wavelengths and have shown to be effective as insecticides.

1.4 Time resolved infrared spectroscopy

Time resolved optical spectroscopic technique has been great employed to probe the structure and properties of excited states of transition metal complexes especially those containing CO or CN ligands. Time resolved techniques are now widely used in photochemical and photophysical studies. The importance of complexes containing CO or CN ligands comes from the high oscillation strengths of the CO or CN stretching vibrations and their π-backbonding relation with the transition metal. Backbonding makes the stretching frequencies and band widths of υ(CO) and υ(CN) infrared bands senstitive to changes in electronic and molecular structure. Following metal based excitation, transient changes occur in these bands on the femtosecond to microsecond timescale. They are often characteristic and can be correlated to changes in electronic structure within the complex. Laser flash photolysis is used to generate intermediates in solutions while ultra-fast IR spectroscopy monitors the photophysical and photochemical processes over time. Infrared CO stretching vibrations with distinct absorbance frequencies allow transient species in metal carbonyl organometallic complexes to be examined.

Time resolved infrared spectroscopy; a combination of UV flash photolysis with fast IR detection is a very important tool for exploring transient species and electronic structure in transition metal complexes containing CO or CN moieties which can act as probes of electron distribution in the excited state.[76, 77] TRIR involves a pump and probe configuration where a laser pulse excites a sample and IR spectroscopy operating in a very fast time range probes the generation of transient excited state species.[78]

The υ(CO) vibrations have high oscillator strengths and their energies are sensitive to changes in electronic structure at the metal. The magnitude of shifts in the υ(CO) band energies between the ground and excited state depends on the electronic origin of the excited state. For example the υ(CO) modes of [(bpy)Re$(CO)_3$Cl] detected from the TRIR spectrum of the complex were assigned to ^{3}MLCT based excited state. In this excited state υ(CO) increases 50 to 100 cm^{-1} compared to that in ground state.[79]This shift of υ(CO) to higher wavenumbers is evidence for a change in electron density on the metal centre which in this example is due to electron transfer from rhenium to bpy ligand and further consequent reduction in back bonding of CO groups.[80] Under appropriate conditions, highly proactive

excited states of the molecules are determined from the collection of TRIR data points following a single laser shot experiment.[81]

TRIR measurements on ultrafast pico and femtosecond timescale are obtained using the pump-probe approach. Two methods are generally used to obtain an ultrafast IR probe, either upconversion of a cw IR signal with a fast visible pulse, or the generation of short IR pulses by difference frequency mixing of two laser pulses.[82]

1.4.1 MLCT excited sates

A major focus of time resolved infrared studies continues to be the identification of the excited states. Excited state of complexes containing CO and CN^- ligands were among the first to be characterised by TRIR because of high υ(CO) and υ(CN) oscillator strengths and ease of measurement in the 1850-2200 cm^{-1} region. Excited state shifts occur in υ(CO) and υ(CN) bands in response to electronic redistribution and its influence of dπ-π* (CO) backbonding.

Figure 1.20 demonstrates a frontier energy level diagram and a metal to ligand excited state transition in a *fac*-$[Re(pp)(CO)_3L]^{n+}$ complex (pp is a polypyridine ligand such as bpy or phen; L is py, CH_3CN etc (n = 1) or Cl^-, H^- etc. (n = 0). Absorption is dominated by direct excitation to a MLCT state, largely singlet in character which relaxes rapidly to lowest-lying, largely triplet states ^{3}MLCT. As a result of population of this ^{3}MLCT excited state, partial oxidation at the metal reduces available electron density for dπ(Re)-π*(CO) back bonding. This increases multiple bond character in CO causing a positive Δυ(CO) shift in excited state of the molecule. [83]

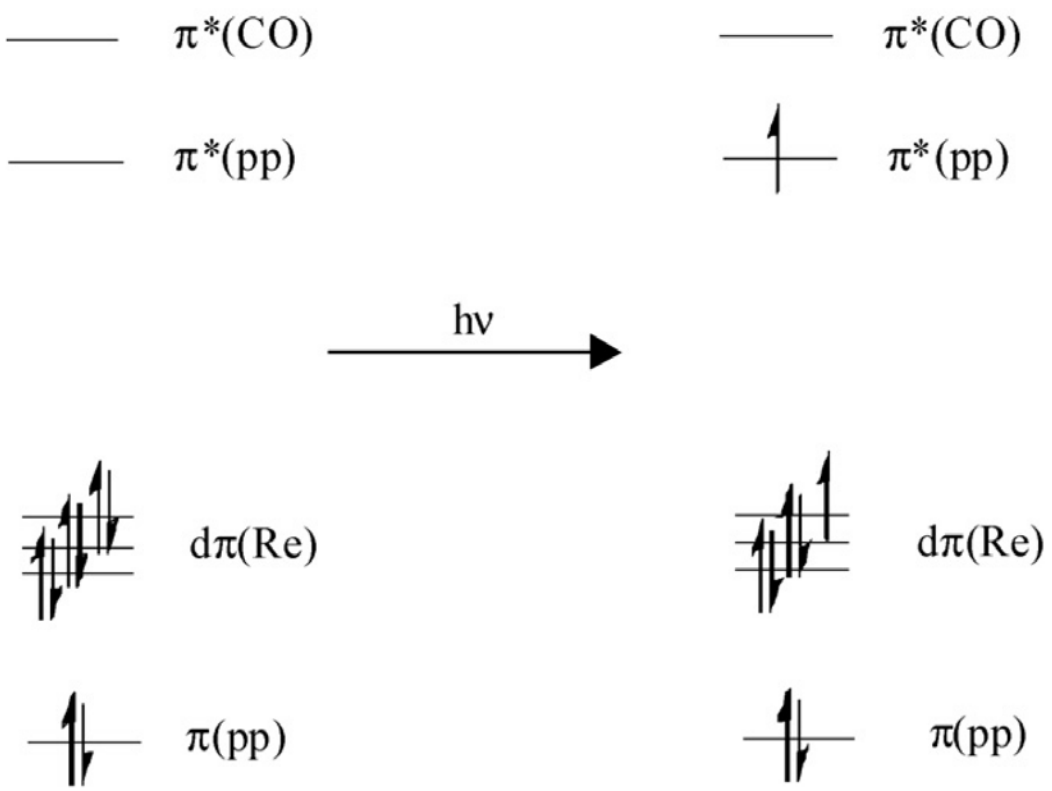

Figure 1.20 *Frontier energy level diagram for $[Re(pp)(CO)_3L]^{n+}$ complex illustrating MLCT excitation to the lowest, largely triplet based MLCT excited state.*

The first application of TRIR to the excited states of transition metal complexes were first reported in 1975 for the complex $[Re(CO)_3Cl(4,4'\text{-bpy})_2]$ (4,4'-bpy = 4,4'-bipyridine).[79] The TRIR spectrum of the complex showed the shifting of two low frequency ground state υ(CO) bands to higher wavenumbers (55-65 cm^{-1}). Initially this shift to higher wavenumbers was assigned to the excited state of the molecule as the Re(I) metal centre is formally oxidised to Re(II). However, full interpretation and significance of the shifts was analysed by the energy factored force field (EFFF) theory.[84] With this approach it was shown that the complex $[Re(CO)_3Cl(4,4'\text{-bpy})_2]$ has higher EFFF force constants (k_{CO}) in its ^{3}MLCT excited state than its ground state. The relationship between k_{CO} and crystallographic bond length (r) is established using equation (1).[85]

$r_{CO} = 1.6196 - 0.1736\ln(k_{CO})$ (1)

This equation provided valuable information in monitoring changes in bond length on excitation. Hence, for the complex $[Re(CO)_3Cl(4,4'\text{-bpy})_2]$ it was concluded that the three C-O bonds were shorten in the excited state, thus the υ(CO) stretching frequencies of the transient species shifts to higher wavenumbers.

Generally, a complex interplay between MLCT and ligand based excited states is known to exist in CO containing polypyridyl complexes of Re(I).[86-88] For example the early time resolved infrared spectroscopic studies on $[Re(phen)(CO)_3(4\text{-Mepy})]^+$ (4Mepy is 4-Methylpyridine) showed formation of a MLCT excited state when excited the molecule was at 355 nm.[89] In the TRIR spectrum it was observed that the broad ground state υ(CO) band at 1931 and 2036 cm^{-1} were observed as a bleach with bands appearing at 1965, 2015 and 2065 cm^{-1}. This increase in υ(CO) is attributed to the partial oxidation of Re(I) to Re(II) and formation of Re(II)($phen^{\cdot-}$) based excited state. The broad band in the ground state consists of two overlapping υ(CO) bands which are resolved in the excited state. Reduction of phen to $phen^-$ decreases the electronic symmetry of the complex which was initially present in the ground state with three facial pyridyl-type ligands (4-Mepy and the two pyridyl rings of phen ligand). Hence, the energies of the υ(CO) bands increase due to a decrease in Re-CO back bonding. This increases the triple bond character of the CO ligands.

Schoonover, Meyer and co-workers have shown a significant difference in the transient infrared difference spectrum of $[Re(CO)_3(PPh_3)(dppz)]^+$ (dppz = dipyrido[3,2-a:2',3'-c]phenazine) complex where the υ(CO) bands shifted to lower frequency upon promotion to the excited state. The υ(CO) bands in the excited state are slightly broadened and decreased in energy by 5 cm^{-1} which is reverse of the general trend being observed for the excited state of the rhenium tricarbonyl complexes.[90] There is no evidence for bands at higher wavenumber characteristic of a MLCT excited state. The relative small shifts in the frequencies of CO bands in dppz complexes are consistent with a ligand localised excited state which is slightly electron donating at the rhenium metal centre relative to ground state of dppz ligand. This low lying excited state is assigned as dppz based ππ* excited state. Similar observations were obtained for $[Re(CO)_3(4\text{-Etpy})(dppz)]^+$complex. Negative υ(CO) shifts in these type of complexes relate to ligand based triplet excited states which is a poorer

π-acceptor than the ground state, resulting in more electron density from Re in the excited state compared to ground state and hence resulting in lowering of υ(CO) stretching frequencies with an increase in π back bonding with the Re carbonyls. **Table 1.1** shows time resolved ground and excited state stretching vibrations for a series of rhenium based tricarbonyl complexes reported in literature (see **Figure 1.21**).

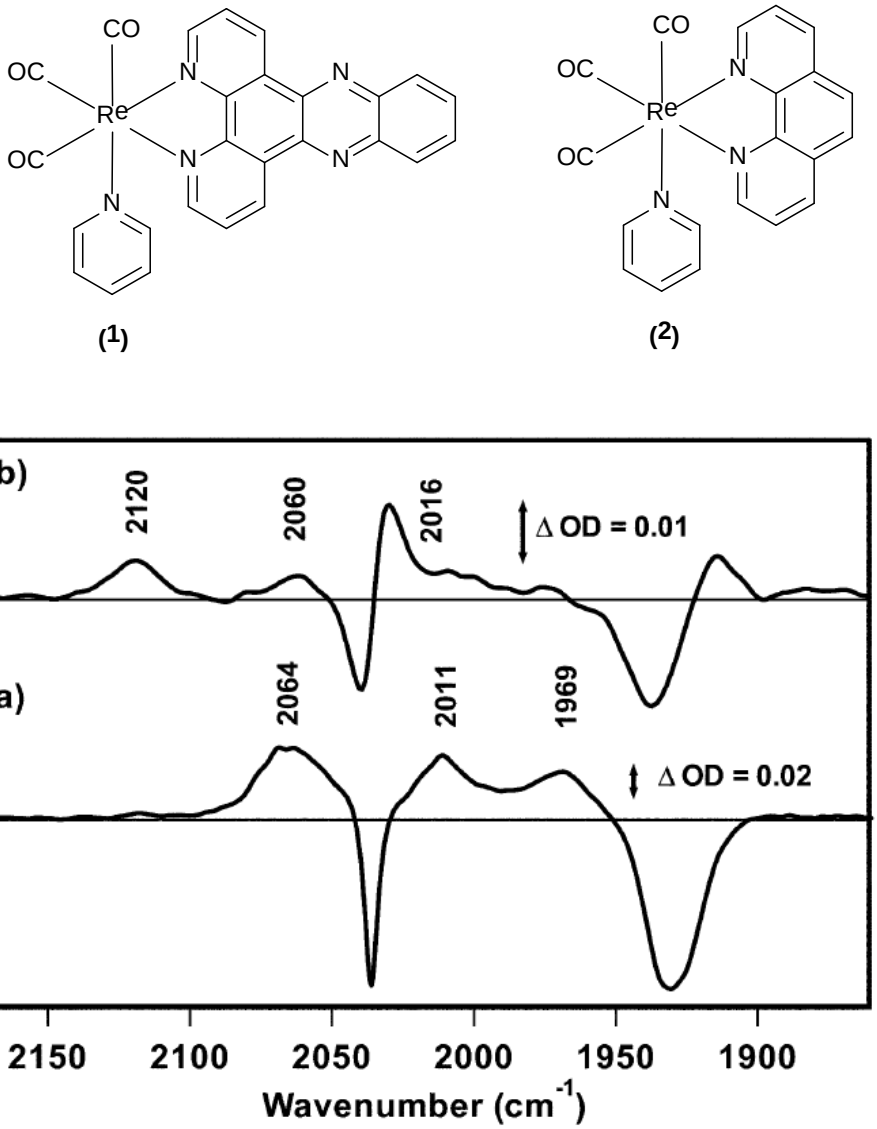

Figure 1.21 *(a) TRIR spectrum of fac-[Re(CO)$_3$(phen)(py)] (**2**) in CH$_3$CN obtained 1.5 μs after 355 nm excitation. (b) TRIR spectrum of fac- [Re(CO)$_3$(dppz)(py)] (**1**) in CH$_3$CN obtained 850 ns after 355 nm excitation*

Table 1.1 *Frequencies of υ(CO) stretching bands (in cm^{-1}) of some of the Re tricarbonyl complexes reported in literature*

Complex	**λ_{ex} (nm)**	**υ(CO) Bands (cm^{-1})**		**Excited State**
		Ground Sate	**Excited State**	
$[Re(CO)_3Cl(4,4'\text{-}bpy)_2]$[91]	308[a]	1957 1936 2027	1957 1992 2055	^{3}MLCT
$[Re(CO)_3Cl(bpy)]$[80]	355[b]	1899 1921 2024	1957 1987 2064	^{3}MLCT
$[Re(CO)_3(4\text{-}Et\text{-}py)(bpy)]^+$[92]	355[b]	1931 2036	1988 2015 2075	^{3}MLCT
$[Re(CO)_3Cl(phen)]$[80]	355[b]	1900 1917 2023	1960 1993 2062	^{3}MLCT
$[Re(CO)_3(Etpy)(dmb)]^+$[93]	400[b]	1930 2013	1970 1913 2068	^{3}MLCT
$[Re(CO)_3Cl(Me_2BPTZ)]$[94]	500[b]	1921 1953 2034	1978 2002 2071	^{3}MLCT
$[Re(CO)_3(4\text{-}Et\text{-}py)(4,4'\text{-}(NH)_2\text{-}bpy)]^+$ [89]	355[b]	1914 2025	1881 1919 2002 2064	π-π*

[a] CH_2Cl_2, [b] CH_3CN

Recently Glusac and co-workers reported the electronic distribution in $[Re(CO)_3Cl(Me_2BPTZ)]$ (Me_2BPTZ = 3, 6-bis(5-methyl-2-pyridine)-1,2,4,5-tetrazine] using ultrafast femtosecond time resolved infrared spectroscopy.[94] Upon excitation at 500 nm, bleaching of the parent υ(CO) bands at 2034, 1953 and 1921 cm^{-1} occur together with the formation of new bands at 2071, 2002 and 1978 cm^{-1}. Within 5 ps, these absorption bands become narrower and shift to higher frequencies. These spectral changes have been attributed to vibrational cooling from the higher vibrational levels of ^{3}MLCT. It was also concluded from further DFT calculations that the excited electron is localised on the central tetrazine ring of Me_2BPTZ and does not involve the pyridine moieties (see **Figure 1.22**).

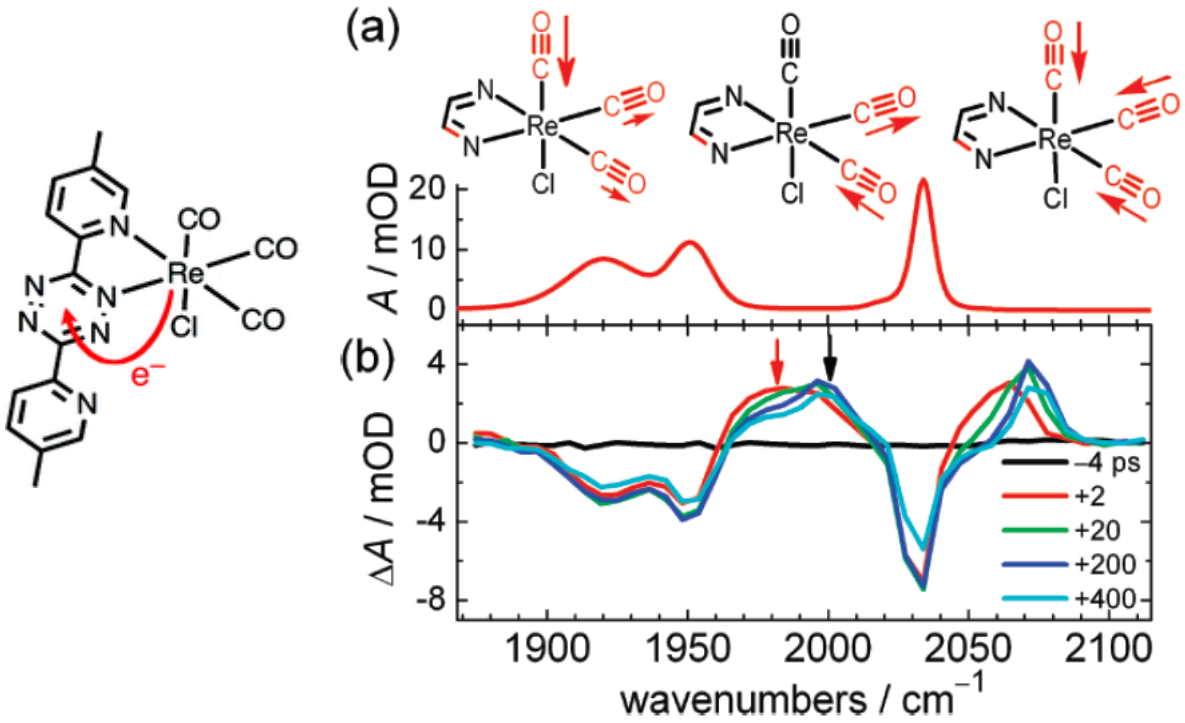

Figure 1.22 *(a) FTIR and (b) TRIR spectra of $Re(CO)_3Cl(Me_2BPTZ)$ (5 mM, $CHCl_3$). For the TRIR measurements, the sample was excited by a 500 nm pump pulse. (c) Decay of the TRIR signal of $Re(CO)_3Cl(Me_2BPTZ)$ at (black) 2002 and (red) 1978 cm^{-1} for (top) shorter and (bottom) longer time scales, showing differences that stem from vibrational cooling*

The shift of υ(CO) to higher frequency for ^{3}MLCT excited states of transition metal carbonyl complexes can also help in elucidating the complex reaction mechanisms. For example the photochemistry of $[Cr(CO)_4(bpy)]$ is very interesting due to dissociation of CO when irradiated into either the LF or MLCT absorption band.[95] Irradiation into the MLCT absorption band resulted in photochemical bond cleavage of the $[W(CO)_5L]$ (L = 4-CN-pyridine or 4-actylpyridine) complex which has been monitored by TRIR. During the time resolved infrared studies the ^{3}MLCT excited state was characterised and its decay to form $[W(CO)_5(solvent)]$ via equilibrium between the MLCT and LF excited states was followed.[96]

Vichova and co-workers found that irradiation into the MLCT absorption band of $[Cr(CO)_4(bpy)]$ produced a short lived (50 ps) intermediate which was assigned to a ^{1}MLCT state; irradiation into the LF transition produced an additional longer lived component (> 10 ns) transient species which was assigned to a ^{3}MLCT excited state.[97] It was demonstrated via the positions of υ(CO) bands of the intermediate that this ^{3}MLCT excited state is actually a solvated intermediate , $[Cr(CO)_3$-(solvent)(bpy)].[98]

Transient infrared measurements have also been used to reveal the co-existence of excited states in the ligand bridged complex $[(4\text{-Etpy})(CO)_3Re^I(\mu\text{-bbpe})Re^I(CO)_3(4\text{-Etpy})]^{2+}$ (see **Figure 1.23**). Following Re to bbpe excitation at 355 nm, characteristic υ(CO) bands are observed for both π-π* and MLCT excited states.[99]

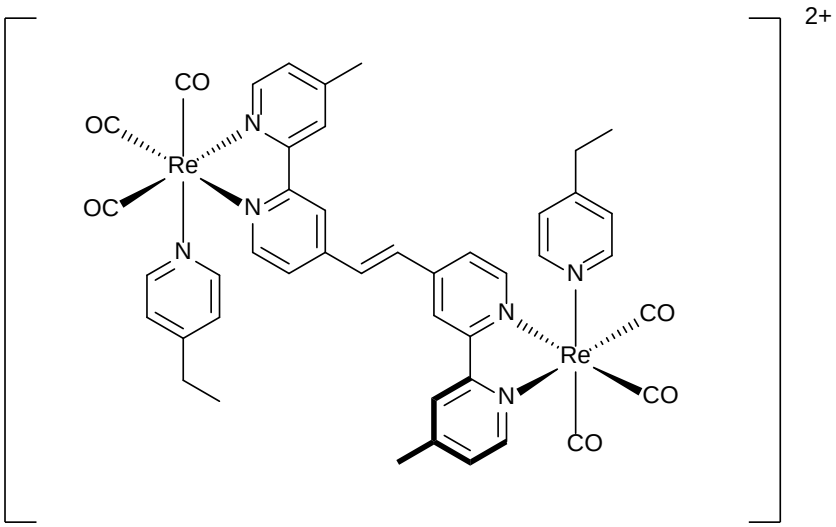

Figure 1.23 *Structure of $[(4\text{-Etpy})(CO)_3Re^I(\mu\text{-bbpe})Re^I(CO)_3(4\text{-Etpy})]^{2+}$*

1.4.2 Electron and energy transfer

Time resolved vibrational spectroscopy has also been used to probe inorganic systems that can undergo electron or energy transfer processes in solution. For example excitation into the rhenium to MLCT band of $[(phen)(CO)_3Re^{I}(CN)Ru^{III}(bpy)_2(CN)]^+$ showed formation of the Re-MLCT followed by energy transfer to the ruthenium-based MLCT excited state.[100] Ultrafast transient infrared measurements on the picosecond timescale provided direct evidence for the initial Re(II) to (phen) based MLCT excited state within 1 ps when excited at 300 nm. Bleaching of the ground state at 1930 and 2030 cm^{-1} is observed with positive shifts in the higher υ(CO). These features decay within 5 ps. The transient spectrum after 5 ps was very similar to the spectrum observed in nanosecond timescale study where the terminal υ(CN) shifted from 2081 to 2108 cm^{-1} , the bridge υ(CN) from 2100 to 2132 cm^{-1} and the υ(CO) from 1930 and 2030 to 1935 and 2035 cm^{-1}. These observations led to the conclusion that the most plausible explanation for the difference in appearance and disappearance kinetics is an intermediate state. A reasonable mechanism given was energy transfer, first from Ru(II) to Re(II), $[(phen^{\cdot-})(CO)_3Re^{II}(CN)Ru^{II}(bpy)_2(CN)]^{+*}$ to $[(phen^{\cdot-})(CO)_3Re^{I}(CN)Ru^{III}(bpy)_2(CN)]^{+*}$ followed by $phen^{\cdot-}$ to bpy, $[(phen^{\cdot-})(CO)_3Re^{I}(CN)Ru^{III}(bpy)_2(CN)]^{+*}$ to $[(phen)(CO)_3Re^{I}(CN)Ru^{III}(bpy^{\cdot-})(bpy)(CN)]^{+*}$.

Another example of electron and energy transfer has been explained using $[(CO)_5W(BL)W(CO)_5]$ (BL is pyrazine or 4,4-bipyridine) complex. From the TRIR experiments it has been demonstrated there are two W environments, i.e. $[(CO)_5W^{+}(4,4'\text{-}bpy)^{-}]$, where the υ(CO) bands of the excited state have shifted to higher frequencies (1970, 2010, 2105 cm^{-1}) and $(4,4'\text{-bpy})W(CO)_5$ where υ(CO) bands of the excited state have shifted to lower frequencies (1875, 1915, 2059 cm^{-1}). Hence, from the time resolved IR spectra it has been confirmed that the lowest excited state of $[(CO)_5W(BL)W(CO)_5]$ involved W to BL ligand charge transfer (see **Figure 1.24**).[101, 102]

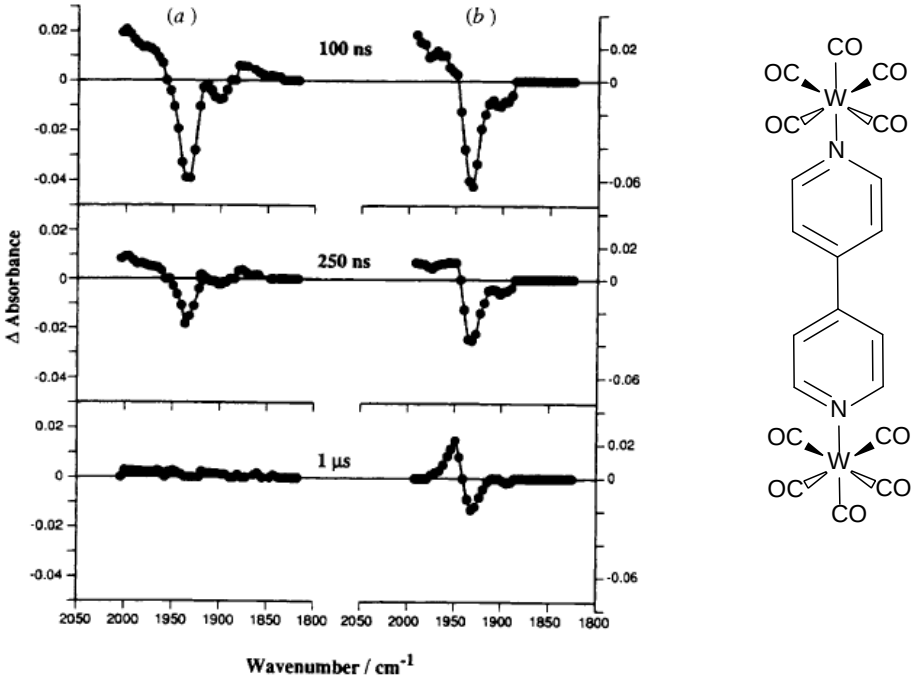

Figure 1.24 *(a) TRIR spectra recorded at 100 ns, 250 ns and 1 µs after flash (460 nm,~10 mJ) of [(OC)$_5$W(4,4'-bipy)W(CO)$_5$] in DCM solution (~ 5 × 10^{-4} mol dm^{-3}, path length 1 mm); (b) TRIR spectra recorded at 100 ns, 250 ns and 1 µs after flash (420 nm,~10 mJ) of [(OC)$_5$W(4,4'-bipy)] in DCM solution (~5 × 10^{-4}mol dm^{-3}, path length 1 mm)*[101]

1.4.3 Detection of efficiency of CO releasing molecules

Recently the potential of tricarbonyl manganese(I) tricarbonyl complexes when bound to ligands such as tris(N-methylimidazol-2-yl)carbinol, tris(pyridine-2-yl)phosphane (tpp), tris(pyrazol-2-yl)methane (tpm) were studied to act as photoactivatable CO releasing molecules using UV/Vis spectroscopy based myoglobin assays as well as time-resolved IR spectroscopy.[103]

Time resolved IR spectroscopy was used to observe the CO release of the compounds such as [Mn(CO)$_3$(tpm)](OTf)] upon irradiation in methanol. The IR spectra taken after 6 minutes showed the decrease in parent bands of Mn(CO)$_3$ moiety and formation of new band in the region of 1840 to 1860 cm^{-1}. This was assumed to be due to formation of dicarbonyl complex following substitution of the π acceptor CO molecule with the σ donor methanol molecule

which resulted in strengthening of the remaining Mn-CO bonds. The appearance of only one new band is explained due to obscurance by the E band of the tricarbonyl species. Dicarbonyl complexes are also photolabile and a low intensity of the band at 1840-1860 cm^{-1} was observed for the formation of this transient species. The time resolved IR spectra of the complexes studied were further compared to the related $[CpMn(CO)_2(thf)]$ complex reported earlier and found to have similar CO stretching frequencies at 1930 and 1861 cm^{-1} (see **Figure 1.25**).[104]

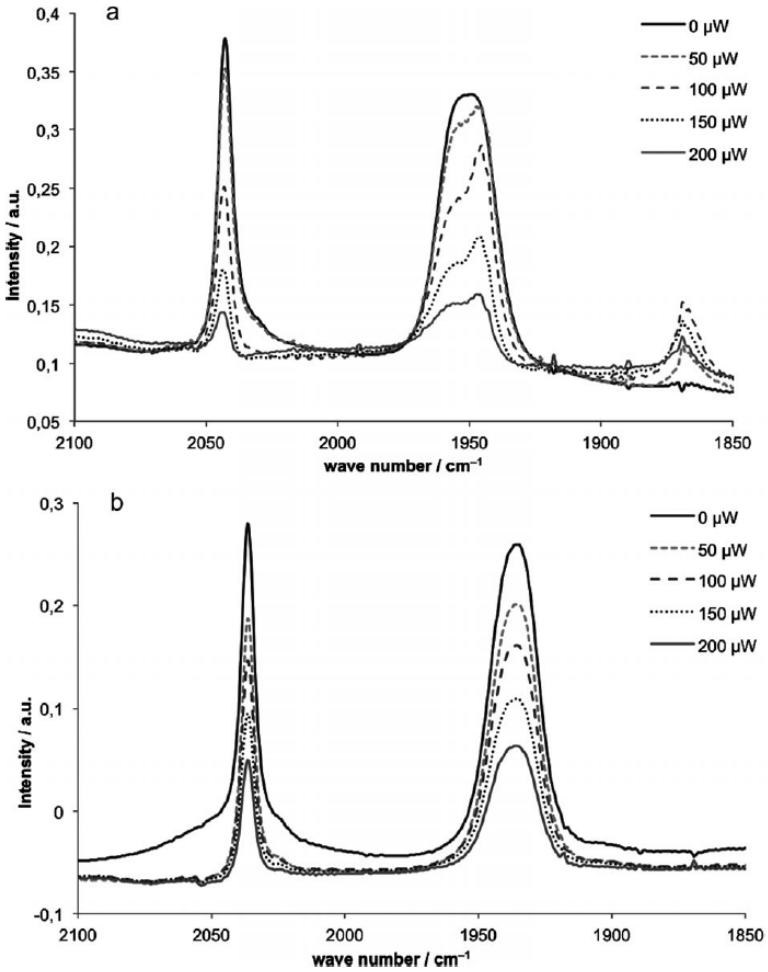

Figure 1.25 *Carbonyl region of solutions of a) $[Mn(CO)_3(2\text{-}tip^{NMe})]$-OTf and b) $[Mn(CO)_3(tpp)]$OTf in methanol (1 wt.-%) after irradiation for 3 min at 360 nm using intensities of 50, 100, 150 and 200 µW.*

TRIR has been shown to be a powerful technique for the elucidation of inorganic excited states and the use of this technique will increase because the major activity of supramolecular photochemistry is in following electron and energy transfer. Recent improvements in step scan FTIR will allow this technique to be used by a much wider community. The detection of vibrations of υ(CO) or υ(CN) in principle allow a more comprehensive structural description of charge transfer excited states.

1.5 Aim of the thesis

The aim of Chapter 2 is to develop novel dipyrrin-based rhenium tetracarbonyl and tricarbonyl complexes, and to study their photochemistry. Emission and picosecond time resolved IR studies are carried out to understand the structure and properties of excited states of the rhenium tetra and tricarbonyl complexes. Picosecond TRIR studies is a direct technique to probe the formation of *intra*-ligand charge transfer excited states for these complexes. This chapter also aims to study the CO releasing ability of these carbonyl complexes using myoglobin assays under both photochemical and thermal (37 ^{o}C) conditions.

The main objective of Chapter 3 is to synthesise and characterise the novel polypyridyl-based rhenium(I) and manganese(I) mononuclear tricarbonyl complexes using NMR, UV and IR spectroscopy and also to study their excited state photochemistry using picosecond TRIR studies. A ruthenium based photosensitiser attached to rhenium tricarbonyl moiety would be very interesting to study the properties of the excited states of the complex and compare with the mononuclear rhenium complex using pico-second TRIR studies. This chapter also aim was to investigate the CO releasing properties of the above mentioned mono- and di-nuclear tricarbonyl complexes. The photochemical CO releasing properties of the manganese based tricarbonyl complexes are anticipated to be efficient using myoglobin assays upon irradiation at visible light, therefore it is worth studying. This chapter also aims to study the electrochemical properties of these metal complexes.

The aim of Chapter 4 is to synthesise and characterise a range of group VI metal carbonyls attached to porphyrins and metallo-porphyrins using NMR, UV and IR spectroscopic tools. These molecules are interesting to study in terms of generating singlet oxygen. The study can

be carried out using different wavelength and different solvent systems. With an aim to develop efficient photosensitisers for singlet oxygen studies, a comparison of the singlet-oxygen quantum yields for these complexes would be highly interesting. Molecules possessing high singlet oxygen quantum yield is highly demanding for photo dynamic therapy against tumour cells. This chapter also see these carbonyl complexes as potential CO releaser therefore also aims to study their CO releasing property under both thermal and photochemical conditions.

Chapter 5 aims to synthesise molybdenum, chromium and tungsten metal based tri and tetracarbonyl complexes tethered to 2,2'-dipyridyl and various arene based ligands. Similar to previous chapters, this chapter also targets to investigate their CO releasing properties of the complexes using UV spectroscopy by converting deoxymyoglobin to carbomonoxyglobin under both photochemical and thermal conditions.

1.6 References

1. J. E. V. L. H.Ali, *Chem.Rev.*, 1999, 2379.

2. M. I. Shazia Rafique, Anwar Nasim, Haji Akbar and Amin Athar, *Biotech. Mol. Biol. Rev.*, 2010, **5**, 38-45.

3. C. N. Lok, T. Zou, J. J. Zhang, I. W.S. Lin and C. M. Che, *Adv. Mater.*, 2014, **26**, 5550-5557.

4. V. Sharma and D. Piwnica-Worms, *Chem. Rev.*, 1999, **99**, 2545-2560.

5. A. R. Battersby, C. J. Fookes, G. W. Matcham and E. McDonald, *Nature*, 1980, **285**, 17-21.

6. A. Jasat and D. Dolphin, *Chem. Rev.*, 1997, **97**, 2267-2340.

7. J. L. Sessler and D. Seidel, *Angew. Chem. Int. Ed.*, 2003, **42**, 5134-5175.

8. J. L. Sessler and R. A. Miller, *Biochem. Pharmacol.*, 2000, **59**, 733-739.

9. S. W. Young, F. Qing, A. Harriman, J. L. Sessler, W. C. Dow, T. D. Mody, G. W. Hemmi, Y. Hao and R. A. Miller, *Proc Natl Acad Sci U S A. 1996, **93**, 6610-5.*

10. H. Rath, J. Sankar, V. Prabhuraja, T. K. Chandrashekar, A. Nag and D. Goswami, *J Am Chem Soc. 2005, **127**, 11608-9.*

11. W. A. Reiter, A. Gerges, S. Lee, T. Deffo, T. Clifford, A. Danby and K. Bowman James, *Coord. Chem. Rev.*, 1998, **174**, 343-359.

12. D. Gorman, A. Drewry, Y. L. Huang and C. Sames, *Toxicology.* , 2003, **187**, 25-38.

13. R. A. Johnson, F. Kozma and E. Colombari, *Braz. J. Med. Biol. Res.*, 1999, **32**, 1-14.

14. M. D. Maines, *Annu. Rev. Pharmacool. Toxicol.*, 1997, **37**, 517-554.

15. B. E. Mann and R. Motterlini, *Chem. Commun.*, 2007, 4197-4208.

16. L. E. Otterbein, M. P. Soares, K. Yamashita and F. H. Bach, *Trends Immunol.*, 2003, **24**, 449-455.

17. A. Yachie, Y. Niida, T. Wada, N. Igarashi, H. Kaneda, T. Toma, K. Ohta, Y. Kasahara and S. Koizumi, *J Clin Invest.* , 1999, **103**, 129-135.

18. R. Foresti, M. Bani-Hani and R. Motterlini, *Intensive Care Med*, 2008, **34**, 649-658.

19. Y. Liu, P. Moenne Loccoz, T. M. Loehr and P. R. O. de Montellano, *J. Biol. Chem.*, 1997, **272**, 6909-6917.

20. P. R. Ortiz de Montellano, *Curr. Opin. Chem. Biol.*, 2000, **4**, 221-227.

21. R. Alberto and R. Motterlini, *Dalton Trans.*, 2007, 1651-1660.

22. A. Nakao, J. S. Neto, S. Kanno, D. B. Stolz, K. Kimizuka, F. Liu, F. H. Bach, T. R. Billiar, A. M. K. Choi, L. E. Otterbein and N. Murase, *Am. J. Transplantation*, 2005, **5**, 282-291.

23. J. S. Neto, A. Nakao, K. Kimizuka, A. J. Romanosky, D. B. Stolz, T. Uchiyama, M. A. Nalesnik, L. E. Otterbein and N. Murase, *Am J Physiol Renal Physiol.* , 2004, **287**, F979-F989.

24. B. A. Moore, L. E. Otterbein, A. Tarler, A. M. K. Choi and A. J. Bauer, *Gastroenterology*, 2003, **124**, 377-391.

25. P. Sawle, R. Foresti, B. E. Mann, T. R. Johnson, C. J. Green and R. Motterlini, *Br. J. Pharmacol.*, 2005, **145**, 800-810.

26. M. G. Bani Hani, D. Greenstein, B. E. Mann, C. J. Green and R. Motterlini, *J Pharmacol Exp Ther.* , 2006, **318**, 1315-1322.

27. R. Fournier, *J. Chem. Phys.*, 1993, **99**, 1801-1815.

28. A. B. Burg and H. I. Schlesinger, *J. Am. Chem. Soc.*, 1937, **59**, 780-787.

29. L. J. Malone and M. R. Manley, *Inorg. Chem.*, 1967, **6**, 2260-2262.

30. R. Motterlini, J. E. Clark, R. Foresti, P. Sarathchandra, B. E. Mann and C. J. Green, *Circul. Res.*, 2002, **90**, e17-e24.

31. J. E. Clark, P. Naughton, S. Shurey, C. J. Green, T. R. Johnson, B. E. Mann, R. Foresti and R. Motterlini, *Circul. Res.*, 2003, **93**, e2-e8.

32. R. Foresti, J. Hammad, J. E. Clark, T. R. Johnson, B. E. Mann, A. Friebe, C. J. Green and R. Motterlini, *Br J Pharmacol.* , 2004, **142**, 453-460.

33. F. Zobi, O. Blacque, R. A. Jacobs, M. C. Schaub and A. Y. Bogdanova, *Dalton Trans.*, 2011, **41**, 370-378.

34. H. Pfeiffer, A. Rojas, J. Niesel and U. Schatzschneider, *Dalton Trans.*, 2009, 4292-4298.

35. P. Sawle, J. Hammad, I. J. S. Fairlamb, B. Moulton, C. T. O'Brien, J. M. Lynam, A. K. Duhme Klair, R. Foresti and R. Motterlini, *J. Pharmacol. Exp. Ther.*, 2006, **318**, 403-410.

36. I. J. S. Fairlamb, J. M. Lynam, B. E. Moulton, I. E. Taylor, A. K. Duhme Klair, P. Sawle and R. Motterlini, *Dalton Trans.*, 2007, 3603-3605.

37. D. E. Bikiel, E. A. GonzaÌ e, M. Solveyra, F. Di S
Eberlin, R. S. CorreÌ, A. J. Ellena, D. A. Estrin and F. Doctorovich, *Inorg. Chem.*, 2011, **50**, 2334-2345.

38. W. Q. Zhang, A. C. Whitwood, I. J. S. Fairlamb and J. M. Lynam, *Inorg. Chem.*, 2010, **49**, 8941-8952.

39. A. J. Atkin, S. Williams, P. Sawle, R. Motterlini, J. M. Lynam and I. J. S. Fairlamb, *Dalton Trans.*, 2009, 3653-3656.

40. I. Ott, B. Kircher, R. Dembinski and R. Gust, *Expert Opin. Ther. Patents*, 2008, **18**, 327-337.

41. C. C. Romao, W. A. Blattler, J. D. Seixas and G. J. L. Bernardes, *Chem. Soc. Rev.*, 2012, **41**, 3571-3583.

42. U. Schatzschneider, *Inorg. Chim. Acta*, 2011, **374**, 19-23.

43. N. E. Brückmann, M. Wahl, G. J. Reiß, M. Kohns, W. Wätjen and P. C. Kunz, *Eur. J. Inorg. Chem.*, 2011, **29**, 4571-4577.

44. R. D. Rimmer, H. Richter and P. C. Ford, *Inorg. Chem.*, 2009, **49**, 1180-1185.

45. R. Kretschmer, G. Gessner, H. Gorls, S. H. Heinemann and M. Westerhausen, *J. Inorg. Biochem.*, 2011, **105**, 6-9.

46. R. Kretschmer, G. Gessner, H. Gorls, S. H. Heinemann and M. Westerhausen, *J Inorg Biochem.* , 2010, **105**, 6-9.

47. W. Q. Zhang, A. J. Atkin, I. J. S. Fairlamb, A. C. Whitwood and J. M. Lynam, *Organometallics*, 2011, **30**, 4643-4654.

48. P. C. Kunz, W. Huber, A. Rojas, U. Schatzschneider and B. Spingler, *Eur. J. Inorg. Chem.*, 2009, **2009**, 5358-5366.

49. G. DoÌrdelmann, H. Pfeiffer, A. Birkner and U. Schatzschneider, *Inorg. Chem.*, 2011, **50**, 4362-4367.

50. B. Chen, L. Guo, C. Fan, S. Bolisetty, R. Joseph, M. M. Wright, A. Agarwal and J. F. George, *Am. J. Pathol.*, 2009, **175**, 422-429.

51. A. B. Stein, Y. Guo, W. Tan, W. J. Wu, X. Zhu, Q. Li, C. Luo, B. Dawn, T. R. Johnson, R. Motterlini and R. Bolli, *J . Mol. Cell. Cardiol.*, 2005, **38**, 127-134.

52. S. Chlopicki, R. Olszanecki, E. Marcinkiewicz, M. Lomnicka and R. Motterlini, *Cardiovasc. Res.*, 2006, **71**, 393-401.

53. B. J. F. A.Sandouka, B.E.Mann,C.J.Green,R.Foresti and R.Motterini, *Kidney Int.*, 2006, **69**, 239-247.

54. Y. Caumartin, J. Stephen, J. P. Deng, D. Lian, Z. Lan, W. Liu, B. Garcia, A. M. Jevnikar, H. Wang, G. Cepinskas and P. P. Luke, *Kidney Int.* , 2011, **79**, 1080-1089.

55. M. C. DeRosa and R. J. Crutchley, *Coord. Chem. Rev.*, 2002, **234**, 351-371.

56. P. Esser, B. Pohlmann, H.D. Scharf, *Angew. Chem.*, 1994, **106**, 2093.

57. B. Heller, P. Wagler, O. Orther, K.H. Funkn, G. Oehme, *Chem. Ing. Technol.*, 1996, **68**, 823.

58. K. Lang, J. Mosinger and D. M. Wagnerova, *Coord. Chem. Rev.*, 2004, **248**, 321-350.

59. W.M. Sharman, C. M. Allen, J. E. van Lier, *Drug Discov. Today*, 1999, **4**, 507.

60. N. L. Oleinick, A. R. Antunez, M. E. Clay, B. D. Rihter and M. E. Kenney, *Photochem. Photobiol.*, 1993, **57**, 242-247.

61. P. G. Calzavara-Pinton, M. Venturini and R. Sala, *J. Eur. Ac. Dermatol. Venereol.*, 2007, **21**, 439-451.

62. R. Bonnett, *Chem. Soc. Rev.*, 1995, **24**, 19-33.

63. A.K. Haylett, F. I. McNair, D. McGarvey, J. V. Moore, *Cancer Letters*, 1997, **112**, 233.

64. Z. Katona, A. Grofusik, P. Baranyai, I. Bitter, G. Grabner, M. Kubinyi, T. Vidoczy, *J. Mol. Struct.*, 1998, **450**, 41.

65. Y. Mikata, M.Shibata, T. Kakuchi, H. Ono, S.Ogura,I. Okura, S. Yano, *Bioorg. Med. Chem. Lett.*, 1998, **8**, 3543.

66. M. Pineiro, M. Pereira, A. R. Gonsalves, L. G. Arnaut, S. J. Formosinho, *J. Photochem. Photobiol.*, 2000, **72**, 217.

67. M. A. Faustino, M. Neves, J. Cavalerio, M. Neumann, H. D. Brauer, G. Jori, *J. Photochem. Photobiol.A:Chem.*, 2001, **138**, 147.

68. R. W. Redmond and J. N. Gamlin, *Photochem, Photobiol.*, 1999, **70**, 391.

69. J. L. Sessler, G. Hemmi, T. D. Mody, T. Murai, A. Burrell and S. W. Young, *Acc. Chem. Res.*, 1994, **27**, 43-50.

70. A. Barnias, P. Keane, T. Krausz, G. Williams, A. A. Epenetos, *Cancer Res.*, 1991, **51**, 724.

71. D. Wohrle, T. Bogdahn Rai, G. Schnurpfeil, M. Shova, *Russ. Chem. Bull*, 1998, **47**, 807.

72. C.M. Allen, W. M. Sharman, C. La Madeleine, J. M. Weber, R. Langois, R. Ouellet, J.E. Vanlier, *J. Photochem. Photobiol.*, 1999, **70**, 512.

73. C. A. Rebeiz, K. N. Reddy, U. B. Nandihalli and J. Velu, *Photochem. Photobiol.*, 1990, **52**, 1099-1117.

74. T. Ben Amor and G. Jori, *Insect Biochem. Mol. Biol.*, 2000, **30**, 915-925.

75. C. A. Rebeiz, L. J. Gut, K. Lee, J. A. Juvik, C. C. Rebeiz, C. E. Bouton and G. H. N. Towers, *Crit. Rev. Plant Sci.*, 1995, **14**, 329-366.

76. M. W. George, M. Poliakoff and J. J. Turner, *Analyst*, 1994, **119**, 551-560.

77. J. J. Turner, M. W. George, F. P. A. Johnson and J. R. Westwell, *Coord. Chem. Rev.*, 1993, **125**, 101-114.

78. Karen McFarlane, Brian Lee, Jon Bridgewater, Peter Ford, 1998, **554**, 49.

79. P. Glyn, M. W. Geroge, P. M. Hodges and J. J. Turner, *J. Chem. Soc., Chem. Commun.*, 1989, 1655-1657.

80. M. W. George, F. P. A. Johnson, J. R. Westwell, P. M. Hodges and J. J. Turner, *J. Chem. Soc., Dalton Trans.*, 1993, 2977-2979.

81. B. D. Rossenaar, M. W. George, F. P. A. Johnson, D. J. Stufkens, J. J. Turner and A. Vlcek, *J. Am. Chem. Soc.*, 1995, **117**, 11582-11583.

82. P. C. Ford, J. S. Bridgewater and B. Lee, *Photochem. Photobiol.*, 1997, **65**, 57-64.

83. J. M. Butler, M. W. George, J. R. Schoonover, D. M. Dattelbaum and T. J. Meyer, *Coord. Chem. Rev.*, 2007, **251**, 492-514.

84. P. S. Braterman, *Academic Press London*, 1975.

85. S. L. Morrison and J. J. Turner, *J. Mol. Str.*, 1994, **317**, 39-47.

86. J. R. Shaw and R. H. Schmehl, *J. Am. Chem. Soc.*, 1991, **113**, 389-394.

87. R. M. Leasure, L. Sacksteder, D. Nesselrodt, G. A. Reitz, J. N. Demas and B. A. DeGraff, *Inorg. Chem.*, 1991, **30**, 3722-3728.

88. A. Juris, S. Campagna, I. Bidd, J. M. Lehn and R. Ziessel, *Inorg. Chem.*, 1988, **27**, 4007-4011.

89. J. R. Schoonover, G. F. Strouse, R. B. Dyer, W. D. Bates, P. Chen and T. J. Meyer, *Inorg. Chem.*, 1996, **35**, 273-274.

90. J. R. Schoonover, K. C. Gordon, R. Argazzi, W. H. Woodruff, C. A. Bignozzi, R. B. Dyer, T. J. Meyer and K. A. Peterson, *J. Am. Chem. Soc.*, 1993, **115**, 10996-10997.

91. D. R. Gamelin, M. W. George, P. Glyn, F.-W. Grevels, F. P. A. Johnson, W. Klotzbuecher, S. L. Morrison, G. Russell, K. Schaffner and J. J. Turner, *Inorg. Chem.*, 1994, **33**, 3246-3250.

92. J. Dyer, W. J. Blau, C. G. Coates, C. M. Creely, J. D. Gavey, M. W. George, D. C. Grills, S. Hudson, J. M. Kelly, P. Matousek, J. J. McGarvey, J. McMaster, A. W. Parker, M. Towrie and J. A. Weinstein, *Photochem. Photobiol. Sci.*, 2003, **2**, 542-554.

93. D. J. Liard, M. Busby, P. Matousek, M. Towrie and A. n. Vlcek, *J. Phys. Chem. A*, 2004, **108**, 2363-2369.

94. G. Li, K. Parimal, S. Vyas, C. M. Hadad, A. H. Flood and K. D. Glusac, *J. Am. Chem. Soc.*, 2009, **131**, 11656-11657.

95. K. A. Rawlins and A. J. Lees, *Inorg. Chem.*, 1989, **28**, 2154-2160.

96. P. Glyn, F. P. A. Johnson, M. W. George, A. J. Lees and J. J. Turner, *Inorg. Chem.*, 1991, **30**, 3543-3546.

97. J. Vichova, F. Hartl and A. Vlcek, *J. Am. Chem. Soc.*, 1992, **114**, 10903-10910.

98. I. G. Virrels, M. W. George, J. J. Turner, J. Peters and A. Vlcek, *Organometallics*, 1996, **15**, 4089-4092.

99. G. F. Strouse, J. R. Schoonover, R. Duesing and T. J. Meyer, *Inorg. Chem.*, 1995, **34**, 2725-2734.

100. J. R. Schoonover, C. A. Bignozzi and T. J. Meyer, *Coord. Chem. Rev.*, 1997, **165**, 239-266.

101. M. W. George, J. J. Turner and J. R. Westwell, *J. Chem. Soc., Dalton Trans.*, 1994, 2217-2219.

102. M. W. George, F. P. A. Johnson, J. J. Turner and J. R. Westwell, *J. Chem. Soc., Dalton Trans.*, 1995, 2711-2718.

103. W. Huber, R. Linder, J. Niesel, U. Schatzschneider, B. Spingler and P. C. Kunz, *Eur. J. Inorg. Chem.*, 2012, **2012**, 3140-3146.

104. M. Melcher, *Ph.D. Thesis, University of Kaiserslautern*, 2000.

Chapter 2

Dipyrrins and their Re metal carbonyl complexes

This chapter deals with a brief introduction to dipyrrin based Re metal carbonyl complexes, photochemistry and their uses. This is followed by discussion on the various forms of spectroscopy employed, NMR, UV, IR, emission and picosecond time resolved IR, to study the properties of the dipyrrins and their Re metal carbonyls. Further the compounds were assessed for their ability to act as CO releasing molecules thermally using myoglobin assays.

2.1 Literature Survey

Over the last two decades borondifluoridedipyrrin (BODIPY) derivatives have emerged as an interesting class of dyes with excellent stability, thus finding various applications in sensing, light harvesting and photodynamic therapy.[1-3] This class of compounds are based on dipyrrinato derivatives.[4, 5] To date many dipyrrin based metal complexes have been explored for their catalytic activity [6-8] and metallic architectures.[9-11] But surprisingly very few dipyrrin molecules have been investigated for their luminescent properties. Several synthetic strategies have recently been developed for the preparation of stable dipyrrinato based metal complexes. In order to enhance the emission quantum yield of the dipyrrin complexes they have been functionalised either at the 5 positions or at 1 and 9 position providing steric hinderance and pseudo-macrocyclic character to the resulting ligands. Different synthetic approaches have been followed to introduce groups at the 1, 5 and 9 positions of the dipyrrin ligand to modify dipyrrin as well as different metal complexes (see **Figure 2.1**).

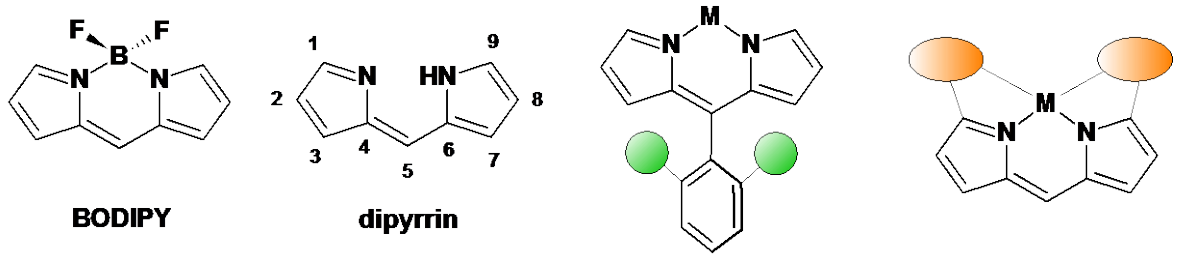

Figure 2.1: *BODIPY dyes, a dipyrrin ligand with the corresponding numbering of the atoms is represented along with the proposal of introduction of groups at position 5 or adding coordinating units at position 1 and 9 to limit the rotational freedom of peripheral aryl moiety.*

In these complexes the attachment of an aryl group at the 5 position of the dipyrrin ligand has a strong effect on the excited state dynamics and luminescent properties of BODIPY molecules.[12] The facile rotation of this group in metal dipyrrin complexes which favours

non-radiative deactivation pathway from the S_1 excited state can be hindered using different functionalisation of the moiety.

Zn(II) dipyrrin metal complexes probably complexes such as those displayed in **Figure 2.2** have been widely studied. Attachment of the mesityl group at the 5 position of the dipyrrin metal complexes resulted in a reduction in the stokes shift, as a result of less conformational freedom leading to an increase in the fluorescence quantum yield when compared to the phenyl based dipyrrin Zn(II) complex.[13]

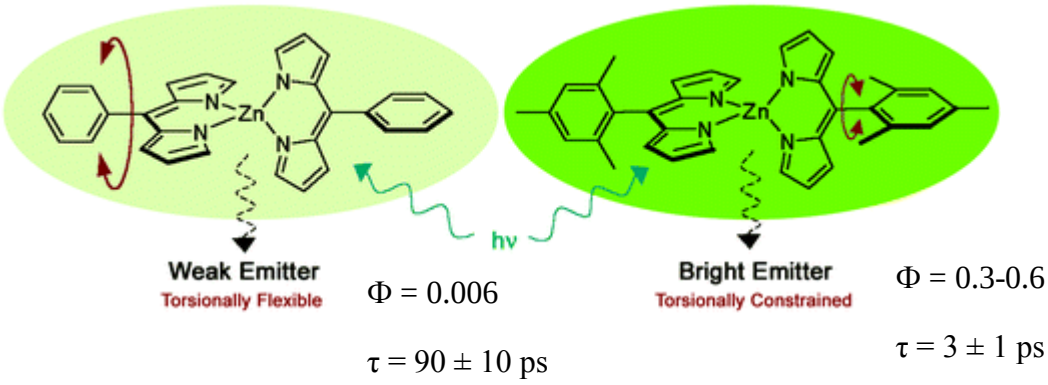

Figure 2.2: *Examples of luminescent Zn dipyrrin complexes (Φ represents the fluorescence quantum yield and τ represents the singlet lifetime values).*

Similar behaviour was reported for 1- and 2-naphthyl appended Zn complexes.[14] It was observed that 1-naphthyl attached Zn dipyrrin complexes showed photoluminescent intensity three times higher than 2-naphthyl appended Zn based dipyrrin complexes in THF solution and ten times greater for films on glass. Further Zn dipyrrin ligands incorporating diazo groups in the position 1 and 9 were found to be weakly luminescent (**Figure 2.3**).[15]

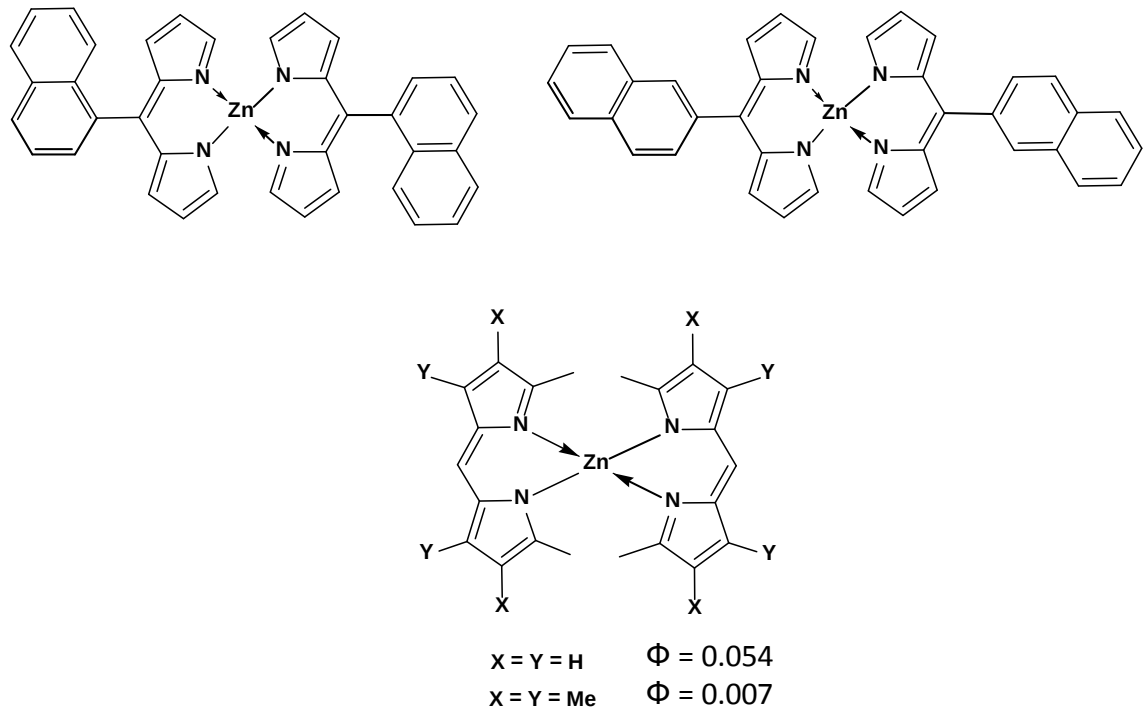

Figure 2.3: *Naphthyl and diazo groups appended Zn dipyrrin complexes; Φ = Fluorescence Quantum Yield*

Although the introduction of bulky groups to the peripheral aryl groups at the 5 position within the Zn dipyrrin or dipyromethene (dpm) complexes results in an increase in fluorescence quantum yield but could not be compared with near unity quantum yields of BODIPY molecules. Comparatively low luminescent properties for these type of complexes were explained due to the thermal transition to non emissive charge separated states of the $(dpm)^{\cdot+}$ - $Zn(dpm)^{\cdot-}$ or $(dpm)^{\cdot-}$ $Zn(dpm)^{\cdot+}$, type from the emissive singlet π-π* (dpm)*Zn(dpm) or (dpm)Zn(dpm)* excited state.[16] However the above mentioned explanation is only favoured for homoleptic complexes. For heteroleptic complexes such as $Zn(azadpm)_2$ complexes, quenching of fluorescence properties occurs as a result of exciton coupling between the transition dipole moments of the dpm and azadpm ligands which remains lower than that for homoleptic $Zn(dpm)_2$ complex (**Figure 2.3**).[17-19]

$M(dpm)_3$ complexes (M = Ga(III), In(III) have been reported by Cohen *et al.* The In(III) derivative was found to be more emissive than Ga(III) which may be due to formation of the triplet excited state (**Figure 2.4**). [20] Fluorescence quantum yields calculated for the In(III) analogue was 0.074 compared to its Ga(III) analogue where the quantum yield was found to be 0.024. No luminescence was observed for benzonitrile appended dpm based Ga dipyrrin complex.

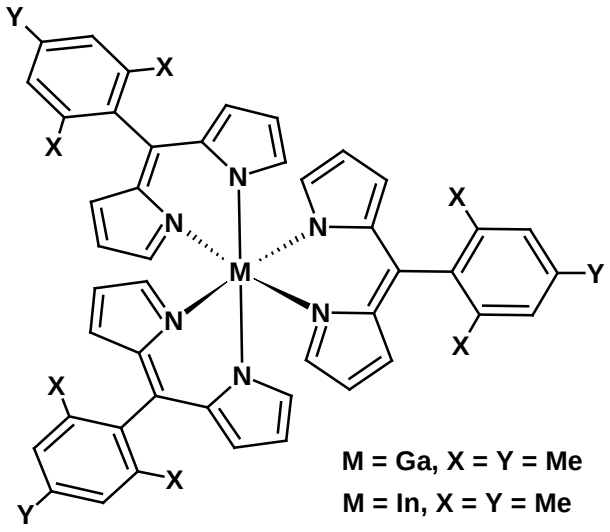

Figure 2.4: *Homoleptic heavy metal dipyrrin complexes; Φ = Fluorescence quantum yield and τ = Singlet lifetime values*

Owing to their optical and electronic properties, metal dpm complexes are highly considered for the preparation of dye-sensitised solar cells. For example, metal dipyrrin complexes having peripheral benzoic acid groups were designed by Telfer and co-workers in order to attach the dyes to TiO_2 for the preparation of dye sensitised solar cells (**Figure 2.5)** .[21] Both complexes were found to be weakly emissive.

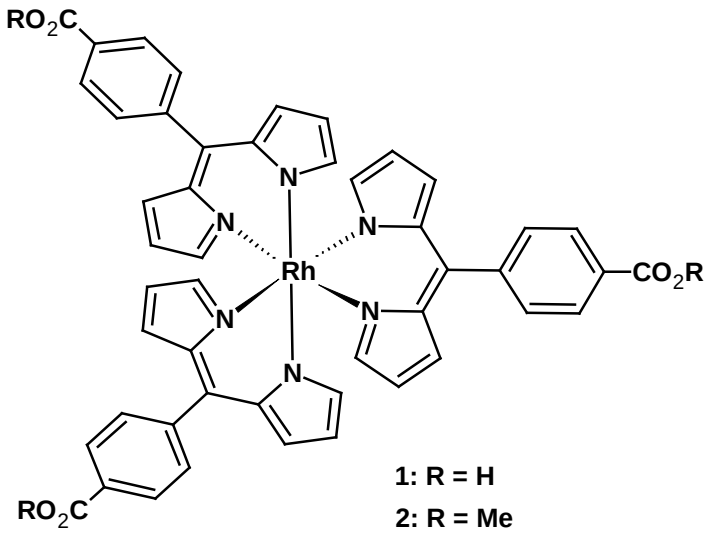

Figure 2.5: *Example of Rhodium based dipyrrin complexes containing benzoic acid groups*

Two Sn(dpm)X complexes having a dpm group with a peripheral mesityl group have been reported by Kawashima *et al.*[22] Both complexes are found to be emissive in benzene solution. Interestingly, the triflate derivative of the complex was found to be more emissive than its chloride derivative. Further, the fluorescent quantum yield for the triflate analogue was found to be ten times higher than the chloride analogue. This was explained via the difference in the location of the lone pair orbital (n) of the Sn(II) cation in the HOMO of the complex. In the case of the chloride incorporated Sn(II)dpm complex n-π* transition is close to the π-π* transition, thus quenching the emission of the complex. Whereas, in the case of the triflate based complex the n-π* transition is much lower in energy than π-π* transitions (**Figure 2.6**).

Cheng and co-workers have reported a series of (dpm)Cu(Phosphine)$_n$ (n = 1 or 2) complexes with various functionalisation of the dipyrrin ligands and with different phosphine groups. Some of the examples have been presented in **Figure 2.6**. The emission from the singlet state in these compounds is based on intraligand charge transfer (dipyrrin based transitions). In these type of complexes, the absence or presence of bromine at 2 and 8 positions of bis-pyrrolic group determines the photophysical properties. The presence of

the bromine group strongly enhances luminescence properties of the complex.[23] Interestingly, in the case of the complex incorporating only one phosphine ligand and a dpm with phenyl units in positions 1, 5 and 9 a red shift was observed in both absorption and emission spectra, while a blue shift was observed for the azadpm derivative.

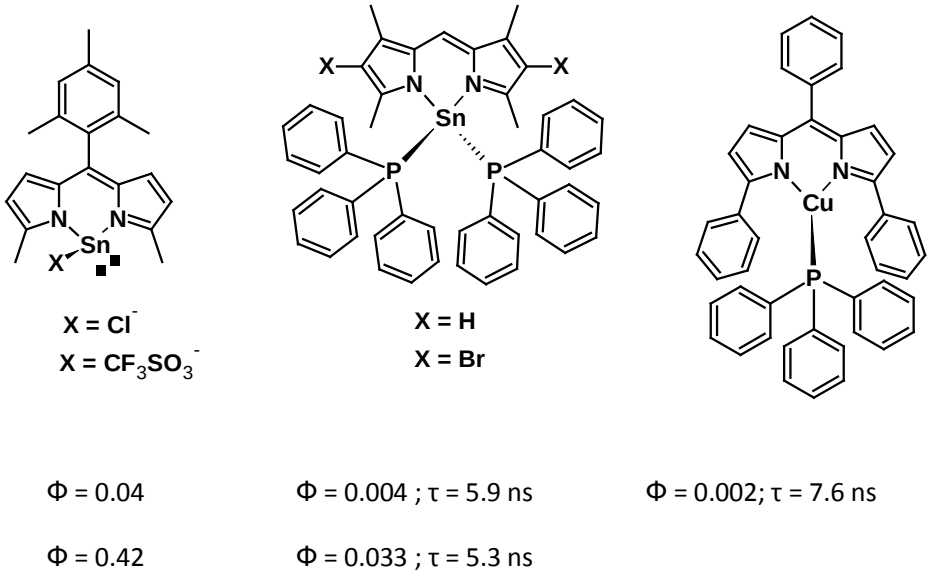

Figure 2.6: *Heteroleptic Sn(II) and Cu(I) complexes. Φ = Fluorescence quantum yield; τ = Singlet lifetime values.*

Another very important class of compounds reported by Telfar *et al.* is based on dipyrromethene and phosphine ligands consisting of dipyrrin based $Re(CO)_3(PR_3)$ coordinated dipyrrin complexes. Stokes shifts for these complexes were observed to be very large when compared to other dpm based complexes which may suggest phosphorescence from a dipyrrin centered based triplet excited state. This is consistent with the heavy atom effect in Re(I) complexes. When the two complexes displayed in **Figure 2.7** are compared, the luminescence quantum yield increases upon introduction of a peripheral mesityl group. When CO is replaced by a triphenylphosphine ligand, no emission was observed.[24]

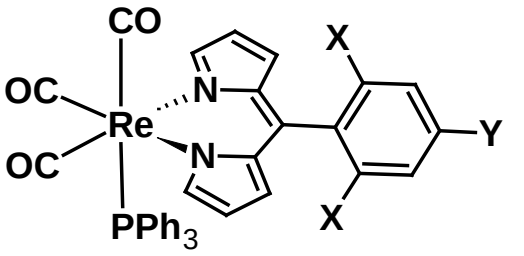

X = Y = H Φ = 0.0026

X = Y = Me Φ = 0.0099

Figure 2.7: *Examples of $Re(CO)_3(PR_3)$ type dipyrrin complexes. Φ = fluorescence quantum yield*

In an attempt to enhance the luminescence properties of dipyrrin complexes, the backbone of the dipyrrin ligand was further rigidified, with the introduction of groups at the 1 and/or 9 positions of pyrrolic moiety.

For example Thompson and co-workers reported a series of Sn(IV) alkyl and phenyl derivatives of dipyrrin complexes and an investigation of photo physical properties of these complexes revealed strong emissive properties due to the rigidification of the dipyrrin ligand with the attachment of functional groups at both the 1 and 9 positions (see **Figure 2.8**).[25]

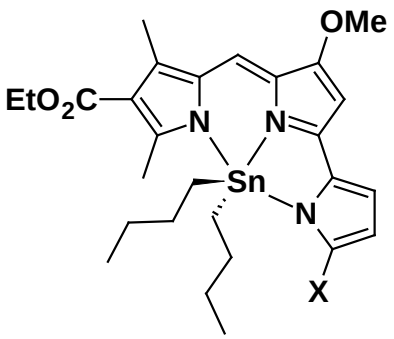

X = H Φ = 0.53

X = C(O)Me Φ = 0.61

Figure 2.8: *Sn(IV) complexes incorporating pyrrolyl dipyrrin complexes. Φ = Fluorescence quantum yield*

Vinogrove and co-workers also reported heteroleptic dipyrrin based metal complexes having ester functional groups at the 1 and 9 positions of the bis-pyrrolic ligand. The Ca(II) and Zn(II) compounds in DMF solutions were found to be strongly emissive when compared to unfunctionalised derivatives (see **Figure 2.9**).[26] The π-extension of the ligand in metallated complexes is red shifted fluorescence compared with unfunctionalised derivatives.

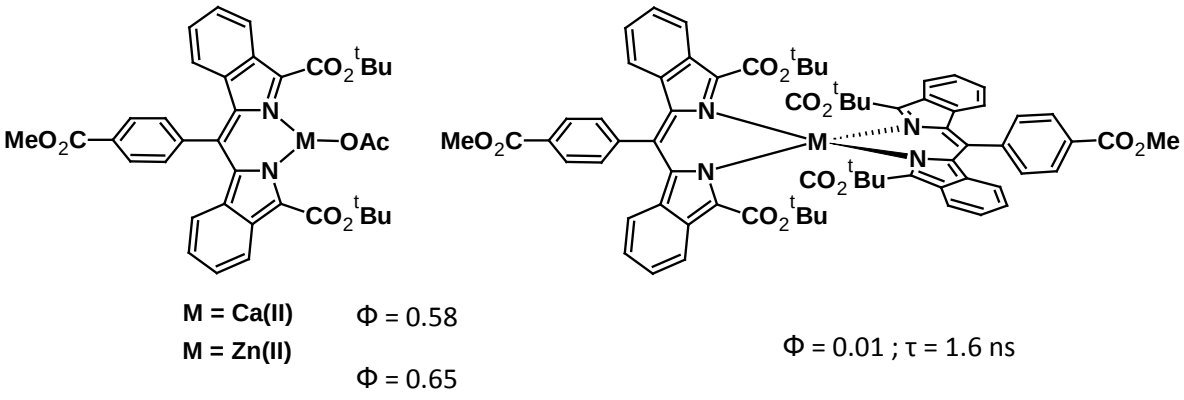

Figure 2.9: *Acetate attached Zn and Ca based dipyrrin complexes. Φ = Fluorescence quantum yield; τ = Singlet lifetime values.*

Dipyrrin based metal complexes have recently appeared as novel interesting species where a careful choice of the ligands in the complex is the key in the development of bright and stable emitters.These dipyrrin based compounds have been applied as metal cation sensors in biological media,[27] as sensitisers for light harvesting systems,[28] OLEDs and for the construction of coordination polymeric architectures.[29] Also, this type of complexes may further be used as sensitisation of these cations on combination with lanthanides as porphyrins and BODIPY compounds have been used for the same purpose.[30]

In this chapter a series of novel dipyrrin ligands consisting of mesityl, pyrenyl and phenyl groups at its 5 position have been synthesised and further reacted with $Re(CO)_5Cl$ to form rhenium tetracarbonyl and tricarbonyl complexes (see **Figure 2.10** and **Figure 2.11**). These

complexes were made with the aim to study their photophysical process and assess their CO loss potential. Photophysical properties of the complexes were investigated through UV-vis, emission, single photon counting and pico-second time resolved infrared spectroscopic techniques. The complexes were studied for their photochemical and thermal CO releasing abilities using myoglobin assays. Furthermore several synthetic attempts were made to synthesise similar dipyrrin based manganese tetracarbonyl and tricarbonyl complexes which, however, were unsuccessful.

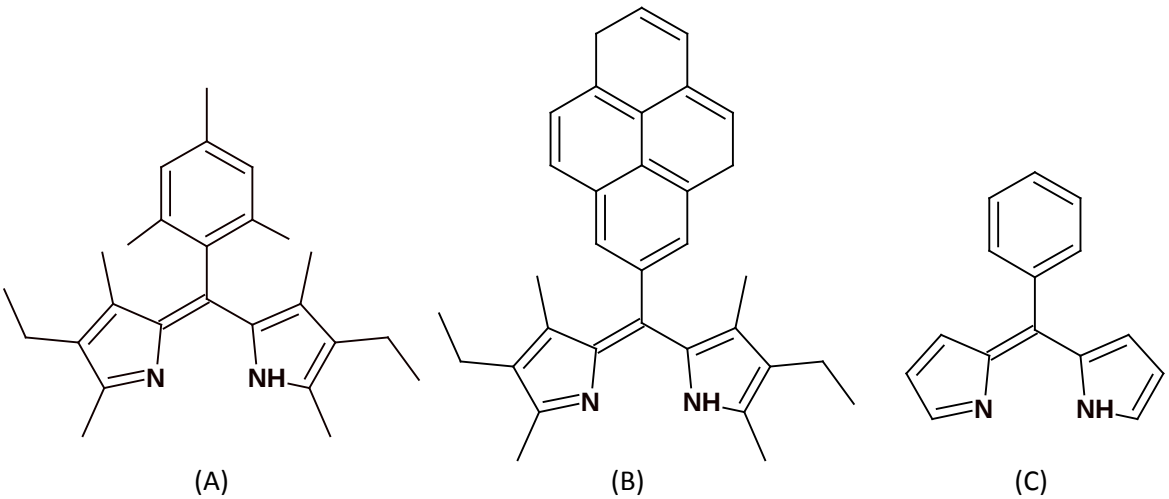

(A) (B) (C)

Figure 2.10: *Structure of the dipyrrin ligands synthesized in this chapter (A) 2,8-diethyl-1,3,7,9tetramethyl-5-mesityl-4,6-dipyrrin (B) 2,8-diethyl-1,3,7,9tetramethyl-5-pyrenyl-4,6dipyrrin (C) 5-phenyl-4,6-dipyrrin.*

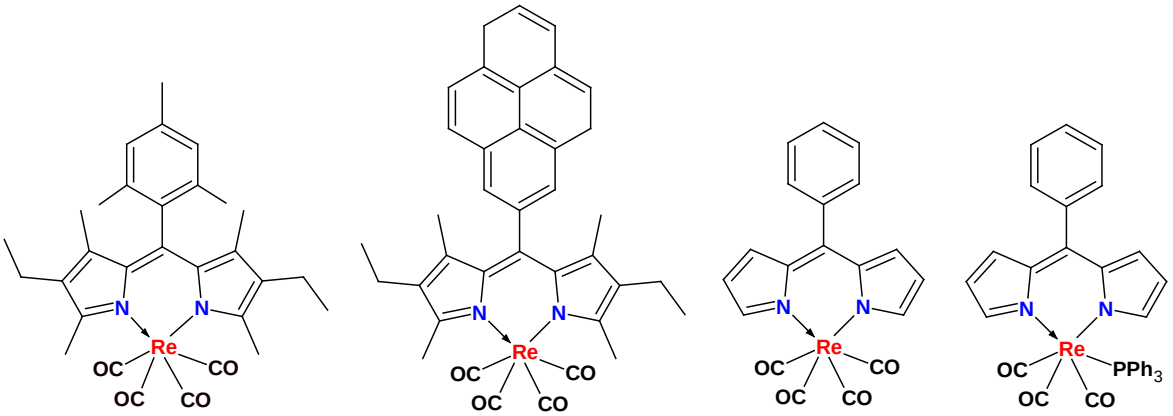

Figure 2.11: *Structure of the Re tetra and tri carbonyl complexes synthesised in this chapter; (A) [2,8-diethyl-1,3,7,9-tetramethyl-5mesityl-4,6-dipyrrinatoRe(CO)$_4$] (B) [2,8-diethyl-1,3,7,9-tetramethyl-5-pyrenyl-4,6-dipyrrinatoRe(CO)$_4$] (C) [5-phenyl-4,6-dipyrrinatoRe(CO)$_4$] (D) [5-phenyl-4,6-dipyrrinatoRe(CO)$_3$PPh$_3$]*

For simplicity, sometimes the IUPAC names of the complexes have been changed and the following names of the complexes are used in this chapter of the thesis:

IUPAC Name	**Common Name**
[2,8-diethyl-1,3,7,9-tetramethyl-5mesityl-4,6dipyrrin]	5-mesityldipyrrin
[2,8-diethyl-1,3,7,9-tetramethyl-5mesityl-4,6-dipyrrinatoRe$(CO)_4$]	[5-mesityldipyrrinatoRe$(CO)_4$]
[2,8-diethyl-1,3,7,9-tetramethyl-5pyrenyl-4,6-dipyrrin]	5-pyrenyldipyrrin
[2,8-diethyl-1,3,7,9-tetramethyl-5pyrenyl-4,6-dipyrrinatoRe$(CO)_4$]	[5-pyrenyldipyrrinatoRe$(CO)_4$]
[5-phenyl-4,6-dipyrrin]	5-phenyldipyrrin
[5-phenyl-4,6-dipyrrinatoRe$(CO)_4$]	[5-phenyldipyrrinatoRe$(CO)_4$]
[5-phenyl-4,6-dipyrrinatoRe$(CO)_3PPh_3$][31]	[5-phenyldipyrrinatoRe$(CO)_3PPh_3$]

2.2 Results and Discussion

2.2.1 NMR Spectroscopy

The rhenium(I) complexes are diamagnetic low spin d^6 species. Assignment of the numbering system to the dipyrrin based complexes is shown in **Figure 2.12**. ^{1}H NMR data for rhenium(I) tetra and tri carbonyl complexes are displayed in **Table 2.1**.

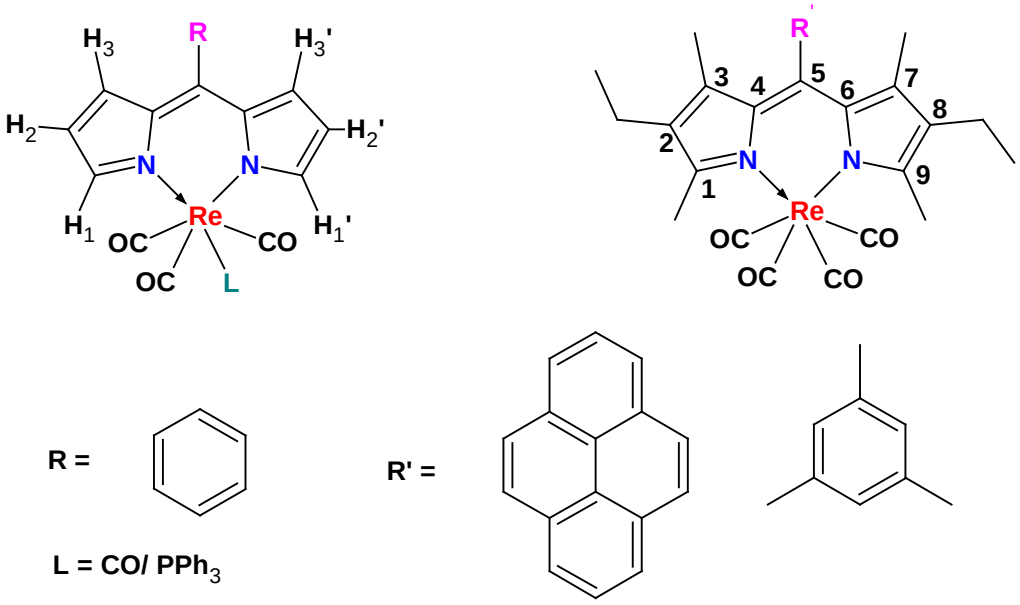

Figure 2.12: *Assignment of numbers to the dipyrrin based molecules*

Table 2.1 *^{1}H NMR data for rhenium(I) tetra and tri carbonyl complexes. All the spectra are recorded in $CDCl_3$.*

Complex	ppm (δ)					
	H_1	**$H_{1'}$**	**H_2**	**$H_{2'}$**	**H_3**	**$H_{3'}$**
[5-phenyldipyrrinatoRe$(CO)_4$]	7.92	7.92	6.66	6.65	6.47	6.45
5-phenyldipyrrinatoRe$(CO)_3PPh_3$]	7.70	7.69	6.42	6.40	6.30	6.29

In the case of **[**5-phenyldipyrrinatoRe$(CO)_4$] all the proton NMR signals for six pyrrolic protons are observed in clusters as shown in **Figure 2.13**. Resonances corresponding to the four protons $H_2/H_{2'}$ and $H_3/H_{3'}$ lie in the region between 6.45 to 6.66 ppm. Whereas signals for H_1/H_1' protons are further shifted down field and appear at 7.92 ppm. It is evident from the ^{1}H NMR spectrum that all the signals for protons from the phenyl ring appear as multiplet, in the region between 7.50-7.44 ppm (**Table 2.1**).

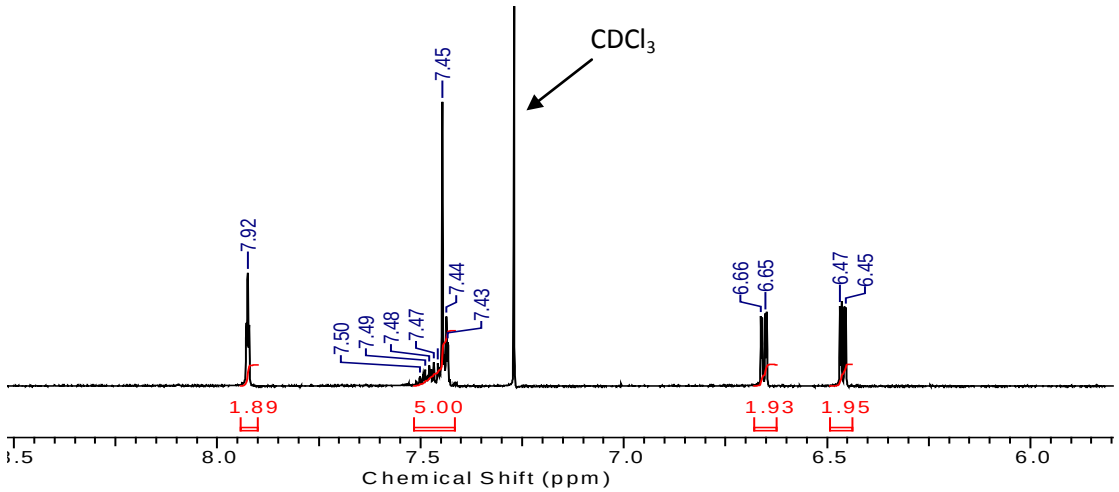

Figure 2.13: *^{1}H NMR spectrum of the [5-phenyl-4,6-dipyrrinatoRe$(CO)_4$] complex recorded in $CDCl_3$*

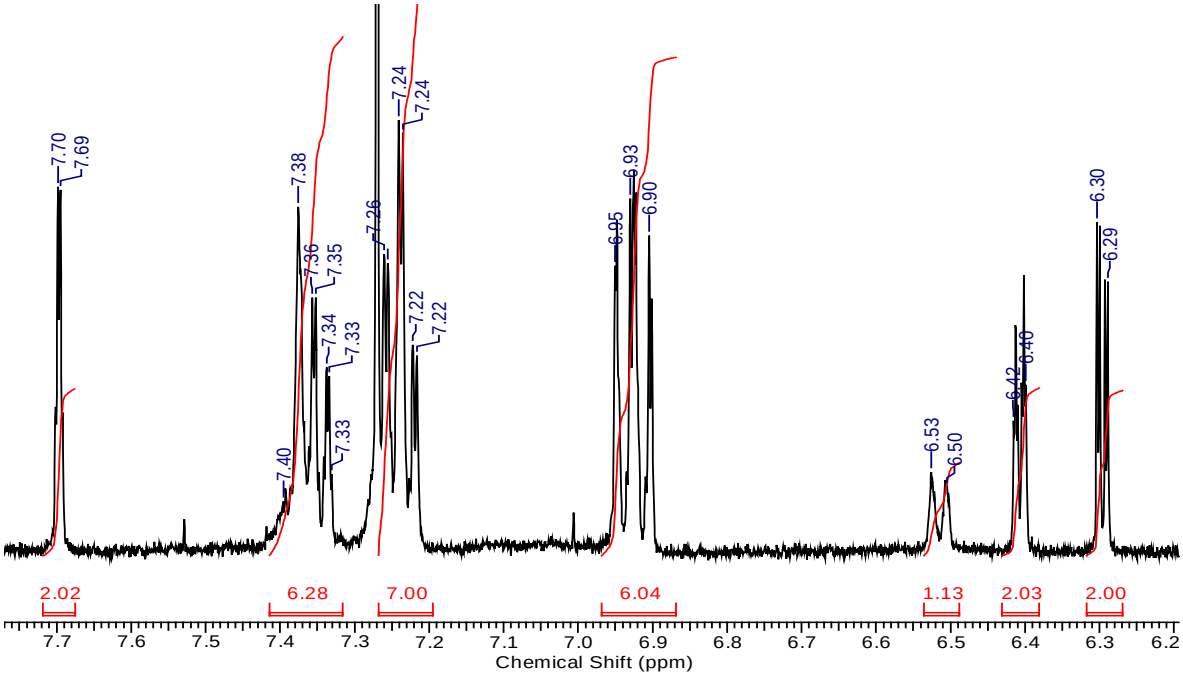

Figure 2.14: *^{1}H NMR spectrum of the [5-phenyl-4,6-dipyrrinatoRe(CO)$_3$PPh$_3$] complex recorded in $CDCl_3$*

Upon inspection of the ^{1}H NMR spectrum of [5-phenyl-4,6-dipyrrinatoRe(CO)$_3$PPh$_3$] (**Figure 2.14**) it is evident that all the signals for pyrrolic protons experience an upfield shift compared to the Re tetracarbonyl analogue which is due to the proximity of the π clouds of the PPh_3 ligand. The remaining resonances appear in the region 6.50 to 7.40 ppm and are due to the protons from the phenyl ring and the three phosphine ligands.

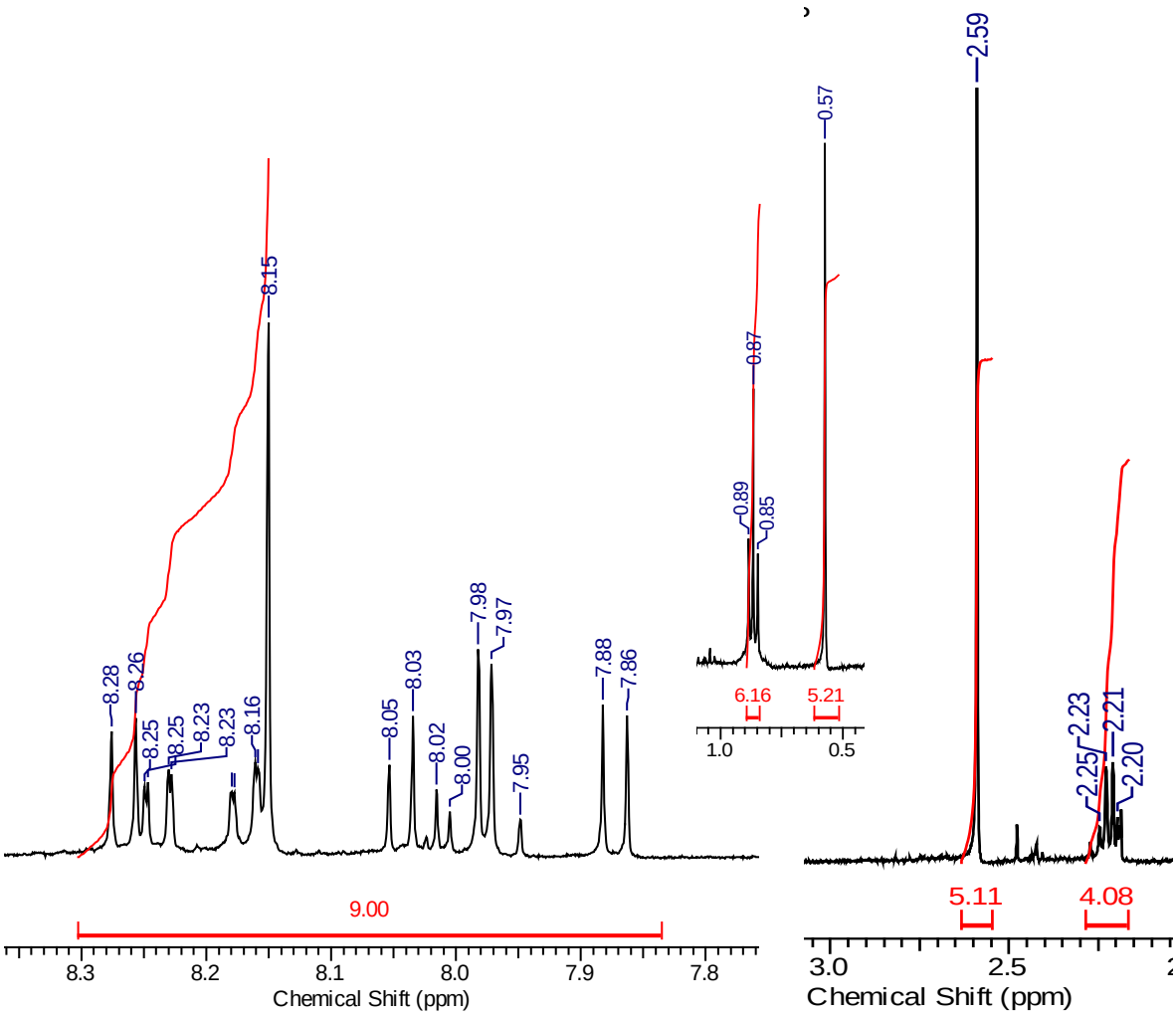

Figure 2.15: *^{1}H NMR spectrum of the [2,8-diethyl-1,3,7,9-tetramethyl-5-pyrenyl-4,6-dipyrrinatoRe(CO)$_4$] complex recorded in $CDCl_3$*

The ^{1}H NMR spectrum (**Figure 2.15**) of the [2,8-diethyl-1,3,7,9-tetramethyl-5-pyrenyl-4,6-dipyrrinatoRe(CO)$_4$] displayed characteristic peaks including two singlets at δ = 0.57 and 2.5 ppm values corresponding to both methyl groups and a triplet (δ = 0.89 ppm) and quartet (δ = 2.29 ppm) for the ethyl groups on the kryptopyrrole unit.

Strong shielding of one of the methyl groups was observed due to its proximity to the electron cloud of the pyrene moiety. All the signals for protons from the pyrene unit appeared as a multiplet between 7.8 and 8.20 ppm values. Also, all the resonance on the

pyrenyl ligand on the dipyrrin Re complex occur upfield shifted compared to the uncoordinated pyrene based dipyrrin ligand due to the presence of back bonding from carbonyl groups.[32]

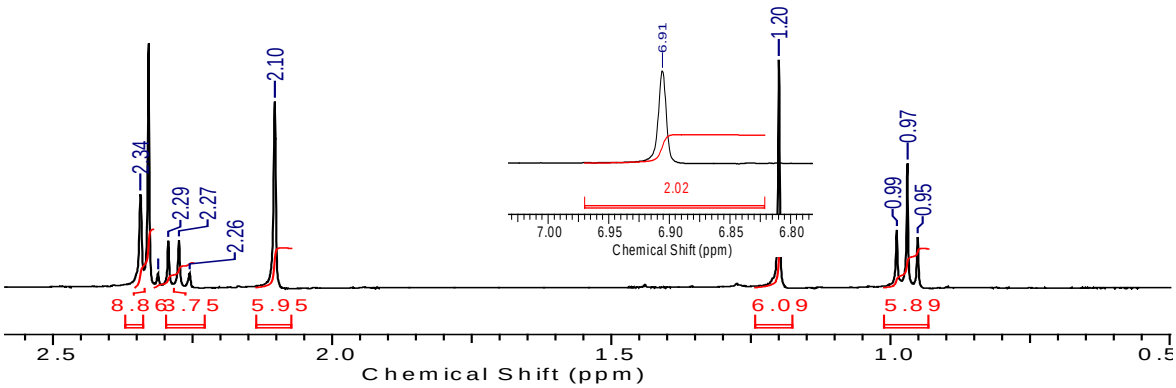

Figure 2.16: *^1H NMR spectrum of the [2,8-diethyl-1,3,7,9-tetramethyl-5-mesityl-4,6-dipyrrinatoRe(CO)$_4$] complex recorded in $CDCl_3$*

Also, the ^{1}H NMR spectrum (**Figure 2.16**) of [2,8-diethyl-1,3,7,9-tetramethyl-5mesityl-4,6-dipyrrinatoRe(CO)$_4$] displayed characteristic peaks including two singlets at δ = 2.1 and 1.0 ppm values corresponding to both methyl groups and a triplet (δ = 0.97 ppm) and quartet (δ = 2.29 ppm) for the ethyl fragments on the kryptopyrrole unit. Two of the methyl groups on the mesityl ring appeared as a singlet which is slightly downfield shifted when compared to the quartet from the ethyl group of pyrrole ring. The two aromatic protons on the mesityl ring appeared as a singlet at 6.91 ppm. [33]

2.2.2 UV- Vis Spectroscopy

The UV-vis spectra of all the ligands and their corresponding Re carbonyl complexes were carried out using spectrophotometric grade pentane. Absorption maxima for all of the compounds synthesised in this chapter have been tabulated in **Table 2.2**.

Table 2.2 *Electronic spectra of dipyrrin ligands and their Re metal based tetra and tricarbonyl complexes. All the spectra were recorded in pentane.*

Compound	**λ_{max} (nm)**	**ε ($\times 10^4$ M^{-1} cm^{-1})(nm)**
2,8-diethyl-1,3,7,9-tetramethyl-5-mesityl-4,6-dipyrrin	315, 400, 470, 505	12 (470)
[2,8-diethyl-1,3,7,9-tetramethyl-5-mesityl-4,6-dipyrrinatoRe$(CO)_4$]	316, 400, 487, 524	8 (524)
2,8-diethyl-1,3,7,9-tetramethyl-5-pyrenyl-4,6-dipyrrin	279, 328, 344, 370, 468	15(468)
[2,8-diethyl-1,3,7,9tetramethyl-5-pyrenyl4,6-dipyrrinatoRe$(CO)_4$]	328, 344, 370, 492, 525	3 (525)
5-phenyl-4,6-dipyrrin	260, 354, 466	9 (466)
[5-phenyl-4,6-dipyrrinatoRe$(CO)_4$]	274, 320, 405, 463, 487	4 (487)
[5-phenyl-4,6-dipyrrinatoRe$(CO)_3PPh_3$]	274, 310, 417, 431, 490	2 (490)

The dipyrrin complexes studied here exhibit a strong absorbance peak in the region 420-580 nm (**Figure 2.17**). These are attributed to $S_0 \rightarrow S_1$ (π -π^*) intraligand transitions centered mainly on the dipyrrinato ligand.[24, 34] A bathochromic shift of 35 nm was observed for the methyl substituted dipyrrins compounds when compared to unsubstituted ones. This is due to the extended conjugation effects of the methyl substituted dipyrrin ligands.[35, 36]

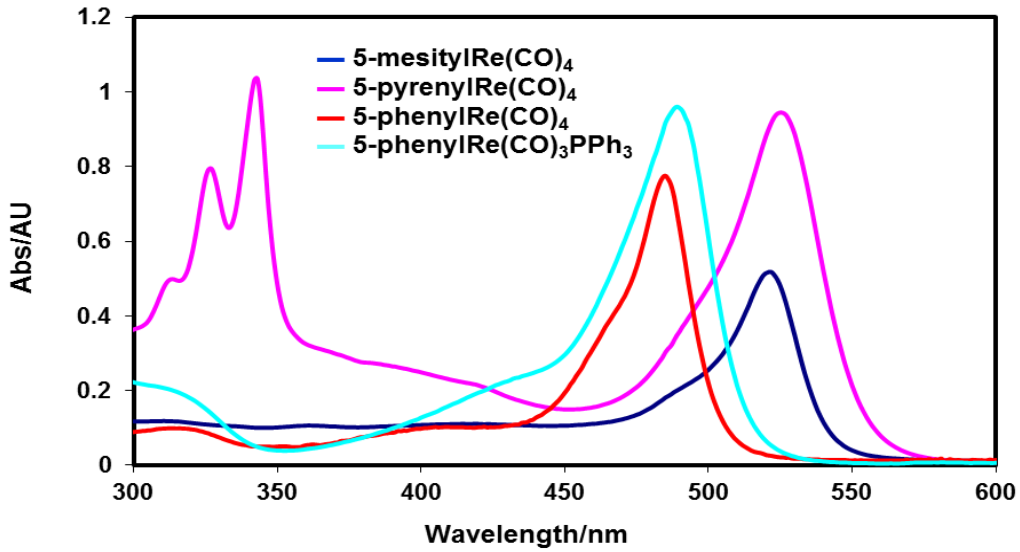

Figure 2.17: *Normalised UV-Vis spectra of [2,8-diethyl-1,3,7,9-tetramethyl-5-mesityl-4,6-dipyrrinatoRe(CO)$_4$] (dark blue line), [2,8-diethyl-1,3,7,9-tetramethyl-5-pyrenyl-4,6-dipyrrinatoRe(CO)$_4$] (pink line), [5-phenyl-4,6-dipyrrinatoRe(CO)$_4$] (red line) and [5-phenyl-4,6-ldipyrrinatoRe(CO)$_3$PPh$_3$] (sky blue line) complexes. All spectra were recorded in spectrophotometric grade pentane at room temperature (20 ± 2 ^{o}C).*

By comparing the complexes with other reported dipyrrinato complexes it can be concluded that this π-π^* transition is relatively insensitive to the identity of the metal ion.[4, 20, 21, 37] Generally, in metal dipyrrinato complexes and BODIPY molecules a weak broader band appears in the region 370 - 400 nm which is due to the dipyrrin based $S_0 \rightarrow S_2$ transition.[38, 39] A similar assignment can be made for dipyrrin compounds. Also, a weak

peak appearing at 320 nm is assigned to an intraligand charge transfer transitions due to the lone pair of nitrogen atoms.[24]

Recently, Re(I) based dipyrrinato complexes with the general formula *fac*[ReL$(CO)_3$Cl]$^-$, *fac* [ReL$(CO)_3PR_3$] and *fac* [ReL$(CO)_2PR_3PR'_3$] have been synthesised by Telfer and co workers as described previously in the chapter. It was further reported that all complexes displayed an intense band centered between 480-491 nm. This band was attributed to an $S_0 \rightarrow S_1$ (primarily π-π^*) transition mainly centered on the dipyrrinato ligand. The minor peaks (or shoulders) present in the absorption spectra of the complexes around 300 nm have been ascribed as dipyrrin based $S_0 \rightarrow S_2$ transitions.[31]

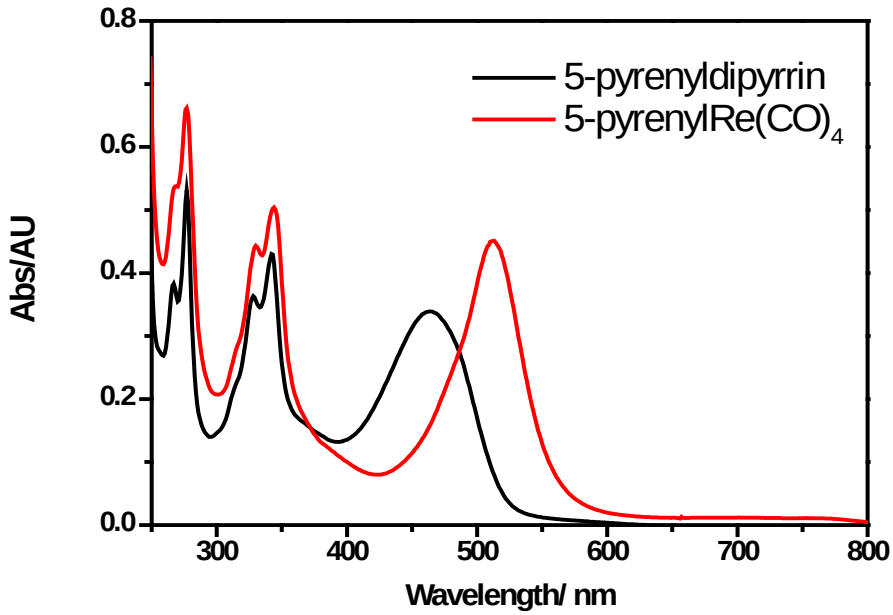

Figure 2.18: *Normalised UV-Vis spectra of 5-pyrenyldipyrrin (black line) and [5-pyrenyldipyrrinatoRe(CO)$_4$] (red line) compounds. All spectra were recorded in spectrophotometric grade pentane at room temperature (20 ± 2°C).*

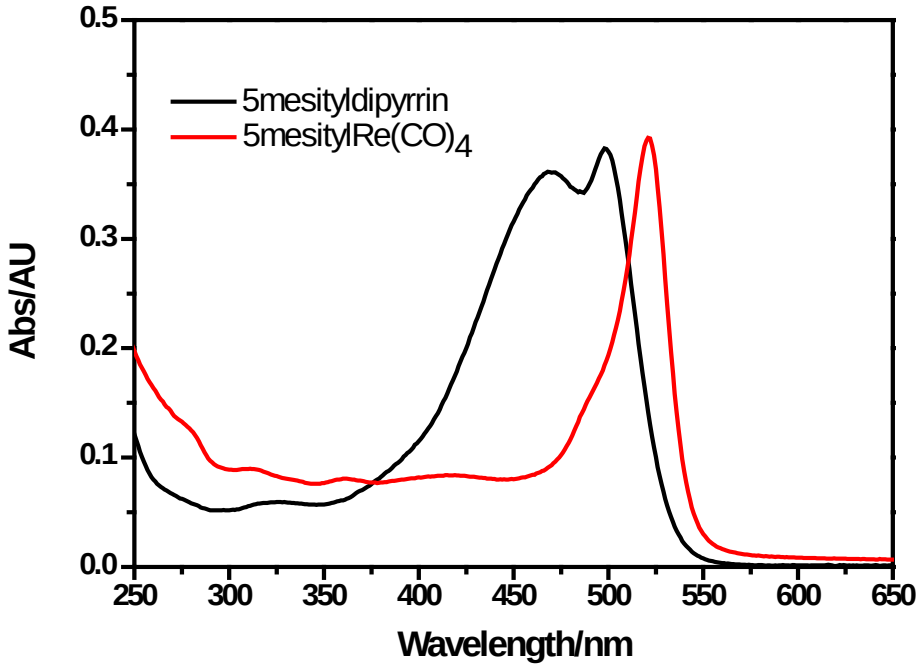

Figure 2.19: *Normalised UV-Vis spectra of 5-mesityldipyrrin (black line), and [5-mesityldipyrrinatoRe(CO)$_4$] (red line) compounds. All spectra were recorded in spectrophotometric grade pentane at room temperature (20 ± 2 ^{o}C).*

In the case of the pyrene based dipyrrin compounds, three new sharp peaks are observed at 279, 328 and 344 nm which may be attributed to π -π* transitions of pyrene chromophore (**Figure 2.18**). [32] The UV-Vis spectrum of the 5-mesityl dipyrrin is significantly broader than the 5-mesityl dipyrrin based Re tetracarbonyl complex which could be due to lower electronic and vibronic coupling between π electrons in the complexed dipyrrin system and the meso substituted mesityl groups (**Figure 2.19**).[40] It is worth noting that the lowest energy peak of all the metallated Re based carbonyl complexes are red shifted when compared to their respective dipyrrin ligand. Generally the lowest energy peak in metallated carbonyl complexes is assigned to a d-d transition of the metal ion which presumably is present in these Re based metal carbonyl complexes. But due to the weakness of the bands they have been concealed by dipyrrin based transitions.

2.2.3 Infrared spectroscopy

All of the IR spectra of Re based tetracarbonyl complexes and tricarbonyl complexes were measured in spectroscopic grade pentane and DCM (**See Table 2.3**).

***Table 2.3**: Comparison of the M-CO stretching frequencies observed for the Re based dipyrrin tricarbonyl and tetracarbonyl complexes in pentane or dichloromethane solution.*

Complexes	**CO Stretching frequencies (cm^{-1})**
[5-mesityldipyrrinatoRe$(CO)_4$]	2094, 1991, 1972, 1930
[5-pyrenyldipyrrinatoRe$(CO)_4$]	2096, 1993, 1974, 1932
[5-phenyldipyrrinatoRe$(CO)_4$]	2105, 2004, 1978, 1933
[5-phenyldipyrrinatoRe$(CO)_3PPh_3$]	2020, 1923, 1896

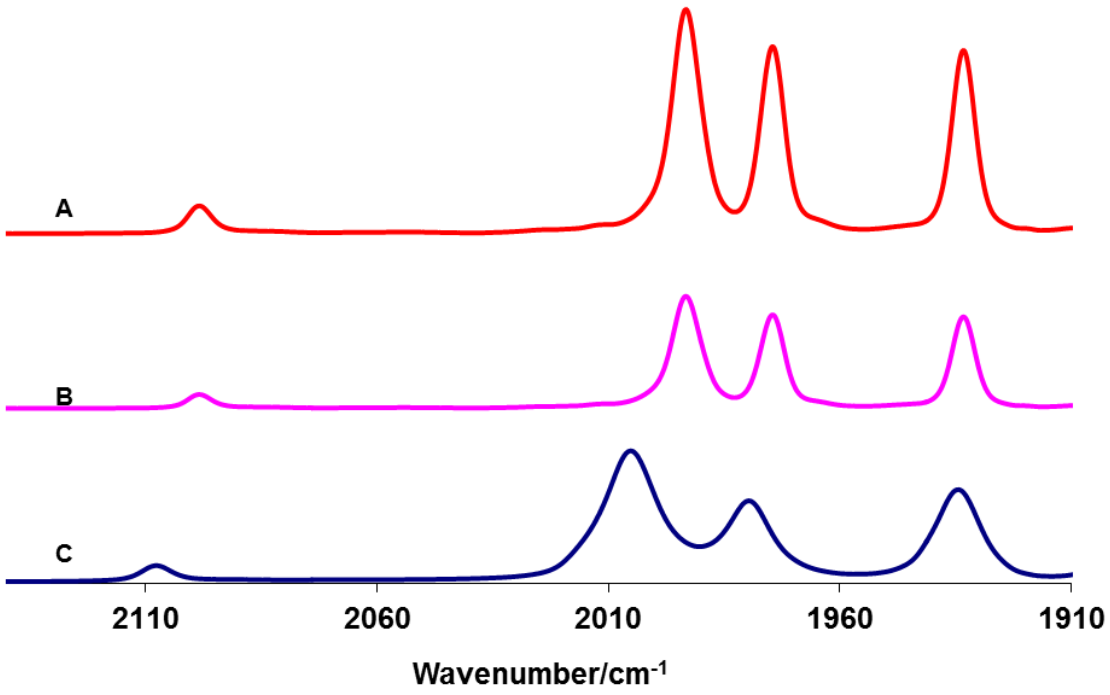

Figure 2.20: *Overlaid IR spectra of [5-pyrenyldipyrrinatoRe(CO)$_4$] (A), [5-mesityldipyrrinatoRe(CO)$_4$] (B) and [5-phenyldipyrrinatoRe(CO)$_4$] (C) in pentane*

As the complexes exhibit C_{2v} symmetry, four C-O stretching modes were observed. [41] All the complexes show four CO stretching bands in the infra red region from 2105-1825 cm^{-1} (**Figure 2.20**). These are attributed to the $2A_1$, B_1 and B_2 modes, and are in agreement with their *cis*-configuration.[42-46] The higher frequency A_1 and B_1 bands are assigned to *trans*-carbonyl ligands, while the lower stretching vibrations to the A_1 and B_2 modes are assigned to *cis*-carbonyl ligands.

For all the Re tetracarbonyl complexes, the υ(CO) band appearing between 2105 and 2085 cm^{-1} are assigned to the trans $Re(CO)_2$ subunits of $Re(CO)_4$ moieties in the complexes as the strong trans influence would weaken the Re-CO π back bonding and thus increase the υ(CO) frequency. Similar υ(CO) stretching frequencies (1916-2081 cm^{-1}) have been

observed for tetracarbonyl(naphthyridylcarbamoyl) and tetracarbonyl(naphthyridylamido) rhenium(I) based complexes reported by Cheung and group.[47]

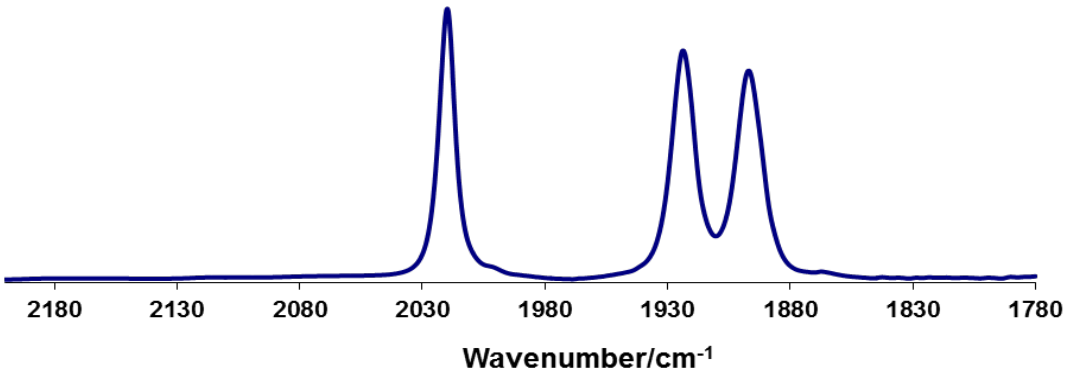

Figure 2.21: *Normalised IR spectrum of [5-phenyldipyrrinatoRe(CO)$_3$PPh$_3$]in DCM*

Three strong bands appear in the range of 1875-2040 cm^{-1} for the [5-phenyldipyrrinatoRe(CO)$_3$PPh$_3$] complex analogue due to the facial coordination of the three carbonyl ligands (**Figure 2.21**).[48] These vibrations can be attributed to totally symmetric in phase vibrations A' (1), and out of phase symmetric vibrations A' (2) and A''.[31, 49, 50]

2.2.4 Emission and lifetime studies

All of the complexes studied in this chapter were studied for luminescence at both room temperature (298K) and at low temperature (77K). The emission spectra were recorded in spectrophotometric grade pentane at room temperature 298K and a 4:1 (v/v) mix of methanol/ethanol at 77K.

The complexes [5-phenyldipyrrinatoRe$(CO)_4$], [5-pyrenyldipyrrinatoRe$(CO)_4$], [5-mesityldipyrrinatoRe$(CO)_4$] and [5-phenyldipyrrinatoRe$(CO)_3PPh_3$] were excited in the range 485 – 522 nm, where the dipyrrin moiety absorbs, however no emission was observed at room temperature 298K. The samples were also prepared in ethanol/methanol (1:4, v/v) mixtures and were cooled to 77K and again no emission was observed for any of the samples when excited in the range 485 – 522 nm. The lack of luminescence spectra for rhenium tri- and tetracarbonyl complexes is in agreement with other dipyrrin complexes reported in literature.[6, 51-53]

However, excitation of the [5-pyrenyldipyrrinatoRe$(CO)_4$] complex, (**Figure 2.23**) into the higher energy absorption region (327- 344 nm), where the pyrene moiety absorbs gives rise to emission comprising of an intense peak at 416 and two weaker peaks at 482 and 545 nm. This observation indicates that the emission at 416 nm is due to pyrene based π-π* transitions.[32 54]

The emission profile of the ligand, 5-pyrenyldipyrrin was also studied in spectrophotometric grade pentane at room temperature (298K). Excitation of the ligand at 344 nm gives rise to emission with a λ_{max} at 389 nm (**Figure 2.24**). No luminescence was observed when the molecule was excited into the dipyrrin based π-π* region (485 nm). In the literature it is suggested that the lack of emission is due to the exchange of the imino proton between the two pyrrolic rings of the dipyrrin ligand.[55, 56]

Further, it can be inferred that the additional weaker bands between 480 – 545 nm observed for the [5-pyrenyldipyrrinatoRe$(CO)_4$] complex when compared to its 5-pyrenyldipyrrin ligand can be attributed to emission due to the addition of the Re carbonyl complex. A Re tetra carbonyl complex, naphthyridylamido [Re$(CO)_4$L] { L = 7-[2-[6-chloropyridylamino]-2,4-dimethyl-1,8-naphthyridine] has been studied, with emission λ_{max} at 499 and 533 nm following excitation in the range 400-430 nm at 77K (**Figure 2.22**).

The emission spectrum for the complex was broad compared to other dipyrrin based rhenium tricarbonyl complexes.[4] The broad emission observed was attributed to a mixture of ^{3}IL transitions involving aromatic diimine groups and ^{3}MLCT transitions within the complex.[47]

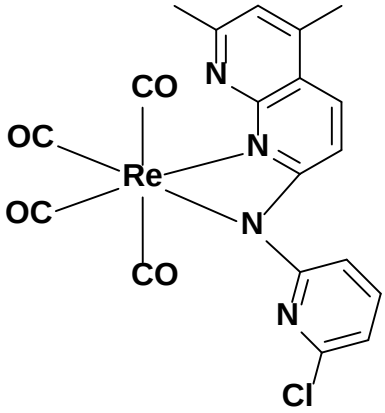

Figure 2.22: *Structure of [Re(CO)$_4$L] { L = 7-[2-[6-chloropyridylamino]-2,4-dimethyl-1,8-naphthyridine]*

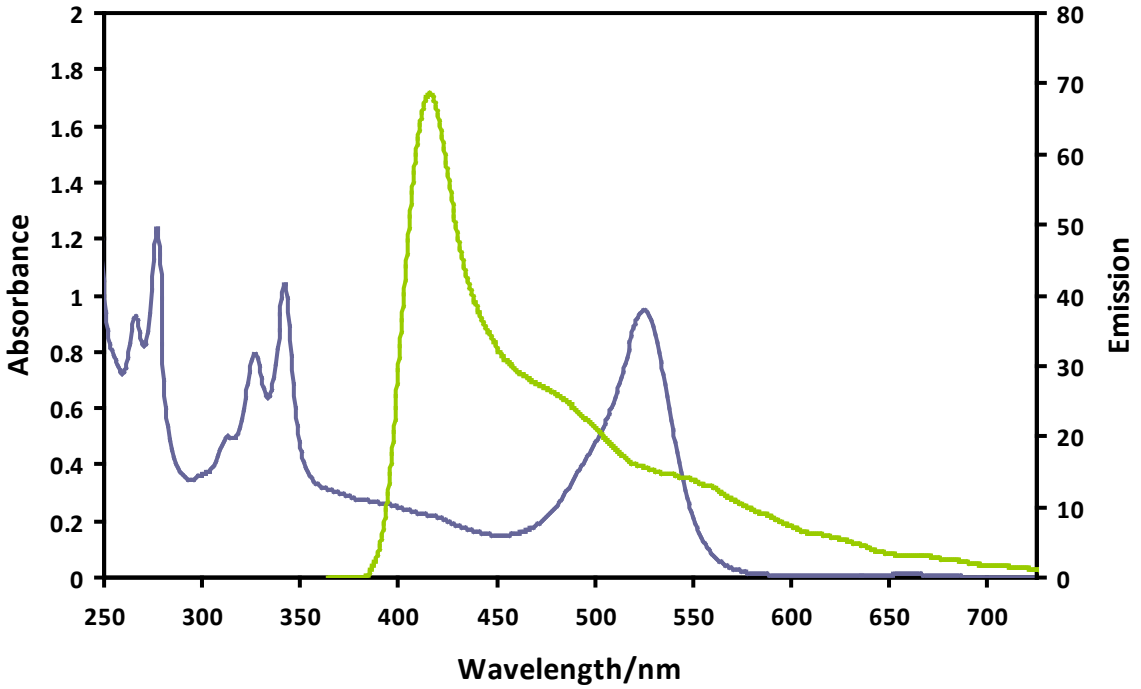

Figure 2.23: *Absorption (in blue) and emission spectra (in green) (λ_{exc} = 344 nm) of [2,8-diethyl-1,3,7,9-tetramethyl-5-pyrenyl-4,6-dipyrrinatoRe(CO)$_4$] (10^{-4}M) recorded in spectrophotometric grade pentane (OD at λ_{exc} = 344 nm is 0.18).*

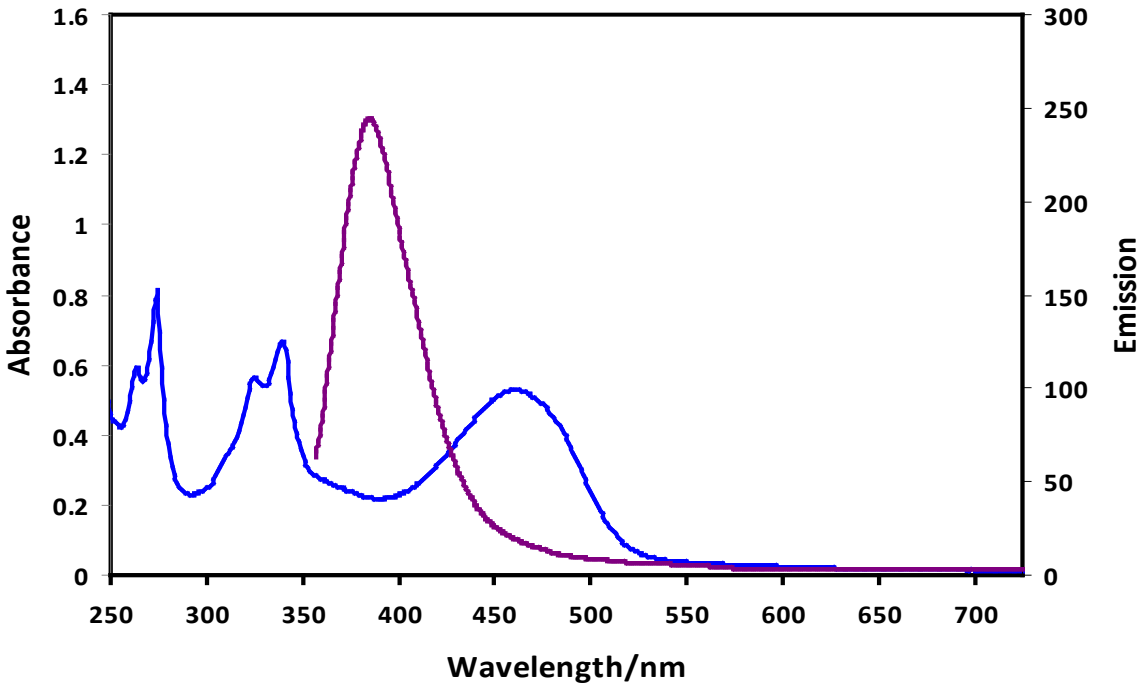

Figure 2.24: *Absorption (in blue) and emission spectra (in purple) (λ_{exc} = 344 nm) of 2,8-diethyl-1,3,7,9-tetramethyl-5-pyrenyl-4,6-dipyrrin (10^{-4}M) recorded in spectrophotometric grade pentane (OD at λ_{exc} = 344 nm is 0.18).*

A significant difference was observed when the emission spectra of 5-pyrenyl dipyrrin was compared to [5-pyrenyl-4,6-dipyrrinatoRe(CO)$_4$] complex (λ_{exc} = 344 nm). The emission intensity is reduced 3 fold in the case of the metallated dipyrrin when compared to the uncoordinated dipyrrin.

The fluorescence lifetimes were recorded in spectrophotometric grade pentane using 360 nm excitation. A lifetime of 7 ± 1 ns was observed for 5-pyrenyldipyrrin and 3.9 ± 1 ns for [5-pyrenyldipyrrinatoRe(CO)$_4$] complex. The singlet lifetimes obtained for the pyrene based rhenium tetracarbonyl complex is in agreement with the literature reported values for dipyrrin complexes.[13, 20, 57] Similar fluorescent lifetime value of 7 ns was reported for pyrene based BODIPY compound (Structure shown in **Figure 2.25**).[32]

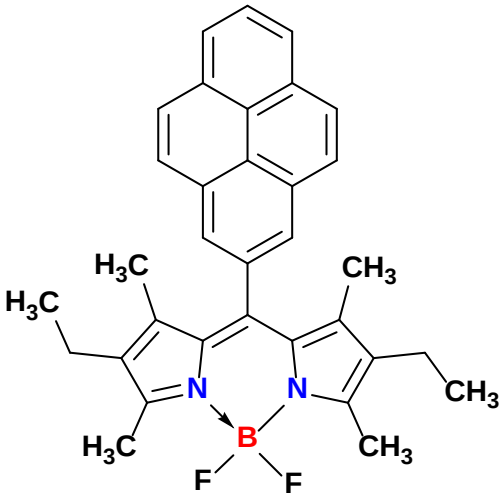

Figure 2.25 *Structure of pyrene based BODIPY compound.*

[5-mesityldipyrrinatoRe(CO)$_4$], [5-phenyldipyrrinatoRe(CO)$_4$] and [5-phenyldipyrrinatoRe(CO)$_3$PPh$_3$] complexes were non emissive and therefore no lifetimes were measured. Typical fluorescence decays observed for 5-pyrenyldipyrrin and [5-pyrenyldipyrrinatoRe(CO)$_4$] in pentane solution are shown in **Figure 2.26** and **Figure 2.27**.

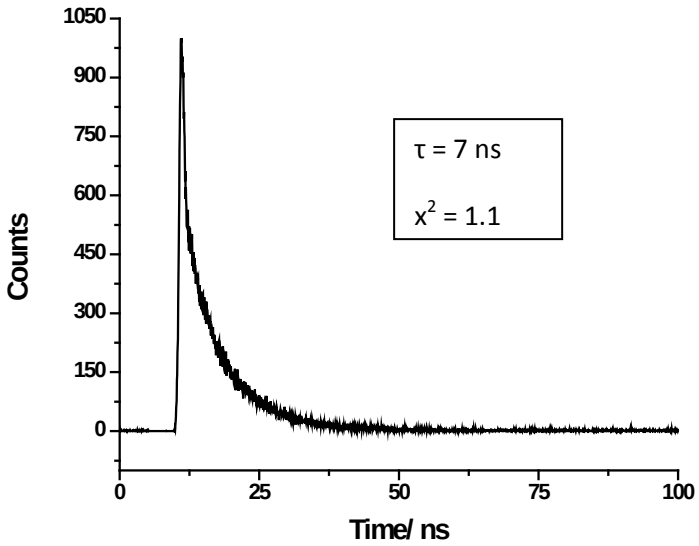

Figure 2.26: *Typical RT Fluoroscence decay observed for 5-pyrenyldipyrrin following excitation at 360 nm. Singlet lifetime is measured in ± 1 ns.*

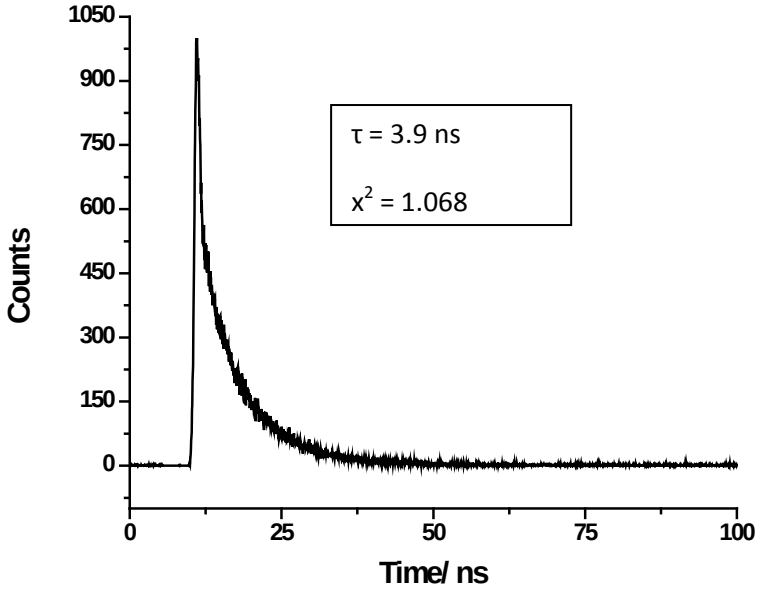

Figure 2.27: *Typical room temperature fluoroscence decay observed for [5-pyrenyldipyrrinatoRe(CO)$_4$] following excitation at 360 nm. Singlet lifetime is measured in ± 1 ns.*

2.2.5. Picosecond Time Resolved Infrared Spectroscopy

A picosecond time resolved infrared study was carried out for [5-phenyldipyrrinatoRe(CO)$_4$], [5-mesityl-4,6-dipyrrinatoRe(CO)$_4$] and the [5-phenyldipyrrinatoRe(CO)$_3$PPh$_3$] complex in solution at room temperature (298 K). Parent and transient bands observed for [5-mesityldipyrrinatoRe(CO)$_4$], [5-phenyldipyrrinatoRe(CO)$_4$] and [5-phenyldipyrrinatoRe(CO)$_3$PPh$_3$]complexes in the TRIR experiments are shown in **Table 2.4**.

Table 2.4 *Parent and transient TRIR bands of the complexes under study*

	TRIR bands (cm^{-1})	
Complexes	**Parent Bands**	**Transient Bands**
[5-mesityldipyrrinatoRe$(CO)_4$]	2094, 1991, 1972	2081, 1981, 1959
[5-phenyldipyrrinatoRe$(CO)_4$]	2105, 2004,1979,1933	2086, 1985, 1969
[5-phenyldipyrrinatoRe$(CO)_3PPh_3$]	2020, 1923, 1896	2010, 1914, 1885

Excitation of the [5-mesityldipyrrinatoRe$(CO)_4$] complex at λ_{exc} = 520 nm in pentane solution at room temperature resulted in depletion of the parent bands at 2094, 1991, 1972 cm^{-1} within the laser pulse together with the growth of new IR bands at 2081, 1981 and 1959 cm^{-1} (**See Figure 2.28**).

(Note: the lowest frequency band at 1930 cm^{-1} was excluded from the spectrum as it was on the periphery of the observation window and reliable information could not be obtained).

The new bands are shifted to lower wavenumbers when compared with their initial ground state depletion. This shift may indicate formation of an IL (π-π*) excited state which is mainly attributed to a π-π* LLCT from the shifting of the electron density from the dipyrrin ligand to the Re carbonyl moiety and hence increasing the back bonding of the CO ligands. Furthermore, after 50ps shifting of initially present band at 1959 cm^{-1} to 1965 cm^{-1} is observed (**See Figure 2.29**). This shift of 6 wavenumbers over 50ps is attributed to vibrational cooling.[58] These bands at 2081, 1981 and 1965 cm^{-1} persist on the nanosecond timescale. Hence, this interesting observation may indicate intraligand charge transfer i.e. interconversion of IL π-π* states localised on the dipyrrin ligand.

This assignment is based on TRIR studies carried out on the complex {*fac*-[Re$(CO)_3$(dppz)(py)]$^+$}(dppz = dipyrido[3,2-a:2'3'-c]phenazine) reported by Weinstein and

co-workers.[59] The picosecond TRIR spectra following 400 nm excitation of this complex has revealed that the parent infrared absorptions at 2036 and 1933 cm^{-1} are bleached within the laser pulse resulting in the formation of two new bands at 2016 and 1907 cm^{-1}. The shifting of the transient bands to lower energy has been assigned to a $\pi \rightarrow \pi^*$ (dppz) excited state. Furthermore, a shift to higher wavenumbers of the υ(CO) IR bands in the photo-generated species was observed over 50 ps which was initially thought to be due to vibrational cooling of the excited states. However, picosecond time resolved raman and absorption experiments further revealed the possibility of interconversion between triplet intraligand excited states. The picosecond TRIR spectrum of the complex suggested that $^3\pi$-π^* (phenathroline) to a $^3\pi$-π^* (phenazine) based excited state might be involved in the early (30 ps) process. The shift to higher wavenumbers of the υ(CO) IR bands over this time scale is due to population of the π^* (phenazine) orbital which would reduce the extent of backbonding to the CO ligands compared to the population of the π^* (phenanthroline) orbital, thus leading to a shift to higher υ(CO) frequency. However, the observed narrowing of the υ(CO) IR bands and shifting to higher wavenumbers has been explained based on two processes; vibrational relaxation and an excited state interconversion $^3\pi$-π^* (phenathroline) to a $^3\pi$-π^* (phenazine) occurring on similar timescale.

In the results presented here there is also some narrowing of the higher frequency band so in addition to a conversion of a IL π-π^* states there is also possible that the complex undergoes vibrational cooling but the two processes overlap in the TRIR spectra.[60]

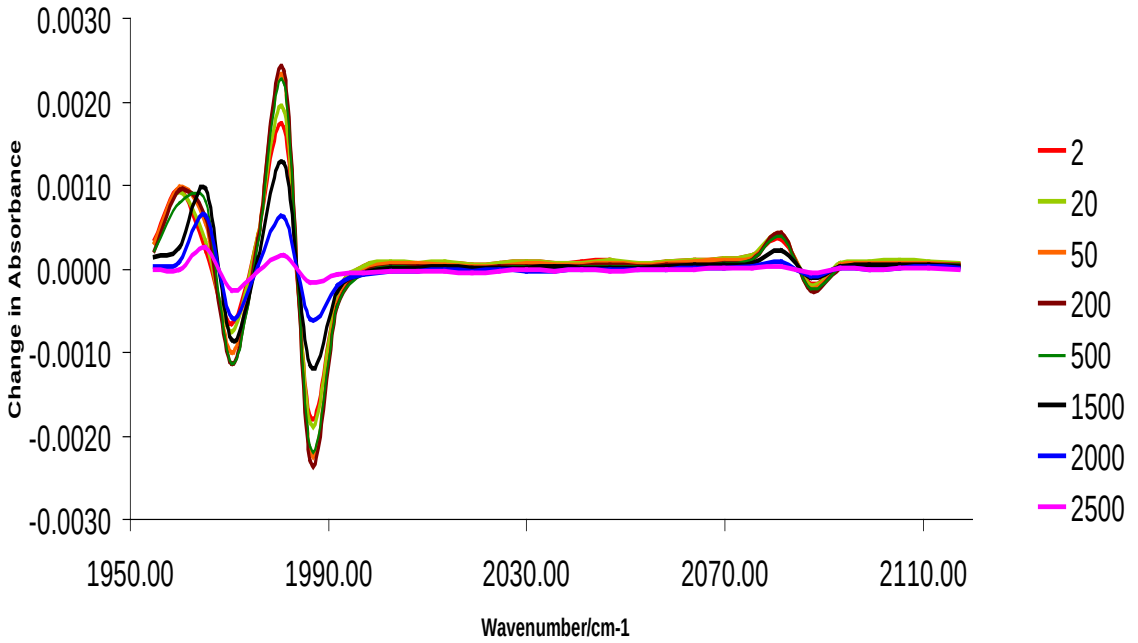

Figure 2.28: *Time resolved infra-red difference spectra following laser photolysis (λ_{exc} = 520 nm) for [2,8-diethyl-1,3,7,9tetramethyl-5-mesityl-4,6-dipyrrinatoRe(CO)$_4$] in heptane. Legend indicates time in ps.*

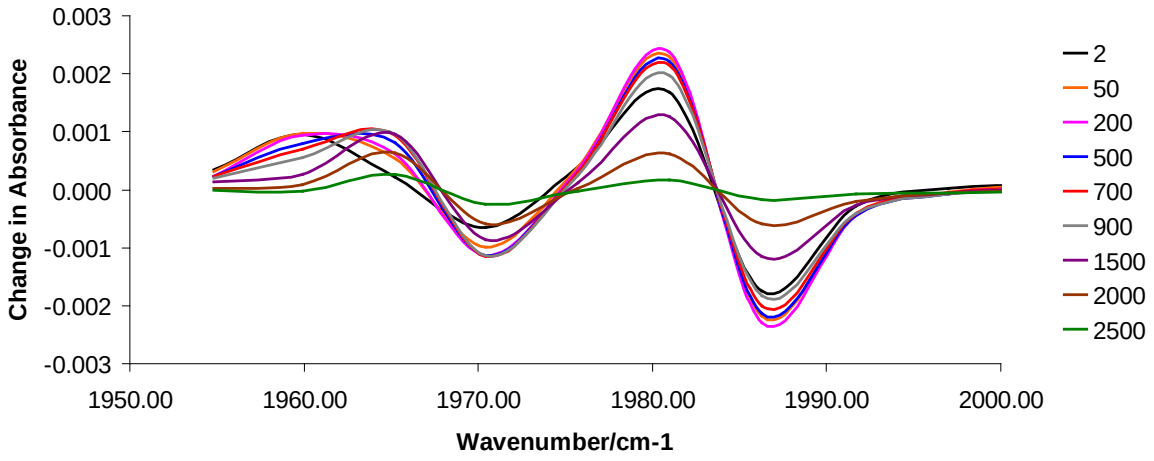

Figure 2.29: *Time resolved infra-red difference spectra following laser photolysis (λ_{exc} = 520 nm) for [2,8-diethyl-1,3,7,9-tetramethyl-5-mesityl-4,6-dipyrrinatoRe(CO)$_4$] in heptane. Legend indicates time in ps.*

Irradiation of [5-phenyldipyrrinatoRe(CO)$_4$] in a heptane solution following excitation at 470 nm excitation resulted in depletion of the parent bands at 2105, 2004, 1978 and 1933 cm^{-1} within 1 ps together with the formation of three new bands at 2086, 1985 and 1969 cm^{-1} (**Figure 2.30**). The newly formed bands began to decay after 9 ps and shifted to higher wavenumbers within the first 50 ps which may be assigned to vibrational cooling of this transient species. The transient band at 1969 cm^{-1} (which is positive in the spectra) and the bands at higher frequency (2086 cm^{-1}) overlap with the bleaching of the parent bands. These newly formed bands can be assigned to the excited state of a π-π* transition of dipyrrin ligand (LLCT) which donates the electron density to the Re carbonyl group resulting in more back bonding and shifting of the υ(CO) bands towards lower wavenumbers. Furthermore, after 50 ps shifting of the initially present excited state bands at 1964 and 2080 cm^{-1} to 1969 and 2086 cm^{-1} is observed. This shifting of the transient bands to higher wavenumber may be linked to an interconversion between IL π-π* states localised on the dipyrrin ligand. Population of the π* orbital of dipyrrin/pyrrole group from π* orbital of phenyl group would reduce the extent of back bonding to the CO ligands, thus, leading to a shift in higher frequencies and the excited state persists on the nanosecond timescale.

This assumption was previously reported for similar type complex {*fac*-[Re(CO)$_3$(dppz)(py)]$^+$}(dppz = dipyrido[3,2-a:2’3’-c]phenazine) as explained in previous section.[59]

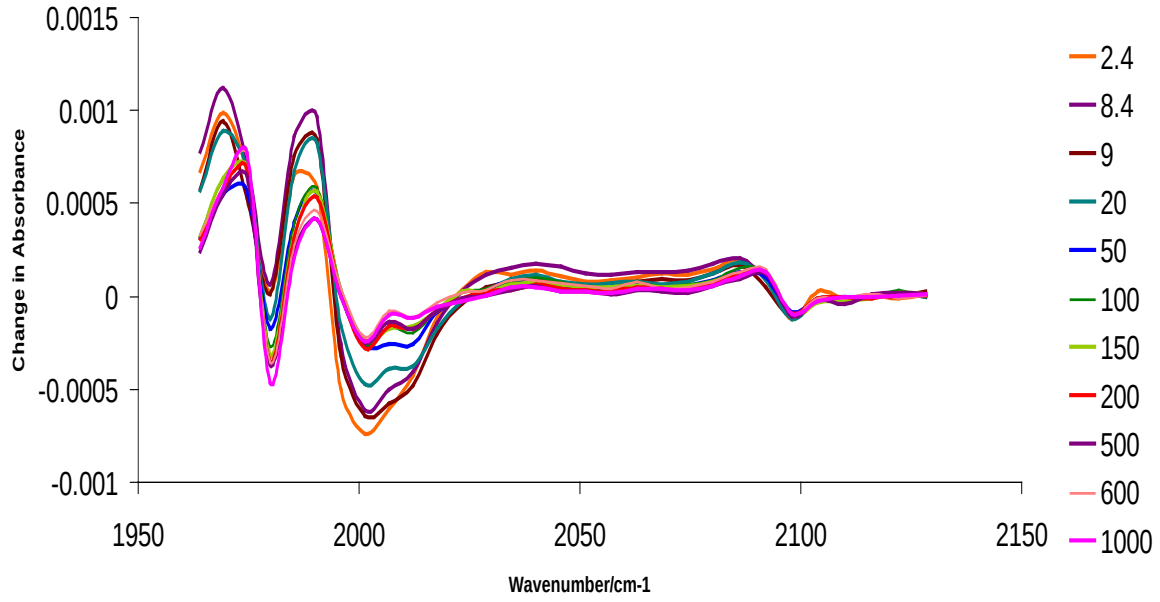

Figure 2.30: *Time resolved infra-red difference spectra following laser photolysis (λ_{exc} = 470 nm) for [5-phenyl-4,6-dipyrrinatoRe(CO)$_4$] in heptane. Legend indicates time in ps.*

The TRIR data for the complex [5-phenyldipyrrinatoRe(CO)$_3$PPh$_3$] was measured in DCM. Upon excitation at 320nm the transient bands are generated within the laser pulse at 1875, 1909 and 2000 cm^{-1} with depletion of parent bands at 2020, 1923 and 1896 cm^{-1}. The newly formed transient bands are assigned to a PPh$_3$ to dipyrrin ^{3}LLCT excited state. This shifting of the excited state bands to lower wavenumbers indicates shifting of electron density to the Re carbonyls and a long lived excited state which persists up to 500 ps.

The above explanation was made based on the results obtained from the similar reported TRIR spectra of [Re(PPh$_2$)(CO)$_3$(bpy)] complex.[61] In this study the excited state bands formed at 1900 and 2000 cm^{-1} after 400 nm excitation are shifted to lower wavenumbers 1881 and 1991 cm^{-1} from their ground state position by approximately 9 cm^{-1}. This shift of the IR bands to lower wavenumbers was assigned to a PPh$_2$→bpy LLCT transition of the lowest triplet excited state of the complex.

2.2.6. Thermal and photochemical CORMs studies

The release of CO from the dipyrrinato rhenium carbonyl complexes were studied spectrophotometrically by measuring the conversion of deoxy-myoglobin (deoxy-Mb) to carbomonoxy myoglobin (Mb-CO). [62, 63] The typical spectra of deoxy-Mb and Mb-CO are represented in **Figure 2.31**. The amount of Mb-CO formed was quantified by measuring the absorbance at 540 nm. A stock solution of myoglobin (lyophilised horse heart 66 μM final concentration) was prepared fresh by dissolving the protein in 0.01 M (pH = 7.4) phosphate buffered saline (PBS). Sodium dithionite (0.1 %) was added to convert the myoglobin stock to deoxy-Mb. A 2 mL quantity of this was measured to obtain a deoxy-Mb spectrum and then bubbled with CO to get an Mb-CO spectrum. CORMs were dissolved in DMSO (8 and 12 mM) and added to deoxy-Mb in the cuvette to give a final CORM concentration of 40 and 60 μM, mixed using a pipette and then overlaid with 500 μL light mineral oil to prevent CO escaping or myoglobin being oxygenated. The CO-release rate was measured both thermally at body temperature (37 ^{o}C) and photochemically. While monitoring the thermal CO release of complexes, the temperature of the water bath (where incubation of cuvettes took place) was held constant for the duration of the experiment. The complexes analysed thermally were covered in tinfoil to ensure that there were no photochemical effects. CO releasing properties from the dipyrrin based Re(I) tetracarbonyl complexes under study is presented in **Table 2.5**.

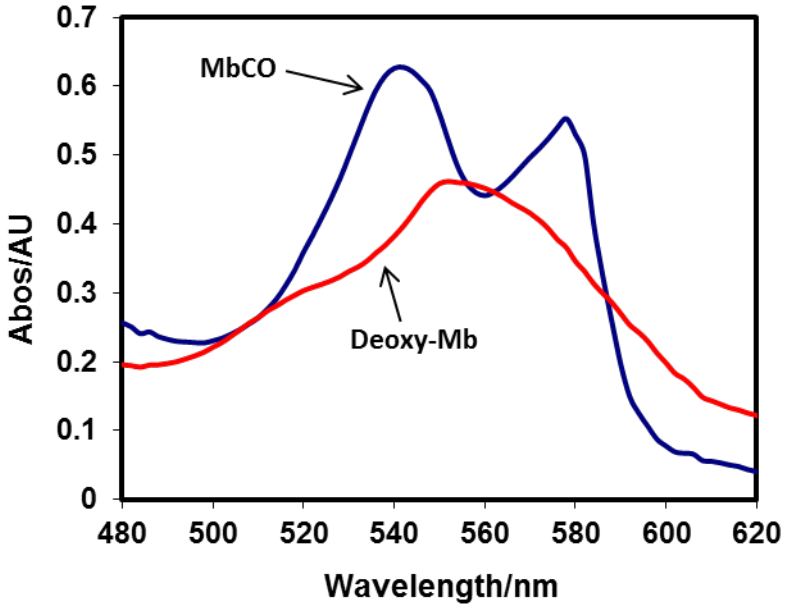

Figure 2.31: *The release of CO by measuring the conversion of deoxy-Mb to Mb-CO*

The amount of [Mb-CO] formation is calculated using following equations

The maximal absorption peak of deoxy-Mb at 560 nm is converted to the two maximal absorption peaks of Mb-CO at 540 and 578 nm. The concentration of myoglobin in the stock solution was calculated from the maximal absorption peak of the Mb-CO solution at 540 nm (Equation 1). Since using 8 and 12 mM solutions the complex released CO instantly, 40 µM and 60 µM solutions were used to carry out all the experiments.

Equation 1

Equation for calculating total myoglobin concentration in a saturated solution of Mb-CO. ε = extinction coefficient of Mb-CO = 15.4 $mM^{-1}cm^{-1}$, OD_{540} = absorbance of Mb-CO solution at 540 nm.

$$\text{Mb-CO}_{max} = \left(\frac{OD_{540}}{\varepsilon}\right)\times 1000$$

From the graph of standard Mb-CO solution, OD_{540} = 0.625885

$$\text{Therefore, Mb-CO}_{max} = \left(\frac{0.625885}{15.4}\right)\times 1000$$

$$= 40.6418 \text{ mM}$$

Intermediate concentrations of Mb-CO are calculated from the OD_{540}. A new extinction coefficient (ε_2) must be calculated to take into account the change in absorbance at 540 nm (ΔOD_{540}). To aid in the accuracy of this calculation, another wavelength is used as a constant reference point. The deoxy-Mb and Mb-CO spectra share four isosbestic (OD_{iso}) points (510, 550, 570, 585 nm). The value at 510 nm (OD_{iso510}) was used in this experiment. The new extinction coefficient was calculated (Equation 2).

Equation 2

Equation needed to calculate unknown Mb-CO extinction coefficient. ΔOD_{iso510} = change in absorbance at the isosbestic point, ΔOD_{540} = change in absorbance at 540 nm, Mb-CO_{max} = maximum concentration of myoglobin. ε_2 = new extinction coefficient.

$$\varepsilon_2 = \frac{(\Delta OD_{540} - \Delta OD_{iso510})\times 1000}{MbCO_{max}}$$

Table 2.5 *Thermal (37 ^{o}C) CO release data from Rhenium based dipyrrin carbonyl complexes, 60 µM represents the concentration of the Re complexes in solution.*

Name of the Complex	**Total Time Required for Thermal CO Release (60 µM) (min)**	**($t_{1/2}$)**
[2,8-diethyl-1,3,7,9-tetramethyl-5-pyrenyl-4,6-dipyrrinatoRe(CO)$_4$]	85	35 min
[2,8-diethyl-1,3,7,9-tetramethyl-5-mesityl-4,6-dipyrrinatoRe(CO)$_4$]	No release	-
[5-phenyl-4,6-dipyrrinatoRe(CO)$_4$]	240	85 min
[5-phenyl4,6-dipyrrinatoRe(CO)$_3$PPh$_3$]	No release	-

The CO-release profile for the [2,8-diethyl-1,3,7,9-tetramethyl-5-pyrenyl-4,6-dipyrrinatoRe(CO)$_4$] complex (60 µM) when studied at body temperature (37 ^{o}C) is illustrated in **Figure 2.32**. At 0 min, there was one distinct absorption peak characteristic of deoxy-Mb. Over time, the intensity of the Q band at approximately 554 nm slowly decreased while the characteristic peaks of Mb-CO appeared at 546 nm and 578 nm. It can be deduced from the overall spectral changes that after 85 mins CO release had ceased as no further changes were observed in the UV-Vis spectra. From the fitted curve the $t_{1/2}$ calculated for the amount of [Mb-CO] formation for the complex [2,8-diethyl-1,3,7,9-tetramethyl-5-pyrenyl-4,6-dipyrrinatoRe(CO)$_4$] is 35 mins (see **Figure 2.33**). Upon irradiation with monochromatic light at 532, 470 and 355nm, no spectral changes that are

characteristic of CO release were observed in the Q band region up to 24 hours. Only one peak characteristic of deoxy-Mb was observed.

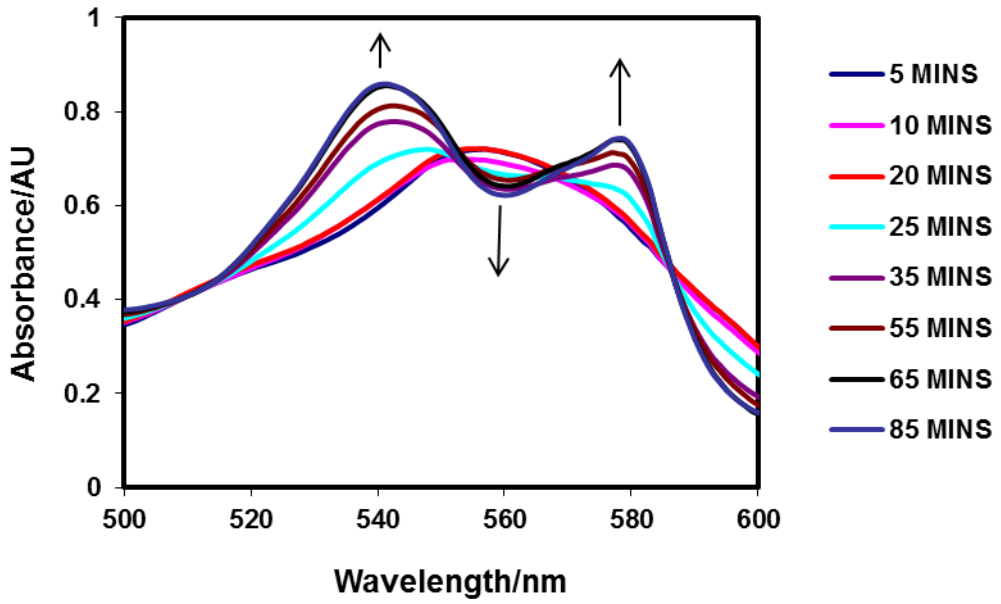

Figure 2.32: *CO-release profile for [2,8-diethyl-1,3,7,9-tetramethyl-5pyrenyl-4,6-dipyrrinatoRe(CO)$_4$] complex (60 µM) recorded at 37 ^{o}C using deoxymyoglobin solution (66 µM). Legend shows time passed in mins.*

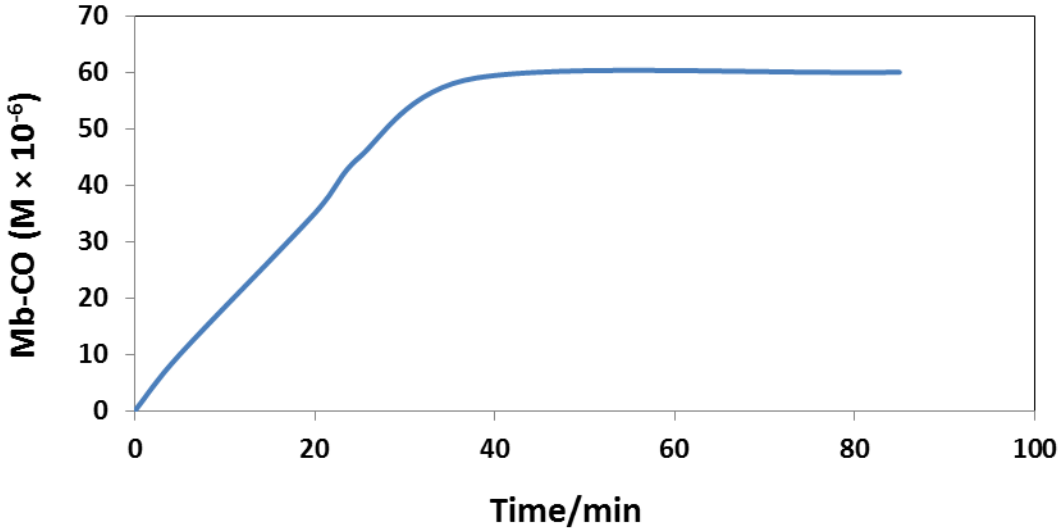

Figure 2.33: *Formation of Mb-CO quantified over time for [2,8-diethyl-1,3,7,9-tetramethyl-5pyrenyl-4,6-dipyrrinatoRe(CO)$_4$] complex (60 µM).*

The [5-phenyl-4,6-dipyrrinatoRe(CO)$_4$] complex was also studied for the release of CO both thermally and photochemically. It was found that the complex released CO only thermally at 37 ^{o}C after 240 mins of carrying out the experiment (see **Figure 2.34**). The $t_{1/2}$ calculated for the formation of amount of Mb-CO for the complex [5-phenyl-4,6-dipyrrinatoRe(CO)$_4$] is 85 mins (see **Figure 2.35**). In presence of light when the complex was irradiated at 470 nm or 355 nm and no spectral changes were observed up to 18 hours, indicating the complex does not release of CO spontaneously under photochemical conditions.

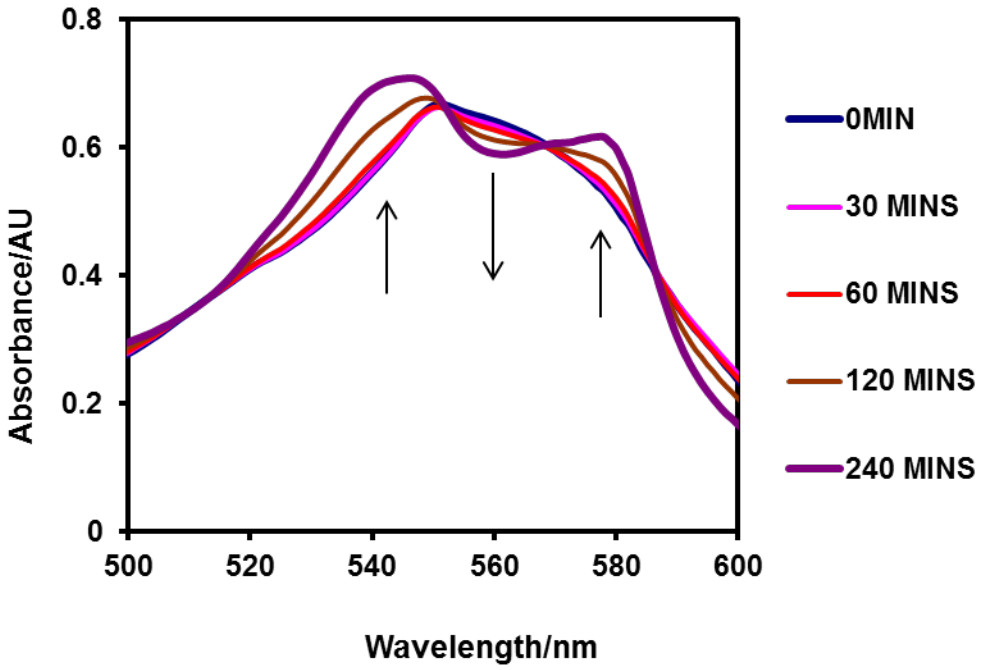

Figure 2.34: *CO-release profile for [5-phenyl-4,6-dipyrrinatoRe(CO)$_4$] complex (60 μM) recorded at 37 ^{o}C using deoxymyoglobin solution (66 μM). Legend shows time passed in mins.*

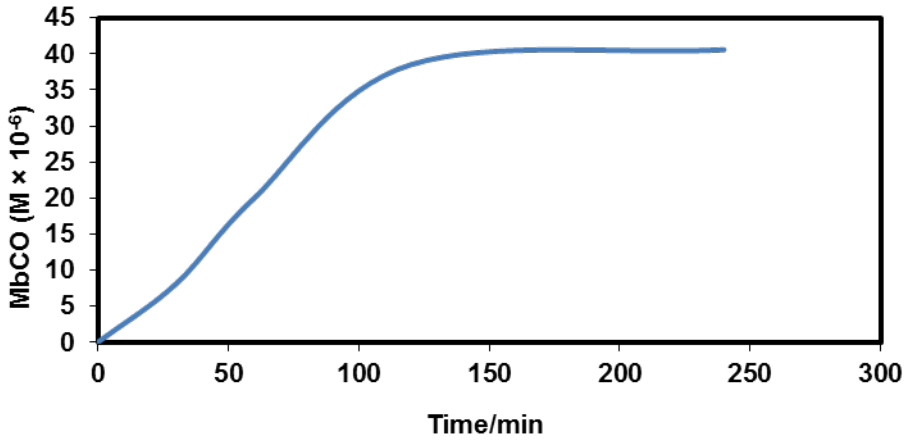

Figure 2.35: *Formation of Mb-CO quantified over time for the [5-phenyl-4,6-dipyrrinato]Re(CO)$_4$ complex recorded at 37 ^oC*

No CO releasing properties were observed for [5-mesityldipyrrinatoRe(CO)$_4$] and [5-phenyldipyrrinatoRe(CO)$_3$PPh$_3$] complexes when assessed using the myoglobin assay both photochemically and thermally at 37 ^oC. The complexes were found to be inert towards the CO releasing investigations.

Clear differences exist between the CORMs evaluated. A comparison of these Re based carbonyl complexes show the importance of pyrenyl substituent at the 5th position of the dipyrrin ligand. The amount of Mb-CO formation for [5-pyrenyldipyrrinatolRe(CO)$_4$] complex was fast and $t_{1/2}$ was found to be 35 min compared to other Re based dipyrrin carbonyl complexes under study. Hence, alteration of this substituent to a mesityl or phenyl group shows a significant loss in CO releasing activity. Whereas existence of methyl and ethyl groups on the dipyrrin ligand does not make a notable change in CO releasing activity. Furthermore it can be confirmed that Re tetracarbonyl complexes are much better CO releasing molecules when compared to Re tri carbonyl complex which might be due to high stability of the latter in DMSO solution.

In the past a number of Rhenium based carbonyl complexes with different attachment of ligands have been studied for their CO releasing abilities both thermally and photochemically.[64, 65] Thus in this study an attempt was made to study the CO releasing properties of the following complexes [5-phenyldipyrrinatoRe(CO)$_4$], [5-

pyrenyldipyrrinatoRe$(CO)_4$], [5-mesityldipyrrinatoRe$(CO)_4$] and [5-phenyldipyrrinatoRe$(CO)_3PPh_3$]. It was found that among all the Rhenium carbonyl complexes, [5-pyrenyldipyrrinatoRe$(CO)_4$] and [5-phenyldipyrrinatoRe$(CO)_4$] were the fastest and slowest thermal CO releaser respectively. [5-pyrenyldipyrrinatoRe$(CO)_4$] complex can be considered as a potential thermal CO releasing molecule and further studies can be carried out to investigate the toxicity of the complex against the cells.

2.3 Conclusion

In this chapter synthesis, characterisation, picosecond time resolved infra-red spectroscopy and CO releasing properties of novel Rhenium tetra and tri carbonyl complexes of dipyrrin complexes were studied. All of the complexes synthesised were characterised using ^{1}H NMR, UV-vis and Infrared spectroscopic techniques. Pico-second TRIR studies were carried out on a number of the carbonyl complexes.

The UV-Vis spectra of the ligands indicate strong absorbance in UV-Vis region of the spectrum. This shows dipyrrin ligand based π-π* transitions. The corresponding tetra and tricarbonyl complexes show a bathchromic shift in the UV-Vis region and sharpening of the peak when compared to respective ligands which primarily is due to π-π* transitions of dipyrrinato ligand with a certain degree of metal-ligand charge transfer.

Excitation of the 5-pyrenyldipyrrin ligand at 344 nm led to emission at 389 nm, which was attributed to pyrene based π-π* transition. Similarly excitation of [5-pyrenyldipyrrinatoRe$(CO)_4$] at 344 nm gave rise to emission comprising an intense peak at 416 nm and two weaker peaks at 482 and 545 nm, which were assigned to a mixture of ^{3}IL and ^{3}MLCT transitions. The non-emissive profile observed for all the complexes when excited in the range of 485 – 522 nm is due to the complexation of the dipyrrin to the rhenium carbonyl moiety.

The infra-red spectra of the tetracarbonyl complexes have metal carbonyl stretching frequencies from 1850-2050 cm^{-1} in form of four bands whereas CO frequencies of tricarbonyl complex of rhenium appear as three bands from 1880-2030 cm^{-1}.

Picosecond TRIR studies were carried out on tetracarbonyl Re dipyrrin complexes in solution, which allowed for the identification of excited states upon laser photolysis. Excitation of the [5-mesityldipyrrinatoRe$(CO)_4$] complex at 520 nm resulted in decay of parent bands of metal tetra carbonyl moiety with formation of IL dipyrrin based excited

state at lower wavenumbers within 1 ps. Shifting of initially present excited state band at 1959 cm^{-1} to 1965 cm^{-1} further suggested that in addition to conversion of a IL π-π* excite state it is also possible that the complex undergoes vibrational cooling but the two process overlap in the TRIR spectra. The excited state is long lived and persisted on the nanosecond timescale. Similarly, excitation of [5-phenyldipyrrinatoRe$(CO)_4$] at 470 nm resulted in formation of transient bands at lower wavenumbers compared to its parent absorptions. This was assigned to the formation of IL π-π* dipyrrin based excited state. Further, shifting of transient bands to slightly higher wavenumbers even after 50 ps was explained due to two processes; vibrational cooling and interconversion between IL π-π* states within the dipyrrin ligand. TRIR spectrum of the complex [5-phenyl-4,6-dipyrrinatoRe$(CO)_3PPh_3$] on excitation at 320 nm in DCM revealed the formation of transient bands at lower wavenumbers are due to phenyl based dipyrrin LLCT character of the excited state of the complex.

Re tetra and tri carbonyl complexes were also studied for their photo and thermal CO release using myoglobin assays. During the CORM studies it was found that tetracarbonyl complexes only release CO thermally at 37 ^oC. The fastest CO releaser among dipyrrin based Re tetracarbonyl complexes was found to be pyrene based dipyrrinato Re tetracarbonyl complex. Hence, it can be concluded that [5-pyrenyldipyrrinatoRe$(CO)_4$] complex can act as potential CO releasing molecule under thermal conditions at pH at 7.4. No CO was released when [5-mesityldipyrrinatoRe$(CO)_4$] and [5-phenyldipyrrinatoRe$(CO)_3PPh_3$] complexes were investigated for their ability to release CO both thermally and photochemically.

Hence, it can be concluded that the results from time resolved infrared studies and photochemical CORM studies agreed with each other and supported the fact that photochemical CO loss from these dipyrrin based complexes is not possible. Further several synthetic methods were tried to synthesise similar bis-pyrrolic based Mn tetra and tricarbonyl complexes. The reactions carried out were not successful.

2.4 Experimental

2.4.1 Materials

All manipulations were carried out under an atmosphere of argon or nitrogen using standard Schlenk techniques. All solvents were supplied by the Sigma Aldrich Chemical Company. Dichloromethane, chloroform, petroleum ether 40:60, pentane and hexane were dried over $MgSO_4$ prior to use. Toulene was distilled over potassium hydroxide before use. Pyrrole was distilled over sodium hydroxide using a short path distillation apparatus prior to use. All other chemicals were obtained commercially and were used without further purification. Silica gel (Merck) was used as received. All mobile phases for column chromatography were dried over $MgSO_4$ before use. All the synthesised Re tetracarbonyl complexes have been submitted for Mass spectroscopic analysis and we await the results.

2.4.2 Equipment

^1H NMR were recorded on a Bruker AC 400 spectrometer in $CDCl_3$ and were calibrated according to the residual solvent peak i.e., $CHCl_3$ at 7.26 ppm for all ^1H spectra. Chemical shifts are given in parts per million (ppm). Proton coupling constants (*J*) are given in Hertz (Hz). XWIN-NMR processor and ACDLABS 12.0 NMR processor software were employed to process the free induction decay (FID) profiles. IR spectra were recorded on a Perkin-Elmer 2000 FT-IR spectrophotometer (2 cm^{-1} resolution) in a 0.1 mm sodium chloride liquid solution cell. All UV-vis spectra were measured on an Agilent Technologies 8453 photodiode array spectrometer using a 1 cm path length quartz cell. Emission spectra (accuracy ±5 nm) were recorded at 298 K using a LS50B luminescence spectrophotometer, equipped with a red sensitive Hammatsu R928 PMT detector, interfaced with Elonex PC466 employing Perkin-Elmer FL WinLab custom built software. All ASCII data were further processed by Microcal Origin 6.0 pro software. The optical densities of all of the sample solution were 0.15- 0.2 A.U. at the excitation wavelength. The lifetimes of samples were determined using an Edinburgh Instruments nf900 ns flashlamp interfaced to a CD900 TAC photon counter. Samples were degassed by bubbling nitrogen through sample for 15 min. Lifetime errors were estimated to be less than 10 %. The TRIR experiments were carried out in Prof. Wybren J. Buma's laboratory, University of Amsterdam and the data obtained were processed and plotted with the help of Prof. Conor Long.

For the transient IR measurements, UV pump and mid-IR probe pulses were generated using a Ti:sapphire laser (Spectra-Physics Hurricane, 600 μJ) with a repetition rate of 1kHz. The UV pump pulse (400nm) was generated by SHG. By DFG of the signal and idler from a BBO-based OPA (Spectra-Physics OPA-800C) in AgGaS2, IR probe pulses were generated. The delay positions were scanned by mechanically adjusting the beam-path of the UV pump using a Newport ESP300 translation stage. The temporal resolution of 200 fs has been obtained from FWHM of the pump probe cross-correlate function. All of the TRIR spectra were obtained after a 150fs laser excitation pulse with energy between 1.5-2.0 μJ.

2.5 Synthesis

2.5.1 Synthesis of 5-phenyl-4,6-dipyrrin

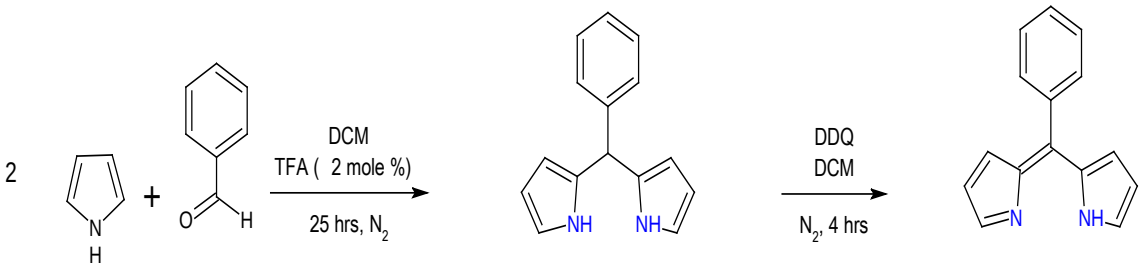

Benzaldehyde (0.01 mol/ 1.1 mL), distilled pyrrole (0.021 mol/1.46 mL) and trifluoroacetic acid (0.1×10^{-3} mol/ 20 μL) were added to nitrogen purged DCM (50 mL) and stirred for 4 hours under inert atmosphere. After this point DDQ (0.01 mol/ 0.265 g) was added and the solution was stirred for 1 hour. The solvent was evaporated and the residue was purified by column chromatography using silica gel and a mobile phase of hexane: ethylacetate (80:20) which afforded a yellow solid. Spectroscopic data were in good agreement with reported data.[31]

Yield: 0.55 g, 0.0025 mol, 25 %.

^{1}H NMR (400 MHz, $CDCl_3$) δ ppm 5.31 (s, 1 H) 6.60 (d, *J*=2.02 Hz, 2 H) 6.78 (d, *J*=4.55 Hz, 2 H) 7.43 - 7.58 (m, 5 H) 8.10 (br. s., 2 H)

2.5.2 Synthesis of 2,8-diethyl-1,3,7,9tetramethyl-5-pyrenyl-4,6-dipyrrin

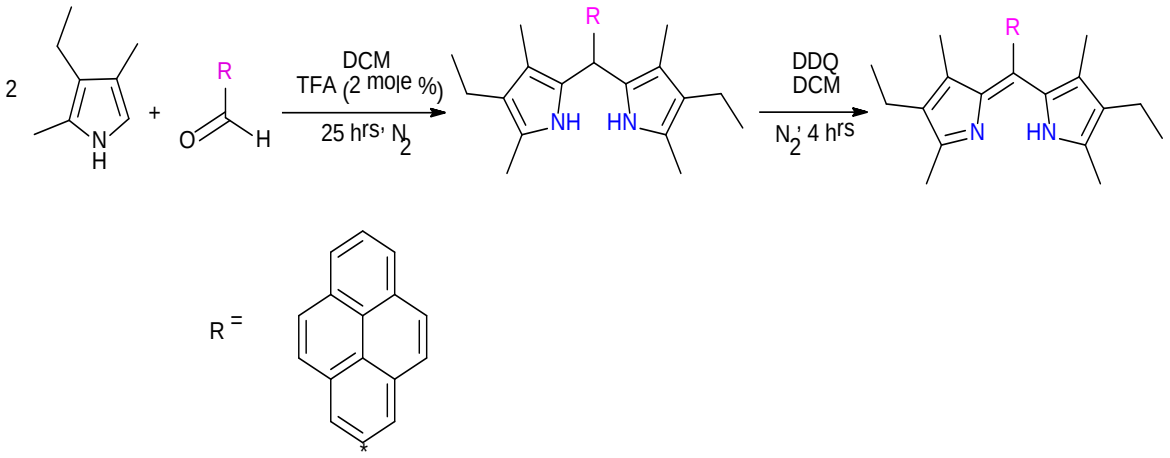

Pyrene-1-carboxaldehyde (0.015 mol/0.253g), kryptopyrrole (0.022 mol/0.3 mL) and trifluoroacetic acid (0.0001 mol/ 20μL) were dissolved in nitrogen purged DCM (50mL). The solution turned dark pink and was stirred for 25hours until aldehyde was fully consumed. Then, DDQ (0.011 mol/0.249 g) was added to the solution and the reaction mixture was further stirred for 4 hours under inert atmosphere. The solvent was evaporated and the residue was purified by column chromatography using silica gel and a mobile phase of hexane: ethylacetate (80:20) which afforded an orange solid.

Yield: 2.7g, 0.006mol, 40 %.

^{1}H NMR (400 MHz, $CDCl_3$) δ ppm 0.66 (s, 5 H) 0.91 (t, *J*=7.45 Hz, 7 H) 2.20 (q, *J*=7.66 Hz, 4 H) 2.39 (s, 6 H) 7.90 - 8.08 (m, 3 H) 8.08 - 8.29 (m, 7 H)

2.5.3 Synthesis of 2,8-diethyl-1,3,7,9-tetramethyl-5-mesityl-4,6-dipyrrin

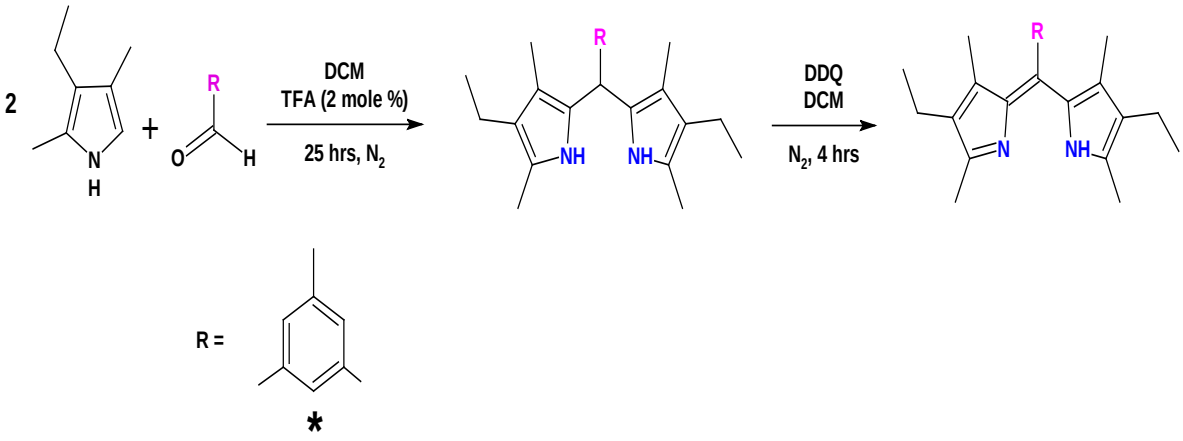

2,8-diethyl-1,3,7,9-tetramethyl-5-mesityl-4,6-dipyrrin was synthesised following the procedure described in 2.5.2. Mesitaldehyde (2.2 mmol/ 0.325 mL), kryptopyrrole (4.4 mmol/ 0.6 mL) and trifluoroacetic acid (0.0002 mol/ 40 µL) were dissolved and stirred in nitrogen purged DCM (100 ml). After 25 hours of stirring the reaction mixture DDQ (2.2 mol/ 0.500 g) was added and the solution was further stirred for 1 hour. The solvent was evaporated and the residue was purified by column chromatography using silica gel and a mobile phase of hexane: ethylacetate (80:20) which afforded an orange solid.

Yield: 0.329 g, 0.88 mmol, 40 %.

^{1}H NMR (400 MHz, $CDCl_3$) δ ppm 0.97 (t, *J*=7.58 Hz, 6 H) 1.20 (s, 6 H) 2.10 (s, 6 H) 2.25- 2.37 (m, 13 H), 2.28 (q, *J*=7.41 Hz, 4 H), 2.32 - 2.35 (m, 9 H)

2.5.4 Synthesis of [5-phenyl-4,6-dipyrrinatoRe(CO)$_4$]

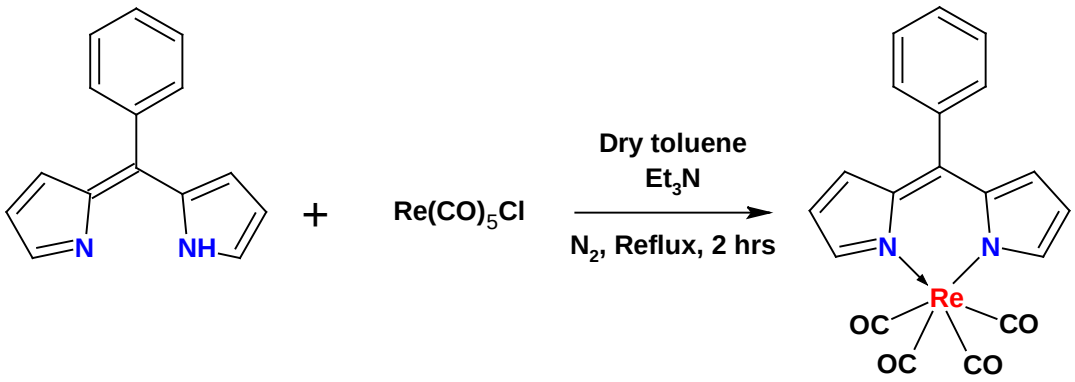

The [5-phenyl-4,6-dipyrrinatoRe(CO)$_4$] complex was synthesised following the work reported by Telfar *et al.*[31] 5-phenyl-4,6-dipyrrin (0.0024 mol/ 0.52 g) and rhenium pentacarbonyl (0.0025 mol /0.9 g) were dissolved in dry toluene (40 mL) and heated to 100 °C. Dry triethylamine (0.0025 mol/0.35 mL) was added and the heating was continued for 2 hours. All the solvents were removed under reduced pressure. An orange coloured product was obtained which was further purified by column chromatography using neutral alumina and the mobile phase hexane:DCM (80:20).

Yield: 0.520 g, 0.001 mol, 42 %.

^{1}H NMR (400 MHz, $CDCl_3$) δ ppm 6.46 (d, *J*=5.81 Hz, 2 H) 6.66 (d, *J*=4.55 Hz, 2 H) 7.42 - 7.52 (m, 5 H) 7.92 (s, 2 H).

^{13}C NMR (400 MHz, $CDCl_3$) δ ppm 118.59, 123.58, 127.38, 128.52, 130.23, 132.70, 137.27, 138.03, 148.87, 154.95, 205.54.

IR ν_{CO} (pentane): 2105, 2004, 1978, 1933 cm^{-1}.

2.5.5 Synthesis of [5-phenyl-4,6-dipyrrinatoRe(CO)$_3$PPh$_3$]

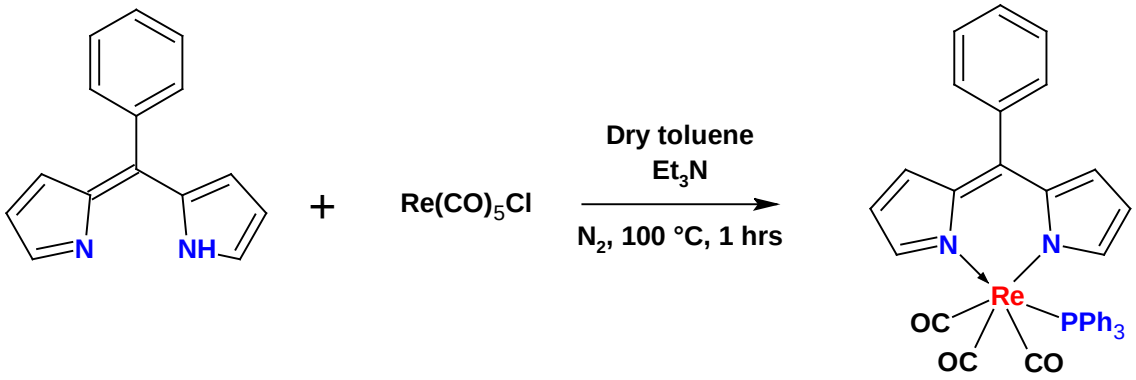

The [5-phenyl-4,6-dipyrrinatoRe(CO)$_3$PPh$_3$] was synthesised using the procedure described in section 2.5.4. 5-phenyl-4,6-dipyrrin (0.0026 mol/ 0.572 g) and rhenium pentacarbonyl (0.003 mol/ 1.13 g) were dissolved in dry toluene (40 mL) and heated to 100 °C under nitrogen atmosphere. Dry triethylamine (0.0026 mol/ 0.36 mL) was added and heating was continued for a further 1 hour. Triphenylphosphine (0.0026 mol/ 0.684 g) was then added and heating was continued for a further 1 hour. Completion of the reaction was monitored by infrared spectroscopy. Solvent was removed and the bright orange colour product was purified by column chromatography using neutral alumina and mobile phase hexane: DCM (80:20) ratio.

Yield: 0.975 g, 0.0013 mol, 50 %.

^{1}H NMR (400 MHz, $CDCl_3$) δ ppm 6.30 (d, *J*=5.81 Hz, 2 H) 6.41 (d, *J*=6.57 Hz, 2 H) 6.52 (d, *J*=8.34 Hz, 1 H) 6.87 - 6.97 (m, 6 H) 7.20 - 7.27 (m, 7 H) 7.32 - 7.41 (m, 7 H) 7.70 (d, *J*=1.26 Hz, 2 H).

^{13}C NMR (400 MHz, $CDCl_3$) δ ppm 118.59, 126.69, 127.06, 128.00, 128.32, 128.39, 129.70, 129.91, 130.24, 130.56, 130.88, 131.87, 133.45, 133.54, 136.68, 138.54, 147.84, 154.21, 196.51.

IR ν_{CO} (pentane): 2020, 1923, 1896 cm^{-1}.

2.5.6 Synthesis of [2,8-diethyl-1,3,7,9tetramethyl-5-pyrenyl-4,6-dipyrrinatoRe(CO)$_4$

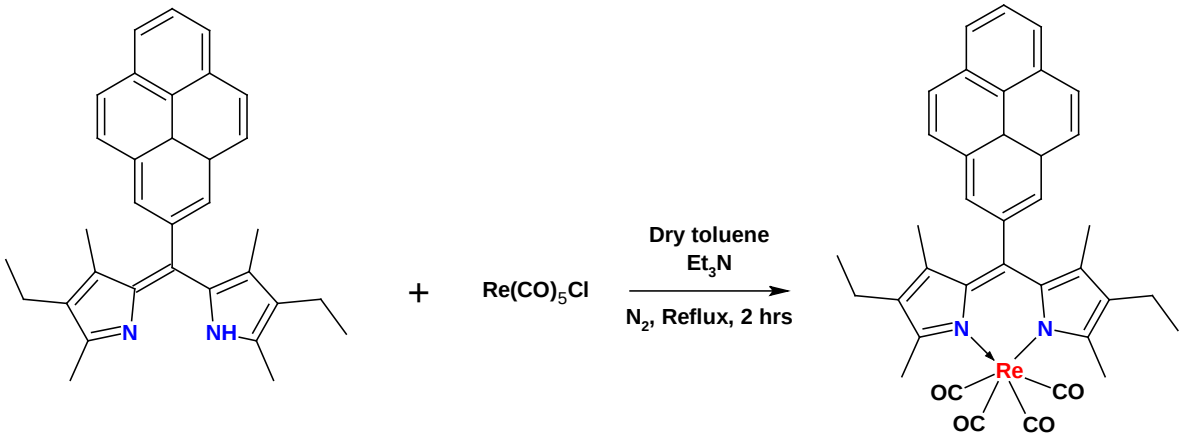

The [5-phenyl-4,6-dipyrrinatoRe(CO)$_4$] was synthesised in similar way as described in section 2.5.4. 2,8-diethyl-1,3,7,9-tetramethyl-5-pyrenyl-4,6-dipyrrin (0.17 mmol/ 0.077 g), rhenium pentacarbonyl (0.17 mmol/ 0.061 g) and dry triethylamine (0.17 mmol/ 0.024 mL) were reacted in dry toluene (20 mL) to obtain an orange colour product. Completion of the reaction was monitored by infrared spectroscopy.

Yield: 0.058 g, 0.08 mmol, 46 %.

^{1}H NMR (400 MHz, $CDCl_3$) δ ppm 0.57 (s, 6 H) 0.87 (t, *J*=7.58 Hz, 7 H) 2.19 - 2.26 (m, 4 H) 2.59 (s, 6 H) 7.87 (d, *J*=7.83 Hz, 1 H) 7.92 - 8.10 (m, 3 H) 8.10 - 8.29 (m, 6 H).

^{13}C NMR (400 MHz, $CDCl_3$) δ ppm 11.22, 14.20, 14.52, 17.52, 21.04, 22.63, 31.60, 60.39, 124.62, 125.15, 126.08, 127.48, 127.64, 130.43, 133.76, 135.58, 136.92, 150.31, 171.14.

IR ν_{CO} (pentane): 2096, 1993, 1974, 1932 cm^{-1}.

2.5.7 Synthesis of [2,8-diethyl-1,3,7,9-tetramethyl-5mesityl-4,6-dipyrrinatoRe(CO)$_4$]

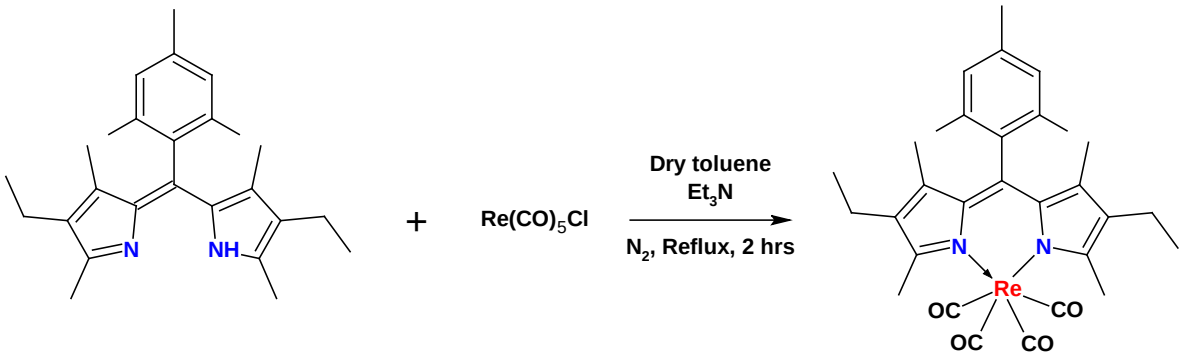

[2,8-diethyl-1,3,7,9-tetramethyl-5-mesityl-4,6-dipyrrinatoRe(CO)$_4$] was synthesised in similar way as described in section 2.5.4. 2,8-diethyl-1,3,7,9-tetramethyl-5mesityl-4,6-dipyrrin (0.3 mmol/ 0.129 g), rhenium pentacarbonyl (0.4 mmol/0.150g) and dry triethylamine (0.3 mmol/ 0.048 mL) were reacted in dry toluene to obtain orange colour product. Completion of the reaction was monitored by infrared spectroscopy.

Yield: 0.09g, 0.135 mmol, 45 %.

^{1}H NMR (400 MHz, $CDCl_3$) δ ppm 0.97 (t, *J*=7.58 Hz, 6 H) 1.20 (s, 6 H) 2.10 (s, 6 H) 2.25- 2.37 (m, 13 H), 2.28 (q, *J*=7.41 Hz, 4 H), 2.32 - 2.35 (m, 9 H).

^{13}C NMR (400 MHz, $CDCl_3$) δ ppm 11.16, 13.83, 17.32, 17.96, 18.80, 20.15, 127.81, 131.22, 134.70, 135.18, 136.03, 137.95, 158.65.

IR ν_{CO} (pentane): 2094, 1991, 1972, 1930 cm^{-1}.

2.6. References

1. A. Loudet and K. Burgess, *Chem. Rev.*, 2007, **107**, 4891-4932.

2. G. Ulrich, R. Ziessel and A. Harriman, *Angew. Chem. Int. Ed.*, 2008, **47**, 1184-1201.

3. N. Boens, V. Leen and W. Dehaen, *Chem. Soc. Rev.*, 2012, **41**, 1130-1172.

4. T. E. Wood and A. Thompson, *Chem. Rev.*, 2007, **107**, 1831-1861.

5. H. Maeda, *Eur. J. Org. Chem.*, 2007, **2007**, 5313-5325.

6. M. Yadav, A. K. Singh and D. S. Pandey, *Organometallics*, 2009, **28**, 4713-4723.

7. E. R. King and T. A. Betley, *Inorg. Chem.*, 2009, **48**, 2361-2363.

8. E. R. King, E. T. Hennessy and T. A. Betley, *J. Am. Chem. Soc.*, 2011, **133**, 4917-4923.

9. D. L. Murphy, M. R. Malachowski, C. F. Campana and S. M. Cohen, *Chem. Commun.*, 2005, 5506-5508.

10. S. R. Halper, L. Do, J. R. Stork and S. M. Cohen, *J. Am. Chem. Soc.*, 2006, **128**, 15255-15268.

11. D. Salazar-Mendoza, S. A. Baudron and M. W. Hosseini, *Chem. Commun.*, 2007, 2252-2254.

12. F. Li, S. I. Yang, Y. Ciringh, J. Seth, C. H. Martin, D. L. Singh, D. Kim, R. R. Birge, D. F. Bocian, D. Holten and J. S. Lindsey, *J. Am. Chem. Soc.*, 1998, **120**, 10001-10017.

13. I. V. Sazanovich, C. Kirmaier, E. Hindin, L. Yu, D. F. Bocian, J. S. Lindsey and D. Holten, *J. Am. Chem. Soc.*, 2004, **126**, 2664-2665.

14. C. H. S. S.Lee, Y. Park, A. Lee,D.H.Jung,S.H.Choi and J. Park, *Mol.Cryst.Liq.Cryst.*, 2010, **531**, 65-72.

15. Y. Li and D. Dolphin, *Can. J. Chem.*, 2011, **89**, 481-487.

16. S. Kusaka, R. Sakamoto, Y. Kitagawa, M. Okumura and H. Nishihara, *Chem. Asian J.*, 2012, **7**, 907-910.

17. T. S. Teets, D. V. Partyka, J. B. Updegraff and T. G. Gray, *Inorg. Chem.*, 2008, **47**, 2338-2346.

18. A. Palma, J. F. Gallagher, H. Muller-Bunz, J. Wolowska, E. J. L. McInnes and D. F. O'Shea, *Dalton Trans.*, 2009, 273-279.

19. S. G. Telfer, T. M. McLean and M. R. Waterland, *Dalton Trans.*, 2011, **40**, 3097-3108.

20. V. S. Thoi, J. R. Stork, D. Magde and S. M. Cohen, *Inorg. Chem.*, 2006, **45**, 10688-10697.

21. J. D. Hall, T. M. McLean, S. J. Smalley, M. R. Waterland and S. G. Telfer, *Dalton Trans.*, 2010, **39**, 437-445.

22. M. Niwa, Y. Kawashima and Y. Murakami, *J. Chem. Soc., Faraday Trans.*, 1985, **81**, 2757.

23. X. Liu, H. Nan, W. Sun, Q. Zhang, M. Zhan, L. Zou, Z. Xie, X. Li, C. Lu and Y. Cheng, *Dalton Trans.*, 2012, **41**, 10199-10210.

24. T. M. McLean, J. L. Moody, M. R. Waterland and S. G. Telfer, *Inorg. Chem.*, 2013, **51**, 446-455.

25. S. M. Crawford, A. Al-Sheikh Ali, T. S. Cameron and A. Thompson, *Inorg. Chem.*, 2011, **50**, 8207-8213.

26. A. Y. L. M.A. Filatov, S.N.Mukhin,S.A.Vinogradov and A.Y. Cheprakhov, *J Am Chem Soc*, 2009, **132**, 9552-9554.

27. Y. Mei, C. J. Frederickson, L. J. Giblin, J. H. Weiss, Y. Medvedeva and P. A. Bentley, *Chem. Commun.*, 2011, **47**, 7107-7109.

28. Y. Rio, D. Sánchez-García, W. Seitz, T. Torres, J. L. Sessler and D. M. Guldi, *Chem. Eur. J.*, 2009, **15**, 3956-3959.

29. C. Clavel, C. Romuald, E. Brabet and F. Coutrot, *Chem. Eur. J.*, 2013, **19**, 2913-2913.

30. R. F. Ziessel, G. Ulrich, L. Charbonnière, D. Imbert, R. Scopelliti and J.-C. G. Bünzli, *Chem. Eur. J.*, 2006, **12**, 5060-5067.

31. T. M. McLean, J. L. Moody, M. R. Waterland and S. G. Telfer, *Inorganic Chemistry*, **51**, 446-455.

32. R. Ziessel, C. Goze, G. Ulrich, M. Césario, P. Retailleau, A. Harriman and J. P. Rostron, *Chem. Eur. J.*, 2005, **11**, 7366-7378.

33. J. K. Laha, S. Dhanalekshmi, M. Taniguchi, A. Ambroise and J. S. Lindsey, *Org. Process Res. Dev.*, 2003, **7**, 799-812.

34. S. J. Smalley, M. R. Waterland and S. G. Telfer, *Inorg. Chem.*, 2008, **48**, 13-15.

35. S. A. Baudron, *Dalton Trans.*, 2013, **42**, 7498-7509.

36. J. E. Fergusson and C. A. Ramsay, *J. Chem. Soc. (Res.)*, 1965, 5222-5225.

37. J. Thomson, I. Jarvis, D. R. H. Green, D. A. Green and T. Clayton, *Geochim. Cosmochim. Acta*, 1998, **62**, 643-656.

38. H. L. Kee, C. Kirmaier, L. Yu, P. Thamyongkit, W. J. Youngblood, M. E. Calder, L. Ramos, B. C. Noll, D. F. Bocian, W. R. Scheidt, R. R. Birge, J. S. Lindsey and D. Holten, *J. Phys. Chem. B*, 2005, **109**, 20433-20443.

39. K. Hanson, A. Tamayo, V. V. Diev, M. T. Whited, P. I. Djurovich and M. E. Thompson, *Inorg. Chem.*, 2010, **49**, 6077-6084.

40. A. Harriman and J. Davila, *Tetrahedron*, 1989, **45**, 4737-4750.

41. M. H. B. Stiddard, *Journal of the Chemical Society (Resumed)*, 1962, **0**, 4712-4715.

42. F. A. Cotton and C. S. Kraihanzel, *J. Am. Chem. Soc.*, 1962, **84**, 4432-4438.

43. P. Datta, P. Gayen and C. Sinha, *Polyhedron*, 2006, **25**, 3435-3440.

44. A. Datta, A. Priyama, S. N. Bhattacharyya, K. K. Mukherjea and A. Saha, *J. Colloid Interface Sci.*, 2008, **322**, 128.

45. P. Datta, A. K. Patra and C. Sinha, *Polyhedron*, 2009, **28**, 525-533.

46. P. A. K. Datta P., Sinha C., *Polyhedron*, 2009, **28**, 525.

47. J.-L. Zuo, W.-F. Fu, C.-M. Che and K.-K. Cheung, *Eur. J. Inorg. Chem.*, 2003, **2003**, 255-262.

48. B. P. Sullivan and T. J. Meyer, *J. Chem. Soc., Chem. Commun.*, 1984, 1244-1245.

49. L. A. Garca-Escudero, D. Miguel and J. A. Turiel, *J. Organomet. Chem.*, 2006, **691**, 3434-3444.

50. M. Wrighton and D. L. Morse, *J. Am. Chem. Soc.*, 1974, **96**, 998-1003.

51. C. Bronner, S. A. Baudron, M. W. Hosseini, C. A. Strassert, A. Guenet and L. De Cola, *Dalton Trans.*, 2010, **39**, 180.

52. M. Yadav, P. Kumar and D. S. Pandey, *Polyhedron*, 2010, **29**, 791-800.

53. M. Yadav, A. K. Singh, B. Maiti and D. S. Pandey, *Inorg. Chem.*, 2009, **48**, 7593-7603.

54. R. J. Shaver and D. P. Rillema, *Inorg. Chem.*, 1992, **31**, 4101-4107.

55. J. A. Pardoen, J. Lugtenburg and G. W. Canters, *J. Phys. Chem.*, 1985, **89**, 4272-4277.

56. M. Buyuktemiz, S. Duman and Y. Dede, *J. Phys. Chem. A*, 2013, **117**, 1665-1669.

57. T. K. Khan, M. S. Shaikh and M. Ravikanth, *Dyes and Pigments*, 2012, **94**, 66-73.

58. M. K. Kuimova, X. Z. Sun, P. Matousek, D. C. Grills, A. W. Parker, M. Towrie and M. W. George, *Photochem. Photobiol. Sci.*, 2007, **6**, 1158-1163.

59. J. Dyer, W. J. Blau, C. G. Coates, C. M. Creely, J. D. Gavey, M. W. George, D. C. Grills, S. Hudson, J. M. Kelly, P. Matousek, J. J. McGarvey, J. McMaster, A. W.

Parker, M. Towrie and J. A. Weinstein, *Photochem. Photobiol. Sci.*, 2003, **2**, 542-554.

60. D. J. Liard, M. Busby, P. Matousek, M. Towrie and A. Vlcek, *J. Phys. Chem. A*, 2004, **108**, 2363-2369.

61. A. Gabrielsson, M. Busby, P. Matousek, M. Towrie, E. Hevia, L. Cuesta, J. Perez, S. ZÃ¡liÅ¡ and A. n. VlcÌŒek, *Inorg. Chem.*, 2006, **45**, 9789-9797.

62. P. Sawle, J. Hammad, I. J. S. Fairlamb, B. Moulton, C. T. O'Brien, J. M. Lynam, A. K. Duhme-Klair, R. Foresti and R. Motterlini, *J. Pharmacol. Exp. Ther.*, 2006, **318**, 403-410.

63. A. J. Atkin, S. Williams, P. Sawle, R. Motterlini, J. M. Lynam and I. J. S. Fairlamb, *Dalton Trans.*, 2009, 3653-3656.

64. F. Zobi, O. Blacque, R. A. Jacobs, M. C. Schaub and A. Y. Bogdanova, *Dalton Trans.*, 2011, **41**, 370-378.

65. P. C. Kunz, W. Huber, A. Rojas, U. Schatzschneider and B. Spingler, *Eur. J. Inorg. Chem.*, 2009, **2009**, 5358-5366.

Chapter 3

Synthesis, time resolved infrared studies, electrochemistry and a thermal assessment of ruthenium (II), rhenium(I) and manganese(I) complexes for their ability to lose CO

Chapter 3 introduces the synthesis, characterisation and photophysical properties of the mononuclear rhenium(I) tricarbonyl, manganese(I) tricarbonyl and mononuclear ruthenium(II) and Ru-Re hetero dinuclear complexes attached to the bis-bipyridine bridging ligand and 2,2'-bipyridine peripheral ligands. The above monomeric and hetero dimeric carbonyl complexes were tested as CO-releasing molecules under different conditions. The pico-second time resolved infrared studies were also carried out for all of the complexes and their electrochemical properties probed.

3.1 Introduction

The design and synthesis of mononuclear and poly-nuclear metal carbonyl complexes are topics of great interest due to their interesting photophysical and photochemical properties.[1, 2] The photophysical and electrochemical properties of theses complexes can be also tuned by varying the ligand architectures coordinating to the metal centres.

This class of metal carbonyl complexes exhibit strong phosphorescence emitting properties possessing long-lived excited states.[3] Therefore these molecules can be used as potential photo-luminescent sensors and supra-molecular photo-devices.[4] Also due to their long-lived excited states they have further been used as active catalysts for the photo and electro-catalytic reduction of CO_2 to various useful chemicals[5-7] as well as used as labelling reagents for biomolecules.[4, 8-11]

3.1.1 Mononuclear rhenium(I) tricarbonyl complexes

Polypyridyl rhenium(I) tricarbonyl complexes have been extensively studied in recent years for their efficient use in photo-driven electron transfer, therapeutic applications as CO releasing molecules and further catalytic purposes in the photo and electrocatalytic reduction of CO_2 to CO. Rhenium(I) tricarbonyl complexes are important candidates for electron and energy transfer systems. The presence of halides in the axial position of complexes of the type $[Re(CO)_3(N\text{^}N)L]$ allows great synthetic freedom and with this, manipulation of the excited state behaviour is possible. For example *fac*-$[Re(CO)_3(bpy)Cl]$ exhibits a broad structureless emission band with a λ_{max} at 610 nm in solution at 298K.[12] In a 77K 4:1 EtOH:MeOH solvent this emission band is blue shifted to 535 nm. This rigidochromic effect is characteristic of the ^{3}MLCT origin of the emissive state of the complex. On cooling to 77K the excited state lifetime increases from 51ns to 2.68μs which is due to the immobility of the solvent dipoles on the timescales involved, resulting in an inability to respond to the change in electronic configuration. Further, Stufkens and co-workers showed the significant importance of the nature of the axial ligand 'X' in *fac*-$[Re(X)(CO)_3(L)]$ complexes where X = Cl, Br, I and L = 2,2′-bipyridine (bpy), pyridine-2-carbaldehyde-N-isopropylimine(iPr-PyCa) and N, N'-di-isopropyl-1,4-diaza-1,3-butadiene(iPr-DAB) (**see Figure 3.1**).[13] Emission maxima of these carbonyl complexes range from 525 nm to 668 nm. The trend in emission wavelength for complexes having a terminal halogen group is as follows; Cl > Br > I. Pyridine based Re(I) complexes have longer lifetimes up to 7.5μs (at 295 K) than that of other Re(I) complexes.

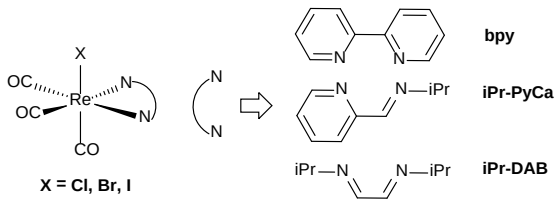

Complex	Emission Max(nm)	Lifetime (μs) (at 298K)
Cl/iPr-DAB	668	0.03
Br/iPr-DAB	666	0.06
I/iPr-DAB	658	0.2
Cl/iPr-PyCa	605	0.4
Br/iPr-PyCa	600	0.7
I/iPr-PyCa	590	1.9
Cl/bpy	532	2.7
Br/bpy	530	3.7
I/bpy	525	7.5

Figure 3.1 *Example of rhenium(I) tricarbonyl complexes*[14]

Time resolved absorption and infrared studies in this class of compounds suggested that the lowest lying excited state transition in *fac*-[Re(L)$(CO)_3$(α-diimine)] is determined by the halide (i.e., X) tethered to the rhenium centre.The excited state character changes predominately from being ^{3}MLCT (Re→α-diimine) in character, when L= Cl to LLCT (X = Br→α-diimine) with bromine. This is attributed to the increased level of mixing between the Re (dπ) and L (pπ) orbitals as the L (pπ) orbital energy increases in going from Cl→Br.

Also it is very important to note that the emission maxima of such systems are very sensitive to the nature of attached polypyridyl ligand and to any substituent on the polypyridyl ligand. For example, there is a considerable shift in the emission wavelength when electron donating or electron withdrawing groups on the bpy ligand in [Re$(CO)_3$(4,4'-X_2-bpy)Cl], are replaced by (X = NEt_2 and NO_2). When X = NEt_2 (electron donating group) the emission wavelength occurs at 575 nm whereas the emission maximum is shifted to 780 nm when X = NO_2 (electron withdrawing group) (see **Figure 3.2**). This effect on emission and absorption spectra of the complexes is due to the change in the HOMO-LUMO energy gap, which varies with the electron withdrawing or electron donating ability of the ligand. [15, 16]

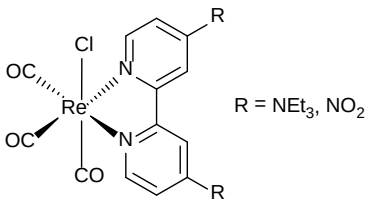

Ligand	Emission Max (nm)
BPY-NO_2	780
BPY-NEt_2	575

Figure 3.2 *Structure of [Re$(CO)_3$(4,4'-X_2-bpy)Cl] type complexes*

Similarly a series of polypyridyl rhenium(I) carbonyl complexes containing isothiocyanate and maleimide groups as electron donating substituents on the polypyridine ligand, result in emission at higher energies than those having electron withdrawing groups. $[Re(phen)(CO)_3(py\text{-}3\text{-}NCS)](CF_3SO_3)$ was found to emit at 530 nm in CH_2Cl_2 solution, while substitution with a more electron withdrawing moiety $[Re(biq)(CO)_3(py\text{-}3\text{-}NCS)](CF_3SO_3)$ (biq = 2,2' biquinolinyl) resulted blue shift in the emission maximum occurring at 642 nm, thus suggesting a ^{3}MLCT Re (d) $\rightarrow\pi^*$ (polypyridine ligand) state.[17]

Wrighton and co-workers first studied the emission states of $[Re(CO)_3(3\text{-}bopy)_2Cl]$ and $[Re(CO)_3(4\text{-}bopy)_2Cl]$ (bopy = 3-benzoylpyridine or 4-benzoylpyridine) where they showed ^{3}MLCT and ^{3}IL states can both be the lowest emission states for these particular type of complexes.[18] Excitation of the complexes $[Re(CO)_3(3\text{-}bopy)_2Cl]$ and $[Re(CO)_3(4\text{-}bopy)_2Cl]$ resulted in broad and structure-less emission spectra with maxima at 560 nm and 600 nm respectively at (RT) which was assigned to a ^{3}MLCT excited state. Excitation of the 4-bopy complex at 77K resulted in an increase in emission intensity with two components, where lifetimes of 18 μs and 1400 μs at room temperature and 77K were observed respectively. The short lived component is assigned to a ^{3}MLCT state while the long lived component is attributed to a ^{3}IL state.[19]

The photophysical properties of acetylide and gold(I) acetylide derivatives of $[Re(CO)_3(phen)Cl]$ complexes were studied using absorbance, luminescence and time resolved spectroscopic techniques with the results revealing the existence of mixed ^{3}MLCT and ^{3}IL excited states.[20] The room temperature excited state decay for the complex [Re(phen-C≡C-H$(CO)_3$Cl] was found to be MLCT character, while upon cooling to 77K a lower lying excited state with ^{3}IL character, localised on the polypyridyl ligand, was observed. Whereas the gold coordinated analogue exhibited a more complex excited state behaviour with mixed MLCT (Re-phen) and ^{3}IL excited state decay character at room temperature.

The ultrafast excited state dynamics of *fac*-$[Re(CO)_3(t\text{-}stpy)(bpy)]^+$ and $[Re(CO)_3(t\text{-}stpy)_2]$ (stpy = strylpyridine) have been recently studied and found to have both ^{3}MLCT and ^{3}IL character.[21] Excitation of the ^{1}MLCT absorption band of *fac*-$[Re(CO)_3(t\text{-}stpy)(bpy)]^+$ results in population of a Re$\rightarrow$bpy(π^*) ^{3}MLCT excited state. This decays over 3.5 ps via an intramolecular energy transfer process to form a ^{3}IL with a *trans*-stpy geometry. This state decays to the ground state and isomerises on the ns timescale. Thus, coordination of the *trans*

4-styrylpyridine moiety allows for population of the reactive ^{3}IL state via ISC from the initially formed ^{3}MLCT state (**See Figure 3.3**).

Another similar analogous system *fac*-[Re(papy)(CO)$_3$(bpy)]$^+$ (papy = phenylazopyridine) when irradiated at 350 nm resulted in *cis-trans* isomerisation of the papy ligand. A TRIR spectroscopic study of *fac*-[Re(CO)$_3$(papy)$_2$Cl] and *fac*-[Re(papy)(CO)$_3$(bpy)]$^+$ indicated that both complexes share a common lowest lying excited state. Irradiation of *fac*-[Re(papy)$_2$(CO)$_3$Cl] populates both the $^1\pi\pi^*$ and ^{1}MLCT (papy) states which undergo ISC to the $^3\pi\pi^*$ state.[22] This is in contrast to previous studies on similar complexes where the ^{3}MLCT state was populated following ISC from the $^1\pi\pi^*$ and ^{1}MLCT states (see **Figure 3.3**). It is proposed that this may be due to either the ^{1}MLCT (papy) state which is populated but decays too quickly to be measured or that population of this state is circumvented by faster ISC to populate the $^3\pi\pi^*$ state via the $^1\pi\pi^*$ and ^{1}MLCT states.

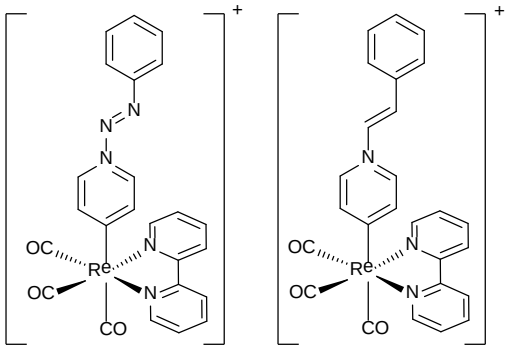

Figure 3.3 *Structure of fac-[Re(papy)$_2$(CO)$_3$(bpy)]$^+$ and fac-[Re(stpy)$_2$(CO)$_3$(bpy)]$^+$ complexes*

Recently a number of phosphido and amido based rhenium complexes [Re(CO)$_3$(ER$_2$)(bpy)] (where ER$_2$ = NHPh or PPh$_2$) were synthesised and studied by Vlcek and co-workers.[23] This class of compounds displayed an unusual absorbance pattern in the region of 590-720 nm in THF. DFT studies suggest that the electronic absorption band is solely due to HOMO-LUMO transition, ER$_2$→bpy LLCT. These complexes were found to be very different from the typical Re(I) carbonyl complexes containing halide or N-donor ligands because charge-transfer occurs largely from a ligand based molecular orbital rather than typical Re→L anti-bonding orbital. TRIR studies suggested a ligand based L→L charge transition is followed

rather than M→L charge transfer and as a result a very small shift in ν_{CO} frequencies was observed.

Another class of chelating ligands based on 4-(2pyridyl)-1,2,3-triazole motifs have been developed by Obata *et al.*[24] A number of 4-(2-pyridyl)-1,2,3-triazole derivatives have been synthesised and studied via click-coupling reactions involving Cu(I) catalysed reactions of an terminal alkyne with an azide group. $[Re(CO)_3Cl(Bn\text{-}pyta)]$ (where bn-pyta = 1-benzyl-4-(2-pyridyl)-1,2,3-triazole) was found to be highly emissive, possessing an emission band at 633 nm in acetonitrile solution, and was blue shifted by almost 100 nm compared to $[Re(CO)_3Cl(bpy)]$. At 77K in Me-THF the excited state lifetime for $[Re(CO)_3Cl(Bn\text{-}pyta)]$ (τ = 8.90 μs) is considerably longer than that observed for $[Re(CO)_3Cl(bpy)]$ (τ = 3.17 μs) under the same conditions.[25]

Li *et al.* showed the use of $Re(CO)_3$-pheanthroline as potential photo-luminoscent in high efficiency organic light emitting diodes (OLEDs). The Re(I) bipyridyl complex $[Re(CO)_3(DDPA)Br]$ (where DDPA = 2,9-dimethyl-4,7-diphenyl-1,10-phenanthroline) was employed in a 4,4'-N,N'-dicarbazole-biphenyl host matrix as an emissive dopant for the fabrication of the OLEDs (see **Figure 3.4**). This system demonstrated high electroluminescence efficiency (21-8 cd/A) and luminescence 8315 cd/cm^2. The high performance was attributed to the structure of the $[Re(CO)_3(DDPA)Br]$ complex.[26]

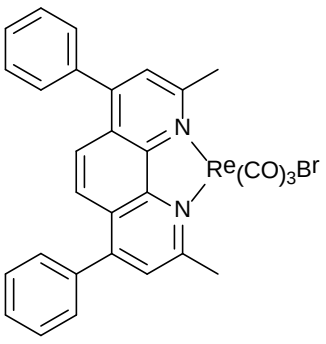

Figure 3.4 *Structure of Re(I) bipyridyl complex $[Re(CO)_3(DDPA)Br]$*

A very interesting rhenium tricarbonyl system incorporating an Avidin-Biotin protein system has been investigated for bio-analytical applications.[27] These rhenium(I) tricarbonyl-biotin complexes exhibit intense long lived ^{3}MLCT emission states. This enhanced emission

intensity is attributed to the hydrophobicity of the avidin moiety as well as a increase in the rigidity of the molecule following avidin binding which is believed to result in a decrease in the efficiency of the non-radiative decay processes (see Figure 3.5).

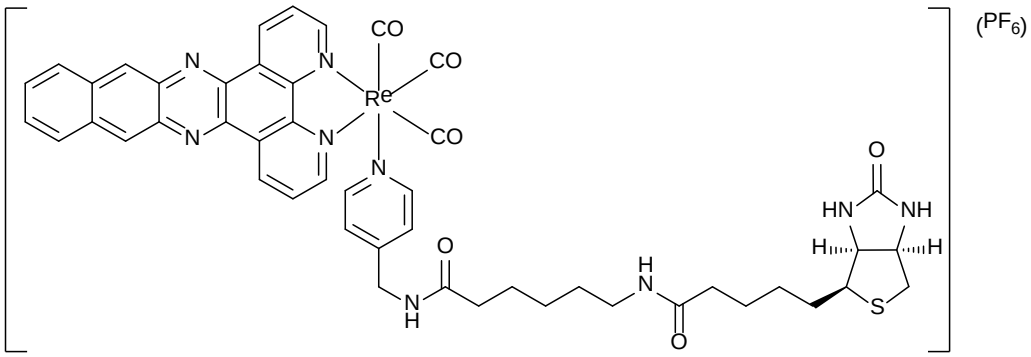

Figure 3.5 *Example of rhenium(I) tricarbonyl-biotin complex*

Recently Perutz and co-workers have studied Zn and Mg metallated porphyrins complexes covalently linked to $[Re(CO)_3(bpy)(pic)]$ (pic = 3-methylpicoline) moiety via an amide linkage (see Figure 3.6).[28]

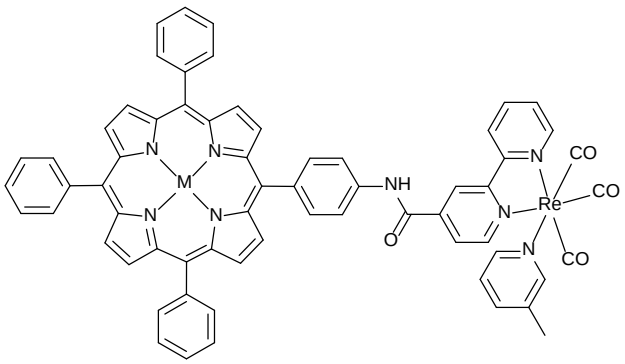

Figure 3.6 *Structure of $[Re(CO)_3(pic)(bpy\text{-}CONH)M(TPP)][OTf]$*

In the same manner the electron donating group 3-methylpyridine (picoline) was introduced to replace the Br atom in $[Re(CO)_3(Br)bpy\text{-}MTPP]$ (where M = Zn and TPP = tetraphenylporphyrin), which indicated no difference on photoinduced electron transfer with the change of axial intermolecular electron donating groups at the rhenium centre. Both $[Re(CO)_3(Br)bpy\text{-}ZnTPP]^+$ and $[Re(CO)_3(pic)bpy\text{-}ZnTPP]^+$ were investigated using steady-state emission spectroscopy, which revealed solvent dependent quenching at the porphyrin centre following irradiation at 560 nm. The emission wavelength of $[Re(CO)_3(pic)bpy\text{-}ZnTPP](OTf)$ was found to be identical to the unit [bpy-ZnTPP], however the emission intensity was substantially reduced for $[Re(CO)_3(pic)bpy\text{-}ZnTPP](OTf)$ when compared to [bpy-ZnTPP].

3.1.2 Dinuclear ruthenium(II)-rhenium(I) complexes

Control of the photophysical, photochemical and electrochemical properties of hetero-nuclear complexes containing Ru(II)-Re(I) bimetallic systems have recently attracted much interest because of their suitable applications in molecular devices,[29] artificial photosynthesis,[30] and in photocatalytic CO_2 reduction[31] and hydrogen production.[32] The photophysical and electrochemical properties of heteronuclear complexes studied so far has indicated that the emission originates from the excited state of the ruthenium core.[33-35]

Two of the Ru(II)-Re(I) complexes containing the asymmetric ligand 2,2′:3′,2″:6″,2‴-quarterpyridine (AB) synthesised by Ward and co-workers are presented in Figure 3.7.[36] This quaterpyridine ligand containing two bpys (A and B) tethered by a single bond are sterically and electronically are not equivalent. The chelating site in B is more sterically hindered compared to A. Both Ru-AB-Re and Re-AB-Ru metal fragments are photochemically and redox active, and exhibit interesting absorption, luminescence and electrochemical properties. The luminescent state of the Ru-AB-Re complex at room temperature is Ru based (i.e. Re→Ru energy transfer) as the emission and photochemical properties are similar to the Ru-AB and Ru-AB-Ru systems studied. However, in the Re-AB-Ru complex, luminescence is centred on the Re moiety (i.e Ru→Re energy transfer), based on the similarity of the lifetimes to those of the Re-AB and Re-AB-Re systems (see **Figure 3.7**).

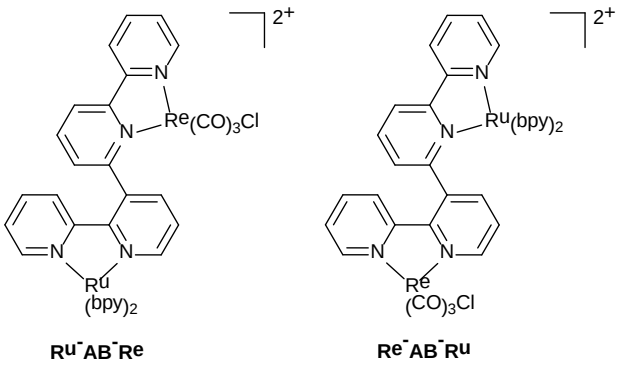

Emission 644nm; **τ** =410 ns **Emission** 623 nm; **τ**=23 ns

Figure 3.7 *Hetero-dinuclear Ru(II)-Re(I) complexes of quaterpyridine ligand AB.*

The mixed metal dinuclear Ru-Re complex, $[Ru(bpy)_2(bpyen)Re(CO)_3(py)]^{3+}$ was found to emit at both 610 nm (Ru) and 540 nm (Re) when excited at 355 nm in dichloromethane.[37] The emission observed at these wavelengths was assigned as being ^{3}MLCT in origin. Communication via the bridging ligand bpyen was poor, but was sufficient to allow Ru→Re energy transfer between the metal centres. The dual-emission observed for this complex is very different from typical Ru(II)-Re(I) dinuclear complexes which exhibited emission originating from the ruthenium based metal centre (see **Figure 3.8**).

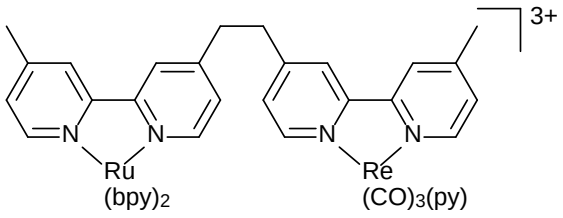

Emission (nm)
610, 540

Figure 3.8 *$[Ru(bpy)_2(\mu\text{-}bpyen)Re(CO)_3(py)]^{3+}$ (Ru-Re complex).*

Another example of dual-emission has been reported by Encinas *et al.* for the $[Ru(bpy)_2(dstyb)Re(CO)_3Cl]^{2+}$ complex.[38] The luminescence spectrum for this complex displayed two distinct emission peaks at 621 nm and 695 nm. The band appearing at 621 nm is assigned to $^3M_{Ru}L_{dstyb}CT$ excited state while the band at 695 nm is attributed to an *intra-*

ligand transition (^{3}IL) from the bridging ligand dstyb (see **Figure 3.9**). Fast deactivation of the ^{3}MLCT is attributed to the lack of rhenium (I) based emission. The relaxation pathways in the heteronuclear complex was established by comparing the excitation spectrum of $[Ru(bpy)_2(dstyb)Re(CO)_3Cl]^{2+}$ with the absorption spectra of $[Ru(bpy)_2(dstyb)Re(CO)_3Cl]^{2+}$ and the mononuclear ruthenium complex $[Ru(bpy)_2(dstyb)]^{2+}$. Emission from the ^{3}IL (dstyb) state is sensitised by the rhenium based absorption, and the ^{3}Ru→LCT emission is not directly sensitised by the rhenium based absorption. It was further concluded that some of the light absorbed by the rhenium based chromophore of $[Ru(bpy)_2(dstyb)Re(CO)_3Cl]^{2+}$ is first transferred to the bridging ligand and then redistributed between the ^{3}IL(dstyb) and ^{3}Ru→dstyb CT levels. The overall excitation process of $[Ru(bpy)_2(dstyb)Re(CO)_3Cl]^{2+}$ involves an indirect Re→Ru energy transfer process mediated by bridging ligand.

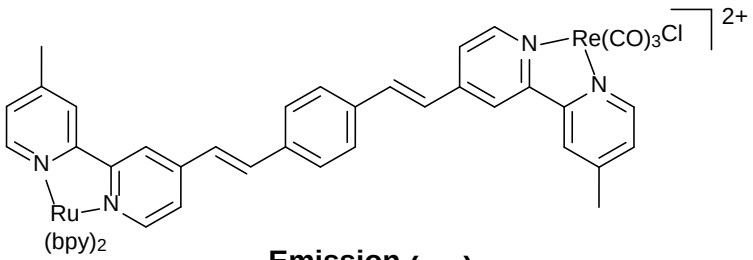

Figure 3.9 *Molecular structure of* $[Ru(bpy)_2(dstyb)Re(CO)_3Cl]^{2+}$ *complex*

In the recent years, polypyridyl transition metal complexes have proven to be excellent probes in detecting the physical properties of DNA. A hetero-di-nuclear Ru-Re complex $[\{Ru(tpm)(dppz)\}(\mu\text{-dpp})\{fac\text{-}(CO)_3Re(dppz)\}]^{3+}$ (where dppz = dipyrido[3,2-a:2'3'-c]phenazine, tpm = tris(1-pyrazolyl)methane and dpp = 4,4'-dipyridylpentane) has been reported to have DNA binding and cleavage properties. The excited states of both metal centres were monitored independently, with ns-TRIR and emission studies clearly demonstrating energy transfer from the Re(I) to Ru (II) centre. The {Ru(dppz)} unit supplies the light-switch function and enhances the binding affinity of the {Ru(dppz)} unit. (see **Figure 3.10**).[39]

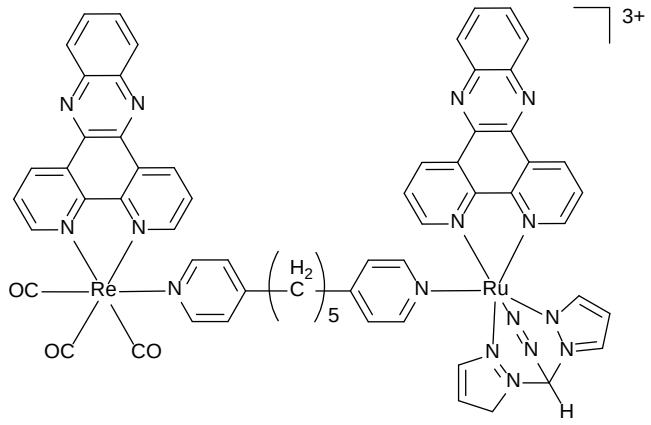

Emission (nm)	**Lifetime (298K)**
430	77 ns

Figure 3.10 *Structure of [{Ru(tpm)(dppz)}(μ-dpp){fac-$(CO)_3$Re(dppz)}]$^{3+}$*

Photocatalytic activity for CO_2 reduction was investigated by Ishitani and co-workers using the Ru(II)-Re(I) bi (**1, 2, 3**) and poly hetero-nuclear (**4**) complexes and turnover numbers of 170 and 240 were reported respectively for CO formation from CO_2 in homogeneous catalytic conditions.[40] (see **Figure 3.11**)

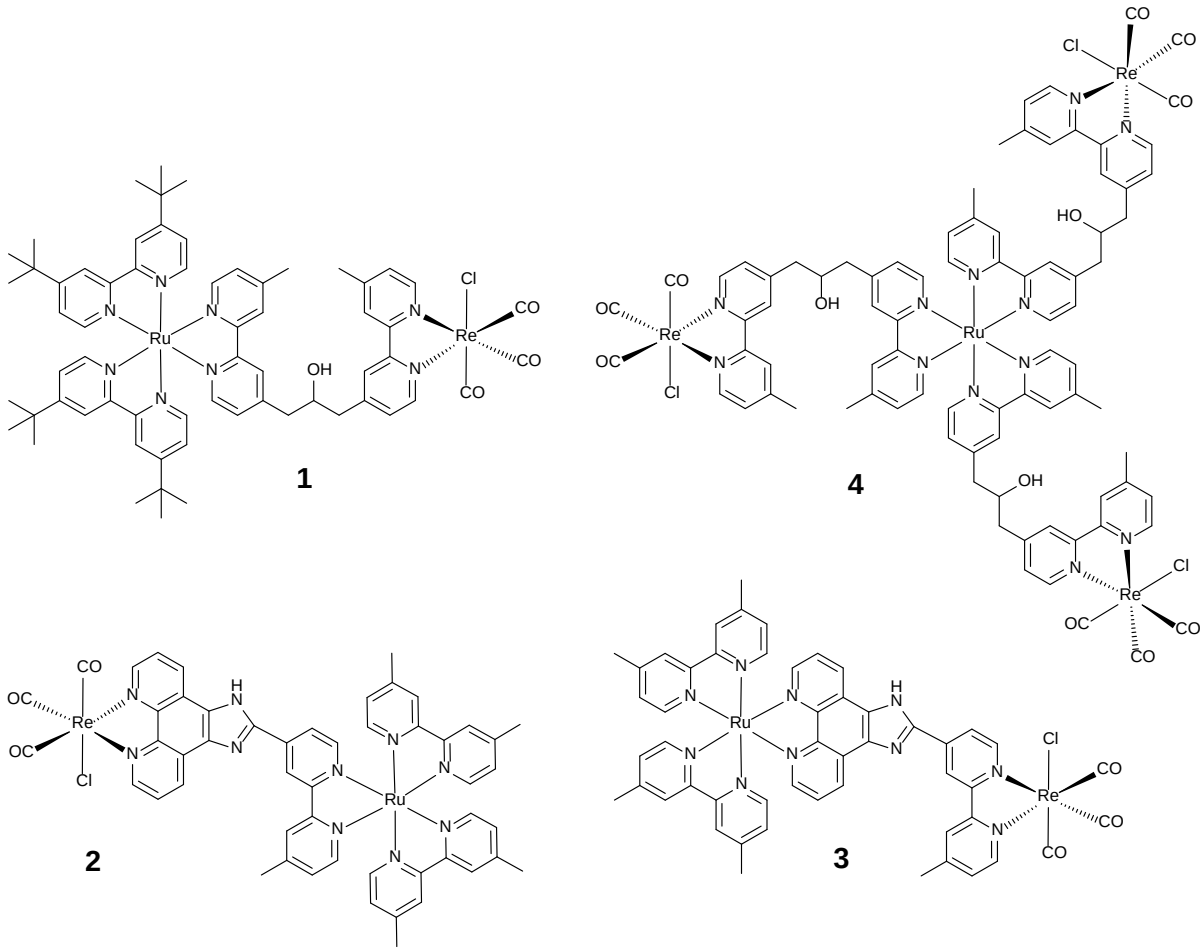

Complex	Emission(nm)	Lifetime(298K)	TON(CO)
1	631	750 ns	240
2	637	1390 ns	28
3	646	930 ns	14
4	638	860 ns	170

Figure 3.11 *Ru(II)/Re(I) bi and poly hetero-nuclear photocatalysts*

Sun and co-workers have prepared and investigated the photophysics of a freebase porphyrin and the triad incorporating zinc-metallated-porphyrins covalently linked both to a ruthenium bipyridyl moiety and a $[Re(CO)_3(bpy)Cl]$ moiety (see **Figure 3.12**).[41] Very weak electronic interactions in both freebase and Zn-metallated-porphyrin systems were indicated through combined electrochemical and photochemical studies. Quenching of the emission intensity for these porphyrin macrocycles when compared to tetraphenyl porphyrin is attributed to electron transfer to the ruthenium unit.

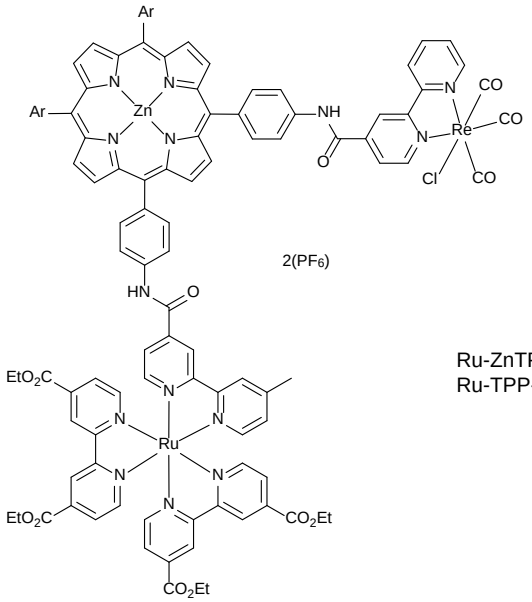

	Emission(nm)
Ru-ZnTPP-Re	614, 664
Ru-TPP-Re	656, 722

Figure 3.12 *Ru-ZnTPP-Re hetero tri-nuclear complex*

3.1.3 Mononuclear Mn(I) complexes

A significant number of Mn carbonyl complexes have been investigated as efficient CO-releasing molecules (CORM)[42-44] as well as electro-catalysts for CO_2 reduction.[45, 46] In this class of compounds the effect of ligand architectures and the nature of metal centres greatly expand the range of different properties and thus enhance their potential applications.

Considering the general trend of replacing unsustainable noble metals by abundant first-row transition metals, manganese complexes are more and more envisioned as promising and safe substitutes to Re counterparts. Recently Mn(I) terpyridine based tricarbonyl complexes were investigated for CO-releasing properties both thermally as well as photochemically (see **Figure 3.13**).[47] The photo-activation study of tri-carbonyl Mn(I) terpy complex has shown the effect of the tridentate terpy ligand on the rate of CO-releasing behaviour from the complex. The rate of the monocarbonylation process for the complex **1b** to **2** (in Figure 3.13) was two times faster than its bpy equivalent species when irradiated at 372 nm.

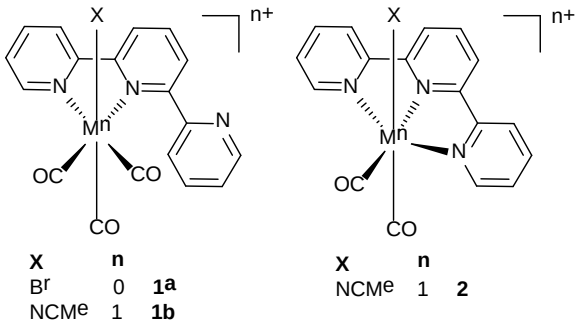

Figure 3.13 *Chemical structure of Mn(I) tricarbonyl complex*

Also, research groups have shown an increasing interest in the study of polypyridyl manganese complexes due to the abundance of manganese metal on the earth's crust which is 1.3 million times more abundant than the rhenium metal.[48]

Recently Mascharak and co-workers have synthesised two Mn(I) carbonyl complexes namely $[MnBr(azpy)(CO)_3]$ and $[Mn(azpy)(CO)_3(PPh_3)](ClO_4)$ (azpy = 2-phenylazopyridine) and have shown rapid release of CO releasing properties upon exposure to lower visible light. These complexes are first examples of biocompatible Photo-CORM that rapidly releases CO upon exposure to low power visible light. The azpy ligand was chosen due to its superior π-acidity and hence the ligand azpy upon coordination with low valent Mn(I), will promote metal to ligand charge transfer in the visible range which in turn will augument CO labilisation. Complex 2 $[Mn(azpy)(CO)_3(PPh_3)](ClO_4)$ (15.28 ± 0.01 min^{-1}) exhibited relatively slower CO release rate than complex 1 $[MnBr(azpy)(CO)_3]$ (21.94 ± 0.01 min^{-1}) under the same experimental conditions using myoglobin assays. The $[MnBr(azpy)(CO)_3]$ complex was found to have significant phototoxicity towards two malignant cell lines HeLa and MDA-MB-231 (see **Figure 3.14**).[49]

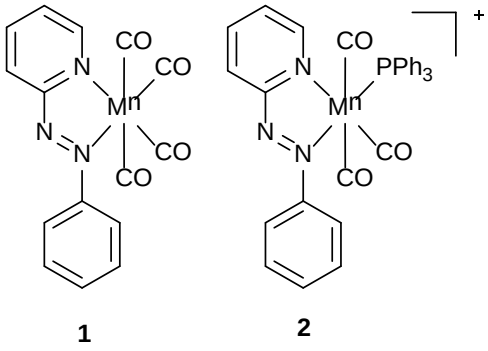

Figure 3.14 *Structures of [MnBr(azpy)(CO)$_3$] (**1**) and [Mn(azpy)(CO)$_3$(PPh$_3$)](ClO$_4$) (**2**)*

Schatzschneider *et al*. have synthesized CO releasing metallodendrimers based on polypyridyl dendrilic scaffolds functionalised with Mn(CO)$_3$ moieties of the general formula [DAB-PPI-{MnBr-(bpy$^{CH3,CH=N}$) (CO)$_3$}$_n$] where DAB = 1,4 diaminobutane, PPI = poly(propyleneimine), bpy = bipyridyl and n = 4 for first or n = 8 for second generation dendrimers and further investigated their CO releasing properties using myoglobin assays. The CO release profile of both the first and second generation dendrimers (4 μM) showed a $t_{1/2}$ of 14.5 min and 16.8 min respectively when irradiated at 410 nm. This class of compounds is an attractive choice due to its monodisperse nature, enhanced permeability and retention effects (see **Figure 3.15**).[50]

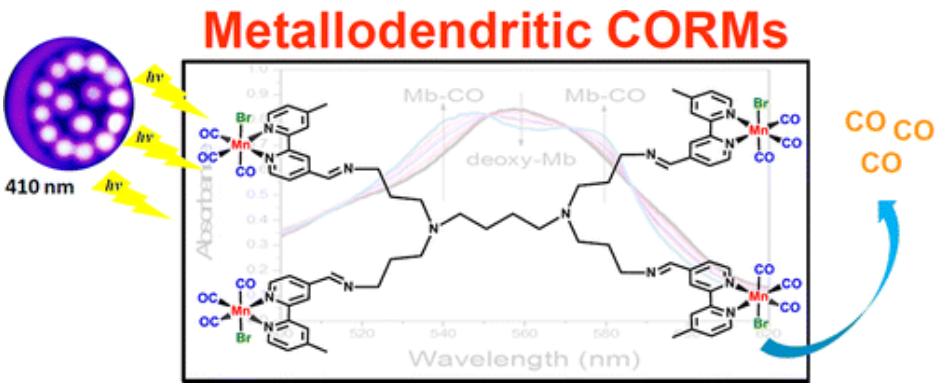

Figure 3.15 *CO release by manganese based metallodendrimers [DAB-PPI-{MnBr-(bpy-CH$_3$,CH=N)(CO)$_3$}$_n$]*[43, 50]

In this chapter mononuclear Mn(I) and Re(I) as well as hetero-di-nuclear Ru(II)-Re(I) carbonyl complexes containing 2,2':5',3":6",2"'-quaterpyridine(bisbpy) as the core ligand were synthesised. Bisbpy contains two 2,2′-bipyridine units and both are attached at the 5 position through a single bond. Following bisbpy as a bridging ligand Ru-Re and Ru-Mn hetero dinuclear carbonyl complexes were synthesised taking $[Ru(II)(bpy)_2(bisbpy)]^{2+}$ as a precursor (see **Figure 3.16**). These complexes were made with the aim of studying their photophysical, electrochemical and CO-releasing properties. Photophysical properties of the complexes were investigated using UV-Vis, emission and pico-second time resolved infrared (TRIR) spectroscopic techniques. CO-releasing properties of these carbonyl complexes were investigated using the myoglobin assay. Electrochemical properties of the bisbpy ligand, and the corresponding mononuclear and dinuclear complexes were investigated using 0.1 M of tetrabutylammoniumhexafluorophosphate($TBAPF_6$) electrolyte in acetonitrile vs Ag/AgCl standard reference electrode. Furthermore, several attempts were made to characterise the synthesised Ru(II)-Re(I) and Ru(II)-Mn(I) hetero-di-nuclear tricarbonyl complex using various spectroscopic tools.

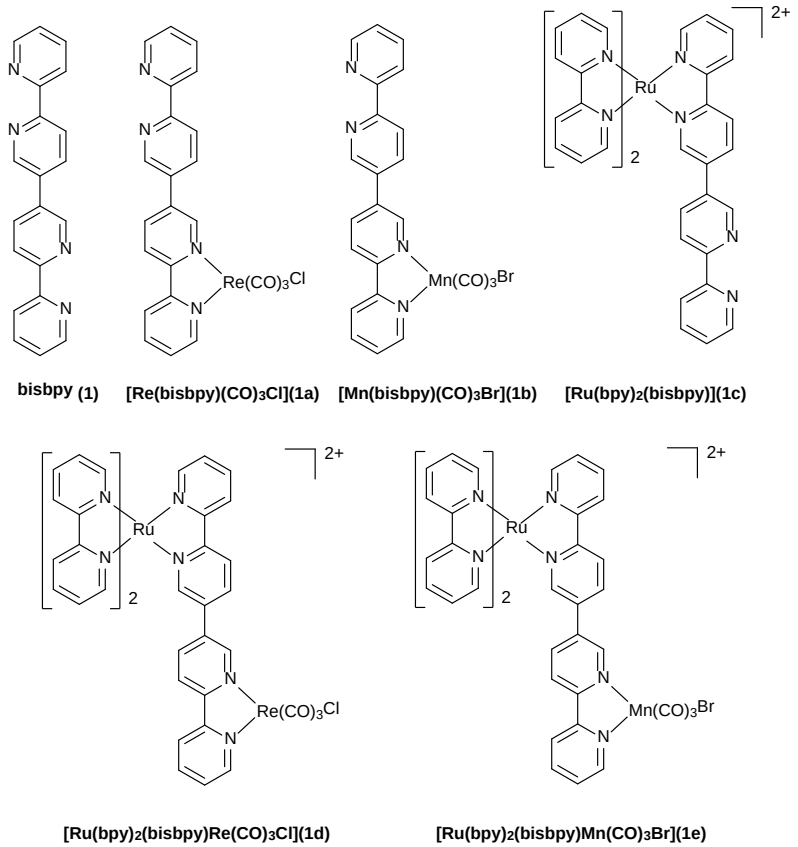

Figure 3.16 *Structures of synthesised Re(I), Mn(I), Ru(II)-Re(I), Ru(II)-Mn(I) complexes*

3.2 Results and Discussion

3.2.1 NMR spectroscopy

3.2.1.1 *5-bromo-2,2'-bipyridine(5Brbpy)*

The ^{1}H NMR and 2D COSY NMR for 5-bromo-2,2'-bipyridine (5Brbpy) are displayed in **Figure 3.17** and **Figure 3.18** respectively. The singlet at 8.82 ppm belongs to H6 as it is next to one nitrogen atom and a Br atom. It occurs further downfield as it is most shielded by the electron clouds of both the Br atom and the lone-pair on the nitrogen atom. From the J-coupling value (^{3}J = 4.67 Hz) and the cosy NMR it is evident that it shares long range coupling with H4 (at 8.2 ppm). The other protons can now be easily assigned following the J-coupling values and the 2D COSY NMR spectra. The assignments for the protons in 5Brbpy are tabulated in **Table 3.1.**

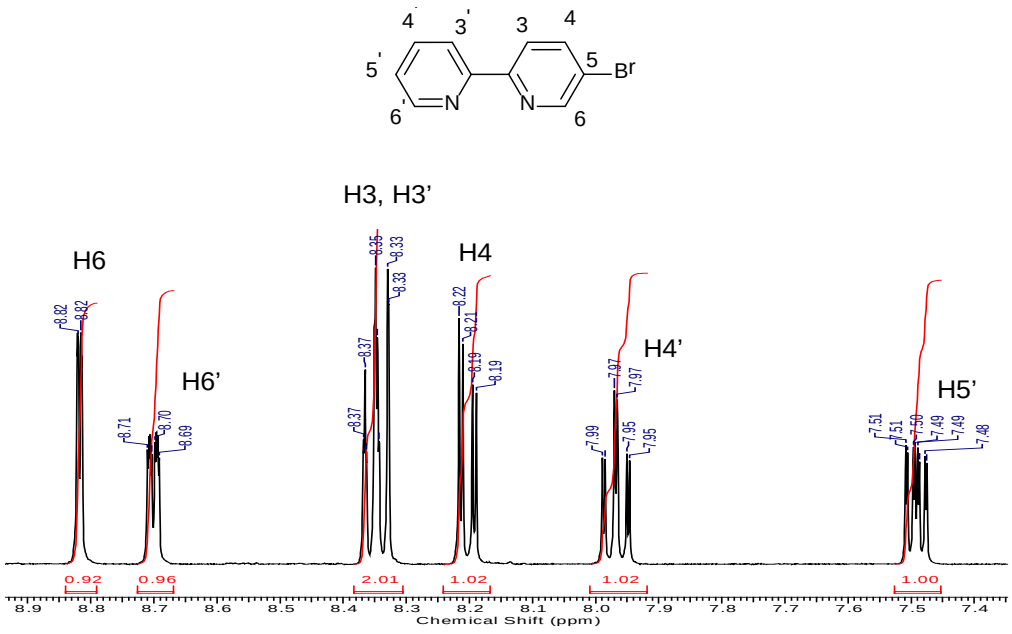

Figure 3.17 *^{1}H NMR (DMSO-d_6, 400 MHz) of 5-bromo-2,2'-bipyridine(5Brbpy)*

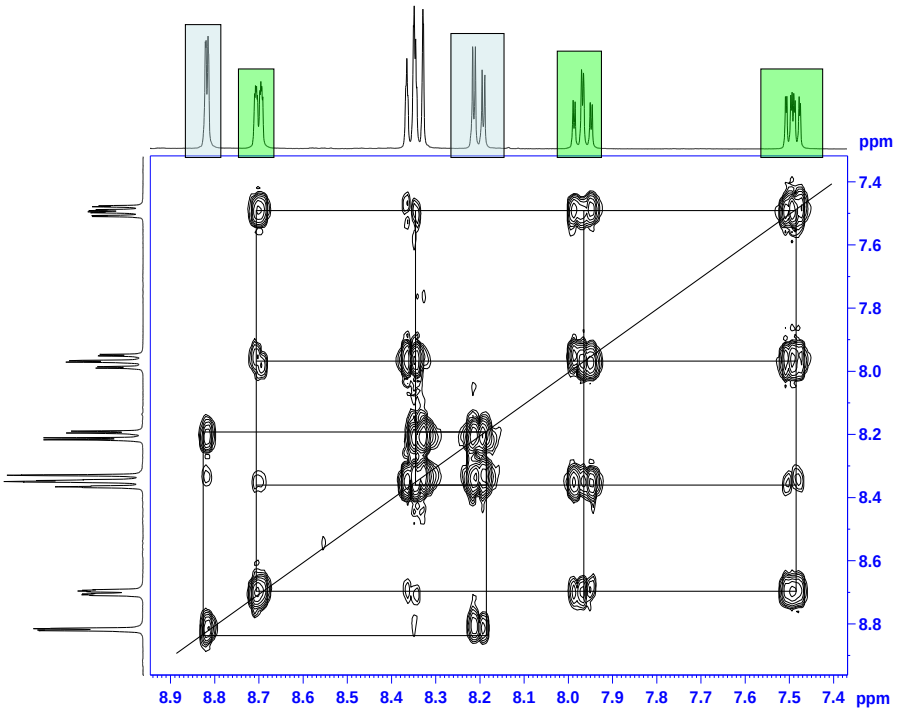

Figure 3.18 *COSY NMR (DMSO-d_6, 400 MHz) of 5-bromo-2,2'-bipyridine(5Brbpy)*

Table 3.1 *^{1}H NMR data for 5-bromo-2,2'-bipyridine(5Brbpy) recorded in DMSO-d_6*

No.	Shift (ppm)
H5′	7.49
H4′	7.97
H4	8.20
H3′, H3	8.35
H6′	8.70
H6	8.82

3.2.1.2 *2,2':5',3'':6'',2'''-quaterpyridine (bisbpy)*

Figure 3.19 and Figure 3.20 show the proton and 2D cosy spectra of 2,2':5',3":6",2"'-quaterpyridine (bisbpy) ligand respectively and which was synthesised using a published method with certain alterations in the synthetic method.[51] The integration shows fourteen

protons in the compound as expected. Both bpy units in bisbpy have an identical chemical environment therefore the NMR spectrum is expected to show proton signals for only one bpy unit. According to the above assumption, H6′ and H2″ have identical chemical shifts. Similarly, H4′, H3′, H6, H5, H4, H3 have identical chemical shifts as H4″, H5″, H6‴, H5‴, H4‴ and H3‴ respectively. The assignments for the protons in bisbpy are tabulated in **Table 3.2.**

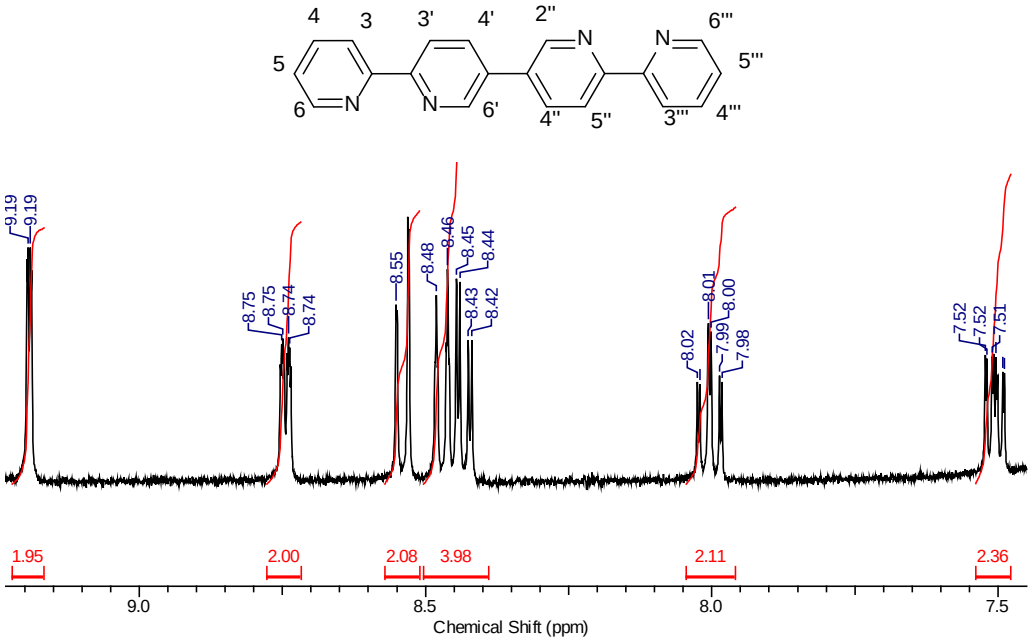

Figure 3.19 *^{1}H NMR (DMSO-d_6, 400 MHz) of 2,2':5',3'':6'',2'''-quaterpyridine(bisbpy)*

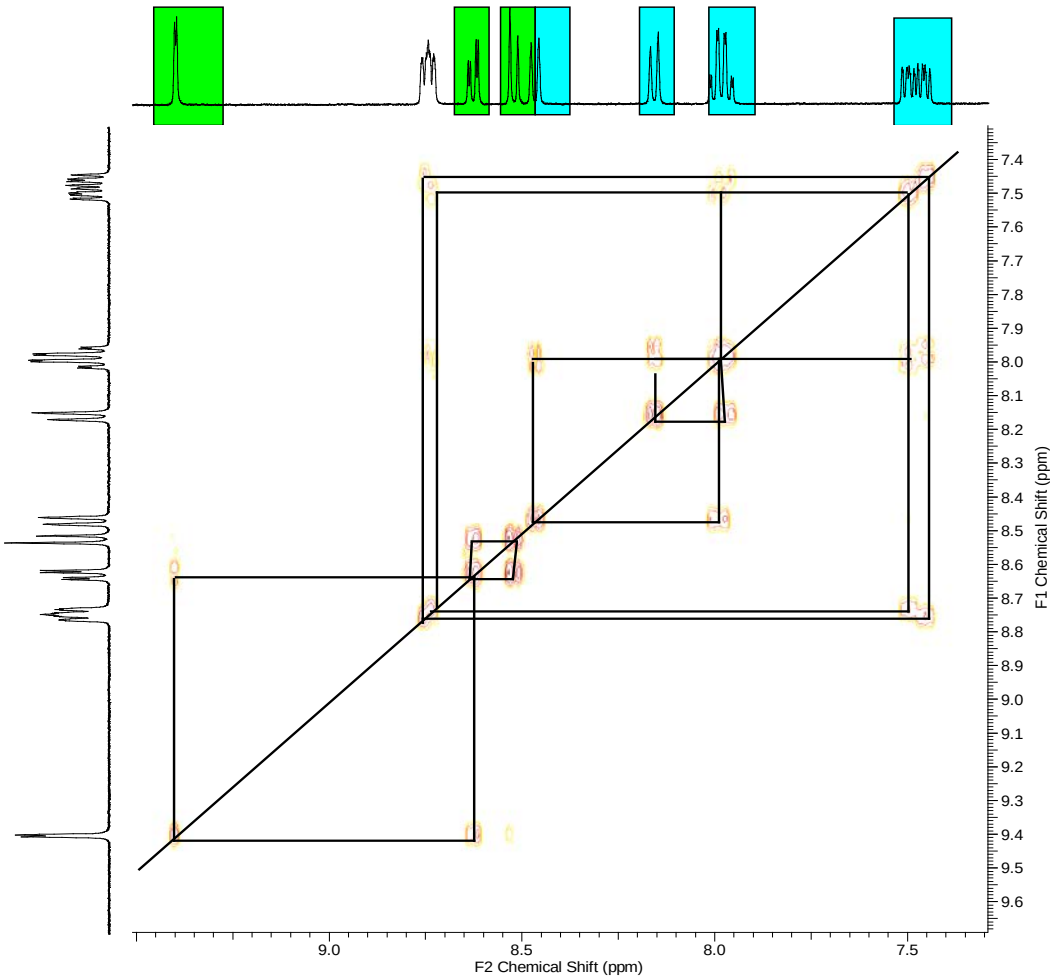

Figure 3.20 *2D COSY NMR (DMSO-d_6, 400 MHz) of 2,2':5',3'':6'',2'''-quaterpyridine(bisbpy)*

Table 3.2 *^{1}H NMR data for 2,2':5',3'':6'',2'''-quaterpyridine (bisbpy) recorded in DMSO-d_6*

No.	Shift (ppm)
H5, H5‴	7.50
H4, H4‴	8.00
H4′, H4″	8.43
H3, H3‴	8.47
H3′, H5″	8.54
H6, H6‴	8.74
H6′, H2″	9.19

3.2.1.3 $[Ru(bpy)_2(bisbpy)](PF_6)_2$

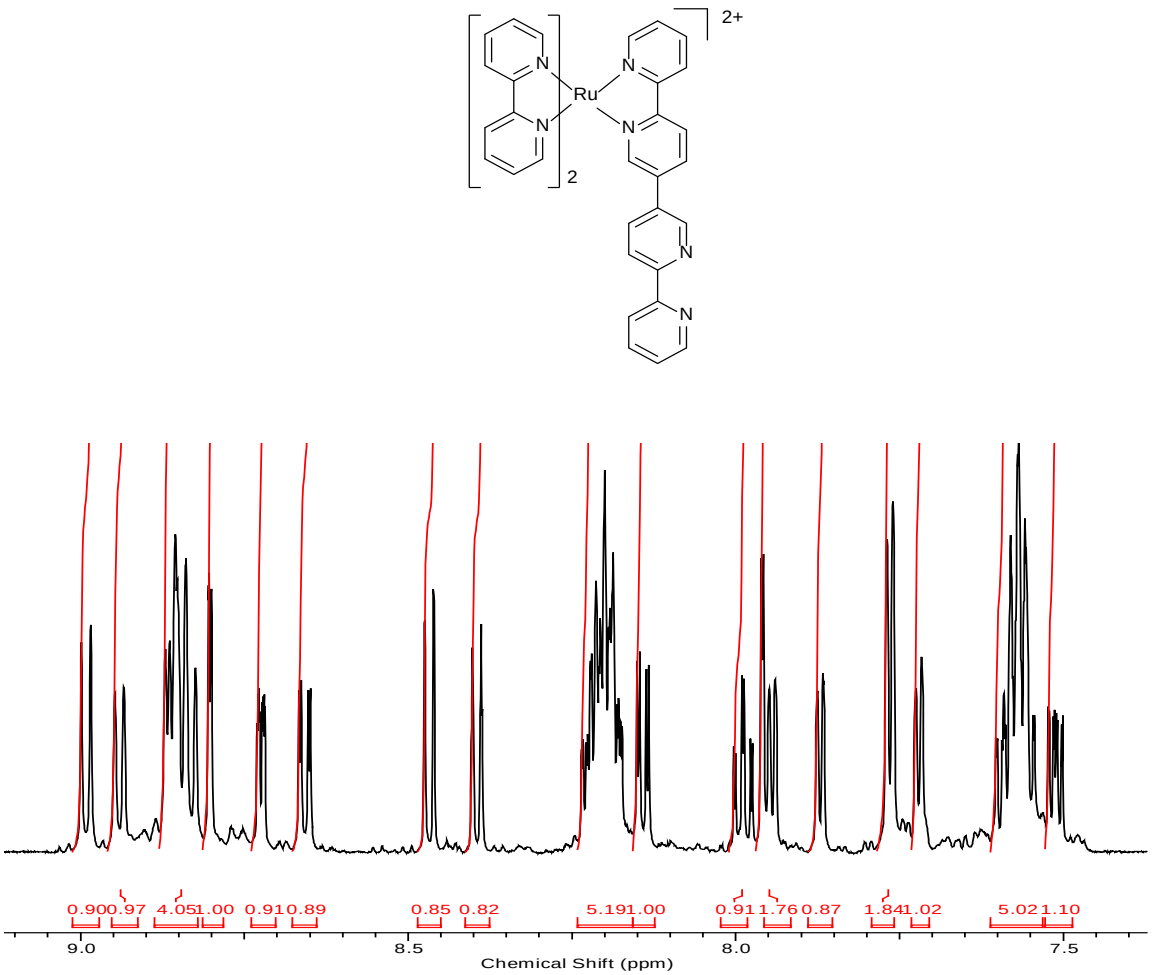

Figure 3.21 *^{1}H NMR (DMSO-d_6, 400 MHz) of $[Ru(bpy)_2(bisbpy)](PF_6)_2$*

The ^{1}H NMR spectrum for $[Ru(bpy)_2(bisbpy)](PF_6)_2$ is shown in **Figure 3.21**. The chemical environment of the free bridging ligand (bisbpy) and the metal coordinated bridging ligand are entirely different. When the bridging ligand is bound to the metal centre, the neighbouring protons to the nitrogen atom (on the bound side of the bridging ligand) will have slightly up-fielded resonance as the shielding effect of nitrogen atom is lowered with coordination. On the other hand the non-coordinated bisbpy moiety has almost identical chemical environments to the uncomplexed ligand and therefore no change in the chemical shift is

anticipated. Chemical shifts for both the free ligand and metal coordinated bridging ligand are provided below **Table 3.3**.

Table 3.3 *The difference in the chemical shift between the free bisbpy and coordinated bisbpy*

Assignment of proton signals with respect to chemical shift (ppm)			
		Free ligand	**Coordinated ligand**
(a)	H5	7.50	7.55
	H4	8.00	8.17
	H4’	8.43	8.63
	H3	8.47	8.92
	H3’	8.54	8.97
	H6	8.74	7.74
	H6’	9.19	7.94
(b)	H5’’’	7.50	7.49
	H4’’’	8.00	7.97
	H4’’	8.43	8.12
	H3’’’	8.47	8.37
	H5’’	8.54	8.44
	H6’’’	8.74	8.70
	H2’’	9.19	8.70

3.2.1.4 $[Ru(bpy)_2(\mu\text{-bisbpy})Re(CO)_3Cl]^{2+}$

The ^1H NMR spectra of the complex $[Ru(bpy)_2(\mu\text{-bisbpy})Re(CO)_3Cl]^{2+}$ shown in **Figure 3.22**. The NMR data is in agreement with the same complex previously synthesised within the group.[51]

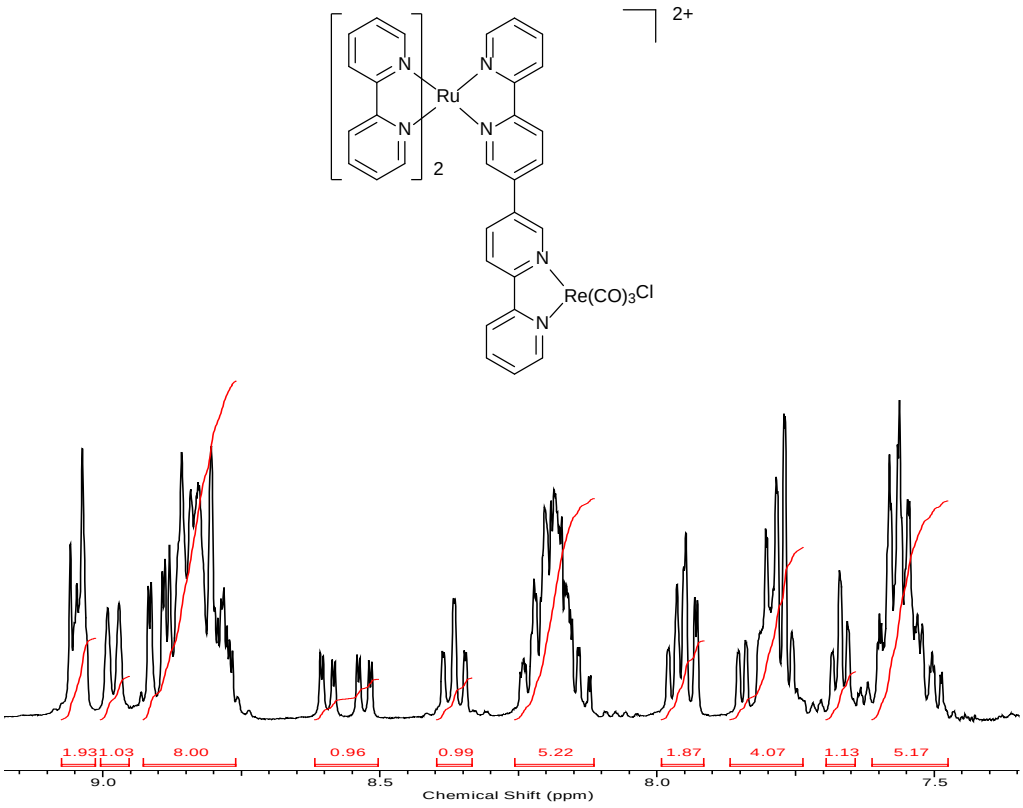

Figure 3.22: *^1H NMR (DMSO-d_6, 400 MHz) of $[Ru(bpy)_2(\mu\text{-bis-bpy})Re(CO)_3Cl]^{2+}$*

3.2.1.5 [(bisbpy)Re(CO)$_3$Cl]

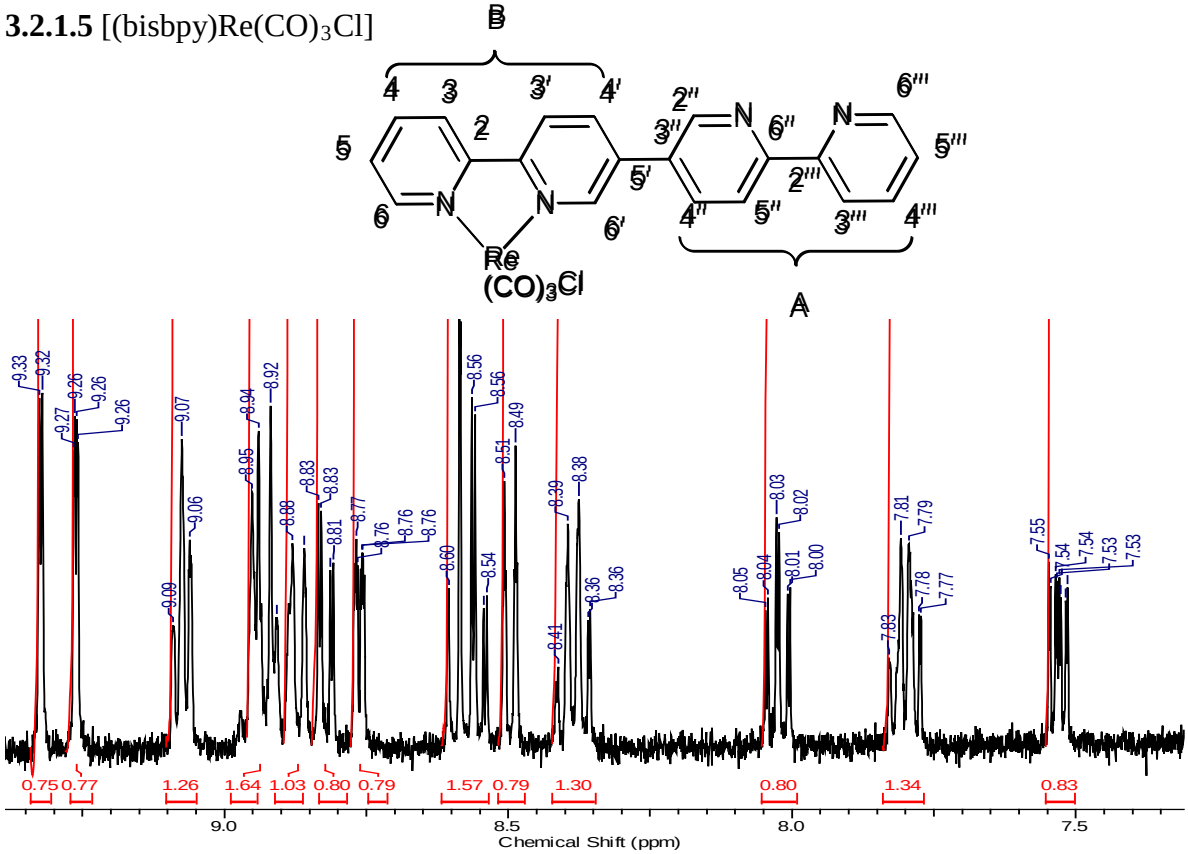

Figure 3.23: *^{1}H NMR (400 MHz, DMSO-d_6) of of [Re(bisbpy)(CO)$_3$Cl]*

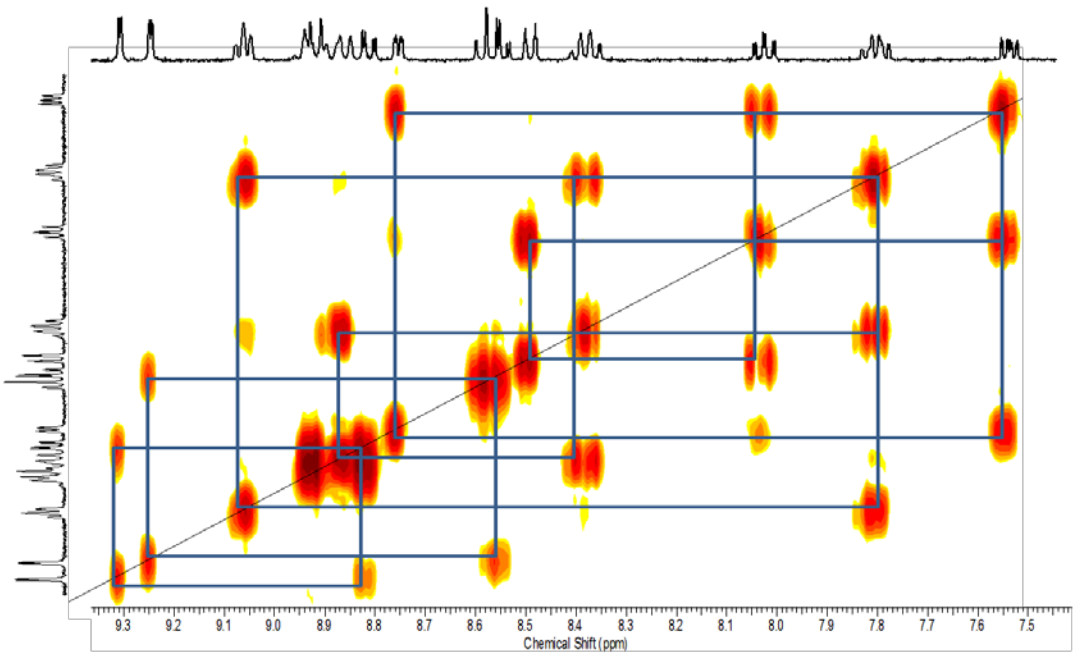

Figure 3.24 *2D COSY NMR (DMSO-d_6, 400 MHz) of [Re(bisbpy)$(CO)_3$Cl]*

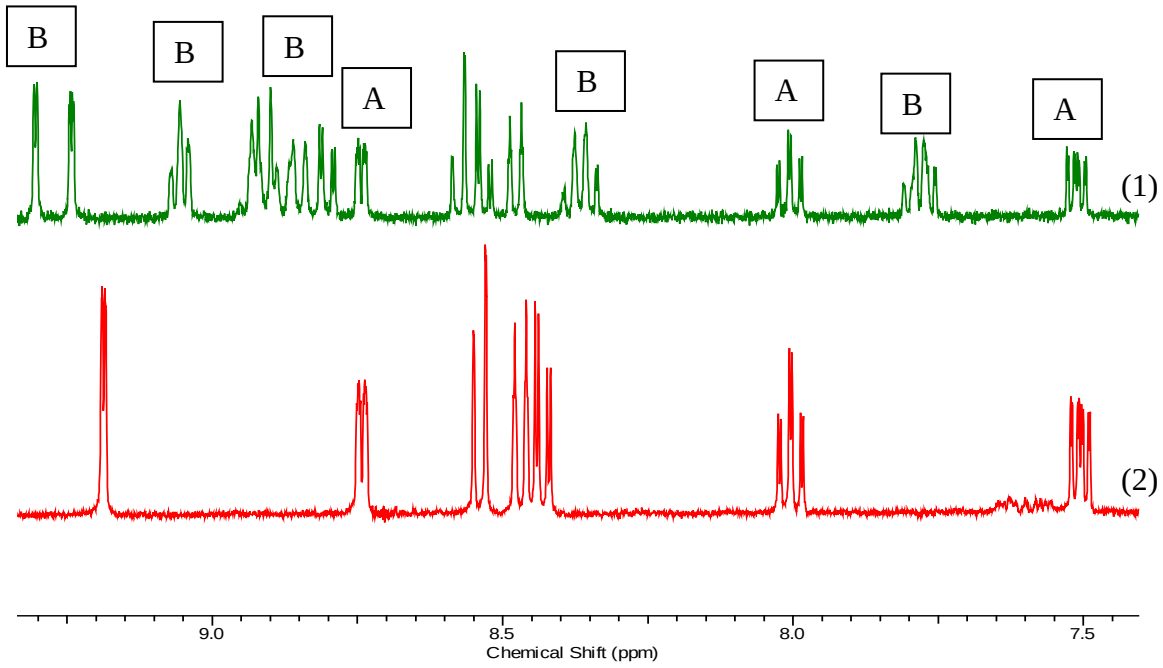

Figure 3.25 *(1) ^{1}H NMR (DMSO-d_6, 400 MHz) of [Re(bisbpy)$(CO)_3$Cl] (2) ^{1}H NMR (DMSO-d_6, 400 MHz) of bisbpy*

From the above **Figure 3.25** it can be inferred that due to metallation the proton signals in the metal attached bpy (B) has been shifted downfield compared to the free bpy moiety (A) in bisbpy. In Figure 3.25, the protons in the non-metallated bpy (A) are unaffected when compared to the metalled bpy moiety (B). It is also noticeable that due to the chlorine atom the singlets (6′ and 2″) near the nitrogen atoms in the middle two pyridine rings are also somehow shielded and shifted to slightly more downfield region. The assignment of the proton signals are tabulated in **Table 3.4**, by taking into account proton and 2D COSY NMR (**Figure 3.23** and **Figure 3.24**) and comparing the proton NMRs of metal complex with free bisbpy ligand. In the COSY, H6' is coupled with a proton at 8.82 which is assigned as H4', and further H4' is coupled with neighbouring H3' at 8.93 ppm. Another singlet at 9.24 ppm is assigned as 2'' which is coupled with H4''. Here the resonance of third pyridine ring is little affected by the complexsation by Re moiety therefore downfield shifts are observed for corresponding protons. As the fourth pyridine ring is mostly unaffected, the doublet at 8.74 ppm can be assigned as H6''' comparing uncomplexed ligand (**Table 3.4**). In similar way

H5’’’(7.53), H4’’’(8.00) and H3’’’(8.47) are assigned and COSY NMR is also supportive with the assignment. As this complex exist as *fac*-isomer, similar downfield shifts are expected for the all the protons in the first pyridine ring attached to Re-moiety. H6 is assigned at 9.06 ppm. H6 further strongly coupled with the proton at 7.79 ppm which is assigned as H5. H5 further couples with H4 (8.37) and H4 to H3 at 8.87 ppm.

Table 3.4 *Difference in chemical shifts for protons in bisbpy and [Re(bisbpy)(CO)$_3$Cl]*

	Protons	**δ ppm (bisbpy)**	**δ ppm [Re(bisbpy)(CO)$_3$Cl]**
B	**H3**	8.47	8.87
	H4	8.00	8.37
	H5	7.50	7.79
	H6	8.74	9.06
	H3′	8.54	8.93
	H4′	8.43	8.82
	H6′	9.19	9.32
A	**H2″**	9.19	9.24
	H4″	8.43	8.56
	H5″	8.54	8.58
	H3‴	8.47	8.47
	H4‴	8.00	8.00
	H5‴	7.53	7.53
	H6‴	8.74	8.74

3.2.2 UV-Vis Spectroscopy

The absorption spectra for all the synthesised complexes were recorded in spectroscopic grade acetonitrile (MeCN) at RT (298K). The absorption data of all the complexes are presented in **Table 3.5**.

Table 3.5 *List of absorption maxima of Re(I) and Mn(I) and Ru-Re type complexes*

Complex	**Absorption (nm)/($\varepsilon \times 10^4$ $M^{-1}cm^{-1}$)**
$[Ru(bpy)_2(bisbpy)](PF_6)_2$	454/(1.16)
$[Ru(bpy)_2(\mu\text{-}bisbpy)Re(CO)_3Cl](PF_6)_2$	450/(1.56)
$[(bisbpy)Re(CO)_3Cl]$	435/ (0.24) , 335/(0.20)
$[(bisbpy)Mn(CO)_3Br]$	435/ (0.50), 315/ (1.20)

Figure 3.26 displays the absorption spectra of $[bisbpyRe(CO)_3Cl]$ (1a) and $[bisbpyMn(CO)_3Br]$ (1b) complexes. The mononuclear $[bisbpyRe(CO)_3Cl]$ complex has a band at 337 nm with a shoulder at 411 nm. The former band is assigned to a π-π* transition of the bisbpy ligand and the latter is assigned to a ^{1}MLCT transition from the rhenium metal orbitals to the unoccupied (π*) orbitals of the bisbpy ligand as similar type transitions were observed for mononuclear rhenium complexes such as $[bpyRe(CO)_3Cl]$ and $[dmpRe(CO)_3Cl]$ (dmp = 6,6'-diaryl-4,4'-bipyrimidine). The absorption spectra for these complexes were dominated by π-π* transitions of the ligand in the UV region and the less intense band at 370 – 464 nm region were assigned to dπ to π* orbital of the ligand based charge transfer.[32, 52, 53]

Similar types of transitions were also observed for the $[(bisbpy)Mn(CO)_3Br]$ where the band at 331 nm is due to a ligand based transition and the 418 nm absorption is attributed to a ^{1}MLCT transition. The absorption band at 318 nm is assigned to dπ(Mn)- π*(bisbpy) MLCT transition as a similar transition is observed for the $[(bpy)Mn(CO)_3Br]$ complex.[54] The band observed at 286 nm is assigned to a bpy based π-π* transition. From **Figure 3.27** it can be

inferred that the Re→bisbpy and Mn→bisbpy transitions have almost identical absorption patterns.

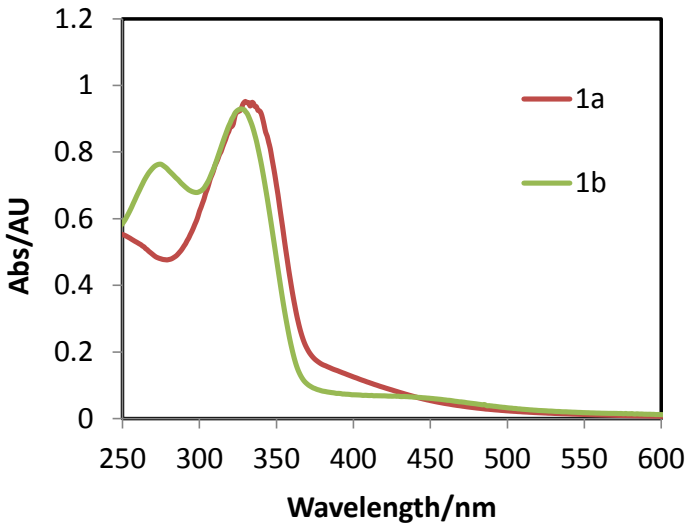

Figure 3.26 *Comparison of absorption spectra of [(bisbpy)Re(CO)$_3$Cl]* ***(1a)*** *and [(bisbpy)Mn(CO)$_3$Br]* ***(1b)****. Absorption spectra for the complexes were recorded in acetonitrile at room temperature (20 ±2 °C)*

Figure 3.27 displays the absorption spectra of the [Ru(bpy)$_2$(bisbpy)(PF$_6$)$_2$] (1c), [Ru(bpy)$_2$(bisbpy)Re(CO)$_3$Cl](PF$_6$)$_2$ (1d) and [bisbpyRe(CO)$_3$Cl] (1a) complexes. [Ru(bpy)$_2$(L)]$^{2+}$ type compounds typically have MLCT bands at 450 nm.[55] The band observed in the visible region at 454 nm for [Ru(bpy)$_2$(bisbpy)(PF$_6$)$_2$] is assigned to a MLCT transition and the absorbance at approximately 300 nm is attributed to bpy based π-π* transition. Sahai *et al*. have reported a series of Ru-/Re heterodimetallic complexes based on the dpm bridging ligand.[34] For example [Ru(bpy)$_2$(dpm)Re(CO)$_3$Cl](PF$_6$)$_2$ has an absorbance at 558 nm and 414 nm with a shoulder at 377 nm. The higher energy transitions for the complex were assigned to a rhenium to dpm based MLCT and the lower transitions were assigned to a ruthenium to dpm based MLCT transitions. The Ru-Re bimetallic complex studied in this chapter, [Ru(bpy)$_2$(bisbpy)Re(CO)$_3$Cl](PF$_6$)$_2$ (1d) has one MLCT band at 450 nm which is due to dπ(Ru) →π*(bisbpy) transition as bisbpy has a lower π* level than bpy. The absorption band at 318 nm is attributed to a dπ(Re) →π*(bisbpy) MLCT transition as a

similar transition is observed for the [(Mebpy-Mebpy)$Re(CO)_3Cl$] complex.[53, 56] The higher energy band observed at 286 nm is assigned to bpy based $\pi \rightarrow \pi^*$ transition.

Generally a red shift in the lowest MLCT band is observed in heterodinuclear complexes containing the bridging ligands with low lying π^* levels which indicates further lowering of the π^* levels of the bridge when attached to the $Re(CO)_3Cl$ moiety.[57, 58] However no shift in the MLCT bands was observed in the case of $[Ru(bpy)_2(\mu\text{-bisbpy})Re(CO)_3Cl](PF_6)_2$ complexes when compared to its mononuclear $[Ru(bpy)_2(bisbpy)](PF_6)_2$ complex. This is due to twisting of two bpy units with respect to each other, when bisbpy is bound to two metal centres. This twisting hinders overlap between the π orbitals on the two bpy units. As a result the Ru to bisbpy MLCT is unaffected following complexation with the rhenium metal centre on the other nitrogen sides of the bisbpy ligand.

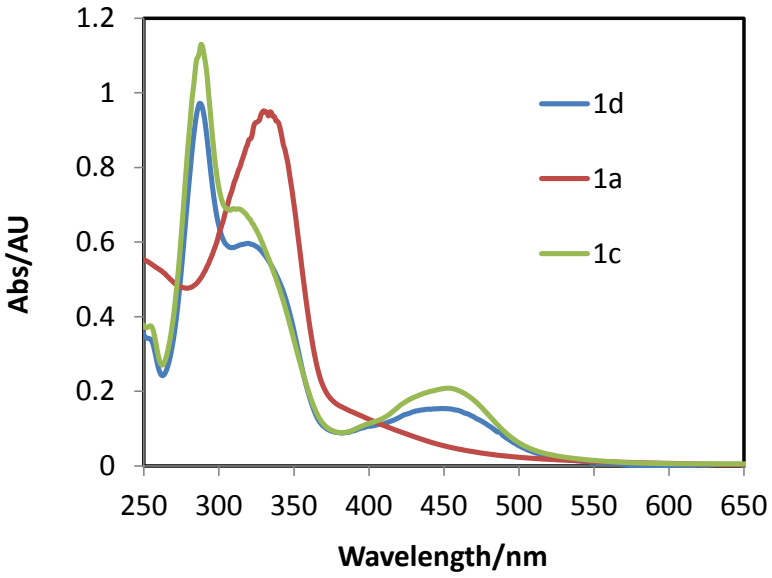

Figure 3.27 *Comparison of the absorption spectra of [(bisbpy)$Re(CO)_3Cl$] (**1a**), $[Ru(bpy)_2(bisbpy)](PF_6)_2$ (**1c**) and $[Ru(bpy)_2(\mu\text{-bisbpy})Re(CO)_3Cl](PF_6)_2$ (**1d**). Absorption spectra for the complexes were recorded in acetonitrile at room temperature (20 ±2 °C)*

3.2.3 Infrared Spectroscopy

A mononuclear rhenium tricarbonyl complex can exist in two types of structural isomers; *fac*-isomer or *mer*-isomer.[59] Typically *fac* and *mer* isomers of tri-carbonyl complexes are characterised by IR spectroscopy and show different CO stretching frequency bands. The FTIR spectra of the mononuclear rhenium and manganese tricarbonyl complexes and ruthenium-rhenium hetero-di-nuclear complex show three bands in the region of 1850-2050 cm^{-1}. These IR bands are assigned to C_s symmetric stretching vibrations [A′(1), A′(2) and A′′].[60, 61]

According to the literature all synthesised complexes are *fac*-isomers as the complexes have only one IR υ(CO) band above 2000 cm^{-1}.[53] Generally *fac*-isomers show three intense IR bands with one band at above 2000 cm^{-1} whereas *mer*-isomers show two intense bands which have lower IR υ(CO) stretching frequencies than 2000 cm^{-1}.[13] The IR bands for the different synthesised metal carbonyl complexes are shown in **Figure 3.28** and the FTIR data are tabulated in **Table 3.6**. All the IR spectra of the complexes were recorded in acetonitrile (solution phase) except for $[Ru(bpy)_2(\mu\text{-bisbpy})Mn(CO)_3Br]^{2+}$ which was recorded in solid phase.

Table 3.6: *IR stretching frequency of Ru-Re, Ru-Mn, Re and Mn based metal carbonyl complexes*

	IR Stretching bands(cm^{-1})		
Complexes	**A'(1)**	**A'(2)**	**A''**
$[(bisbpy)Re(CO)_3Cl]$	2022	1915	1898
$[(bisbpy)Mn(CO)_3Br]$	2024	1939	1913
$[Ru(bpy)_2(\mu\text{-bisbpy})Re(CO)_3Cl]^{2+}$	2022	1917	1899
$[Ru(bpy)_2(\mu\text{-bisbpy})Mn(CO)_3Br]^{2+}$	2022	1915 (Br)	

In the case of [(bisbpy)Mn(CO)$_3$Br], the metal carbonyl bands in the IR appear at a slightly higher wavenumber when compared to the rhenium carbonyl complex [(bisbpy)Re(CO)$_3$Cl], which is due to the fact that dπ- orbital of the rhenium metal favour more π-back donation to the carbonyl groups compared to the manganese metal. As a result the CO bond becomes slightly longer and the rhenium carbonyl bands appear at lower frequency in the IR spectra (**see Figure 3.28**).

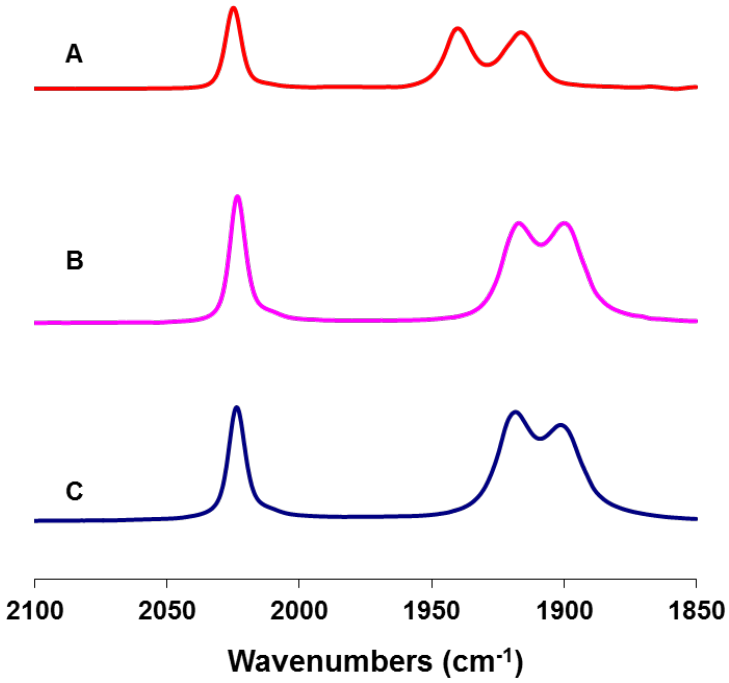

Figure 3.28 *Comparison of FTIR (in Acetonitrile) spectra of fac-[(bisbpy)Mn(CO)$_3$Br](A), fac-[(bisbpy)Re(CO)$_3$Cl](B) and fac-[Ru(bpy)$_2$(μ-bisbpy)Re(CO)$_3$Cl](PF$_6$)$_2$(C)*

In the case of the [Ru(bpy)$_2$(μ-bisbpy)Mn(CO)$_3$Br](PF$_6$)$_2$ complex, the IR spectrum was recorded in the solid phase as the complex decomposed in acetonitrile (**Figure 3.29**).In this case the lower region IR band is not resolved due to the overlapping of bands. This phenomenon might be explained by the electronic effect from the charged ruthenium centre on the bridging ligand as well as on the manganese metal centre. The electronic effect may also be facilitating the π-back donation from manganese metal centre to the carbonyl groups and further results in overlapping of the IR bands.

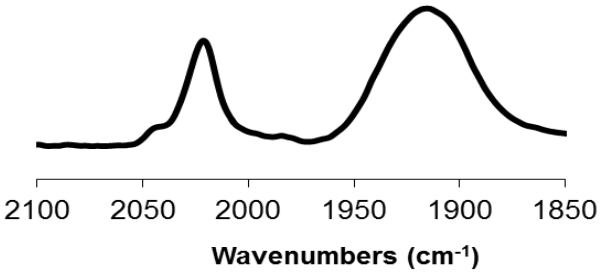

Figure 3.29 *FTIR (in solid state) spectrum of fac-[Ru(bpy)$_2$(μ-bisbpy)Mn(CO)$_3$Br](PF$_6$)$_2$*

3.2.4 Emission Studies

Room temperature emission spectra were recorded in spectrophotometric grade acetonitrile for all complexes and are summarised in **Table 3.7**.

Table 3.7 *Summary of the emission maxima for all Re(I), Mn(I) and Ru-Re complexes*

Complex	Excitation Wavelength (nm)	Emission Wavelength (nm)
[(bisbpy)Re(CO)$_3$Cl]	335	375
[(bisbpy)Mn(CO)$_3$Br]	315	372
[Ru(bpy)$_2$(μ-bisbpy)]$^{2+}$	450	635
[Ru(bpy)$_2$(μ-bisbpy)Re(CO)$_3$Cl]$^{2+}$	450	675

The emission spectra of [(bisbpy)Re(CO)$_3$Cl] were recorded at 298K. No emission was observed when the complex was excited at 400±20 nm which corresponds to the MLCT bands of the complex. However, when the complex was excited at 335 nm, luminiscence was observed at 375 nm which is due to ligand based π→π* transitions. A similar emission spectra was previously reported for [Re(CO)$_3$(phen)Cl] and [Re(CO)$_3$(dceb)Cl] type

complexes. In agreement with our study these latter complexes did not emit when excited at their respective MLCT absorption band.[51]

Similarly, in the case of the [(bisbpy)Mn(CO)$_3$Br] complex, no luminiscence was observed when the complex was excited at 400±20 nm which may again indicate metal→ligand charge transfer, but when the complex was excited at 315 nm, emission was observed at 372 nm which is assigned to a π→π* based emission (see **Figure 3.30 and 3.31**).

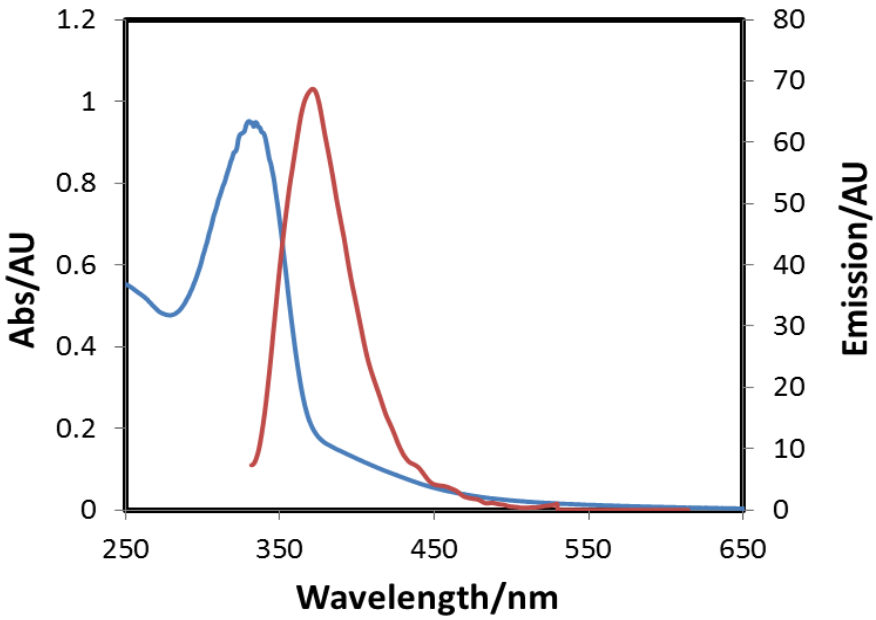

Figure 3.30 *Absorption (blue line) and emission spectra (red line) (λ_{exc} = 335 nm) of* [(bisbpy)Re(CO)$_3$Cl] *(10^{-4}M for absorbance) recorded in spectrophotometric grade acetonitrile. (OD at λ_{exc} = 335 nm is 0.18)*

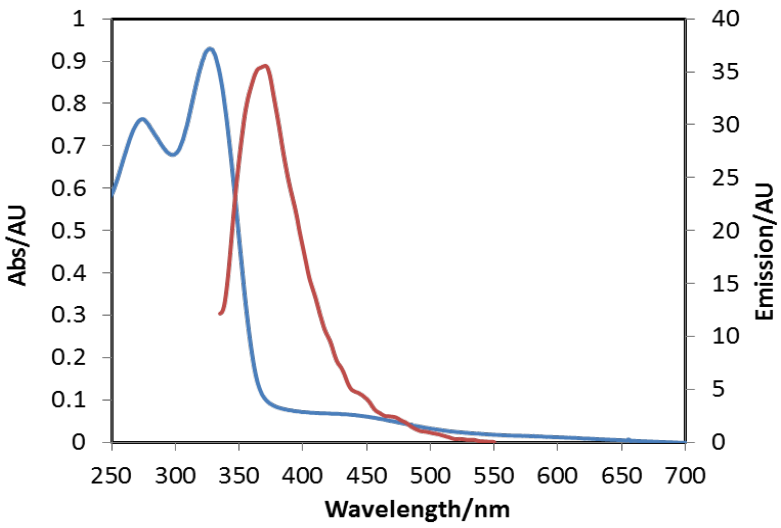

Figure 3.31 *Absorption (blue line) and emission spectra (red line) (λ_{exc} = 315 nm) of* [(bisbpy)Mn(CO)$_3$Br] *(10^{-4}M for absorbance)) recorded in spectrophotometric grade acetonitrile .(OD at λ_{exc} = 315 nm is 0.19)*

In the case of the $[Ru(bpy)_2(bisbpy)]^{2+}$ mononuclear complex the emission is observed at 635 nm following excitation at 450 nm which is assigned to a emission based on the Ru to bisbpy ^{3}MLCT state. When this emission spectrum is compared to that of the Ru-Re analogue $[Ru(bpy)_2(\mu\text{-bisbpy})Re(CO)_3Cl]^{2+}$ the emission spectrum moves to lower energy 675 nm, upon excitation at the same wavelength which is also assigned to a ruthenium based ^{3}MLCT transition. Also, bisbpy is a strong π accepting ligand and hence its π levels are stabilised by the coordination of the Re(CO)$_3$Cl moiety resulting in a red shift in the emission maxima and substantial quenching in the emission intensity (see **Figure 3.32**). [34, 62]

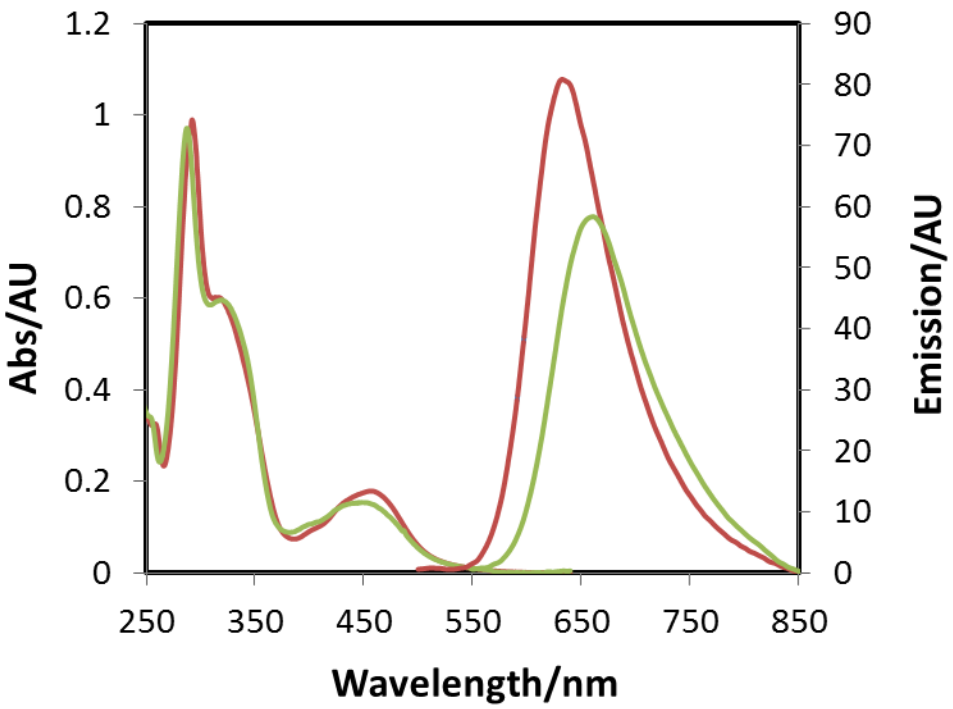

Figure 3.32 *Absorption and emission spectra (λ_{exc} = 450 nm) of $[Ru(bpy)_2(bisbpy)]^{2+}$ (10^{-5}M for absorbance) (Red) OD at λ_{exc} = 450 nm is 0.17) and $[Ru(bpy)_2(\mu\text{-bisbpy})Re(CO)_3Cl]^{2+}$ (10^{-5}M for absorbance) (Green) OD at λ_{exc} = 450 nm is 0.16) recorded in spectrophotometric grade acetonitrile.*

3.2.5 Pico-second time resolved infra-red (TRIR) spectroscopy

A picosecond time resolved infrared (TRIR) study was carried out for [(bisbpy)Re(CO)$_3$Cl], [(bisbpy)Mn(CO)$_3$Br] and [Ru(bpy)$_2$(μ-bisbpy)Re(CO)$_3$Cl](PF$_6$)$_2$ in acetonitrile at 20 ± 2 ^{o}C. All of the TRIR spectra were obtained following excitation with a laser pulse at 320 or 450 nm. The IR stretching vibrations for the parent material and the transient species generated are given in **Table 3.8**.

Table 3.8 *Parent and transient TRIR bands of the complexes in this study*

	TRIR bands (cm^{-1})	
Complexes	**Parent Bands**	**Transient Bands**
[(bisbpy)Re(CO)$_3$Cl]	2010, 1905, 1890	2055, 1978, 1947
[Ru(bpy)$_2$(μ-bisbpy)Re(CO)$_3$Cl]$^{2+}$	2013, 1909, 1890	2010, 1875

Excitation of [(bisbpy)Re(CO)$_3$Cl] at λ_{exc} = 320 nm in an acetonitrile solution at room temperature resulted in depletion of the parent bands at 2010, 1905, 1890 cm^{-1} within 1 ps together with formation of new IR bands at 2055, 1978 and 1947 cm^{-1}. The spectral pattern for the parent complex and the new bands observed υ(CO) in the TRIR experiments are quite similar. The time resolved infrared (TRIR) spectrum of the [(bisbpy)Re(CO)$_3$Cl] complex shown in **Figure 3.33** is similar to other rhenium tricarbonyl complexes which have been reported in literature.[28, 63, 64] The TRIR bands formed following excitation of the [(bisbpy)Re(CO)$_3$Cl] complex between 1 to 20 ps are broad, after 20 ps the bands become narrower along with a blue shift of the transient IR bands due to vibrational cooling.[65]

The shifting of IR bands to a higher energy than their ground state counterparts is very typical for tricarbonyl polypyridyl based rhenium complexes. For example, in the case of the

[Re(Cl)(CO)$_3$(4,4'-bipyridine)$_2$] and [Re(Cl)(CO)$_3$(bpy)] complexes, a shifting of the transient bands to higher wavenumbers is assigned to a ^{3}MLCT excited state (Re→polypyridyl transition).[61, 65-68] Hence, the positive shifts of the υ(CO) bands for the [(bisbpy)Re(CO)$_3$Cl] complex formed upon excitation agrees with previous studies on similar complexes and consequently these new bands are assigned to a Re→bisbpy based ^{3}MLCT excited state. The shifting of the transient bands to higher wavenumbers is due to reduction of π back bonding in the ^{3}MLCT excited state resulting from depletion of the electron density at the metal centre. The excited state formed is long-lived and does not decay completely even after 1 ns.

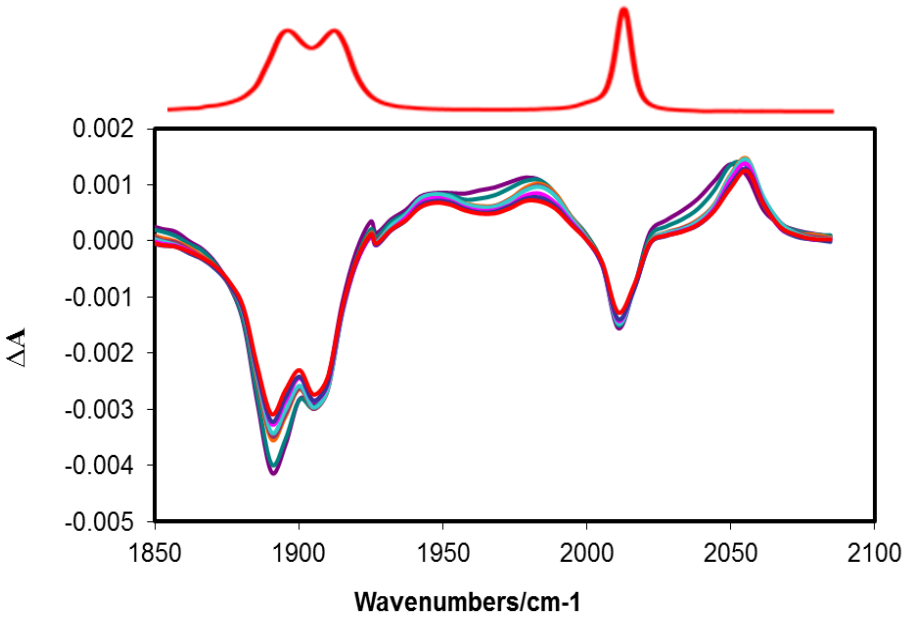

Figure 3.33 *Time resolved infra-red difference spectra following laser photolysis (λ_{exc} = 320 nm) for* [(bisbpy)Re(CO)$_3$Cl] *complex in acetonitrile. The spectrum above illustrates the parent υ(CO) stretches at t = 0 ps in acetonitrile.*

Excitation of the [Ru(bpy)$_2$(μ-bisbpy)Re(CO)$_3$Cl](PF$_6$)$_2$ complex at λ_{exc} = 450 nm in an acetonitrile solution at room temperature also resulted in depletion of parent bands at 2013, 1909, 1890 cm^{-1} within 1 ps together with the formation of new IR bands at 2010 and 1875 cm^{-1}. The new bands are shifted to lower wavenumbers when compared to their ground state indicating an increase in electron density at the Re metal hence, leading to an increase in π-

back bonding which shifts the υ(CO) bands to lower frequencies. This observation led to suggest a population of the anti-bonding orbitals of the bisbpy bridging ligand which is slightly more electron donating in nature. Similar observations were noted by Ward and co-workers for their $[(bpy)_2Ru^{II}(AB)Re^{I}(CO)_3Cl]^{2+}$ and $[(bpy)(CO)_3Re^{I}(AB)Ru^{II}(bpy)_2]^{2+}$ complexes where AB is an asymmetric bridging ligand 2,2′:3′,2″:6″,2‴- quaterpyridine (**see Figure 3.34**).[69] Irradiation into either the Re or Ru MLCT transition of $[(bpy)_2Ru^{II}(AB)Re^{I}(CO)_3Cl]^{2+}$, resulted in depletion of the parent bands at 1902, 1918 and 2023 cm^{-1} and formation of new signals at 1888, 1910 and 2016 cm^{-1}. The shifting of the υ(CO) bands to lower wavenumbers was assigned to the formation of the Ru→AB bridging ligand based MLCT state $[(bpy)_2Ru^{III}(AB)Re^{I}(CO)_3Cl]^{2+}$. However TRIR data for another isomer $[(bpy)(CO)_3Re^{I}(AB)Ru^{II}(bpy)_2]^{2+}$ showed bleaching of the parent bands at 1902, 1922 and 2028 cm^{-1} and the formation of new bands at 1892, 1912 and 2018 cm^{-1} as well a broad band at 1965 cm^{-1}. These observations have been assigned to the formation of both Re and Ru based MLCT excited states $[(bpy)(CO)_3Re^{II}(AB)^{-}Ru^{II}(bpy)_2]^{2+}$ and $[(bpy)(CO)_3Re^{I}(AB)^{-}Ru^{III}(bpy)_2]^{2+}$.

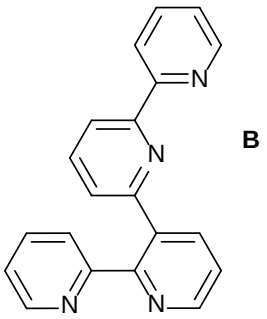

Figure 3.34 *Structure of 2,2':3',2":6",2''' quaterpyridine ligand (AB).*

Hence, it can be concluded from the TRIR spectra in the studies performed here on $[(bpy)_2Ru^{II}(\mu\text{-bisbpy})Re^{I}(CO)_3Cl]^{2+}$ that the shift to higher frequency of all the υ(CO) bands formed upon excitation at 450 nm agrees with the previous studies on similar $[(bpy)_2Ru^{II}(AB)Re^{I}(CO)_3Cl]^{2+}$ type complexes and consequently these new bands are assigned to a relaxed Ru^{II} to bisbpy bridging ligand based MLCT state

$[(bpy)_2Ru^{III}(bisbpy)Re^{I}(CO)_3Cl]^{2+}$. The difference was that no new broad band was observed around 1965 cm^{-1} which was assigned to Re based MLCT excited state in case of $[(bpy)(CO)_3Re^{I}(AB)Ru^{II}(bpy)_2]^{2+}$. The excited state formed was very long lived and did not decay even after 1 ns. No recovery of the parent bands was observed (see **Figure 3.35**). (Note: the lowest frequency band was excluded from the spectrum as it was at the periphery of the observation window and reliable information could not be obtained).

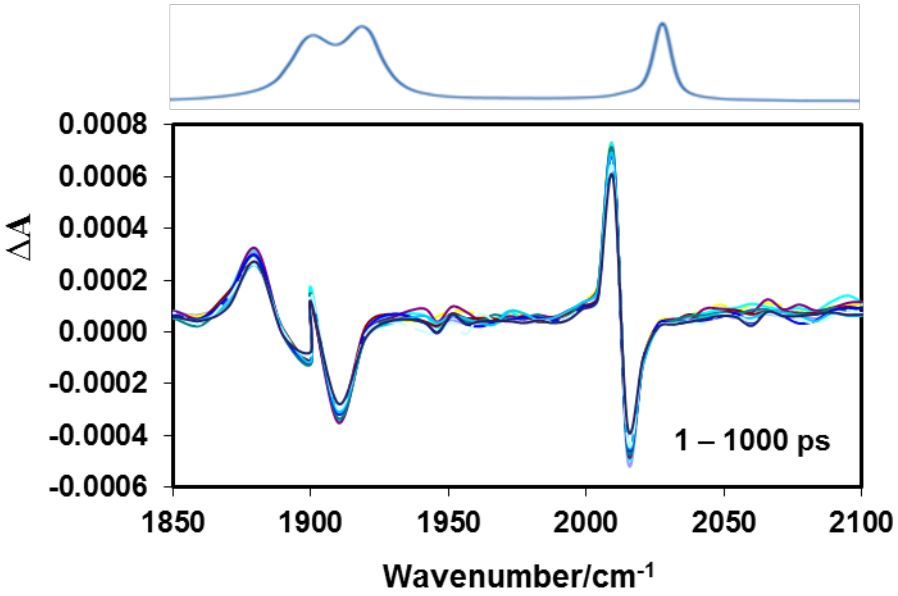

Figure 3.35 *Time resolved infra-red difference spectra following laser photolysis (λ_{exc} = 450 nm) for* $[Ru(bpy)_2(\mu\text{-bisbpy})Re(CO)_3Cl](PF_6)_2$ *complex in acetonitrile. Above spectrum illustrates the parent ν(CO) streches at t = 0 ps in acetonitrile.*

All the TRIR experiments for $[(bisbpy)Re(CO)_3Cl]$ and $[Ru(bpy)_2(\mu\text{-bisbpy})Re(CO)_3Cl](PF_6)_2$ complexes were carried out in a static IR cell. Attempts to perform TRIR on the $[(bisbpy)Mn(CO)_3Br]$ complex in a static IR cell when excited at 320 nm were unsuccessful due to decomposition of the molecule within the laser pulse. Therefore, for $[(bisbpy)Mn(CO)_3Br]$ complex a flow through IR cell is required to carry out the TRIR experiments.

3.2.6 Electrochemical Studies

The electrochemical study for all compounds was performed in 0.1M $TBAPF_6/CH_3CN$ and the observed data are tabulated in Table 3.9. The electrochemical data were recorded vs. Ag/AgCl standard reference electrode at a glassy carbon (GC) working electrode with scan rate of 0.1 V/s.

Table 3.9 *Redox properties of* bisbpy, $[(bisbpy)Re(CO)_3Cl]$, $[Ru(bpy)_2(bisbpy)]^{2+}$, *and* $[Ru(bpy)_2(bisbpy)Re(CO)_3Cl]^{2+}$ *vs. Ag/AgCl, at a glassy carbon electrode. The electrolyte employed was 0.1 M* $TBAPF_6$ *in acetonitrile*

Compound	**Oxidation Potential (V)**		**Reduction Potential (V)**		
	E_{pa} Oxi(V)	**E_{pc} Oxi(V)**	**E_{pa} Red(V)**	**E_{pc} Red(V)**	**$E_{1/2}$ Red(V)**
bisbpy	+1.25[a]	1.10[a]	-1.70[c] -1.91[c]	-1.78[c] -2.0[c]	-
$[(bisbpy)Re(CO)_3Cl]$	+0.90[c] +1.26[a]	+0.75[c] +1.09[a]	-1.14[c] -1.23[c] -1.91[c]	-0.96[a] -1.00[c] -1.39[c] -2.0[c]	-
$[Ru(bpy)_2(bisbpy)]^{2+}$	+1.01[c] +1.75[a]	+0.8[c]	-1.51[b] -1.77[b] -2.0[b] -2.17[b]	-1.54[b] -1.80[b] -2.06[b] -2.20[b]	-1.54 -1.80 -2.06 -2.20
$[Ru(bpy)_2(bisbpy)Re(CO)_3Cl]^{2+}$	+1.35[a] +1.51[c] +1.95[a]	+1.25[a] +1.40[c]	-1.20[c] -1.50[c] -1.72[c]	-1.25[c] -1.74[c] -1.82[c]	-

*** 'a'** *indicates an irreversible wave;* ***'b'*** *indicates a reversible wave;* ***'c'*** *indicates a quasi-reversible wave.*

Figure 3.36 below displays the electrochemical behaviour of the bisbpy ligand. A quasi reversible bisbpy based oxidation is observed at 1.25 V. The two reduction potentials observed at -1.78 and -2.0 V are associated with the reduction of the bisbpy ligand. Similar observations were reported for another (3,5-bis(pyridine-2-yl)-1,2,4-triazole) polypyridyl ligand.[70]

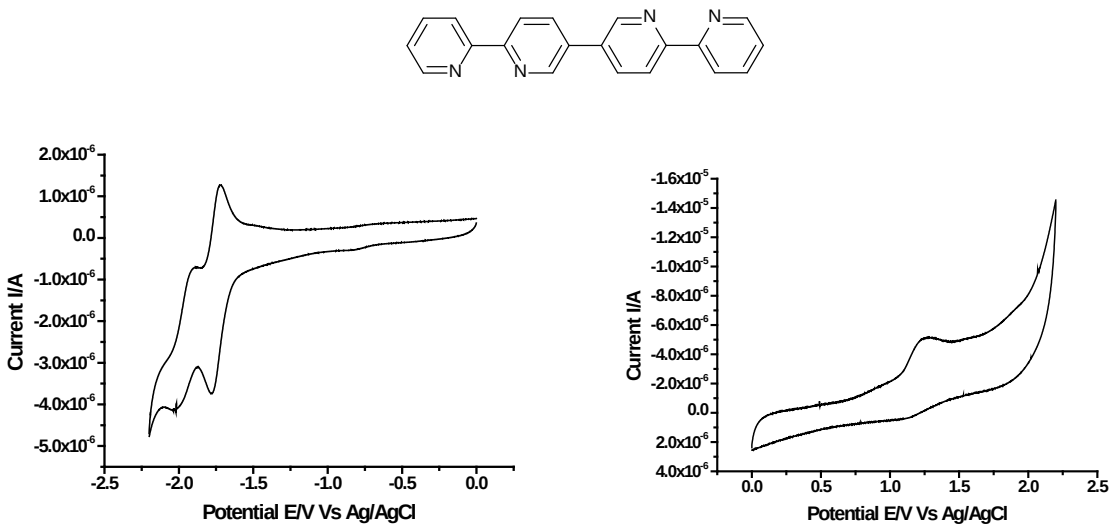

Figure 3.36 *Cyclic Voltammogram of bisbpy ligand showing oxidation and reduction waves vs. Ag/AgCl in 0.1M TBAPF$_6$/MeCN at a scan rate of 0.1 Vs^{-1}*

The cyclic voltammogram of the complex [Ru(bpy)$_2$(bisbpy)](PF$_6$)$_2$ is presented in **Figure 3.37**. A quasi reversible Ru(II)/Ru (III) oxidation is observed at 1.01 V. All the reduction potentials observed for the [Ru(bpy)$_2$(bisbpy)](PF$_6$)$_2$ complex are completely reversible processes.[71] The first and second reduction potential of the complex are assigned to the reduction of the coordinated bipyridyl ligands. The two reduction potentials observed at -2.0 V and -2.17 V are associated with the reduction of the bisbpy ligand.

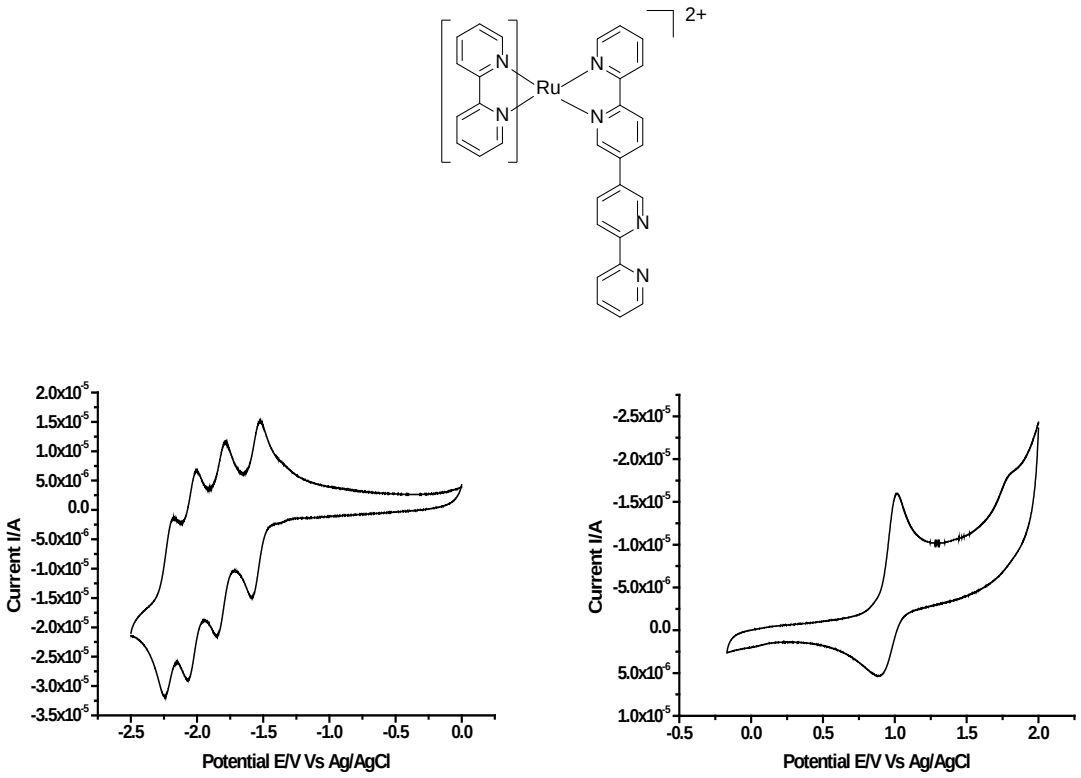

Figure 3.37 *Cyclic Voltammogram of* $[Ru(bpy)_2(bisbpy)](PF_6)_2$ *showing oxidation and reduction waves vs. Ag/AgCl in 0.1M TBAPF$_6$/MeCN at a scan rate of 0.1 Vs^{-1}*

The cyclic voltammogram of the complex $[Ru(bpy)_2(\mu\text{-bisbpy})Re(CO)_3Cl](PF_6)_2$ is presented in **Figure 3.38**. The irreversible Re(I) oxidation wave was found at 1.97 V. The irreversible nature of the Re(I)/Re(II) couple is typical of rhenium tricarbonyl complexes. The reduction wave for the bridging ligand can be at -1.25 V. Another two reduction waves at -1.57 V and -1.82 V are likely to correspond to a bpy based reduction and an irreversible Re(I) reduction respectively. Electrochemistry of similar complexes has been previously studied by Dr. Mary Pryce's group.[72]

Another important point to be noted is that first Ru(II)/Ru(III) couple of the dinuclear complex is observed at 1.51 V which is higher than the oxidation potential of the Ru(II)/Ru(III) couple in mononuclear complex $[Ru(bpy)_2(bisbpy)](PF_6)_2$ observed at 1.01 V. This is due to the fact that upon coordination to the $Re(CO)_3Cl$ moiety, the electron density

of the bisbpy ligand is shared between the ruthenium and the rhenium moiety. As a result less electron density is present at the metal centres. This results in the ruthenium centre oxidising at a higher oxidation potential. Such differences in oxidation potentials have been observed between the mononuclear $[Ru(bpy)_2bpzt]^+$ and dinuclear $[\{Ru(bpy)_2\}_2bpzt]^{3+}$ complexes (where bpzt is 3,5-di(pyraz-2-yl)-1,2,4-triazole).[73] The first Ru(II)/Ru(III) oxidation of $[\{Ru(bpy)_2\}_2bpzt]^{3+}$ is observed at 1.16 V while oxidation of the ruthenium mononuclear complex $[Ru(bpy)_2bpzt]^+$ is observed at 0.99 V. In the mononuclear complex $[Ru(bpy)_2bpzt]^+$, the negative charge of the bpzt anion is delocalised onto the metal centre through the N2 of the triazole ring. Addition of the second metal results in a delocalisation of electron density over two metal centres hence reducing the electron density over both the metal centres and increasing the first oxidation potential of $[\{Ru(bpy)_2\}_2bpzt]^{3+}$ compared to $[Ru(bpy)_2bpzt]^+$.

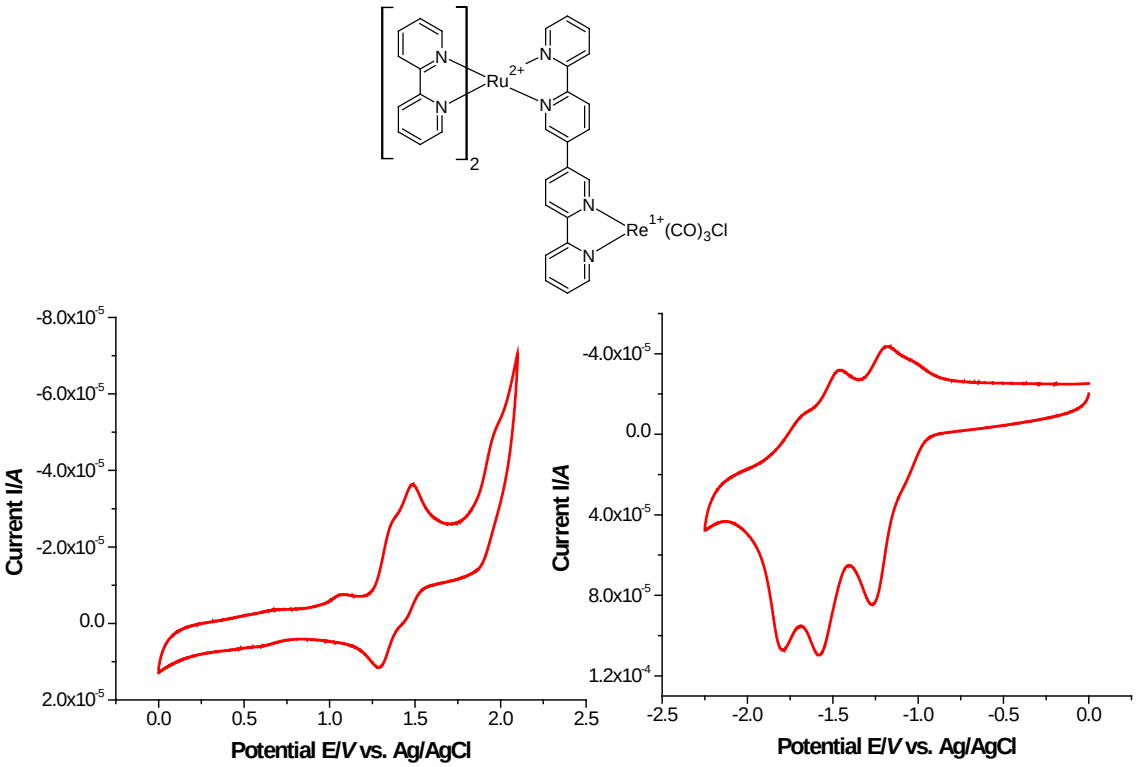

Figure 3.38 *Cyclic Voltammogram of* $[Ru(bpy)_2(bisbpy)Re(CO)_3Cl](PF_6)_2$ *showing oxidation and reduction waves vs. Ag/AgCl in 0.1M* $TBAPF_6$*/MeCN at a scan rate of 0.1* Vs^{-1}

Both the oxidation and reduction process for [(bisbpy)Re(CO)$_3$Cl] are complicated in nature. The cyclic voltammogram of the complex [(bisbpy)Re(CO)$_3$Cl] is presented in Figure 3.39. A quasi reversible oxidation of the bisbpy ligand is observed at 1.09 V. A series of quasi-reversible and irreversible reduction waves are observed at -1.00 V, -1.39 V, -2.0 V and -0.96 V respectively. These reduction processes most likely are a result of reduction of the irreversible Re(I) and bisbpy ligand followed by chloride dissociation processes as observed for [Re(CO)$_3$(bpy)Cl] and other rhenium polypyridyl complexes.[74, 75]

The cyclic voltammogram of the complex [(bisbpy)Mn(CO)$_3$Br] could not be performed due to decomposition of the complex upon undergoing electrochemical measurements.

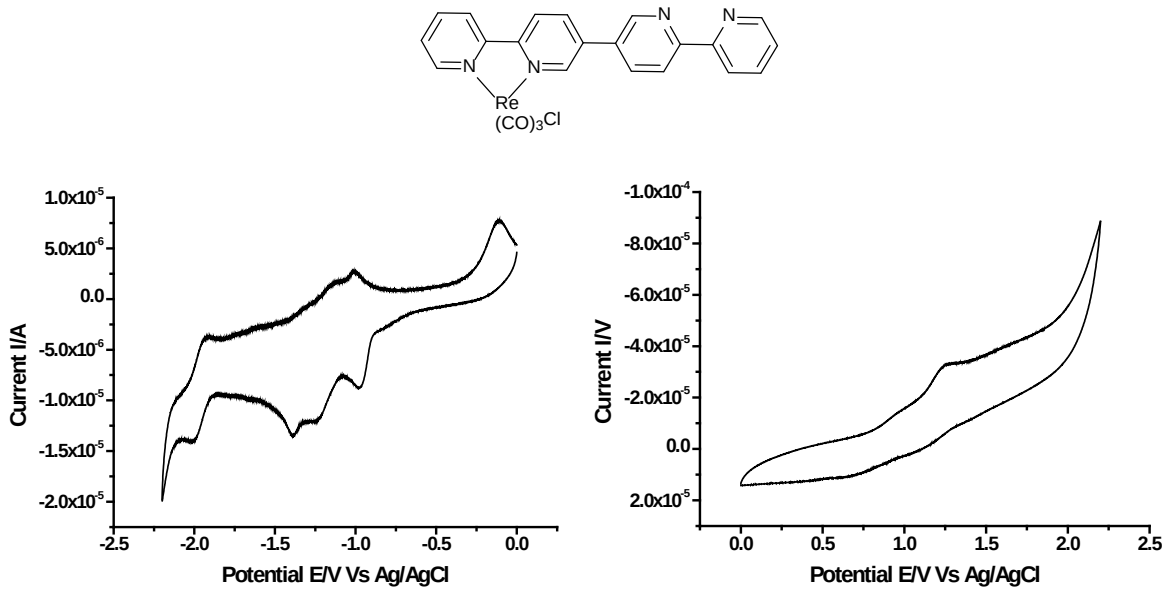

Figure 3.39 *Cyclic voltammogram of [(bisbpy)Re(CO)$_3$Cl] showing oxidation and reduction waves vs. Ag/AgCl in 0.1M TBAPF$_6$/MeCN at a scan rate of 0.1 Vs^{-1}*

3.2.7 CO Releasing Properties

CO release from the bisbpy based manganese and rhenium tricarbonyl complexes were attempted by measuring the conversion of deoxy-myoglobin (deoxy-Mb) to carbomonoxy myoglobin (Mb-CO) using UV-Vis spectroscopy and the amount of Mb-CO formed was quantified by measuring the absorbance value at 540 nm outlined in chapter 2.[76, 77]

The manganese and rhenium tricarbonyl complexes studied in this chapter were monitored for CO release both thermally and photochemically. No CO was detected using this approach when the carbonyl complexes were investigated under thermal condition (at 37 °C).

The complexes were assessed for photochemical CO release at different wavelengths (λ = 355, 436, 470 nm). CO release from manganese tricarbonyl complexes using the myoglobin assay was only observed at 436 nm. **Table 3.10** represents the overall profile for photochemical CO release at 436 nm from manganese and rhenium tricarbonyl complexes.

Table 3.10 *Photochemical CO release data for Rhenium and Manganese based carbonyl complexes, 60 μM and 40 μM represents the concentration of the Re/Mn complexes in solution.*

Name of the Complex	**Total Time Required for Photochemical (λ=436 nm) CO Release**		**Half Life ($t_{1/2}$)**
	60 μM	**40 μM**	
[(bpy)Mn(CO)$_3$Br]	60 mins	150 mins	19 mins (60 μM) 35 mins (40 μM)
[(bpy)Re(CO)$_3$Cl]	No release		
[(bisbpy)Mn(CO)$_3$Br]	30 mins	70 mins	7 mins (60 μM) 18 mins (40 μM)
[(bisbpy)Re(CO)$_3$Cl]	No release		
[Ru(bpy)$_2$(μ-bisbpy)Re(CO)$_3$Cl]$^{2+}$	No release		

From the literature survey the majority of Mn-based photo-CORMS reported so far exhibit CO release only upon exposure to a high power UV light source.[50, 78-80] However, [(bpy)Mn(CO)$_3$Br] (60 μM in DMSO) when exposed to 436 nm wavelength light source resulted in rapid CO-release as evident by the reduced myoglobin (Mb) assay (see **Table 3.10**). To test the suitability as photoactivatable CO releasing molecules (Photo-CORMs), the CO releasing properties of [(bpy)Mn(CO)$_3$Br] was investigated using the myoglobin assay which is the standard method to assess the CO releasing properties of metal carbonyl complexes. In a typical experiment, a 60 μM and 40 μM solution of the complex dissolved in DMSO was irradiated for time intervals of 5 min at 436 nm. This wavelength was chosen to induce carbon monoxide release from the complexes, as the compounds absorb in this region. The recorded spectra were then corrected to the isobestic point 510 nm (see **Figure 3.40** and **3.41**). From the comparison of the half-life ($t_{½}$) calculated for 60 μM solution ($t_{½}$ = 19 mins) and 40 μM solution ($t_{½}$ = 35 mins) that formation of [Mb-CO] is much faster at 60 μM than at 40 μM. **Figure 3.42** shows the formation of Mb-CO over time for the [(bisbpy)Mn(CO)$_3$Br] (60 μM in DMSO) when irradiated at 436 nm.

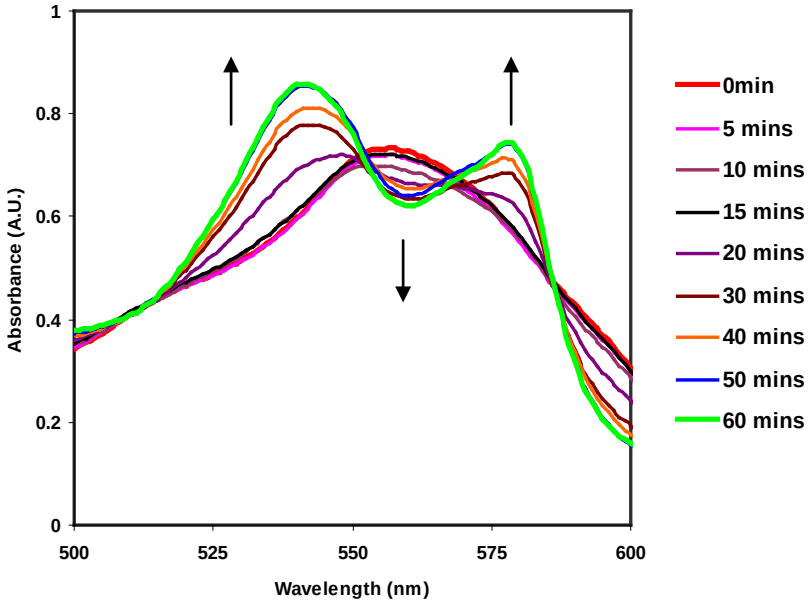

Figure 3.40 *CO-release profile for [(bpy)Mn(CO)$_3$Br]complex (60 μM) upon irradiation at 436 nm using deoxymyoglobin solution (66 μM).*

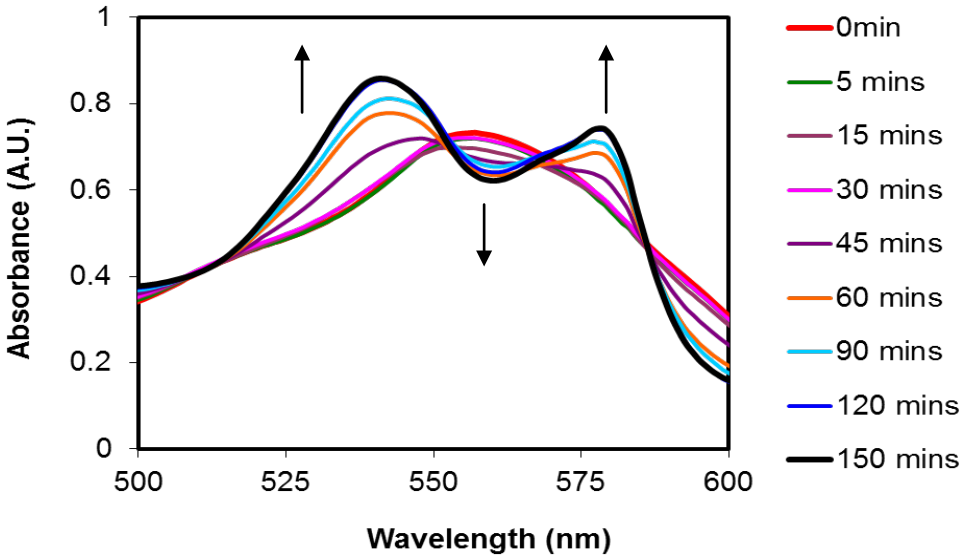

Figure 3.41 *CO-release profile for [(bpy)Mn(CO)$_3$Br]complex (40 μM) upon irradiation at 436 nm using deoxymyoglobin solution (66 μM). Legend shows time passed in mins.*

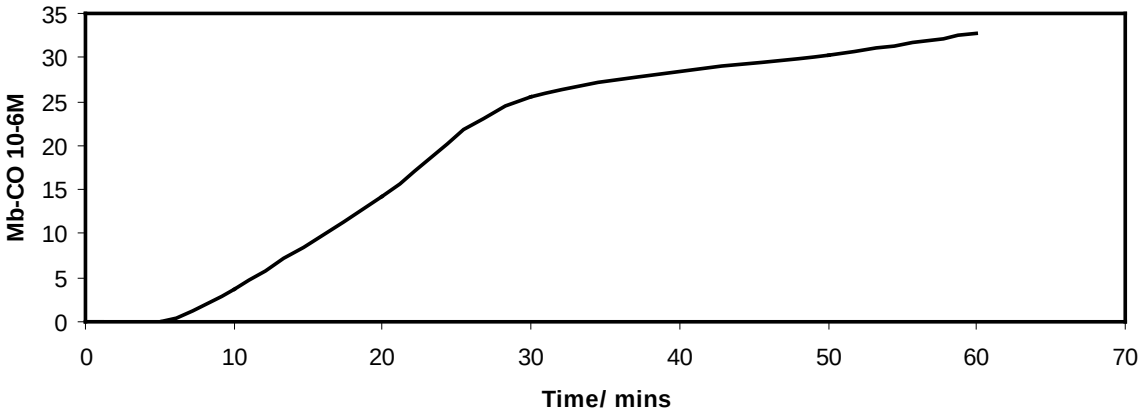

Figure 3.42 *Formation of Mb-CO quantified over time for [bpyMn(CO)$_3$Br] complex (60 μM) irradiated at 436 nm*

Similarly, the photochemical CO releasing properties of [(bisbpy)Mn(CO)$_3$Br] was investigated using the myoglobin assay and phosphate buffer solutions. [(bisbpy)Mn(CO)$_3$Br] complex was studied at two different concentrations 40 μM and 60 μM to compare the [Mb-CO] formation over the period of time (**Figure 3.43** and **3.44**). From the comparison of CO release at two different concentrations it was found that the [Mb-CO] formation is much faster ($t_{½}$ = 7 min) at 60 μM than ($t_{½}$ = 18 min) at 40 μM. Overall CO release for the the [(bisbpy)Mn(CO)$_3$Br] complex was faster with a half life of 7 mins when compared to [(bpy)Mn(CO)$_3$Br] complex which has a half life of 19 mins for 60 μM concentrations. **Figure 3.45** shows the formation of Mb-CO quantified over time for [(bpy)Mn(CO)$_3$Br] complex (60 μM) irradiated at 436 nm.

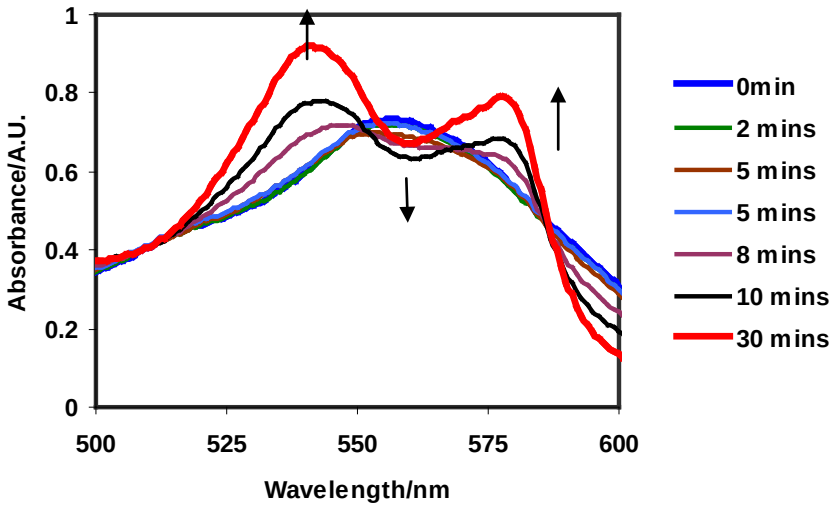

Figure 3.43 *CO-release profile for [(bisbpy)Mn(CO)$_3$Br]complex (60 μM) recorded at 436 nm using deoxymyoglobin solution (66 μM). Legend shows time passed in mins.*

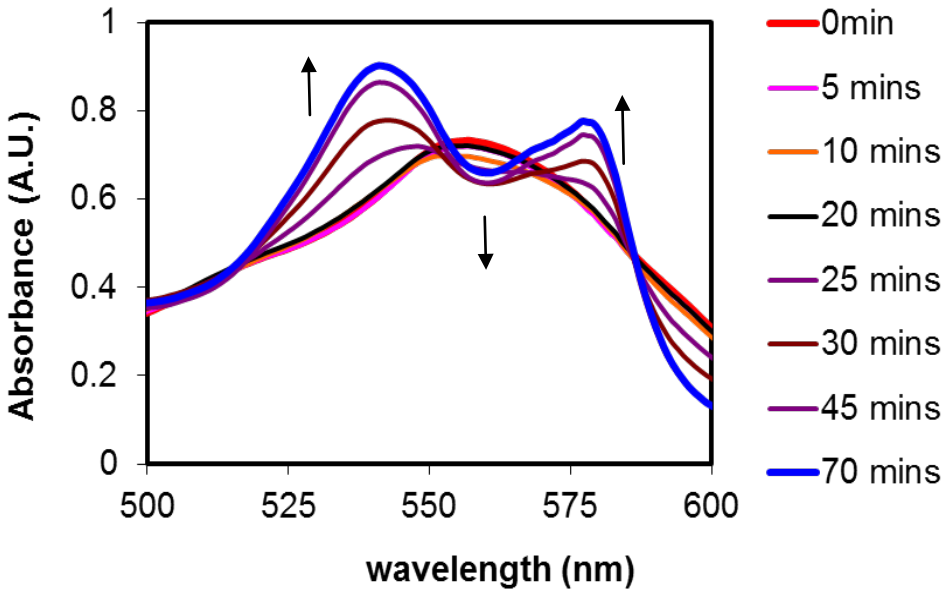

Figure 3.44 *CO-release profile for [(bisbpy)Mn(CO)$_3$Br]complex (40 μM) recorded at 436 nm using deoxymyoglobin solution (66 μM). Legend shows time passed in mins.*

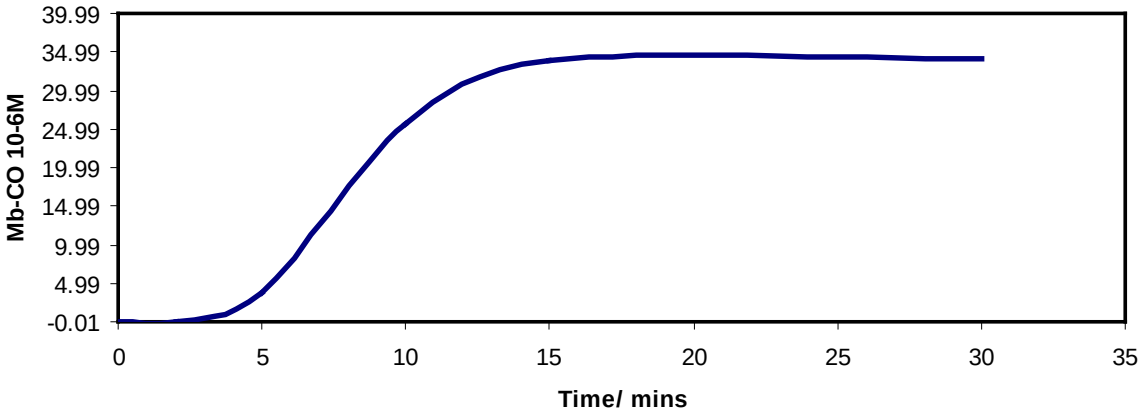

Figure 3.45 *Formation of Mb-CO quantified over time for [bisbpyMn(CO)$_3$Br] complex (60 μM) irradiated at 436 nm*

Compared to other Mn based CORMs such as the [(2-TIP^{NMe})Mn(CO)$_3$]OTf complex [(bisbpy)Mn(CO)$_3$Br] was found to be a much faster CO releasing molecule than the former system. The [(2-TIP^{NMe})Mn(CO)$_3$]OTf complex released CO completely after 60 mins however [(bisbpy)Mn(CO)$_3$Br] complex released CO completely after 30 min under photochemical conditions.[79] Also in the case of the [(2-TIP^{NMe})Mn(CO)$_3$]OTf complex to release CO irradiation at UV region is required whereas in case of [(bisbpy)Mn(CO)$_3$Br] complex less energy is needed to release CO photochemically. Also, the [(bpy)Mn(CO)$_3$Br] complex released CO rapidly over a period of 1 hour. This complex also needed much lower energy exposure to release CO photochemically compared to majority of reported Mn based Photo-CORMs which exhibited CO releasing properties only when exposed to UV light source.[78-80] No release of CO was detected for any of the rhenium based tricarbonyl complexes studied in this chapter either photochemically and thermally.

3.3 Conclusion

In this chapter, picosecond time resolved infra-red spectroscopy, electrochemistry and CO releasing properties of mononuclear rhenium and manganese as well as dinuclear ruthenium-rhenium tri-carbonyl complexes were studied. All complexes synthesised were characterised using ^{1}H NMR, UV-Vis and infrared spectroscopic techniques.

The UV-Vis spectra of the mononulclear rhenium and manganese complexes indicate strong absorbance in the UV region. This shows bisbpy ligand based $\pi \rightarrow \pi^*$ transitions. Whereas dinuclear tri-carbonyl complexes showed strong absorbance in the visible region, the MLCT band at 450 nm was observed for Ru-Re hetero di-nuclear complex which is attributed to $d\pi(Ru) \rightarrow \pi^*$(bisbpy) transition.

A study of emission properties revealed that the emission in the $[Ru(bpy)_2(\mu\text{-bisbpy})Re(CO)_3Cl]^{2+}$ complex is red shifted when compared to the $[Ru(bpy)_2(\mu\text{-bisbpy})]^{2+}$ monomer. This is due to the coordination of the $Re(CO)_3Cl$ moiety which stabilises the π^* level of bisbpy. No emission was detected at room temperature when the mononuclear rhenium and manganese tri-carbonyl complexes were excited at their MLCT bands. However these mononuclear complexes showed ligand-centred emission while they were excited at higher energy.

The infra-red spectra of the tricarbonyl complexes of rhenium and manganese have metal carbonyl stretching frequencies in the region of 1850-2050 cm^{-1}. From the IR spectrum patterns it can be concluded that all the complexes exist as *fac*- isomer.

Furthermore a picosecond time resolved infrared spectroscopic study of $[Ru(bpy)_2(bisbpy)Re(CO)_3Cl](PF_6)_2$ at λ_{exc} = 450 nm in acetonitrile solution resulted in formation of a relaxed Ru(II) to bisbpy bridging ligand based MLCT excited state ($[(bpy)_2Ru^{III}(bisbpy)Re^{I}(CO)_3Cl]^{2+}$) whereas the time resolved infrared spectroscopic study of $[(bisbpy)Re(CO)_3Cl]$ at λ_{exc} = 320 nm led to the shifting of IR υ(CO) bands to higher energy than their ground state counterparts which correspond to a Re to bisbpy based MLCT excited state.

Re and Mn based tri-carbonyl complexes were also studied for their photo and thermal CO releasing properties. $[bisbpyMn(CO)_3Br]$ and $[bpyMn(CO)_3Br]$ complexes have shown excellent photochemical CO releasing properties using myoglobin assays; complexes were irradiated at 436 nm. The $[bisbpyMn(CO)_3Br]$ complex showed better photochemical CO

releasing properties compared to the [bpyMn(CO)$_3$Br] complex. Both Mn based tricarbonyl complexes can be considered as potential photo CORMs as they use visible light for their photochemical release of CO.

3.4 Experimental

3.4.1. Materials and instrumental techniques

All solvents used for spectroscopy were of spectroscopic grade. $RuCl_3.3H_2O$, 2,2'-bipyridine, anhydrous DMF, [Pd(PPh_3)$_4$], PPh_3, [Ni_2Cl_2] and 2-Pyridylzincbromide in THF used for the reactions below were obtained from Sigma-Aldrich and used without further purification. All other solvents and reagents used were reagent grade. 5-bromo-2,2'-bipyridine(5Brbpy)[81], [(bpy)Mn(CO)$_3$Br][82] and [(bpy)Re(CO)$_3$Cl][83] were synthesised according to reported literature. Previously synthesised [Ru(bpy)$_2$Cl$_2$] by Dr. Mary Pryce's group was used to carry out the synthesis of [Ru(bpy)$_2$(bisbpy)](PF$_6$)$_2$. Schlenk technique was applied for all air sensitive reactions in anhydrous solvents. ^{1}H NMR (400 MHz) spectra were recorded in deuterated solvents (d_6-DMSO, d_3-acetonitrile) on a Bruker AC400 NMR and AC600 NMR Spectrometer with TMS or residual solvent peaks as reference. The XWIN-NMR processor and ACDLABS 12.0 NMR processor software were employed to process the free induction decay (FID) profiles. The H-H 2D COSY NMR involved the accumulation of 128 FIDs of 16 scans. Elemental analysis (CHN) was carried out using Exador Analytical CE440 by the Microanalytical Department, University College Dublin, Ireland. UV-Vis absorption spectra were recorded on a Shimadzu 3100 UV-Vis/NIR spectrophotometer interfaced to an Elonex PC575 desktop computer using 1 cm path length quartz cell. The detection wavelength was 190-900 nm. The ASCII data for each UV-Vis spectra were further processed using Microcal Origin 8 pro software. Emission spectra were recorded on a Perkin-Elmer LS0B luminescence spectrophotometer. The solvent used for the room temperature emission spectroscopy was spectroscopic grade acetonitrile. All spectra were initially generated by Perkin-Elmer FL Winlab custom built software and further the ASCII data were processed by Microcal Origin 8 pro software. The optical densities of all sample solutions were approximately 0.15 A.U. Cyclic voltammetry (CV) was carried out using a CH Instruments CHI version 2.07 software controlled potentiostat (CH Instuments Memphis 660). CV's of the complexes were obtained in a 0.1 M solution of tetrabutylammonium tetrafluoroborate ($TBABF_4$) in anhydrous acetonitrile. The solution was purged with N_2 (10 min) and an N_2 atmosphere was maintained throughout the experiment. The three electrodes

employed consisted of a Standard glassy carbon electrode (working, 2 mm diameter), platinum wire (counter) and Ag/Ag^+ half-cell reference. Extensive pre-treatment of the working electrodes were performed prior to each CV. Pre-treatment generally consisted of polishing the electrode surface with decreasing grades of alumina polish (1μm, 0.5μm) in distilled water with finely graded polishing pads in a figure of eight motion. Excess alumina particles on the surface of the electrodes were removed by sonication in distilled water for 10 min periods. The electrodes were then allowed to air dry. A CV of the solvent was obtained prior to each electrochemical measurement in order to ensure that all peaks noted in CVs were due to the sample being examined.

The ultrafast TRIR systems facility at the Van't Hoff Institute of Molecular Sciences, University of Amsterdam provided pump and probe spectroscopy with pico second time resolution. For the transient IR measurements, UV pump and mid-IR probe pulses were generated using a Ti:sapphire laser (Spectra-Physics Hurricane, 600 μJ) with a repetition rate of 1kHz. The UV pump pulse (400nm) was generated by SHG. By DFG of the signal and idler from a BBO-based OPA (Spectra-Physics OPA-800C) in AgGaS2, IR probe pulses were generated. The delay positions were scanned by mechanically adjusting the beam-path of the UV pump using a Newport ESP300 translation stage. The temporal resolution of 200 fs has been obtained from FWHM of the pump probe cross-correlate function. The laser pulse was 150 fs and energy output between was 1.5 - 2.0 μJ.

3.5 Synthesis

3.5.1 Synthesis of 5*Br-bpy*

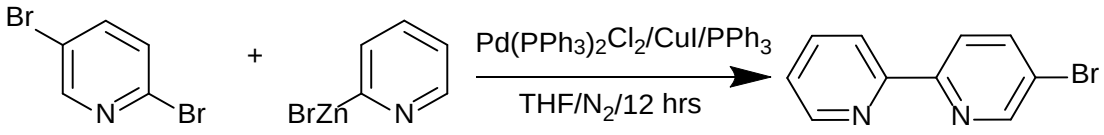

0.14 g (0.2 mmol) of $Pd(PPh_3)_2Cl_2$, 0.038 g (0.2mmol) of CuI, 0.105 g (0.4 mmol) of PPh_3 and 1.18 g (5 mmol) of 2,5-dibromopyridine were taken in a dried two neck round bottom flask under N_2 atmosphere. After that 19.35 mL (8.4 mmol) of 2-pyridylzincbromide (in dry THF) was added to the reaction mixture. The whole reaction mixture was stirred for 12 hours at room temperature under nitrogen atmosphere. After 12 hours of stirring the reaction mixture was poured into a saturated aqueous solution of EDTA/Na_2CO_3 until some yellow flakes appeared. The aqueous phase was extracted with DCM three times and dried over $MgSO_4$. DCM solvent was evaporated in air and the crude product was purified by alumina column using hexane/ethyl acetate (9:1) as eluent.

Yield: 1.058 g , 4.5 mmol, 90 %

^{1}H NMR (400 MHz, DMSO-d_6) δ ppm 7.49 (dd, J = 7.45, 4.80 Hz, 1 H), 7.97 (td, J = 7.71, 7.71 Hz, 1 H), 8.20 (dd, J = 8.46, 2.40 Hz, 1 H), 8.30 - 8.39 (m, 2 H), 8.67 - 8.73 (m, 1 H), 8.82 (d J = 2.40, 1 H)

3.5.2 Synthesis of *2,2':6'',2'''-quaterpyridine (bisbpy)*

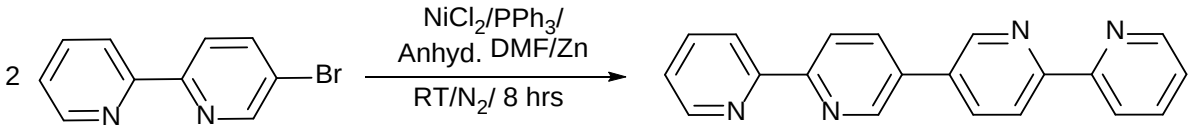

403 mg (1.7 mmol) of $NiCl_2.6H_2O$ was dissolved in 10 mL of anhydrous DMF under N_2 atmosphere. The reaction mixture became green. After $NiCl_2.6H_2O$ was completely dissolved in DMF, 891 mg (3.4 mmol) of PPh_3 was added to the DMF solution. The solution was then purged with nitrogen for 15 minutes at 20 ^oC. The solution turned deep blue in colour after adding PPh_3. 111 mg (3.4 mmol) of zinc-powder was added and the solution was stirred for another 30 minutes under a N_2 atmosphere. The solution turned green gradually and finally turned to deep brown solution. 400 mg (1.7 mmol) of 5Br-bpy was added to the deep brown solution and stirred for a further 18 hours at 20 ^oC under N_2 atmosphere. The reaction mixture was then poured into 150 mL of 3M aqueous NH_3. The product was extracted three times from the aqueous phase with 3 × 50 ml of ethyl acetate. Ethyl acetate was evaporated by a rotary evaporator and the remaining solvent containing DMF was removed using a liquid nitrogen pump. An off-white coloured sticky product was obtained. The crude product in hexane was sonicated for 30 minutes and then filtered under vacuum to get rid of excess of PPh_3. The process was repeated 4 times. TLC was checked with 80:20 hexane: ethyl acetate to ensure that there was no PPh_3 present in product. A white colour solid was finally collected as product.

Yield: 209 mg, 0.67 mmol, 79%.

^1H NMR (400 MHz, DMSO-d_6) δ ppm 7.50 (dd, *J* = 7.52, 4.74 Hz, 2 H), 8.00 (td, *J* = 7.83, 7.77 Hz, 2 H), 8.43 (dd, *J* = 8.34, 2.53 Hz, 2 H), 8.47 (d, *J* = 7.83 Hz, 2 H), 8.54 (d, *J* = 8.08 Hz, 2 H), 8.74 (d, *J* = 4.11 Hz, 2 H), 9.19 (d, *J* = 1.77 Hz, 2 H).

3.5.3 Synthesis of *[(bisbpy)Re(CO)$_3$Cl]*

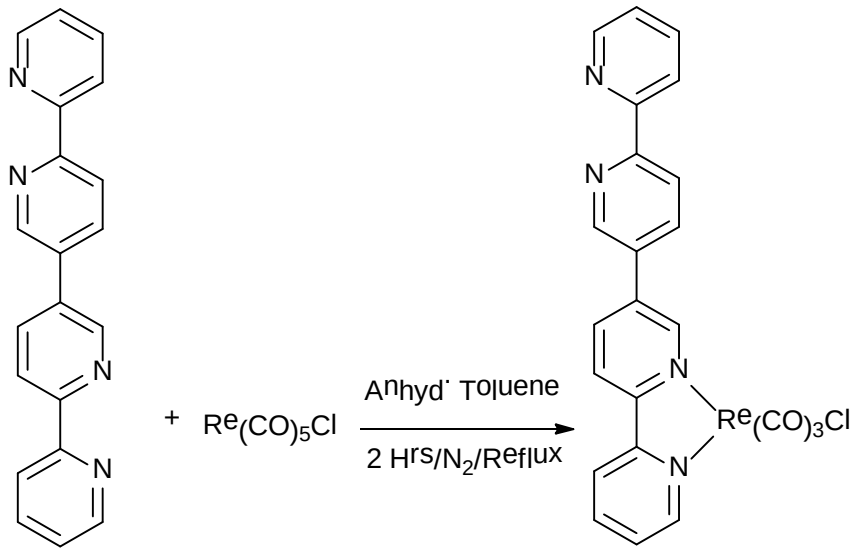

102 mg (0.33 mmol) of bisbpy and 50 mL anhydrous toluene were taken in a 100 mL round-bottom flask under N_2 atmosphere. 100 mg (0.77 mmol) of $Re(CO)_5Cl$ was added slowly over a period of 1 hour to the solution with slow stirring of the reaction mixture. After the addition of $Re(CO)_5Cl$, the reaction mixture was refluxed for 2 hours under N_2 atmosphere. The reaction was stopped and cooled to room temperature after 2 hours. An orange colour precipitate formed and was washed with cold toluene to remove the unreacted $Re(CO)_5Cl$ from the product. The product was then recrystallised from acetonitrile/diethyl-ether solvent mixture to remove the dinuclear bisbpy$[Re(CO)_3Cl]_2$ species formed as by product during the reaction. The infra-red (IR) spectra of the product was checked and recorded using acetonitrile to confirm the formation of product.

Yield: 152 mg, 0.25 mmol, 75%.

^{1}H NMR (400 MHz, DMSO-d_6) δ ppm 7.53 (ddd, *J*=7.39, 4.74, 1.26 Hz, 1 H) 7.76 - 7.83 (m, 1 H) 8.03 (td, *J*=7.71, 1.77 Hz, 1 H) 8.34 - 8.41 (m, 1 H) 8.50 (d, *J*=8.08 Hz, 1 H) 8.53 - 8.62 (m, 2 H) 8.76 (dd, *J*=3.66, 0.88 Hz, 1 H) 8.82 (dd, *J*=8.59, 2.02 Hz, 1 H) 8.87 (d, *J*=8.34 Hz, 1 H) 8.91 - 8.95 (m, 2 H) 9.05 - 9.10 (m, 1 H) 9.26 (dd, *J*=2.27, 0.76 Hz, 1 H) 9.32 (d, *J*=2.27 Hz, 1 H)

Elemental analysis for $C_{23}H_{14}ClN_4O_3Re$. M.W. = 616.04; Calc: C 44.84, H 2.29, N 9.09. Found: C 45.05, H 2.20 and N 9.41%.

IR ν_{CO} CH_3CN: 2022, 1915, 1898 cm^{-1}

3.5.4 Synthesis of *[(bisbpy)Mn(CO)$_3$Br]*

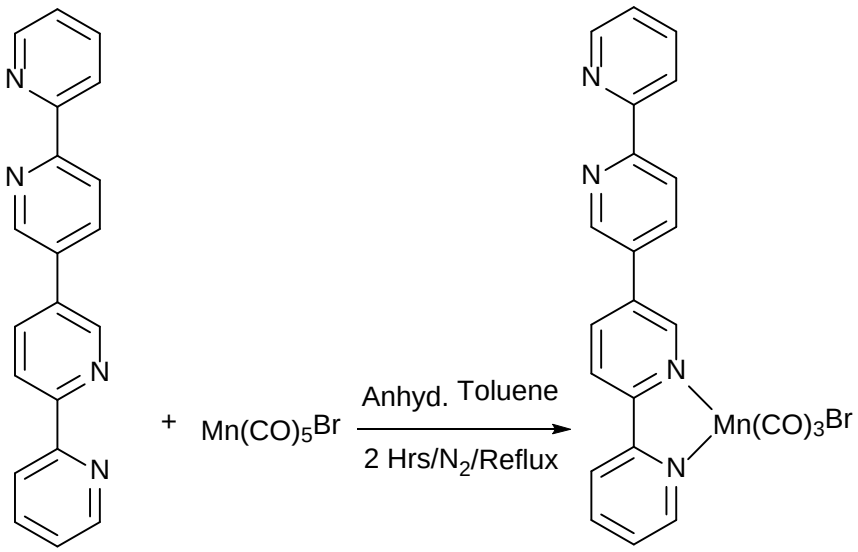

100 mg (0.32 mmol) of bisbpy ligand was dissolved in 50 mL anhydrous toluene in a 100 ml round-bottom flask under N_2 atmosphere. 59 mg (0.21 mmol) of $Mn(CO)_5Br$ was added slowly over a period of 1 hour to the solution with slow stirring of the reaction mixture. The reaction mixture was then refluxed for 2 hours under N_2 atmosphere. The reaction was stopped and cooled to room temperature after 2 hours. An orange coloured precipitate was formed and washed with cold toluene to remove unreacted $Mn(CO)_5Br$ from the product. The infra-red (IR) spectra of the obtained product was checked and recorded using acetonitrile to confirm the formation of product.

Yield: 110 mg, 0.21 mmol, 65%.

Elemental analysis of $C_{23}H_{14}BrN_4O_3Mn$, M.W = 529.22 Calc: C 52.20, H 2.67, N 10.59. Found: C 52.18, H 2.41 and N 10.53 %.

IR ν_{CO} CH_3CN: 2024, 1939, 1913 cm^{-1}

3.5.5 Synthesis of $[Ru(bpy)_2(bisbpy)](PF_6)_2$

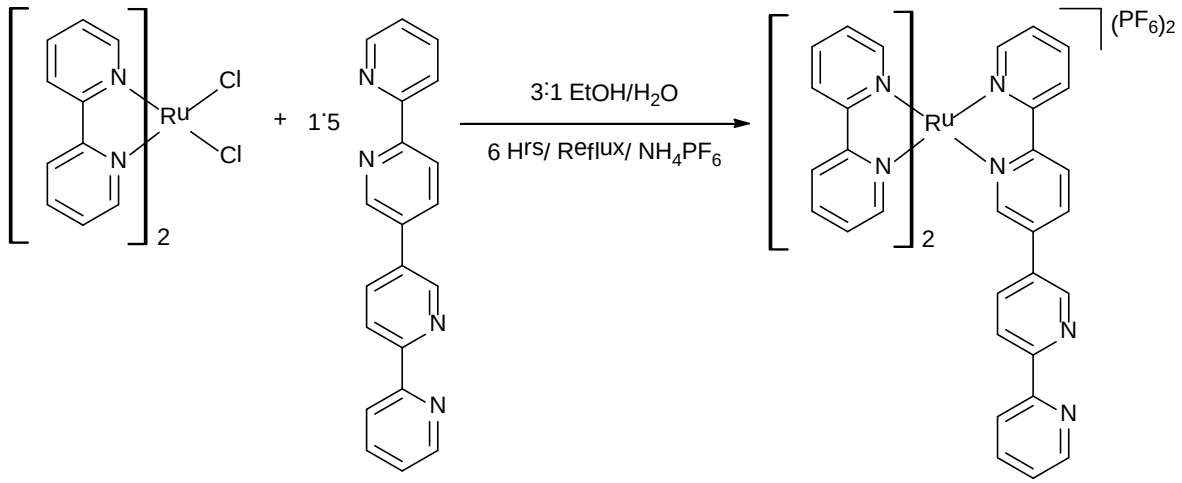

179 mg (0.577 mmol) of bisbpy were dissolved in 30 mL ethanol/water (3:1) and heated for 15 minutes. 200 mg (0.384 mmol) of $[Ru(bpy)_2Cl_2].2H_2O$ in ethanol was added slowly over 30 minutes. The total volume of the reaction mixture was kept to 50 mL and the reaction mixture was refluxed for further 6 hours. The reaction mixture turned dark red. The ethanol was completely removed by rotary evaporation and another 20 mL of water was added to the reaction mixture. The red aqueous reaction mixture was filtered twice and an aqueous solution of NH_4PF_6 was added in excess to the filtrate to yield a brick red precipitate. The precipitate was washed with diethyl ether and collected by filtration. Initial ^{1}H NMR analysis showed the formation of 20% of the dimer along with the formation of the required product. Hence, the crude product was further purified by recrystallisation using toluene/acetone solution.

Yield: 441 mg, 0.433 mmol, 75%.

^{1}H NMR (400 MHz, DMSO-d_6) δ ppm 1.30 - 1.40 (m, 12 H) 4.39 - 4.49 (m, 8 H) 7.56 (dd, *J* = 7.58, 5.94 Hz, 1 H) 7.59 - 7.67 (m, 2 H) 7.74 (dd, *J* = 5.94, 1.64 Hz, 1 H) 7.79 (dd, *J*= 5.81, 1.77 Hz, 1 H) 7.88 (dd, *J* = 5.94, 1.64 Hz, 2 H) 8.00 (dd, *J* = 6.06, 1.77 Hz, 1 H) 8.03 (d, *J* = 7.83 Hz, 1 H) 8.05 - 8.19 (m, 4 H) 8.31 - 8.40 (m, 1 H) 8.60 (d, *J* = 8.08 Hz, 1 H) 8.99 (d, *J* = 5.56 Hz, 1 H) 9.25 - 9.32 (m, 4 H).

IR ν_{CO} CH_3CN: 2024, 1939, 1913 cm^{-1}

Elemental analysis of $C_{40}H_{30}F_{12}N_8P_2Ru$: M.Wt = 1049.75 Calc: C 45.77, H 3.26, N 10.67. Found: C 46.15, H 2.86 and N 10.09 %.

3.5.6 Synthesis of $[Ru(bpy)_2(\mu\text{-bisbpy})Re(CO)_3Cl](PF_6)_2$

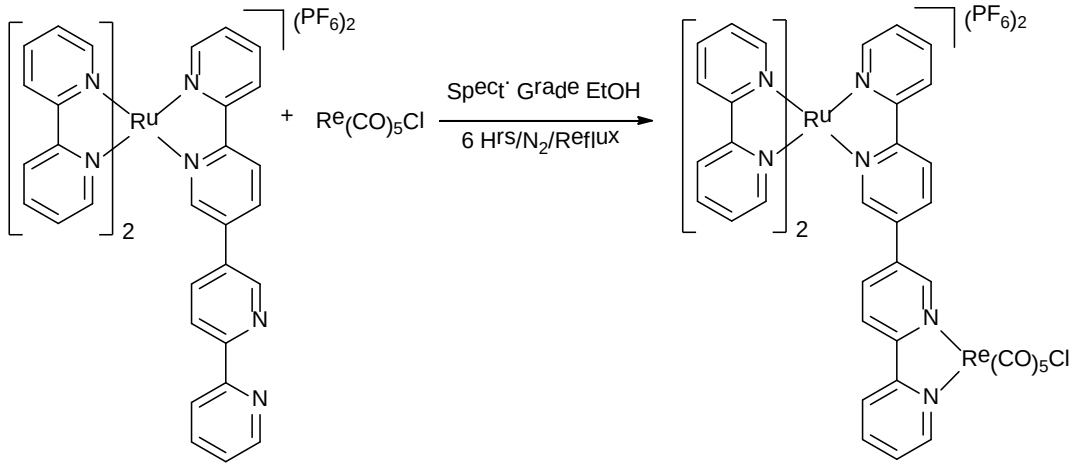

40 mL of spectroscopic grade ethanol was purged with nitrogen for 30 minutes. 77 mg (0.075 mmol) of $[Ru(bpy)_2(bis\text{-}bpy)](PF_6)_2$ and 32.8 mg (0.09 mmol) of $Re(CO)_5Cl$ were added to the purged ethanol. The reaction mixture was then refluxed in the dark for a further 6 hours under nitrogen atmosphere. The reaction was monitored by TLC and IR. The solvent was removed immediately by rotary evaporation after 6 hours of reaction. The crude product was washed with *n*-pentane and diethyl ether. The bright red coloured product was further purified by careful recrystallisation from acetone/toluene solution.

Yield: 86 mg, 0.065 mmol, 87%.

^{1}H NMR (400 MHz, DMSO-d_6) δ ppm 1.32 - 1.39 (m, 12 H), 4.41 - 4.48 (m, 8 H), 7.51 - 7.61 (m, 1 H), 7.75 - 8.05 (m, 10 H), 8.07 - 8.20 (m, 1 H), 8.23 - 8.31 (m, 1 H), 8.36 (t, *J*=8.34 Hz, 1 H), 8.62 - 8.70 (m, 1 H), 8.73 - 8.90 (m, 4 H), 8.98 - 9.05 (m, 2 H), 9.08 (dd, *J*=8.59, 3.03 Hz, 1 H), 9.19 (d, *J*=16.93 Hz, 1 H), 9.25 (d, *J*=8.08 Hz, 1 H), 9.32 (d, *J*=8.34 Hz, 2 H).

Elemental analysis for $C_{43}H_{30}ClF_{12}N_8O_3P_2ReRu.4H_2O.0.2$(toluene) M.Wt = 1409.9 Calc: C 37.82, H 2.83, N 7.94 Found: C 37.48, H 2.44 and N 7.45%

IR ν_{CO} in CH_3CN: 2022, 1917, 1899 cm^{-1}.

3.5.7 Synthesis of *[Ru(bpy)$_2$(bisbpy)Mn(CO)$_3$Br](PF6)$_2$*

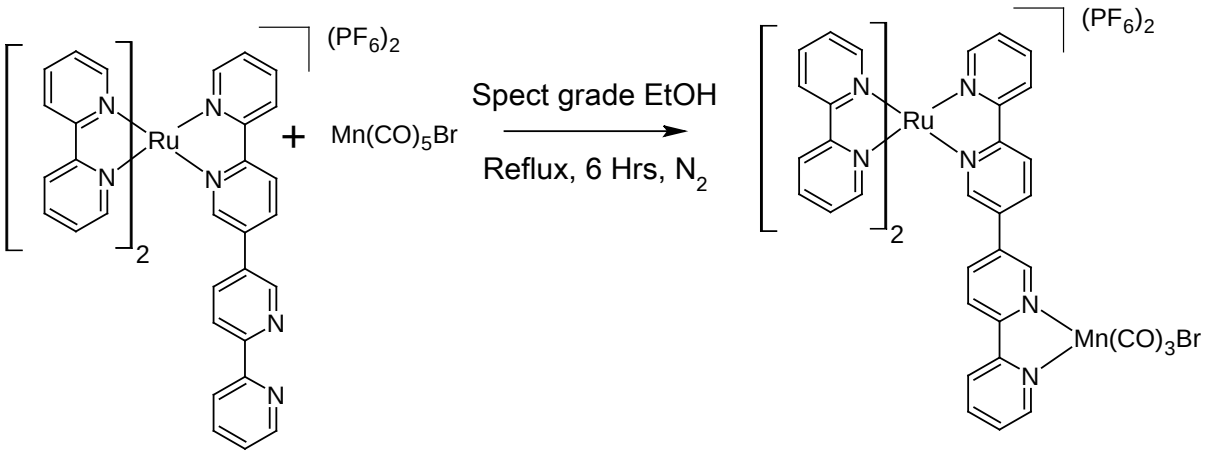

30 mL of spectroscopic grade ethanol was purged with nitrogen for 30 minutes. 50 mg (0.049 mmol) of $[Ru(bpy)_2(bis\text{-}bpy)](PF_6)_2$ and 20.0 mg (0.074 mmol) of $Mn(CO)_5Br$ were added to the purged ethanol. The reaction mixture was then refluxed in the dark for a further 6 hours under nitrogen atmosphere. The reaction was monitored by TLC and IR. The solvent was removed immediately by rotary evaporation after 6 hours of reaction. Bright red crude product was washed with *n*-pentane and diethyl ether. The formation of the product was check by infrared spectroscopy.

Yield: 48.5 mg, 0.039 mmol, 80%.

IR ν_{co} in solid state: 2022, 1915 (broad) cm^{-1}.

3.5.8 Synthesis of *[(bpy)Re(CO)$_3$Cl]*

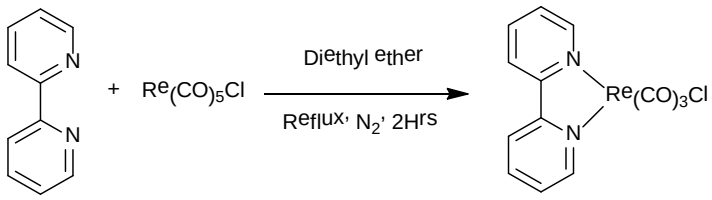

43 mg of bpy (0.28 mmol) and 100 mg of rhenium pentacarbonyl chloride (0.72 mmol) were dissolved in 20 mL of diethylether stirred and refluxed for 3 hours under nitrogen atmosphere. After cooling to room temperature the yellow coloured powder obtained by precipitation was washed with diethyl ether and dried under vacuum.

Yield: 111mg, 0.24 mmol, 91%

^{1}H NMR (400 MHz, $CDCl_3$) δ ppm 7.62 (m, 2 H), 8.37 (m, 2 H), 8.72 (d, *J* = 8.3 Hz, 2 H), 9.12 (d, *J*= 4.5 Hz, 2 H).

IR ν_{CO} in CH_3CN: 2018, 1917, 1892 cm^{-1}.

3.5.9 Synthesis of *[(bpy)Mn(CO)$_3$Br]*

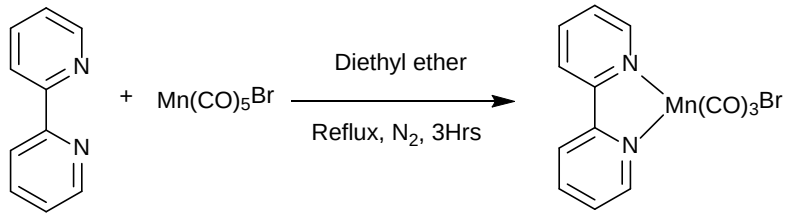

111 mg of bpy (0.71 mmol) and 199 mg of manganese pentacarbonyl bromide (0.72 mmol) were dissolved in 30 mL of diethylether stirred and refluxed for 3 hours under nitrogen atmosphere. After cooling to room temperature the yellow coloured power obtained by precipitation was washed with diethyl ether and dried under vacuum.

Yield: 200 mg, 0.53 mmol, 75%

^{1}H NMR (400 MHz, $CDCl_3$) δ ppm 7.62 (t, *J* = 6.0 Hz, 2 H), 8.12 (td, *J* = 7.7 Hz, 1.2 Hz, 2 H), 8.35 (d, *J*=8.1 Hz, 2 H), 9.24 (d, *J*= 4.8 Hz, 2 H).

IR ν_{CO} in CH_3CN: 2028, 1933 (Broad) cm^{-1}.

3.6 References

1. J. V. Caspar and T. J. Meyer, *J. Phys. Chem.*, 1983, **87**, 952-957.

2. L. A. Worl, R. Duesing, P. Chen, L. D. Ciana and T. J. Meyer, *J. Chem. Soc., Dalton Trans.*, 1991, 849-858.

3. M. Leirer, G. Knör and A. Vogler, *Inorg. Chem. Commun.*, 1999, **2**, 110-112.

4. A. Juris, S. Campagna, I. Bidd, J. M. Lehn and R. Ziessel, *Inorg. Chem.*, 1988, **27**, 4007-4011.

5. J. Hawecker, J.-M. Lehn and R. Ziessel, *J. Chem. Soc., Chem. Commun.*, 1983, 536-538.

6. H. Hori, J. Ishihara, K. Koike, K. Takeuchi, T. Ibusuki and O. Ishitani, *J. Photochem. Photobiol. A: Chem.*, 1999, **120**, 119-124.

7. F. P. A. Johnson, M. W. George, F. Hartl and J. J. Turner, *Organometallics*, 1996, **15**, 3374-3387.

8. K. K.-W. Lo, W.-K. Hui, C.-K. Chung, K. H.-K. Tsang, D. C.-M. Ng, N. Zhu and K.-K. Cheung, *Coord. Chem. Rev.*, 2005, **249**, 1434-1450.

9. V. W.-W. Yam, K. M.-C. Wong, V. W.-M. Lee, K. K.-W. Lo and K.-K. Cheung, *Organometallics*, 1995, **14**, 4034-4036.

10. D. I. Yoon, C. A. Berg-Brennan, H. Lu and J. T. Hupp, *Inorg. Chem.*, 1992, **31**, 3192-3194.

11. C. A. Berg-Brennan, D. I. Yoon, R. V. Slone, A. P. Kazala and J. T. Hupp, *Inorg. Chem.*, 1996, **35**, 2032-2035.

12. D. J. Stufkens and A. VlÄ□ek Jr, *Coord. Chem. Rev.*, 1998, **177**, 127-179.

13. G. J. Stor, S. L. Morrison, D. J. Stufkens and A. Oskam, *Organometallics*, 1994, **13**, 2641-2650.

14. C. Berg-Brennan, P. Subramanian, M. Absi, C. Stern and J. T. Hupp, *Inorg. Chem.*, 1996, **35**, 3719-3722.

15. B. D. Rossenaar, D. J. Stufkens and A. n. VlcÌŒek, *Inorg. Chem.*, 1996, **35**, 2902-2909.

16. L. Yang, A. M. Ren, J. K. Feng, X. J. Liu, Y. G. Ma, M. Zhang, X. D. Liu, J. C. Shen and H. X. Zhang, *J. Phys. Chem. A*, 2004, **108**, 6797-6808.

17. K. Kam-Wing Lo, D. Chun-Ming Ng, W.-K. Hui and K.-K. Cheung, *J. Chem. Soc., Dalton Trans.*, 2001, 2634-2640.

18. S. M. Fredericks, J. C. Luong and M. S. Wrighton, *J. Am. Chem. Soc.*, 1979, **101**, 7415-7417.

19. M. H. Chisholm, R. L. Kelly, F. A. Cotton and M. W. Extine, *J. Am. Chem. Soc.*, 1978, **100**, 2256-2257.

20. I. E. Pomestchenko, D. E. Polyansky and F. N. Castellano, *Inorg. Chem.*, 2005, **44**, 3412-3421.

21. M. Busby, P. Matousek, M. Towrie and A. Vlcek, Jr., *The journal of physical chemistry. A*, 2005, **109**, 3000-3008.

22. V. Wing-Wah Yam, V. Chor-Yue Lau and L.-X. Wu, *J. Chem. Soc., Dalton Trans.*, 1998, 1461-1468.

23. A. Gabrielsson, M. Busby, P. Matousek, M. Towrie, E. Hevia, L. Cuesta, J. Perez, S. ZÃ¡liÅ¡ and A. n. VlcÌŒek, *Inorg. Chem.*, 2006, **45**, 9789-9797.

24. M. Obata, A. Kitamura, A. Mori, C. Kameyama, J. A. Czaplewska, R. Tanaka, I. Kinoshita, T. Kusumoto, H. Hashimoto, M. Harada, Y. Mikata, T. Funabiki and S. Yano, *Dalton Trans*, 2008, 3292-3300.

25. V. V. Rostovtsev, L. G. Green, V. V. Fokin and K. B. Sharpless, *Angew. Chem. Int. Ed.*, 2002, **41**, 2596-2599.

26. M. Casanova, E. Zangrando, E. Iengo, E. Alessio, M. T. Indelli, F. Scandola and M. Orlandi, *Inorg. Chem.*, 2008, **47**, 10407-10418.

27. K. K.-W. Lo and K. H.-K. Tsang, *Organometallics*, 2004, **23**, 3062-3070.

28. A. Gabrielsson, F. e. Hartl, H. Zhang, J. R. Lindsay Smith, M. Towrie, A. n. VlcÌŒek and R. N. Perutz, *J. Am. Chem. Soc.*, 2006, **128**, 4253-4266.

29. F. Barigelletti and L. Flamigni, *Chem. Soc. Rev.*, 2000, **29**, 1-12.

30. T. Muckerman James and E. Fujita, in *Chemical Evolution II: From the Origins of Life to Modern Society*, American Chemical Society, Editon edn., 2009, vol. 1025, pp. 283-312.

31. H. Takeda, K. Koike, H. Inoue and O. Ishitani, *J. Am. Chem. Soc.*, 2008, **130**, 2023-2031.

32. H. Takeda and O. Ishitani, *Coord. Chem. Rev.*, 1999, **254**, 346-354.

33. A. Vogler and J. Kisslinger, *Inorg. Chim. Acta*, 1986, **115**, 193-196.

34. R. Sahai, D. P. Rillema, R. Shaver, S. Van Wallendael, D. C. Jackman and M. Boldaji, *Inorg. Chem.*, 1989, **28**, 1022-1028.

35. K. Kalyanasundaram and M. K. Nazeeruddin, *J. Chem. Soc., Dalton Trans.*, 1990, 1657-1662.

36. D. A. Bardwell, F. Barigelletti, R. L. Cleary, L. Flamigni, M. Guardigli, J. C. Jeffery and M. D. Ward, *Inorg. Chem.*, 1995, **34**, 2438-2446.

37. S. Van Wallendael and D. P. Rillema, *J. Chem. Soc., Chem. Commun.*, 1990, 1081-1082.

38. S. Encinas, A. M. Barthram, M. D. Ward, F. Barigelletti and S. Campagna, *Chem. Commun.*, 2001, 277-278.

39. S. P. Foxon, T. Phillips, M. R. Gill, M. Towrie, A. W. Parker, M. Webb and J. A. Thomas, *Angew. Chem. Int. Ed.*, 2007, **46**, 3686-3688.

40. B. Gholamkhass, H. Mametsuka, K. Koike, T. Tanabe, M. Furue and O. Ishitani, *Inorg. Chem.*, 2005, **44**, 2326-2336.

41. X. Liu, J. Liu, J. Pan, R. Chen, Y. Na, W. Gao and L. Sun, *Tetrahedron*, 2006, **62**, 3674-3680.

42. J. S. Ward, J. M. Lynam, J. W. B. Moir, D. E. Sanin, A. P. Mountford and I. J. S. Fairlamb, *Dalton Trans.*, 2012, **41**, 10514-10517.

43. U. Schatzschneider, *Inorg. Chim. Acta*, 2011, **374**, 19-23.

44. B. E. Mann and R. Motterlini, *Chem. Commun.*, 2007, 4197-4208.

45. K. Koike, J. Tanabe, S. Toyama, H. Tsubaki, K. Sakamoto, J. R. Westwell, F. P. A. Johnson, H. Hori, H. Saitoh and O. Ishitani, *Inorg. Chem.*, 2000, **39**, 2777-2783.

46. J. L. Smithback, J. B. Helms, E. Schutte, S. M. Woessner and B. P. Sullivan, *Inorg. Chem.*, 2006, **45**, 2163.

47. J.-D. Compain, M. Bourrez, M. Haukka, A. Deronzier and S. Chardon-Noblat, *Chem. Commun.*, 2014, **50**, 2539-2542.

48. J. Qiao, Y. Liu, F. Hong and J. Zhang, *Chem. Soc. Rev.*, 2014, **43**, 631-675.

49. S. J. Carrington, I. Chakraborty and P. K. Mascharak, *Chem. Commun.*, 2013, **49**, 11254-11256.

50. P. Govender, S. Pai, U. Schatzschneider and G. S. Smith, *Inorg. Chem.*, 2013, **52**, 5470-5478.

51. A. Paul, *PhD thesis, Dublin City University*, 2012.

52. D. J. Stufkens and A. Vlcek, *Coord. Chem. Rev.*, 1998, **177**, 127-179.

53. H. Takeda and O. Ishitani, *Coord. Chem. Rev.*, 2009, **254**, 346-354.

54. H. K. Van Dijk, J. Van der Haar, D. J. Stufkens and A. Oskam, *Inorg. Chem.*, 1989, **28**, 75-81.

55. F. Barigelletti, L. De Cola, V. Balzani, R. Hage, J. G. Haasnoot, J. Reedijk and J. G. Vos, *Inorg. Chem.*, 1989, **28**, 4344-4350.

56. Z.-Y. Bian, K. Sumi, M. Furue, S. Sato, K. Koike and O. Ishitani, *Inorg. Chem.*, 2008, **47**, 10801-10803.

57. S. Van Wallendael, R. J. Shaver, D. P. Rillema, B. J. Yoblinski, M. Stathis and T. F. Guarr, *Inorg. Chem.*, 1990, **29**, 1761-1767.

58. B. J. Yoblinski, M. Stathis and T. F. Guarr, *Inorg. Chem.*, 1992, **31**, 5-10.

59. I. Moldes and R. Mathieu, *J. Organomet. Chem.*, 1994, **480**, 185-189.

60. L. W. Houk and G. R. Dobson, *Inorg. Chem.*, 1966, **5**, 2119-2123.

61. D. R. Gamelin, M. W. George, P. Glyn, F.-W. Grevels, F. P. A. Johnson, W. Klotzbuecher, S. L. Morrison, G. Russell, K. Schaffner and J. J. Turner, *Inorg. Chem.*, 1994, **33**, 3246-3250.

62. K. Kalyanasundaram, M. Graetzel and M. K. Nazeeruddin, *Inorg. Chem.*, 1992, **31**, 5243-5253.

63. G. Li, K. Parimal, S. Vyas, C. M. Hadad, A. H. Flood and K. D. Glusac, *J. Am. Chem. Soc.*, 2009, **131**, 11656-11657.

64. J. R. Schoonover, C. A. Bignozzi and T. J. Meyer, *Coord. Chem. Rev.*, 1997, **165**, 239-266.

65. D. M. Dattelbaum, K. M. Omberg, J. R. Schoonover, R. L. Martin and T. J. Meyer, *Inorg. Chem.*, 2002, **41**, 6071-6079.

66. D. J. Liard, M. Busby, P. Matousek, M. Towrie and A. n. VlcÌŒek, *J. Phys. Chem. A*, 2004, **108**, 2363-2369.

67. A. Vlcek Jr, I. R. Farrell, D. J. Liard, P. Matousek, M. Towrie, A. W. Parker, D. C. Grills and M. W. George, *J. Chem. Soc., Dalton Trans.*, 2002, 701-712.

68. M. W. George, F. P. A. Johnson, J. R. Westwell, P. M. Hodges and J. J. Turner, *J. Chem. Soc., Dalton Trans.*, 1993, 2977-2979.

69. J. R. Schoonover, A. P. Shreve, R. B. Dyer, R. L. Cleary, M. D. Ward and C. A. Bignozzi, *Inorg. Chem.*, 1998, **37**, 2598-2601.

70. H. A. Nieuwenhuis, J. G. Haasnoot, R. Hage, J. Reedijk, T. L. Snoeck, D. J. Stufkens and J. G. Vos, *Inorg. Chem.*, 1991, **30**, 48-54.

71. R. Hage, A. H. J. Dijkhuis, J. G. Haasnoot, R. Prins, J. Reedijk, B. E. Buchanan and J. G. Vos, *Inorg. Chem.*, 1988, **27**, 2185-2189.

72. C. Brennan, *PhD Thesis, Dublin City University*, 2007.

73. R. H. J.M.de wolf, J.G. Haasnoot, J. Reedijk, J.G.Vos, *New. J. Chem.*, 1991, **15**, 501.

74. H. E. A. K. C. V. W.Kaim, J.Rieker, *J.Organomet.Chem*, 1989, 107.

75. A. Klein, C. Vogler and W. Kaim, *Organometallics*, 1996, **15**, 236-244.

76. P. Sawle, J. Hammad, I. J. S. Fairlamb, B. Moulton, C. T. O'Brien, J. M. Lynam, A. K. Duhme-Klair, R. Foresti and R. Motterlini, *J. Pharmacol. Exp. Ther.*, 2006, **318**, 403-410.

77. A. J. Atkin, S. Williams, P. Sawle, R. Motterlini, J. M. Lynam and I. J. S. Fairlamb, *Dalton Trans.*, 2009, 3653-3656.

78. J. Niesel, A. Pinto, H. W. P. N'Dongo, K. Merz, I. Ott, R. Gust and U. Schatzschneider, *Chem. Commun.*, 2008, 1798-1800.

79. P. C. Kunz, W. Huber, A. Rojas, U. Schatzschneider and B. Spingler, *Eur. J. Inorg. Chem.*, 2009, **2009**, 5358-5366.

80. G. DoÌˆrdelmann, H. Pfeiffer, A. Birkner and U. Schatzschneider, *Inorg. Chem.*, 2011, **50**, 4362-4367.

81. Y.-Q. Fang and G. S. Hanan, *Synlett*, 2003, **2003**, 0852,0854.

82. M. Bourrez, F. Molton, S. Chardon-Noblat and A. Deronzier, *Angew. Chem. Int. Ed.*, 2011, **50**, 9903-9906.

83. M. Wrighton and D. L. Morse, *J. Am. Chem. Soc.*, 1974, **96**, 998-1003.

Chapter 4

Singlet oxygen and CO release studies of porphyrin-based metal-carbonyl complexes

A range of porphyrins including free base and metallomacrocycles were studied for this ability to generate singlet oxygen. In addition, metal carbonyl tethered porphyrin macrocycles were also studied. The latter systems were further investigated for their ability to act as CO releasing molecules both thermally and photochemically.

4.1 Introduction

Porphyrin metal complexes represent an important field of research. The unique physicochemical properties of porphyrins have prompted the incorporation of these macrocycles in a large number of systems where their role is to harvest light efficiently and once photo excited, to act as an electron donor for an acceptor moiety.[1, 2]

Extensive studies have been done on the systems that undergo electron transfer processes involving porphyrin macrocycles to covalently linked to transition metal complexes.[3] These compounds display a rich electrochemistry and versatile catalytic and photochemical properties. Porphyrin molecules coordinated to a transition metal are of great interest as these supramolecular systems can mimic the electron transfer process observed in photosynthesis. Porphyrins absorb within the therapeutic window (600 – 800 nm) where diseases may be treated effectively upon irradiation. Porphyrin molecules have been investigated for their role as photosensitisers in singlet oxygen studies as described in chapter 1.[4]

Singlet oxygen is generated via electron transfer process from a photosensitiser. First the photosensitizer is excited to the first singlet state ($S_0 \rightarrow S_1$). Then the singlet excited state undergo intersystem crossing to the lower excited triplet state ($S_1 \rightarrow T_1$). Upon collision ground state triplet molecular oxygen undergo energy transfer from the triplet excited state of photosensitiser to produce singlet oxygen species (see **Figure 4.1**).

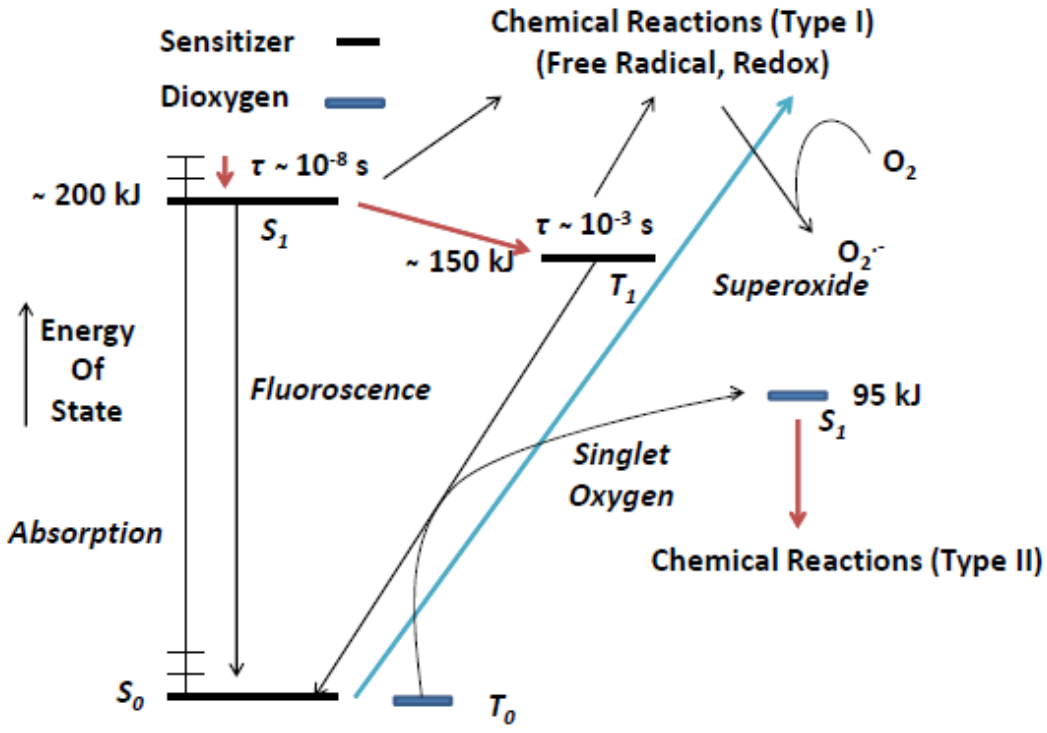

Figure 4.1: *Generation of excited photosensitiser states and reactive dioxygen species.*

Porphyrin ring is aromatic, planar and highly stable. It contains four pyrrole subunits linked together by methine bridges. The porphyrin ring consists of 22π electrons with each atom in macrocycle being sp^2 hybridised but only 18π electrons are completely delocalised.

Figure 4.2 shows the chemical structure and backbone of simplest porphyine ring upon which all porphyrins are derived. The high degree of conjugation is also visible in its electronic absorption spectrum. The visible spectrum of a typical porphyrin molecule consistes of a very intense absorption band around 400 nm known as Soret band, which is attributed to $S_0 \rightarrow S_2$ transition. The other absorption bands between 500 and 650 nm are known as the Q band and represents the $S_0 \rightarrow S_1$ transition. The Q band contains multiple peaks corresponding to different vibrational modes. Irradiation of the porphyrin molecule leads to formation of second excited singlet state which decays to the first excited singlet state and undergo intersystem crossing to the first triplet state. The long lived triplet excited state and high triplet quantum yield of most porphyrin molecules make them efficient photosensitizers for singlet oxygen generation.[5]

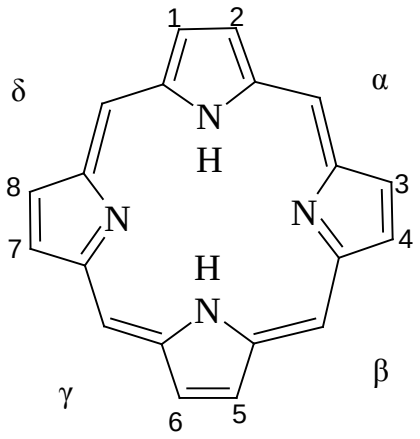

Figure 4.2: *Structure of Porphine*

Pyridyl porphyrins have attractive spectroscopic, photophysical and redox properties and are building blocks for the construction of photoactive supramolecular systems. A variable number of 4-pyridyl (*n*) and phenyl (4 - *n*) groups at the *meso* position(s) of the porphyrin macrocycle. The *meso* pyridyl groups provide great flexibility to synthesise metal complexes of various coordination numbers and geometries to porphyrin ring as the peripheral nitrogen atom(s) of the pyridyl ring can be coordinated to the metal complexes. The *meso* pyridyl group plays an important role as a ligand for metal sites that are held at fixed distances and angles to the porphyrin molecule. A new class of porphyrins are designed on complexation of the peripheral pyridyl nitrogen atom of the porphyrin molecules with the metal complexes (**Figure 4.3**).

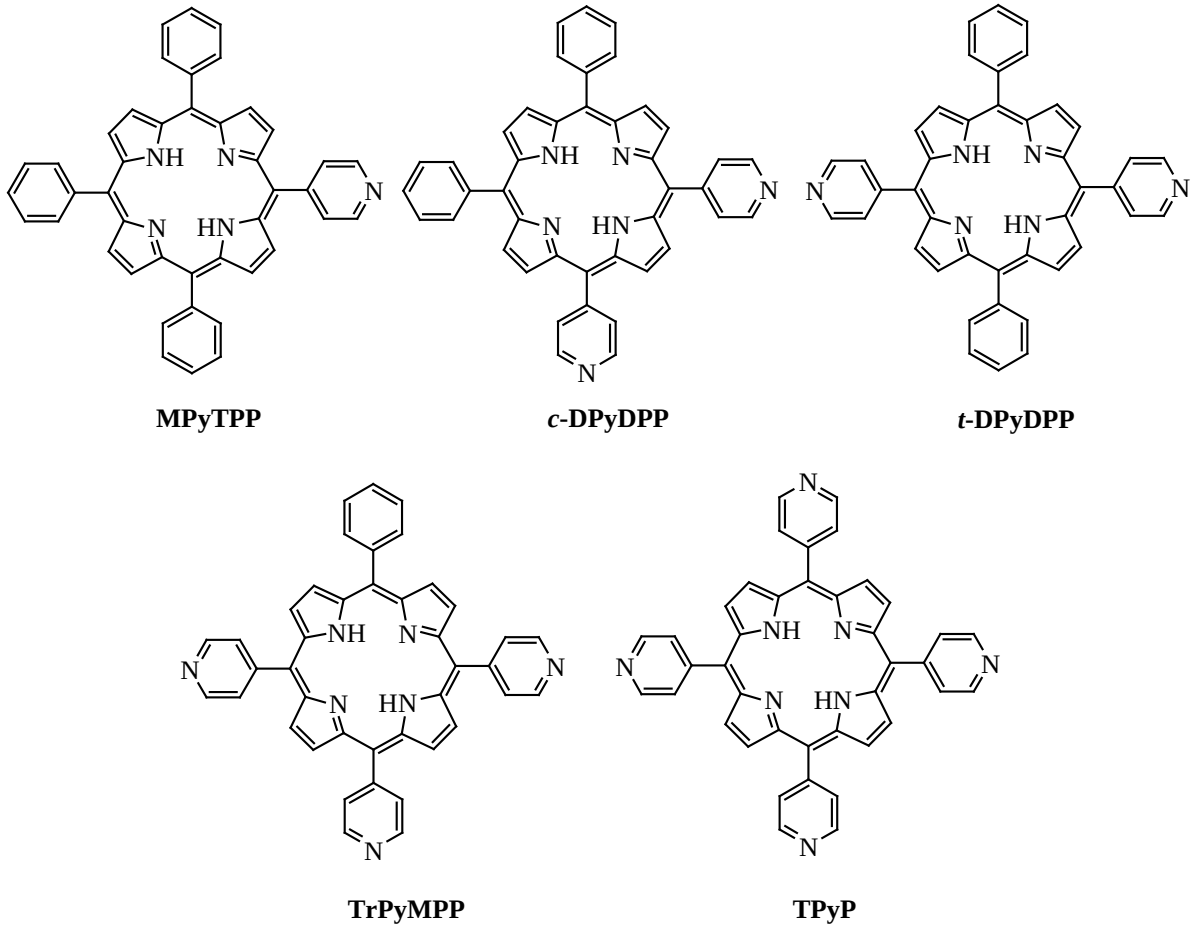

Figure 4.3: *Five 4-pyridyl (n) and phenyl (4 - n) meso substituted porphyrins*

Extent of electron transfer is extensively studied between metal carbonyls coordinating to a porphyrin molecule as it provides valuable data for the excited states of the individual porphyrin and metal carbonyl fragments. For example, transition metal carbonyls including (μ-H)-$Os(CO)_{10}$, $Re(CO)_3Cl$, $RuCl_2(DMSO)_2CO$, $Cr(CO)_3$ and $W(CO)_5$ coordinated to various porphyrin molecules have been investigated to study the efficiency of communication between the porphyrin and a metal carbonyl moiety across π substituents at the *meso* position of the porphyrin macrocycle and study photophysical measurements.[6-9]

For example Perutz and co workers reported freebase and zinc metalled porphyrins tethered to $W(CO)_5$ moiety via a pyridyl linker (**Figure 4.4**). This series of porphyrins were investigated to study the interactions between metal carbonyl and mono pyridyl porphyrin molecules. The UV-Vis spectra for both complexes **1** and **2** were dominated by porphyrin transitions with no shift in band position observed upon metallation with $W(CO)_5$. Time

resolved absorbance spectroscopy was used to probe the $^3(\pi\text{-}\pi^*)$ excited states of complexes **1** and **2**. The transient spectra were typical of porphyrin based $^3(\pi\text{-}\pi^*)$ excited state and no change in spectra was observed for $W(CO)_5$ coordinated porphyrin compounds. The fluorescence spectra of Zn metallated porphyrin without $W(CO)_5$ coordination exhibited two emission bands at 610 and 610 nm when excited the molecule at 355 nm. The fluorescence spectrum for the tungsten metal coordinated porphyrin complex showed an extra emission at 630 nm which authors suggested is due to photoinduced electron transfer process. [8]

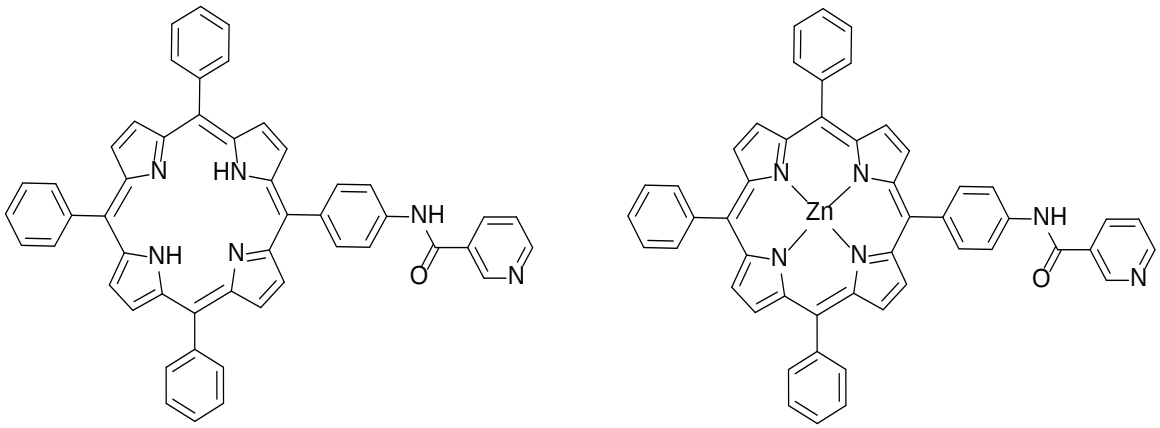

1 **2**

Figure 4.4: *Structures of freebase (**1**) and zinc metallated porphyrin (**2**) molecules bound to $W(CO)_5$ moiety.*

Mimicking green plants' extraordinary ability to absorb a vast number of photons and harness their energy is a longstanding goal in artificial photosynthesis. In recent years porphyrin molecules have gain much attention for their ability to function as light harvesting dyads.[10-12] These significant applications of porphyrins have lead to the synthesis of a vast array of free base and metallated porphyrins. Our group is interested in the ability of porphyrins to generate singlet oxygen, and also in the case of metal carbonyl linked porphyrins, their potential to act as CO releasing molecules.

In this chapter a series of freebase and Zn, Cu and Pd metallated porphyrin molecules as well as tungsten and chromium pentacarbonyl groups tethered to the nitrogen of the pyridyl ring of

the porphyrin macrocycles were synthesised and characterised using proton NMR, IR and UV-vis spectroscopic techniques. These molecules were synthesised with an aim to study their singlet oxygen generation and CO releasing properties using myoglobin assays both thermally and photochemically. Further, two sets of experiments using two different solvents toluene and DCM were carried for all the synthesised porphyrin molecules to investigate and calculate the quantum yield of singlet oxygen generation (**See Figure 4.5**). Porphyrin molecules highlighted in (*) have been synthesised previously within the Dr. Pryce research group.[13] For simplicity, the IUPAC names of the porphyrin moieties have been changed and the following names of the porphyrin macrocycles are used in this chapter of the thesis.

IUPAC Name	Common Name
5,10, 15, 20-tetraphenyl porphyrin	TPP
5-(4-Pyridyl)-10,15,20-triphenyl porphyrin	MPyTPP

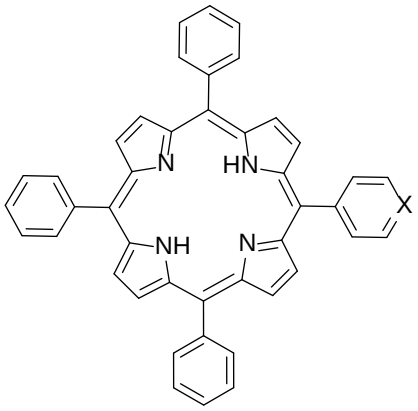

X		
C	TPP	(1)
N	MPyTPP	(2)

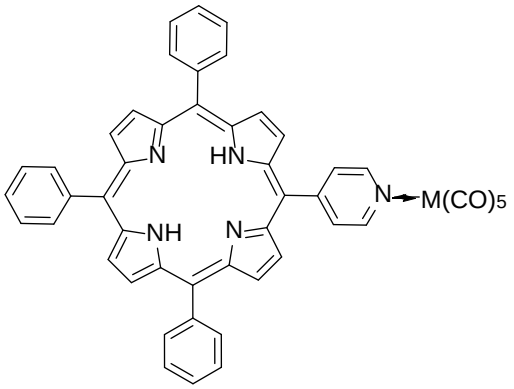

M		
Cr	$MPyTPPCr(CO)_5$	(9)
W	$MPyTPPW(CO)_5$	(10)

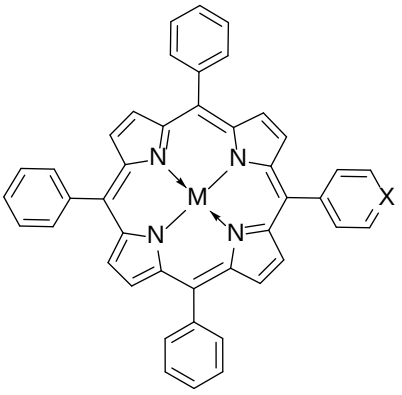

M	**X**		
Zn	C	ZnTPP	(3)
Zn	N	ZnMPyTPP	(4)
Cu	C	CuTPP	(5)
Cu	N	CuMPyTPP	(6)
Pd	C	PdTPP	(7)
Pd	N	PdMPyTPP	(8)

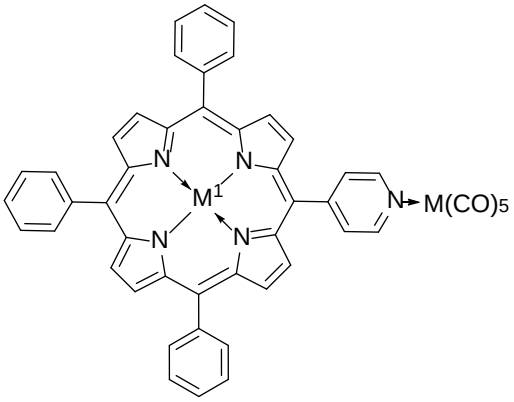

M^1	**M^2**		
Zn	Cr	$ZnMPyTPPCr(CO)_5$	(11)
Zn	W	$ZnMPyTPPW(CO)_5$	(12)
Cu	Cr	$CuMPyTPPCr(CO)_5$	(13)
Cu	W	$CuMPyTPPW(CO)_5$	(14)

Figure 4.5: *Structures of MPyTPP*, TPP*, ZnMPyTPP*, ZnTPP*,, CuMPyTPP, CuTPP, PdMPyTPP, PdTPP, MPyTPP-$Cr(CO)_5$,* ZnMPyTPP-$Cr(CO)_5$*, MPyTPP-$W(CO)_5$*, ZnMPyTPP-$W(CO)_5$*, CuMPyTPP-$Cr(CO)_5$ and CuMPyTPP-$W(CO)_5$ porphyrin macrocycles synthesised in this chapter.*

4.2 Results and Discussion

4.2.1 Absorption Spectroscopy

The UV-Vis spectrum of the uncomplexed freebase porphyrin, H_2MPyTPP (see in **Figure 4.6**), was reported previously and is similar to that of H_2TPP.[14] It displayed a Soret λ_{max} at 418 with four Q bands in the range 514 – 644 nm (**Table 4.1**). The freebase pyridyl porphyrins complexed with metal pentacarbonyls, H_2MPyTPP-W(CO)$_5$ and H_2MPyTPP-Cr(CO)$_5$ have an intense Soret band and four Q bands, with the Soret band red shifted by only 2 and 4 nm respectively, and a 2 nm red shift was observed in all Q bands (**Table 4.1**). The small but consistent bathochromic shift of the Soret and Q bands indicates very weak electronic interaction between the metal carbonyl centre and the porphyrin macrocycle.[15] The UV-Vis spectrum of ZnMPyTPP (**Figure 4.6**) has also been reported previously and is very similar to that of ZnTPP with a Soret λ_{max} observed at 418 nm and two Q bands at 562 and 604 nm (**Table 4.1**).[13] The UV-Vis spectrum of ZnMPyTPP show a red shift of Q bands by 404 nm when compared to PdMPyTPP complex.

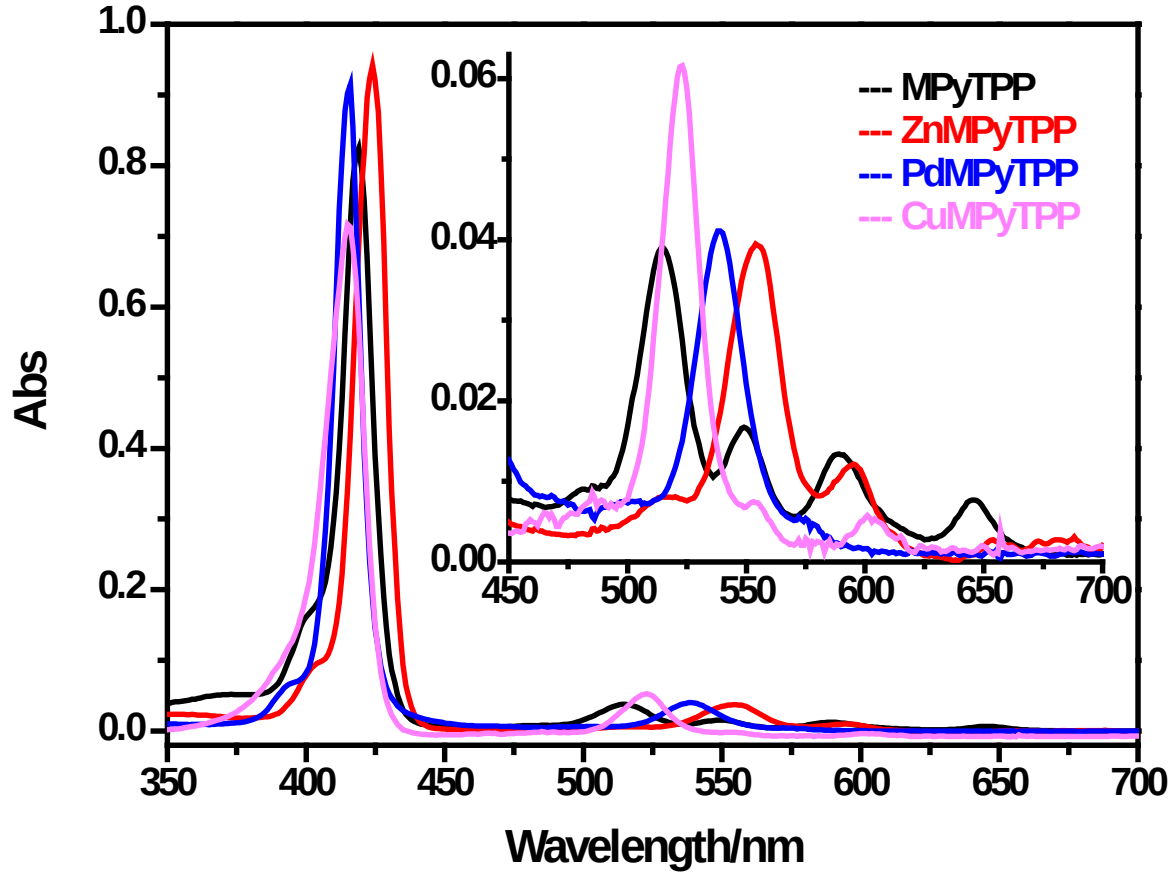

Figure 4.6: *UV-Vis spectra of MPyTPP, ZnMPyTPP, PdMPyTPP and CuMPyTPP, recorded in* CH_2Cl_2 *at 20* ^oC

***Table 4.1**: Absorbance maxima of freebase and Zinc(II), Palladium(II) and Copper(II) porphyrins and metal-pentacarbonyl-porphyrin complexes recorded in spectroscopic grade CH_2Cl_2.*

Compound	**Soret band (nm)**	**Q bands (nm)**
MPyTPP	418	514, 548, 588, 644
ZnMPyTPP	418	562, 604
MPyTPP-$W(CO)_5$	422	516, 552, 590, 646
ZnMPyTPP-$W(CO)_5$	420	548, 588
MPyTPP-$Cr(CO)_5$	420	516, 552, 590, 646
ZnMPyTPP-$Cr(CO)_5$	422	548, 588
CuMPyTPP-$W(CO)_5$	416	536, 578
CuMPyTPP-$Cr(CO)_5$	415	538, 576
TPP	418	515, 549, 589, 645
ZnTPP	419	536, 589
PdTPP	416	524, 557
CuTPP	417	536, 578
CuMPyTPP	418	537, 579
PdMPyTPP	417	525, 560

The UV-Vis spectrum of MPyTPP, ZnMPyTPP, PdMPyTPP and CuMPyTPP are displayed in **Figure 4.6**. The overall profile of the absorbance spectra are similar to those reported.[16-18] Following complexation of the porphyrins (MPyTPP, ZnMPyTPP, CuMPyTPP) with $W(CO)_5$ and $Cr(CO)_5$, the UV-Vis spectra are dominated by porphyrin based transitions with only a slight shift in the band position. No tungsten or chromium based absorbance phenomena were detected for the porphyrin metal carbonyl complexes. The electronic absorbance spectral features of the porphyrins synthesised in this study are listed in **Table 4.1**.

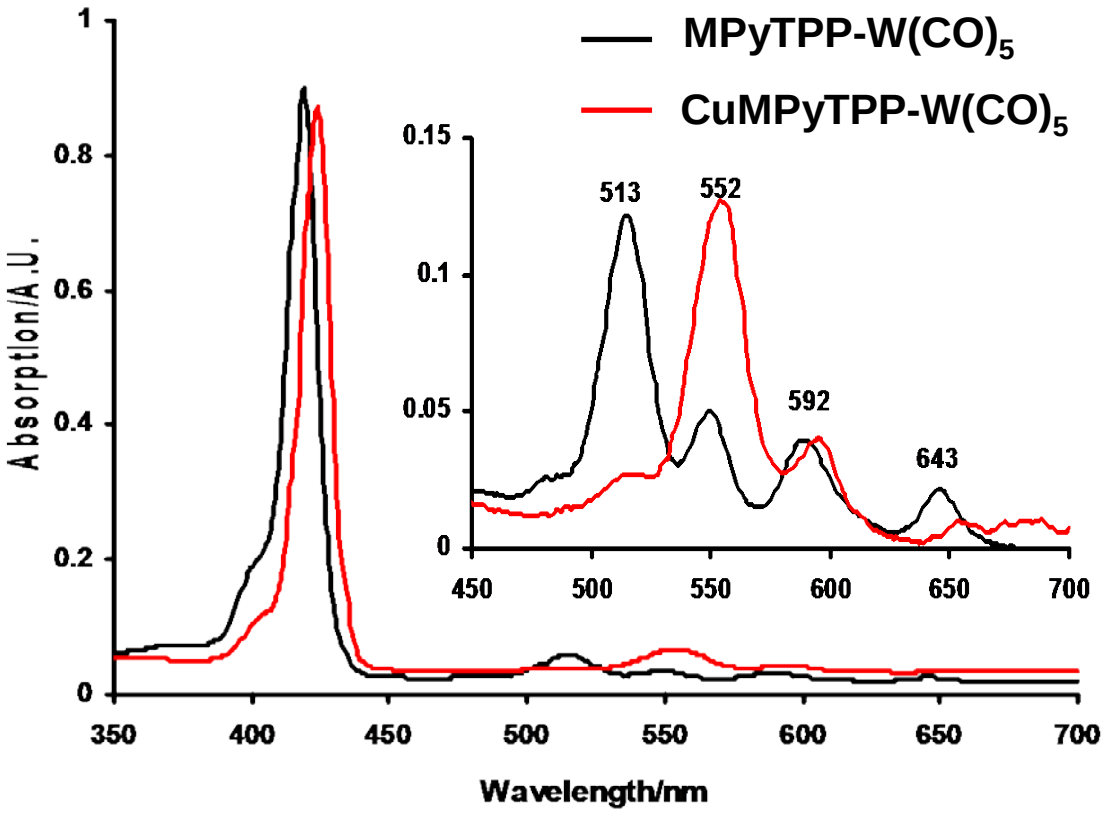

Figure 4.7: *UV-Vis spectra of MPyTPP-W(CO)$_5$ (black line) and CuMPyTPP-W(CO)$_5$ (red line) recorded in CH_2Cl_2 at 20 ^oC.*

Pyridine is known to coordinate to the metal centre of a metalloporphyrin and in this case the N atom of the pyridine unit coordinates to the Zn atom of another, leading to the formation of a polymer. However Q bands of PdMPyTPP were similar to that of PdTPP suggesting non

polymerisation of the molecule. Complexation of the zinc porphyrin with the metal pentacarbonyl moiety produced electronic absorbance spectra that were similar to that of the uncomplexed zinc porphyrins. However substantial blue shifts were observed in the Q band region of 14 – 16 nm. The reason for this large shift in the Q bands (compared to the 2 nm red shift observed with freebase analogues) is that the environment of the meso-pyridyl group was changed more dramatically.

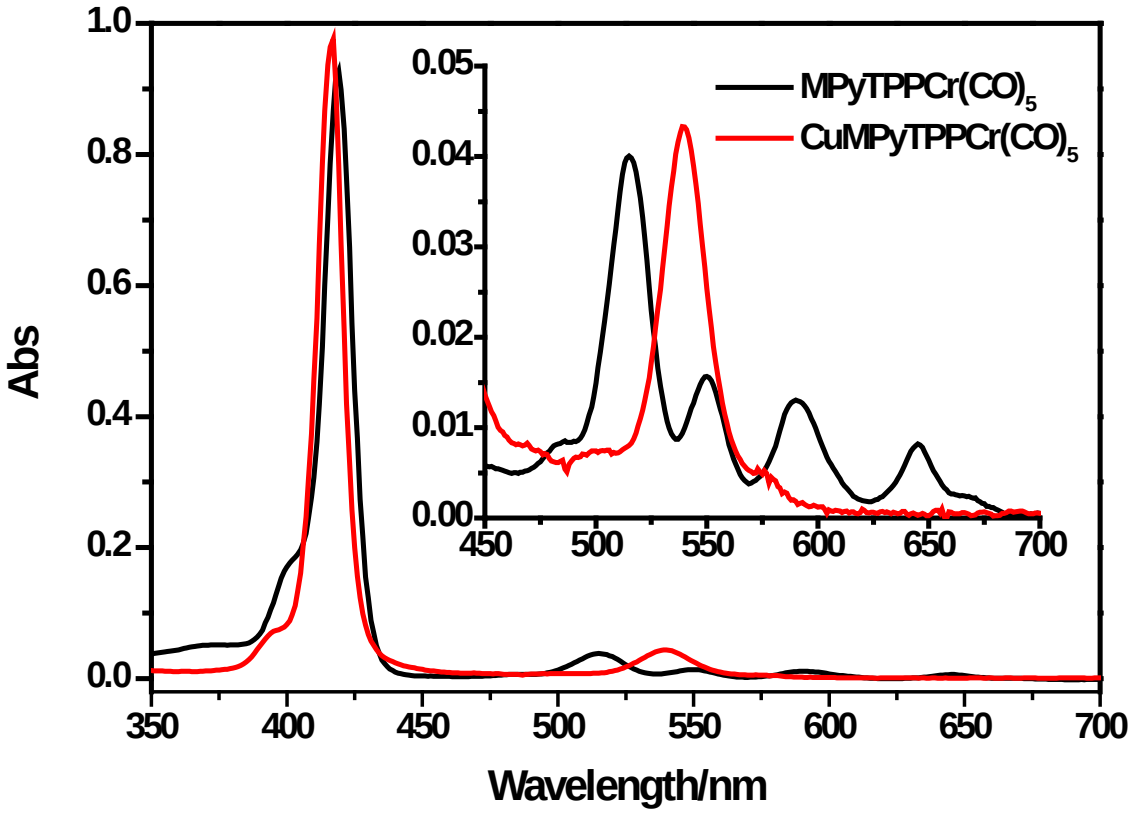

Figure 4.8: *UV-Vis spectra of MPyTPP-Cr(CO)$_5$ (black line) and CuMPyTPP-Cr(CO)$_5$ (red line) recorded in CH_2Cl_2*

The UV-Vis spectra are dominated by porphyrin transitions and no tungsten based absorbances were detected for the porphyrin molecules tethered to tungsten based pentacarbonyl moieties (**see Figure 4.7**). As the tungsten (or chromium) based absorption

bands were masked hence, the extinction coefficients of the porphyrin are higher than that of the free pyridine metal pentacarbonyl. Similar observations were also noted for the complexation of CuMPyTPP with chromium based pentacarbonyl moiety (**Figure 4.8)**.

4.2.2 Infrared Spectroscopy

The ground state IR spectrum of pyridine-$W(CO)_5$ was reported previously and display three IR active ν(CO) stretching vibrations bands at 2071, 1930 and 1918 cm^{-1}. The pyridyl porphyrin based carbonyl complexes display similar IR vibrations to those of pyridine-$M(CO)_5$.[19, 20] The IR spectra of the freebase and Zn(II) pyridyl porphyrin chromium and tungstun pentacarbonyl complexes are shown in **Figure 4.9**. Also, the IR spectra of pentacarbonyl chromium and tungsten Cu(II) pyridyl porphyrins are shown in **Figure 4.10**.

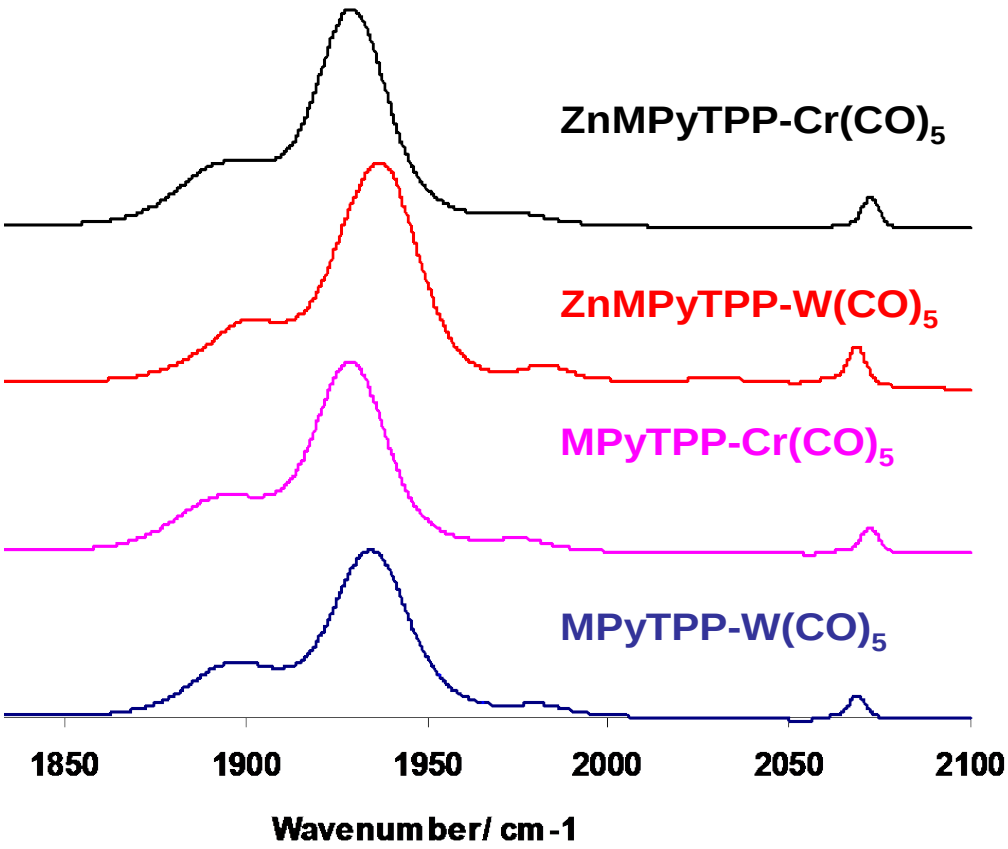

Figure 4.9: *IR spectra of ZnMPyTPP-$Cr(CO)_5$ (black line), ZnMPyTPP-$W(CO)_5$ (red line), MPyTPP-$Cr(CO)_5$ (pink line) and MPyTPP-$W(CO)_5$ (blue line) were recorded in CH_2Cl_2.*

Pyridine-$W(CO)_5$ was reported to have a C_{4v} local symmetry and as such displays three IR-active ν(CO) vibrations at 2071, 1930 and 1918 cm^{-1}, which correspond to $2A_1$ and E stretching vibrations.[21, 22] The infrared spectrum was dominated by the strong E band. The weak A_1^2 band attributed to in-phase stretching vibrations of the four *cis* CO ligands occurs at higher frequency. The A_1^1 ν(CO) vibration, involving mainly the *trans* CO ligand, occurs on the lower energy side of the E band.

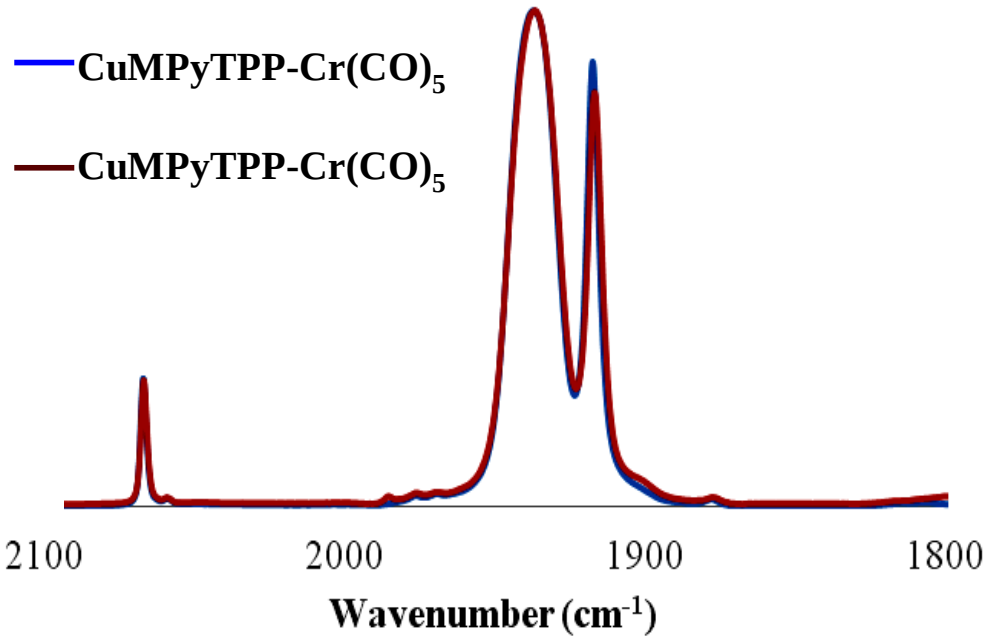

Figure 4.10: *IR spectra of CuMPyTPP-Cr(CO)$_5$ (blue line) and CuMPyTPP-W(CO)$_5$ (red line), were recorded in CH_2Cl_2.*[13]

The IR spectroscopic data (metal carbonyl region) for the freebase and zinc monopyridylporphyrin $M(CO)_5$ complexes are presented in **Table 4.2**. Three bands in the range 1895 – 2072 cm^{-1} are displayed in the ground state infrared spectra. This is consistent with the C_{4v} symmetry of the pentacarbonyl moiety. IR spectra of the pentacarbonyl complexes were dominated by three bands.[23]

Table 4.2: *Carbonyl stretching frequencies of porphyrin metal pentacarbonyl complexes measured in spectrophotometric grade* CH_2Cl_2.

Porphyrin Complexes	**ν_{CO} (cm^{-1})**
MPyTPP-$W(CO)_5$	2070, 1928, 1896
ZnMPyTPP-$W(CO)_5$	2071, 1929, 1894
CuMPyTPP-$W(CO)_5$	2070,1927,1892
MPyTPP-$Cr(CO)_5$	2068, 1935, 1898
ZnMPyTPP-$Cr(CO)_5$	2069, 1934, 1892
CuMPyTPP-$Cr(CO)_5$	2068, 1933, 1896

As observed for pyridine-$W(CO)_5$, the strongest stretching vibration was the E band, a weak $A_1{}^2$ band that was assigned to in-phase stretching vibrations of the four *cis* carbonyl ligands at higher frequencies. The $A_1{}^1$ ν(CO) vibration, involving mainly the *trans* CO ligand, was attributed to the low-energy side of the E band.[24] Formation of the pentacarbonyl complex with the porphyrin macrocycle was further confirmed from Kolodziej *et al*. studies.[25]

4.2.3 Singlet oxygen studies

This work describes a comparison of the singlet-oxygen quantum yields in solution by means of luminescence techniques.[26, 27] Two sets of experiments were carried out using toluene and DCM as solvents. In order to study the effect of molecular oxygen dissolved in solvents, the desired porphyrin molecules were dissolved and purged with oxygen and argon for 15 mins to obtain oxygen saturated and argon saturated solutions respectively. The singlet oxygen

quantum yield (Φ_Δ) was measured in terms of its phosphorescence emission intensity at 1270 nm using a 532 nm CW laser (Cobolt, 10 mW) with detection using an Andor idus-InGaAs diode array on a Shamrock 303 spectrograph. The spectrograph was fibre coupled to a cuvette holder and the excitation and fluorescence from the sample was recorded using two Semrock filters (532 and 1064 long pass). UV-Vis spectra of the solutions were checked before and after running the experiment using a JASCO V630 spectrophotometer in 1cm path-length quartz cuvettes. The $^1O_2$ quantum yields of the porphyrins were determined in DCM and toluene relative to the reference compound meso-tetraphenylporphyrin H_2TPP (Φ_Δ = 0.68 for toluene and 0.63 for DCM) using equation 1, where Φ_Δ is the singlet oxygen quantum yield, G is the integrated area under the emission spectrum and A is the absorbance at the excitation wavelength. Superscripts and subscripts of REF and S correspond to the reference and sample respectively. An optical density of 0.30 at the excitation wavelength (532 nm) was maintained for all the samples.[28]

$$\Phi_\Delta^S = \Phi_\Delta^{REF} \times \left(\frac{\eta_S}{\eta_{REF}} \right)^2 \frac{G_\Delta^S}{G_\Delta^{REF}} \times \frac{A_{REF}}{A_S} \qquad \textbf{(1)}$$

Table 4.3: *Quantum yield of Singlet Oxygen formation of the two sets of experiments (oxygen purged and Ar purged) carried out using toluene and DCM as solvents.*

	Quantum yield of Singlet Oxygen Generation			
	Toluene		**DCM**	
	Oxygen Purged	**Argon Purged**	**Oxygen Purged**	**Argon Purged**
TPP	0.68	0.68	0.63	0.63
CuTPP	0.77	0.81	0.63	0.95
PdTPP	0.90	0.87	0.77	0.78
ZnTPP	0.62	0.67	0.63	0.63
MPyTPP	0.91	0.77	0.72	0.71
CuMPyTPP	0.69	0.72	0.53	0.74
PdMPyTPP	0.61	0.60	0.50	0.25
ZnMPyTPP	0.47	0.33	0.64	0.64
$MPyTPPCr(CO)_5$	0.57	0.48	0.53	0.55
$MPyTPPW(CO)_5$	0.76	0.68	0.79	0.65
$ZnMPyTPPCr(CO)_5$	0.59	0.57	0.35	0.28
$ZnMPyTPPW(CO)_5$	0.84	0.43	0.47	0.63
$CuMPyTPPCr(CO)_5$	0.64	0.74	0.67	0.62
$CuMPyTPPW(CO)_5$	0.73	0.78	0.68	0.75

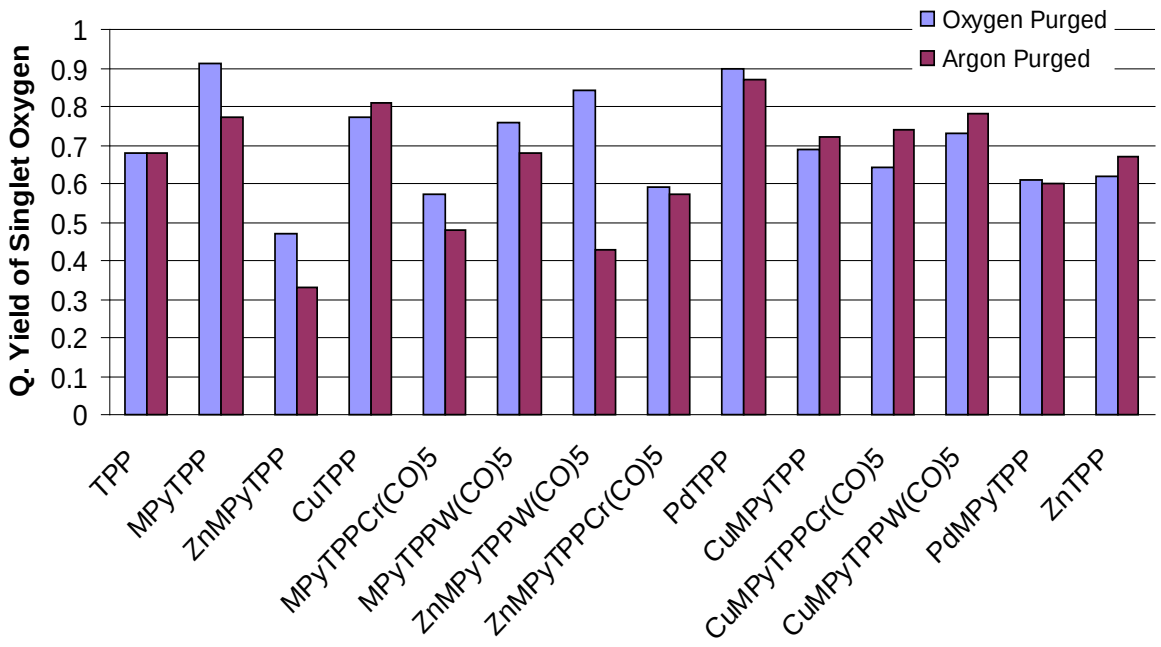

Figure 4.11: *Comparison of singlet oxygen quantum yields for the synthesised porphrins. (All the measurements were made in toluene solutions with TPP taken as reference)*

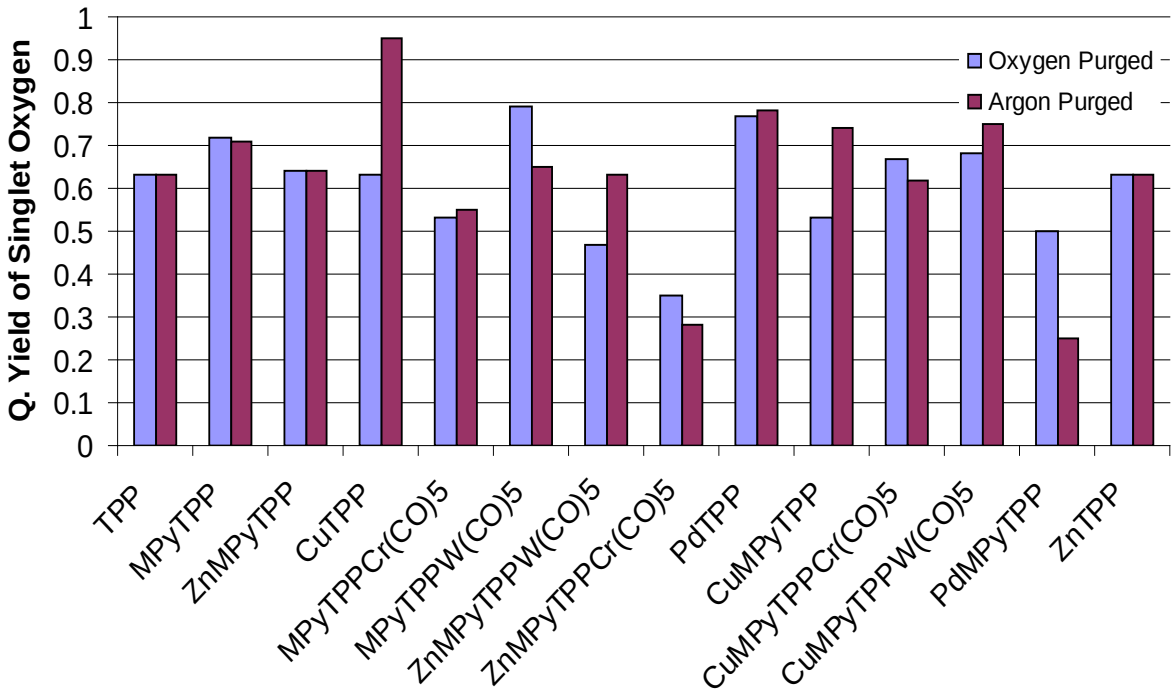

Figure 4.12: *Comparison of singlet oxygen quantum yields for the synthesised porphrins. (All the measurements were made in DCM solutions with TPP taken as reference)*

In the present study a range of freebase and metallated mesoporphyrins are investigated for their ability to act as photosensitiser for the generation of singlet oxygen. It allows a different charge distribution over the periphery of the tetrapyrollic macrocycle and consequently creates the possibility of controlling the transport of the photosensitizer molecule and its location at the cellular level without significant change of spectroscopic and photosensitizing properties.[29] An unsymmetrical charge distribution over the macrocycle periphery of the tetrapyrollic ring is responsible for the slight amphoteric character that favours the transport of the photosensitiser to the cellular targets, both in polar (the external environment of the cell) and nonpolar (the lipidic double layer of the cellular membrane) media. Also, the rationale behind choosing pyridyl based porphyrins is due to their high quantum yield for singlet oxygen generation and hence potentially acting as better PDT agents.[30-32]

For example Kawanishi and co-workers reported 5,10,15,20-tetrakis(N-methyl-4-pyridyl)-21H,23H-porphyrin(TMPyP) macrocycle as a potential photosensitisers for singlet oxygen studies. The porphyrin molecules were further tested for its toxicity against carcinoma cells. From the studies it was revealed that TMPyP is a potential reagent for photo dynamic therapy.

From the analysis of the singlet oxygen quantum yields of the porphyrins with oxygen purged solutions in toluene a first observation can be made: similar and even higher values for singlet oxygen quantum yields were found for all the complexes except for ZnMPyTPP where a drop of 20% was observed in comparison to the reference TPP (Φ_{Δ} = 0.68) (**Figure 4.11**). In general there was a ± 10% variation in results for singlet oxygen quantum yields.

The better efficiency of singlet oxygen quantum yields for the free base and Zn metallated tungsten pentacarbonyl porphyrin molecules is due to the longer lifetime of triplet state of the photosensitisers as previously reported by the DCU group.[33] The triplet state exists on the μs timescale which is long enough to sensitise the singlet oxygen. Among all the porphyrins mentioned in this chapter, it should be noted that MPyTPP has the highest singlet oxygen quantum yield due to relatively long lifetime of its triplet state (τ = 30 μs) and higher absorption coefficients.[33] From the literature it can be inferred that quantum yields of singlet oxygen generation for metalloporphyrins are higher compared to freebase porphyrins.[34, 35]

Similarly, analysis of the singlet oxygen quantum yields of the porphyrins with oxygen purged solutions in DCM showed similar or slightly higher values for all the synthesised complexes. The singlet oxygen quantum yield for ZnMPyTPPW$(CO)_5$ and

$ZnMPyTPPCr(CO)_5$ complexes, however were 20-25% lower than that for the reference TPP(Φ_Δ = 0.63) (see **Figure 4.12**) . Slightly higher quantum yield of the copper based porphyrin complexes could not be explained satisfactorily as generally much shorter triplet lifetimes and low quantum yield of singlet oxygen formation are observed in these complexes Further study is required to calculate the singlet and triplet state lifetimes for these complexes in order to explain the present results. In both the solvents, zinc metallated tungsten based pentacarbonyl to porphyrin complex increases the singlet oxygen quantum yield efficiency compared to chromium pentacarbonyl when attached to a zinc metallated porphyrin which can be attributed to the low energy charge-transfer states from the porphyrin to tungsten pentacarbonyl moiety which may accelerate the sensitisation of singlet oxygen, but also opens other radiation less channels that waste a significant part of the energy absorbed.[12]

Furthermore from the analysis of the singlet oxygen quantum yields of porphyrins, argon purged toluene and DCM solutions showed similar or slightly lower values for all the complexes in comparison to those of the reference TPP, which can be explained due to relatively high concentration of molecular oxygen dissolved in DCM and toluene (10 mmol/L).

A comparison of singlet oxygen quantum yields of the synthesised porphyrin complexes in DCM and toluene solutions (**Table 4.3**) clearly indicates that better results are achieved when toluene was used a solvent. In the case of the pentacarbonyl complexes of tungsten and chromium are more stable and do not decompose as quickly in toluene as opposed to DCM.

From the above study it can inferred that there was no dramatic difference in the quantum yields for singlet oxygen, when oxygen saturated and non-saturated solutions of toluene and DCM were used, for most of the complexes while carrying out the singlet oxygen measurements. Overall it can be concluded that the free base and metallated porphyrins and their W/Cr based pentacarbonyl complexes are effective photosensitisers towards singlet oxygen formation when compared with the literature except for the copper based macromolecules which need more photophysical studies in order to explain the enhanced singlet oxygen quantum yields.

4.2.4 CORMs Studies

To assess the efficiency of the synthesised porphyrin pentacarbonyl complexes to act as efficient CO releasing molecules, the compounds were studied spectrophotometrically using the myoglobin assay by measuring the conversion of deoxygenated-myoglobin (deoxy-Mb)/ carbomonoxy-myoglobin (Mb-CO) as discussed in the experimental **Section 4.4**. Changes in the UV-Vis spectra of the complexes for thermal (37 ^{o}C) and photochemical (470 nm and 355 nm) experiments were monitored for an extended period of time. It was necessary to ensure that the deoxy-myoglobin was stable for the duration of the analyses. This was confirmed by measuring the UV-Vis spectrum of two controls; a control solution containing DMSO, deoxy-Mb and mineral oil, and one containing deoxy-Mb only. The result proved that the deoxy-Mb was stable in both cases up to a time frame of 48 hours. Monitoring of CO release was carried out in some cases up to 24 hours. Therefore, the stability of deoxy-Mb was not affected.

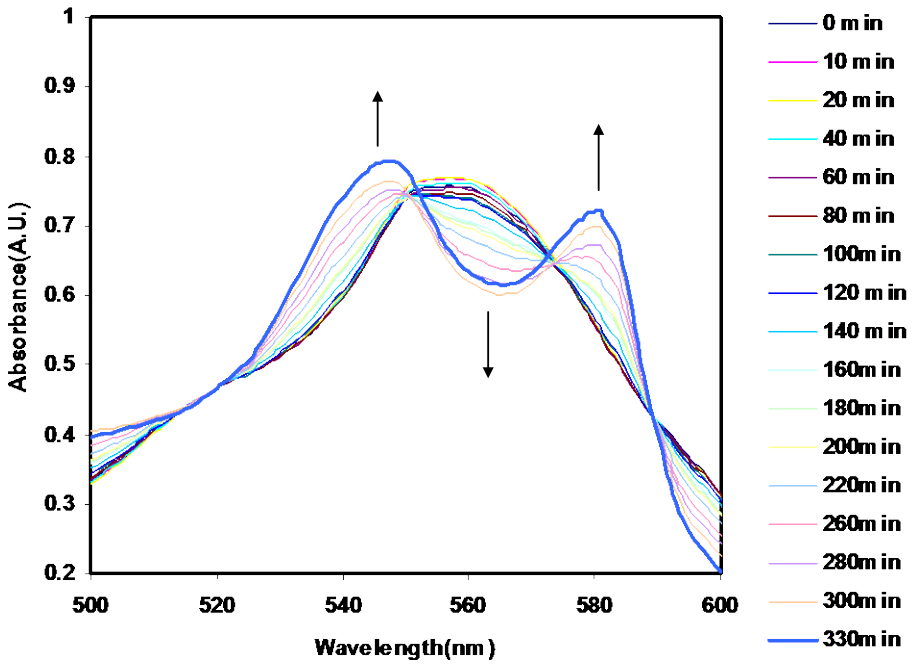

Figure 4.13 *The changes in the UV-Vis spectrum of myoglobin (66 µM) at 37 °C as CO is released from [Zn(MPyTPP)W(CO)$_5$] (8 µM).*

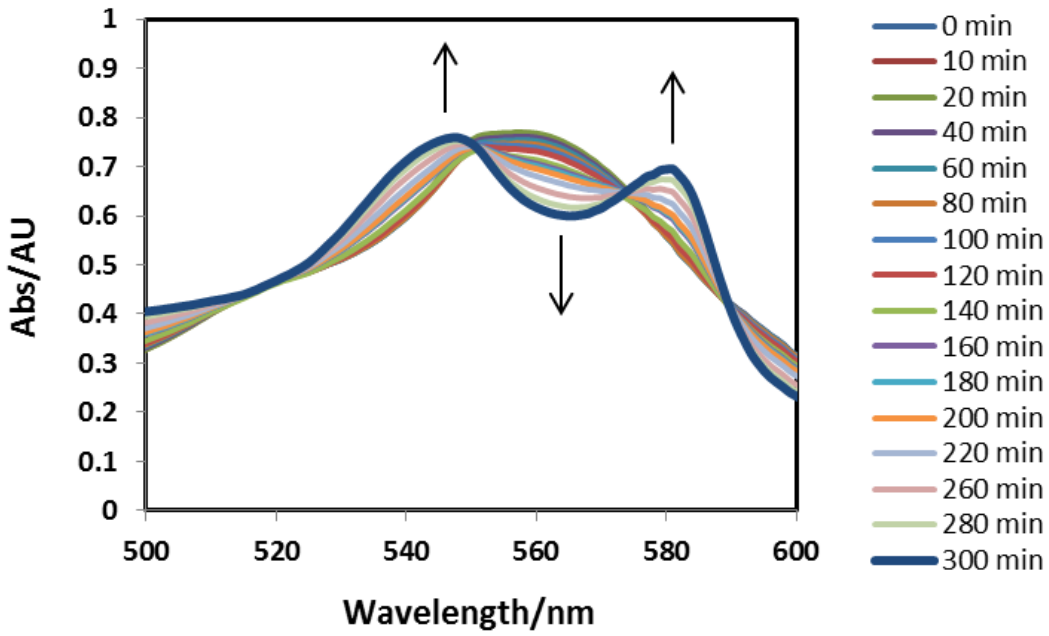

Figure 4.14: *The changes in the UV-Vis spectrum of myoglobin (66 µM) at 37 °C as CO is released from [Zn(MPyTPP)Cr(CO)$_5$] (8 µM).*

A series of Group 6 complexes containing amino ester groups based on M(CO)$_5$ framework (M = Cr, Mo, W) exhibited rapid CO release as shown by the myoglobin assay.[36] A range of free base and metalloporphyrins tethered to W/Cr pentacarbonyl moieties were synthesised in order to investigate their CO releasing properties both photochemically and thermally under physiological conditions. The CO-release profile for one of the CO releasing porphyrin [Zn(MPyTPP)W(CO)$_5$] (8 µM) is illustrated in **Figure 4.13**. Thermally at 37 ^{o}C, the spectral changes that are characteristic of CO release were demonstrated in the Q band region of the myoglobin. At 0 min, there was one distinct absorption peak characteristic of deoxy-Mb. Over time, the intensity of the Q band at approximately 554 nm slowly decreased while the characteristic peaks of Mb-CO appeared at 546 nm and 578 nm (indicated by the arrows). It can be deduced from the overall spectrum that after 330 mins, [Zn(MPyTPP)W(CO)$_5$] completely released the maximum amount of CO as there were no further spectral changes for observed after this time. To ensure that this is the maximum concentration of CO liberated, the spectrum was compared with the reference standard spectrum of Mb-CO. [37]

Table 4.4: *Thermal (37 ^{o}C) and photochemical CO releasing studies carried out on the pentacarbonyl porphyrins synthesised in this chapter. 8μM represents the concentration of the complexes in DMSO solution.*

Name of complex	**Total time required for Thermal (37 ^{o}C) CO Release (8μM)**	**Total time required for Photo CO Release**	
		470 nm (8μM)	**355 nm (8μM)**
ZnMpyTPPCr(CO)$_5$	300 mins	No Release	No Release
MpyTPPCr(CO)$_5$	320 mins	No Release	No Release
CuMpyTPPW(CO)$_5$	270 mins	No Release	No Release
ZnMpyTPPW(CO)$_5$	330 mins	No Release	No Release
MpyTPPW(CO)$_5$	720 mins	No Release	No Release

Photochemical loss of CO from these Cr/W tethered pentacarbonyl complexes is dependent on the wavelength at which the porphyrin molecule is irradiated as observed previously by Dr. Mary Pryce research group using TRIR studies.[13] From the studies it was concluded that upon irradiation at lower wavelength led to the cleavage of W/Cr-CO bond and photo induced CO loss occurred only when the molecule was irradiated at higher wavelength. However, there was no liberation of CO observed at room temperature when the freebase and metallated porphyrin molecules tethered to chromium or tungsten pentacarbonyl complexes using myoglobin assays were irradiated at 470 nm or at 355 nm as no significant changes were observed in the UV-Vis spectra. Similarly, CO release was measured in the same fashion for each of the pentacarbonyl porphyrin complexes; (MPyTPP)W(CO)$_5$, Cu(MPyTPP)W(CO)$_5$, Cu(MPyTPP)Cr(CO)$_5$ and Zn(MPyTPP)Cr(CO)$_5$ **(Table 4.4)**. The

complexes were measured up to a time frame of 24 hours. Among all the porphyrins, thermally at 37 ^{o}C Cu(MPyTPP)W$(CO)_5$ was the fastest CO releaser (270 mins) with the slowest being (MPyTPP)W$(CO)_5$ (720 mins). Among chromium based pentacarbonyl porphyrin complexes, thermal CO liberation at 37 ^{o}C, ZnMPyTPPCr$(CO)_5$ complex was found to be the fastest (**Figure 4.14**).

Tungstun based pentacarbonyl macrocycles acted as thermally slower CO releasers than the Cr carbonyls, which is similar in behaviour to that reported in the literature. A series of group 6 pentacarbonyl complexes containing amino ester groups namely [$M(CO)_5(NH_2CH(R)CO_2R')$] [M = Cr, Mo, W] have been investigated by Fairlamb and co-workers. The reported complexes were assessed thermally for the release of CO using myoglobin assays. In all the complexes the tungsten motif was a far slow CO releaser than the corresponding molybdenum and chromium complexes.[36] However the UV-Vis absorption of these molecules at 8μM solutions was observed to be extremely low and might be the reason for the slow release of CO when irradiated with light.

It should be noted that exact concentrations of the liberated CO may be determined from the absorption information obtained for Mb-CO using the molar extinction co-efficient (ε = 15.4 mmol/L^{-1}.cm^{-1}) and then applying the Beer-Lambert law.[38] All the spectra in **Figures 4.13 - 4.14** have been passed through four isobestic points. External factors such as turbidity effect the accuracy of Mb-CO concentration calculations and should be taken into account by the use of these isobestic points which occur at a certain wavelength where two chemical species have the same molar absorption coefficient value.[39] They were used as an internal reference. As stated by Atkin *et al.* "an isobestic point, otherwise known as a point of intersection in the spectra of two interconverting species (deoxy-Mb→Mb-CO) should remain constant throughout the course of the assay".[40] Therefore, any shifts that may have appeared in the spectra are translated at the various intersection points to ensure accurate result. Half-life ($t_{1/2}$) for all the pentacarbonyl porphyrin complexes was not calculated as they were found to be very slow CO releasing molecules.

4.3 Conclusion

Free base and metallated porphyrins tethered to chromium and tungsten based pentacarbonyl moieties were successfully synthesised and characterised by NMR, UV and IR spectroscopy in addition to a range of other porphyrins. The quantum yields of the singlet oxygen formation by these porphyrin molecules were extensively studied by carrying out two sets of experiments with oxygen saturated and argon degassed solutions of toluene and DCM. It can be concluded that all the porphyrin moieties were efficient photosensitisers when compared with similar porphyrins reported in literature except for the copper based porphyrins which require further study so as to explain the singlet oxygen quantum yield measurements presented in this chapter. Quantum yields for the formation of singlet oxygen were in general higher in toluene as opposed to DCM as solvent.

The release of CO from these complexes was assessed spectrophotometrically by measuring the conversion of deoxymyoglobin to carboxymyoglobin. The CO releasing ability of synthesised porphyrin pentacarbonyl complexes was evaluated. Libration of CO was monitored thermally (37 ^{o}C) and photochemically (470 nm and 355 nm). CuMPyTPPCr(CO)$_5$ (8μM) and ZnMPyTPPCr(CO)$_5$ (8μM) acted as relatively fast CORMs compared to other porphyrin pentacarbonyl complexes. These pentacarbonyl complexes released the maximum output of CO thermally after 270 mins and 300 mins, respectively. In comparison, the pentacarbonyl complexes, MPyTPPCr(CO)$_5$ and ZnMPyTPPW(CO)$_5$ (8μM) liberated CO after 300 mins by thermal means (37 ^{o}C) only. The most promising complexes are CuMPyTPPW(CO)$_5$ and MPyTPPW(CO)$_5$ which released CO thermally (37 ^{o}C) after 300 mins. Most of the pentacarbonyl porphyrin complexes did not appear to be good photo CO releasers under the condition employed in this study.

4.4 Experimental

4.4.1 Materials

All solvents were supplied by the SigmaAldrich Chemical Company. Chloroform, dichloromethane, pentane, diethyl ether, and hexane were dried over $MgSO_4$ prior to use. All organic reagents were purchased from the SigmaAldrich and used without further purification unless stated otherwise. Tetrahydrofuran (THF) was distilled from sodium metal and benzophenone and used immediately prior to synthesis. Pyrrole was distilled over KOH under reduced pressure prior to use. The hexacarbonyls, $W(CO)_6$ and $Cr(CO)_6$ were used without further purification. All mobile phases for column chromatography were dried over $MgSO_4$ and silica gel (Merck) was used as received. All syntheses were carried out under an atmosphere of argon or nitrogen using standard Schlenk techniques unless otherwise stated. All the novel porphyrin molecules synthesised in this chapter were submitted for mass spectroscopic analysis and results are awaited.

4.4.2 Instrumentation

NMR spectra were recorded on a Bruker model AC 400 MHz spectrophotometer and Bruker model ANC 600MHz spectrophotometer using $CDCl_3$ as solvent. All NMR spectra were calibrated according to the residual solvent peak, i.e. $CHCl_3$ at 7.27 ppm for all ^1H spectra. Chemical shifts (δ) are given in parts per million (ppm). Proton coupling constants (*J*) are given in Hertz (Hz). All UV-vis spectra were measured on an Agilent Technologies 8453 photodiode array spectrometer using a 1 cm^3 quartz cell. IR spectra were recorded on a Perkin-Elmer 2000 FT-IR spectrophotometer (2 cm^{-1} resolution) in a 0.1 mm sodium chloride liquid solution cell. Experimental setup for the singlet oxygen measurements at 532nm was carried out using DPSS CW laser (25 mW, Cobalt lasers) in Dr. Wesley Browne's laboratory, University of Groningen, Netherlands.

4.4.3 General Procedure for the study of Myoglobin assay

This procedure was undertaken in the same manner as reported by Atkin *et al.* and Fairlamb et al.[37, 41-44] required amount of the sample was dissolved in DMSO to make a particular concentration of the complex. The deoxymyoglobin (deoxy-Mb) standard solution was prepared by weighing 0.0115 g of myoglobin, 0.01g of sodium dithionite and dissolving them in 10mL of phosphate buffer solution (PBS). A UV-Vis spectrum of this standard deoxymyoglobin solution was run. The solution was then purged with CO gas for 30 mins

forming carboxymyoglobin (Mb-CO). A UV-Vis spectrum of this standard was then taken. 2mL of the standard deoxy-Mb, 10 µL of the complex / DMSO solution and 500 µL of mineral oil were placed into a plastic cuvette. The overall concentration of the solution being tested was 8 µM. The CO release was monitored by performing UV-Vis analysis after particular interval of time on the solutions by thermal means (37 ^{o}C). The solution was allowed to stand wrapped in tinfoil (to prevent light entering) at body temperature (37 ^{o}C). The CO release was also measured by photochemical means in the same way (the cuvette containing the solution to be measured was placed in front of a LED light source and was placed 10 cm away. A control experiment was performed. The temperature of the solution placed in front of the LED light was recorded after certain time intervals to ensure that there was only a photochemical effect and not photochemical and thermal effect acting on the solution under investigation. This was confirmed as the temperature of the solution remained constant.

4.5 Synthesis

All porphyrins and their pentacarbonyl complexes were synthesised as described using an adapted method by Adler *et al.* [45] and by Stromeier *et al.* respectively.[46]

4.5.1 5-(4-Pyridyl)-10,15,20-triphenyl porphyrin and 5,10, 15, 20-tetraphenyl porphyrin

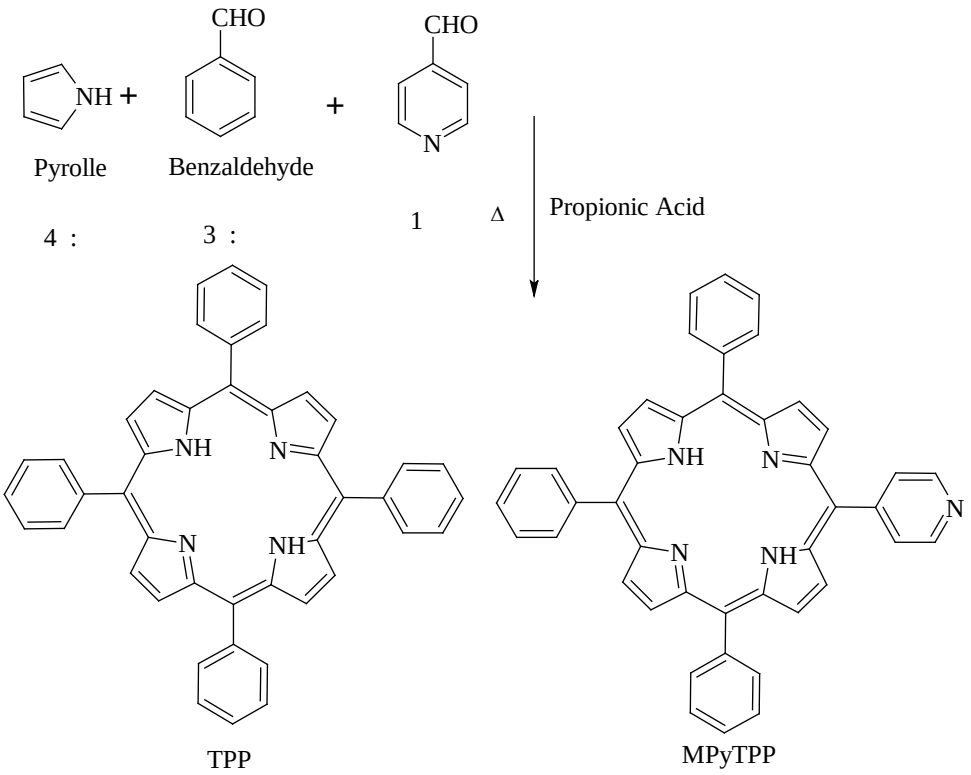

The monopyridyltriphenyl porphyrin was synthesised *via* a mixed aldehyde condensation reaction. Freshly distilled pyrrole (100 mmol / 7.0 mL), benzaldehyde (75 mmol / 8.0 mL) and 4-pyridine carboxaldehyde (25 mmol / 2.35 mL) were refluxed for 2 hours in 99 % propionic acid (250 mL). The acidic solution gradually turned black and the mixture was allowed to cool and placed in the fridge overnight for crystallisation. The black solution was filtered under vacuum and the purple crystals collected were washed several times with methanol to give a bright purple crystalline solid. Typically this method gave a yield of 2 g of crude product.

Thin layer chromatography using chloroform: ethanol (98: 2) as mobile phase indicated the presence of a mixture of six porphyrins formed during the reaction. The compounds formed were 5,10,15,20-tetraphenylporphyrin (**H_2TPP**), 5-pyridyl-10,15,20-triphenylporphyrin (**MPyTPP**), *cis*-5,10-dipyridyl-15,20-diphenylporphyrin (***cis*-DPyDPP**), *trans*-5,15-dipyridyl-10,20-diphenylporphyrin (***trans*-DPyDPP**), 5,10,15-pyridyl-20-phenylporphyrin (**TPyMPP**) and 5,10,15,20-tetrapyridylporphyrin (**TPyP**).

The crude porphyrin mixture was initially purified on a silica gel column using chloroform: ethanol (98: 2) solvent ratio as eluent and the first fraction eluted was **H_2TPP**. Slowly the percentage of polarity of the eluent was increased (chloroform: ethanol (97:3) and chloroform: ethanol (96: 4)) to separate the remaining porphyrins. Only **H_2TPP** and **MPyTPP** were required for this study. Spectroscopic data were in good agreement with the reported data.[13]

H_2TPP

Yield: 107mg, 17.50mmol, 70%

^{1}H NMR (400 MHz, $CDCl_3$) δ ppm 8.87 (8H,m), 8.15 (8H, m), 7.77-7.75 (14H, m), -2.79 (2H, s) .

UV-Vis : (λ, CH_2Cl_2): 417, 512, 544, 586, 642 nm.

MPyTPP

Yield: 100 mg,16.25mmol, 65%

^{1}H NMR (400 MHz, $CDCl_3$) δ ppm 9.04 (2H,d), 8.86(8H,m), 8.22 (8H, m), 7.77 (9H, m), -2.83 (2H, s) .

UV-Vis (λ, CH_2Cl_2): 418, 514, 548, 588, 644 nm.

4.5.2 Zinc(II) 5-(4-pyridyl)-10,15,20-triphenyl porphyrin (ZnMPyTPP)

ZnMPyTPP was synthesised *via* Lindsey's method for the metallation of porphyrins.[847, 48]The freebase porphyrin, **MPyTPP**, (0.30 mmol / 200 mg) was dissolved in *ca.* 50 mL chloroform an the solution was purged with nitrogen for 15 mins. An excess of zinc acetate $Zn(OAc)_2$ (0.45 mmol / 73 mg) was first dissolved in *ca.* 5 mL MeOH and then added to the porphyrin solution. The reaction mixture was allowed to stir overnight at room temperature under a nitrogen atmosphere. All solvents were removed under reduced pressure leaving a purple solid. This solid was dissolved in CH_2Cl_2 and washed several times with 5 % aqueous sodium bicarbonate $NaHCO_3$, followed by water using separating funnel. The organic layer was dried over $MgSO_4$ and the solvent was removed under reduced pressure. The product obtained was purified by column chromatography using silica and chloroform (dried over $MgSO_4$) as mobile phase.

MPyTPP ZnMPyTPP

The ^{1}H NMR spectrum showed evidence of aggregation for zinc pyridyl porphyrins. Aggregation occurs in non-coordinating solvents and these solutions are a darker blue colour compared to the purple colour of **ZnTPP**.[49] Spectroscopic data were in good agreement with the reported data.[13]

Yield: 0.143 g,0.21mmol, 70%

^{1}H NMR (400 MHz, $CDCl_3$) δ ppm 8.81 (m, 4H), 8.46 (d, 2H), 8.13 (d, 2H) 8.03 (d, 4H) 7.69-7.56 (m, 9H), 7.34 (d, 2H), 2.08 (s, 4H) .

UV-Vis (λ_{max}, CH_2Cl_2): 418, 551, 601 nm.

4.5.3 Zinc (II) 5, 10,15,20-tetraphenylporphyrin (ZnTPP)

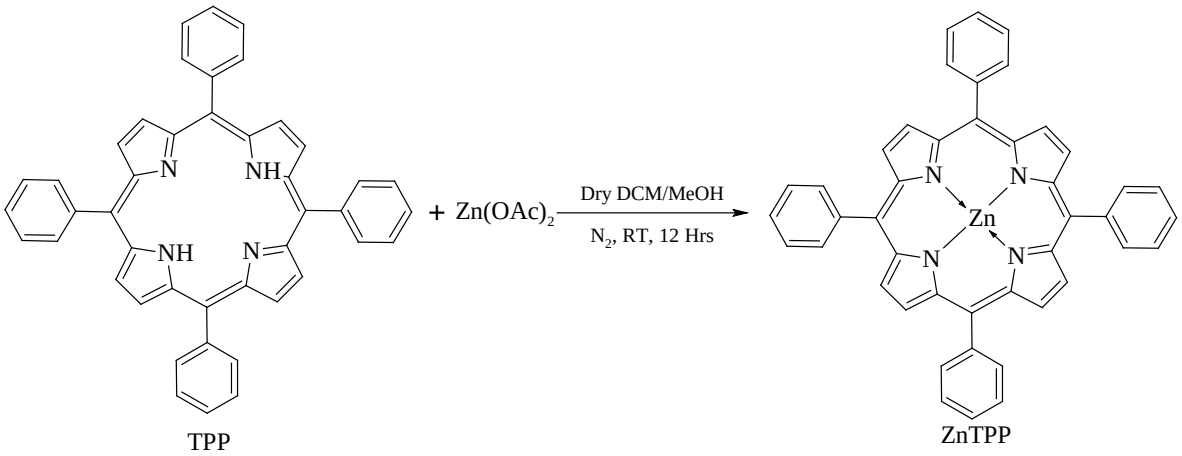

The metalloporphyrin was synthesised and purified following the synthesis of Zinc (II) 5-(4-pyridyl)-10, 15, 20-triphenyl porphyrin (ZnMPyTPP) where free base porphyrin taken was TPP instead of MPyTPP. Tetraphenylporphyrin (0.32 mmol/200mg) were reacted with (0.43 mmol/73 mg) of zinc acetate. Spectroscopic data were in good agreement with the reported data.[13]

Yield: 0.183g, 0.27 mmol, 90%

^{1}H NMR (400 MHz, $CDCl_3$) δ ppm 8.87 (m, 8H), 8.15 (m, 8H), 7.69-7.56 (m, 12H) .

UV-Vis (λ_{max}, CH_2Cl_2): 418, 550, 604 nm.

4.5.4 Copper (II) 5-(4-pyridyl)-10,15,20-triphenyl porphyrin (CuMPyTPP)

This metalloporphyrin (CuMPyTPP) was synthesised and purified following the synthesis of Zinc (II) 5-(4-pyridyl)-10, 15, 20-triphenyl porphyrin (ZnMPyTPP) where (0.43 mmol/78 mg) of copper acetate was taken instead of zinc acetate and reacted with (0.30 mmol/200 mg) of MPyTPP**.**

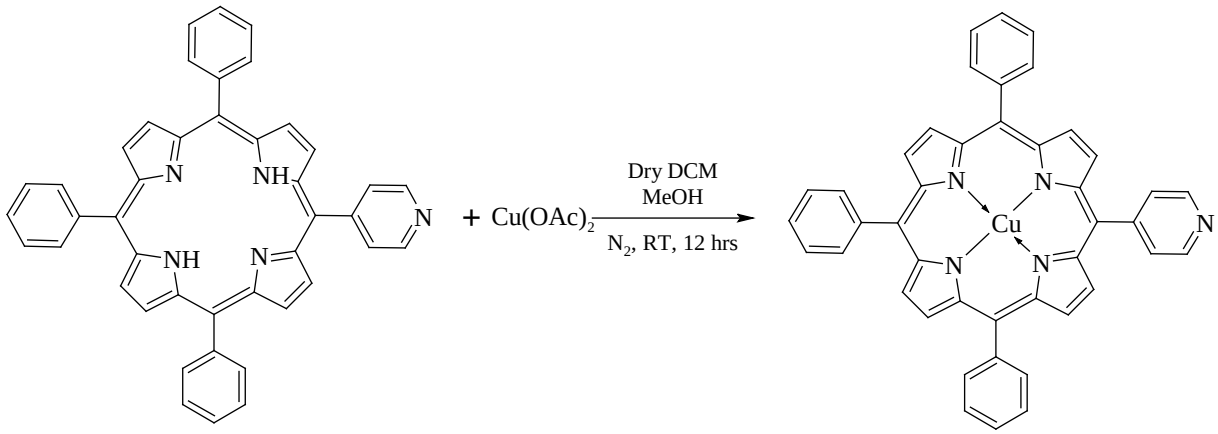

MPyTPP CuMPyTPP

Yield: 0.182g, 0.27 mmol, 90%

UV-Vis (λ_{max}, CH_2Cl_2): 418, 551, 601 nm.

4.5.5 Copper (II)5,10,15,20-tetraphenylporphyrin (CuTPP)

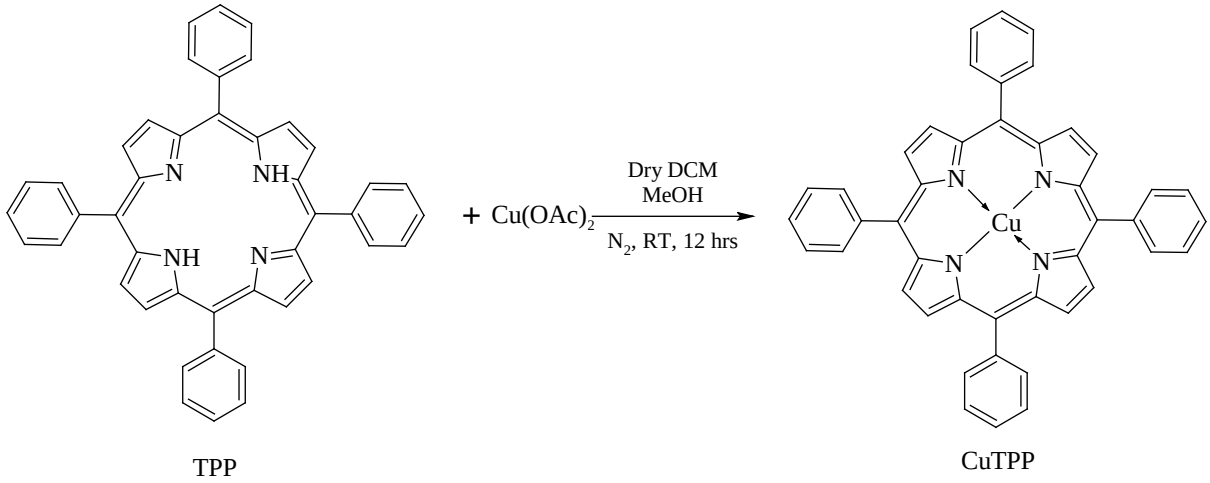

TPP CuTPP

This metalloporphyrin was synthesised and purified following the synthesis of Copper (II) 5-(4-pyridyl)-10, 15, 20-triphenyl porphyrin (CuMPyTPP) where free base porphyrin taken was TPP (0.32 mmol/200 mg) instead of MPyTPP and reacted with (0.43 mmol/ 78 mg) of copper acetate. The NMR data (Broad due to paramagnetic nature) is in good agreement with the reported literature.[50]

Yield: 0.172g, 0.255 mmol, 85%

^{1}H NMR (400 MHz, $CDCl_3$) δ ppm 7.64 (br, 12H), 7.49 (br, 16H) .

UV-Vis (λ_{max}, CH_2Cl_2): 418, 550, 604 nm.

4.5.6 Palladium(II)5-(4-pyridyl)-10,15,,10,15,20-tetraphenylporphyrin (PdMyTPP)

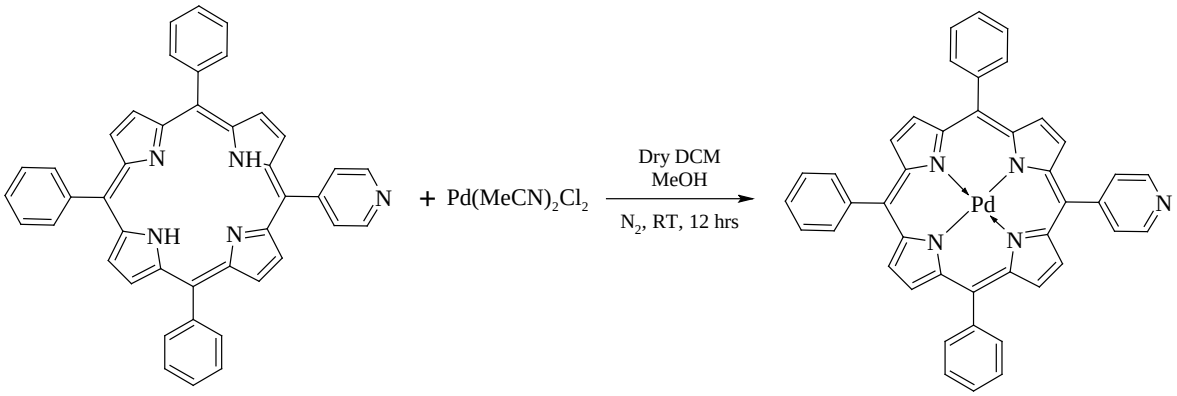

MPyTPP PdMPyTPP

This metalloporphyrin was synthesised and purified following the synthesis of Zinc (II) 5-(4-pyridyl)-10, 15, 20-triphenyl porphyrin (ZnMPyTPP) where (0.43 mmol/ 111 mg) of bis(acetonitrile)dichloropalladium (II) was taken instead of zinc acetate and reacted with (0.30 mmol/ 200mg) of MPyTPP.

Yield: 0.173g, 0.24 mmol, 80%

^{1}H NMR (400 MHz, $CDCl_3$) δ ppm 8.74 (m, 8H), 8.11 (m, 8H), 7.72-7.64 (m, 12H) .

UV-Vis : (λ_{max}, CH_2Cl_2): 418, 524, 604 nm.

4.5.7 Palladium (II) 5,10,15,20-tetraphenylporphyrin (PdTPP)

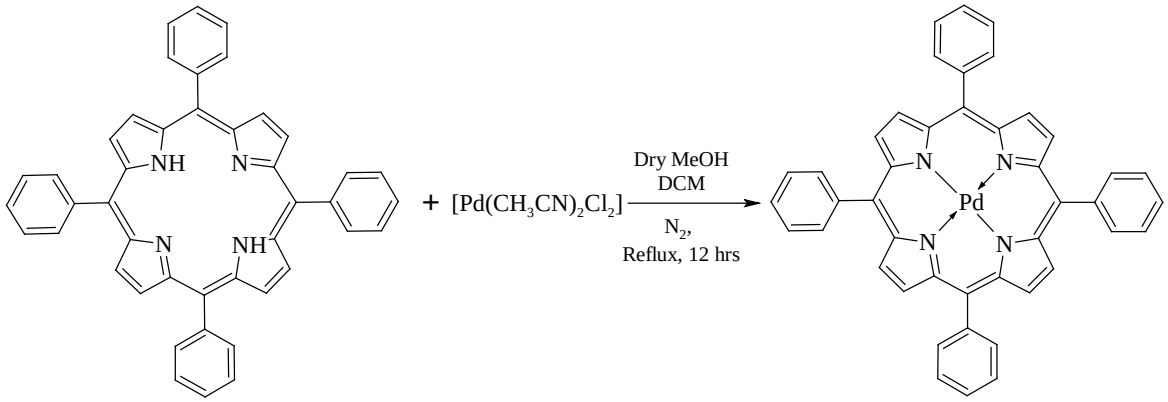

TPP PdTPP

This metalloporphyrin was synthesised and purified following the synthesis of Palladium (II) 5-(4-pyridyl)-10, 15, 20-triphenyl porphyrin (PdMPyTPP) where free base porphyrin taken was TPP (0.32 mmol / 200mg) instead of MPyTPP and reacted with (0.43 mmol / 111mg) bis(acetonitrile)dichloropalladium (II). Characterisation data is in good agreement with reported literature.[51]

Yield: 0.184g, 0.255 mmol, 85%

^{1}H NMR (400 MHz, $CDCl_3$) δ ppm 8.81 (s, 8H), 8.16 (d, 8H, J=6.5Hz), 7.72 (m, 12H) .

UV-Vis (λ_{max}, CH_2Cl_2): 418, 550, 604 nm.

4.5.8 5-(4-pyridyl)-10,15,20-triphenylporphyrinchromiumpentacarbonyl (MPyTPP-Cr(CO)$_5$)

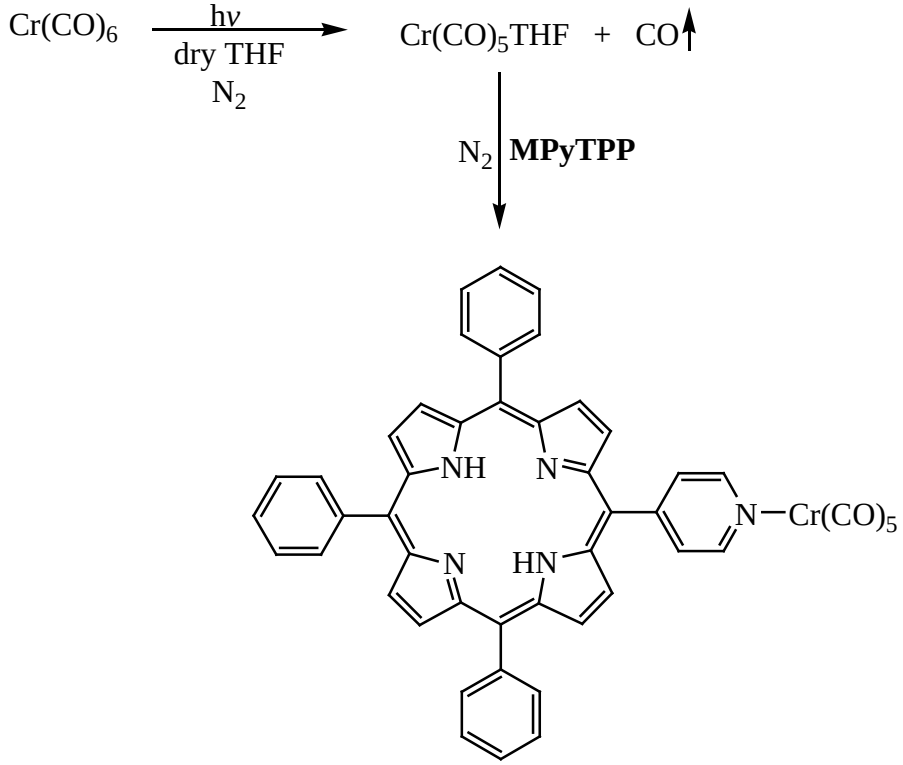

Initially chromium hexacarbonyl (0.68 mmol / 150 mg) was photolysed using an Hg lamp in freshly distilled THF (150 mL) that had been degassed for 15 mins with nitrogen. The solution was continually purged with nitrogen while stirring the solution and after about 40 mins the solution had turned a strong orange colour. Completion of photolysis and the formation of $Cr(CO)_5THF$ was determined by IR spectroscopy. Depletion of the hexacarbonyl peak at 1979 cm^{-1} and formation of the new pentacarbonyl peaks (2072, 1936 and 1893 cm^{-1}) indicated completion of the reaction. Following this, 5-(4-pyridyl)-10,15,20-triphenylporphyrin (0.32 mmol / 200 mg) was added to the $Cr(CO)_5THF$ under an atmosphere of nitrogen and allowed to stir overnight in darkness under an inert atmosphere. The solvent THF was removed under reduced pressure on the rotary evaporator. The complex was then dissolved in chloroform and purified on a silica gel column using chloroform/pentane (90:10) as mobile phase. Unreacted hexacarbonyl was eluted initially from the column with any further hexacarbonyl impurities removed by sublimation under

reduced pressure. The complex was recrystallised from cold pentane affording purple crystals. The formation of the final product was confirmed by the spectroscopic data which were in good agreement with reported data.[13, 33]

Yield: 0.168 g, 0.21 mmol, 65 %.

^{1}H NMR (400 MHz, $CDCl_3$) δ ppm 9.01(2H,d), 8.81 (8H, m), 8.20 (8H, m), 7.75 (9H, m), -2.83 (2H, s) .

IR ν_{CO} (CH_2Cl_2): 2068, 1935, 1898 cm^{-1}.

UV-Vis (λ_{max}, CH_2Cl_2): 420, 516, 552, 590, 646 nm.

4.5.9 5-(4-Pyridyl)-10,15,20-triphenyl porphyrin tungsten pentacarbonyl (MPyTPP-W(CO)$_5$)

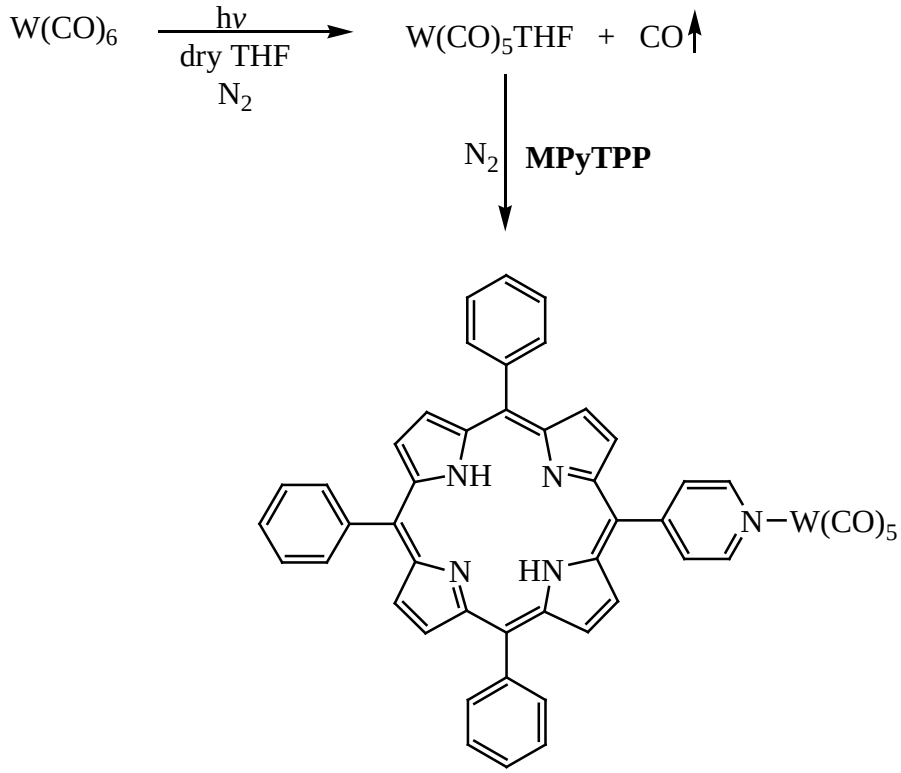

The porphyrin tungsten pentacarbonyl derivative, **MPyTPPW(CO)$_5$**, was also synthesised by first producing the W(CO)$_5$THF adduct. Tungsten hexacarbonyl (0.43 mmol / 150 mg)

was added to freshly distilled THF (150 mL) which had been purged for the previous 15 mins with nitrogen. The solution was placed in the photolysis chamber and continually purged with nitrogen gas. After ~30 mins irradiation the solution had turned a strong yellow colour. Formation of the $W(CO)_5THF$ adduct and hence completion of the reaction was monitored by IR spectroscopy. Depletion of the parent hexacarbonyl peak at 1976 cm^{-1} and generation of new bands at 2073, 1930 and 1890 cm^{-1} were observed. The freebase porphyrin, **MPyTPP**, (0.32 mmol / 200 mg) was then added to the THF solution. The reaction mixture was allowed to stir, covered in tin foil and under a nitrogen atmosphere, overnight **.** The THF was then removed under reduced pressure and the crude complex was redissolved in chloroform. Purification on a silica gel column using chloroform/pentane (90:10) as mobile phase eluted most of the unreacted hexacarbonyl followed by the porphyrin complex. Any further hexacarbonyl impurities were removed by sublimation under reduced pressure. The product was recrystallised from cold pentane affording brownish-purple crystals. Spectroscopic data were in good agreement with reported data.[33]

Yield: 0.204 g, 0.22 mmol, 68 %.

^1H NMR (400 MHz, $CDCl_3$) δ ppm 9.13 (2H,d), 8.86 (8H, m), 8.22 (8H, m), 7.77 (9H, m), -2.83 (2H, s) ppm.

IR ν_{CO} (CH_2Cl_2): 2070, 1928, 1896 cm^{-1}.

UV-Vis (λ_{max}, CH_2Cl_2): 422, 516, 552, 590, 646 nm.

4.5.10 Zinc(II)5-(4-pyridyl)-10,15,20-triphenyl porphyrin chromium pentacarbonyl (ZnMPyTPP-$Cr(CO)_5$)

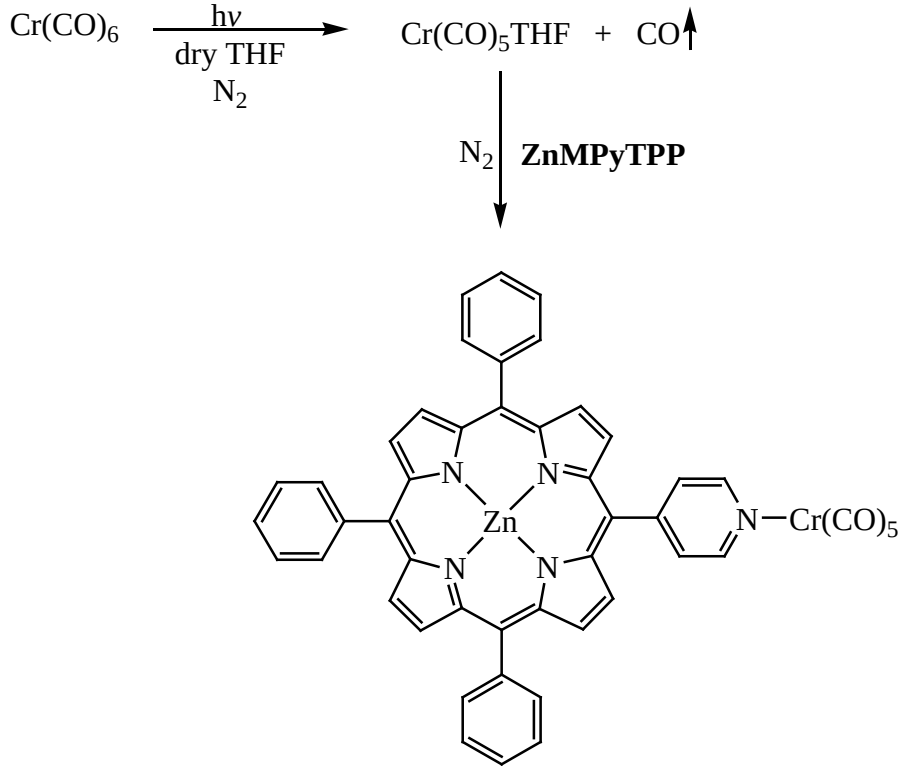

Synthesis of the zinc derivative was carried out in the same manner. Chromium hexacarbonyl (0.45 mmol / 100 mg) was dissolved in freshly distilled THF (100 mL) that had been degassed for 15 mins with nitrogen. The solution was photolysed using an Hg lamp while being continually purged with nitrogen to avoid an oxidation effects. After about 20 mins the solution had turned a strong orange colour and completion of photolysis (and therefore formation of $Cr(CO)_5THF$) was monitored by IR spectroscopy. Depletion of the hexacarbonyl peak at 1979 cm^{-1} and formation of the new pentacarbonyl peaks (2072, 1936 and 1893 cm^{-1}) indicated completion of the reaction. Following this, **ZnMPyTPP** (0.074 mmol / 50 mg) was added to the $Cr(CO)_5THF$ solution and allowed to stir overnight under an atmosphere of nitrogen wrapped in tinfoil. THF was removed under reduced pressure on the rotary evaporator. The complex was then dissolved in chloroform and purified on a silica gel column using chloroform/pentane (90:10) as mobile phase. Unreacted hexacarbonyl was eluted initially from the column with any further hexacarbonyl impurities removed by sublimation under reduced pressure. The complex was recrystallised from cold pentane affording purple crystals. Spectroscopic data were in good agreement with reported data.[33]

Yield: 0.034g, 0.039 mmol, 53 %.

^{1}H NMR (400 MHz, $CDCl_3$) δ ppm 9.20(2H, d), 8.85 (8H, m), 8.19 (8H, m), 7.75 (9H, m) ppm.

IR ν_{CO} (CH_2Cl_2): 2069, 1934, 1895 cm^{-1}.

UV-Vis (λ_{max}, CH_2Cl_2): 422, 548, 588 nm.

4.5.11 Zinc(II) 5-(4-pyridyl)-10,15,20-triphenyl porphyrin tungsten pentacarbonyl (ZnMPyTPP-W(CO)$_5$)

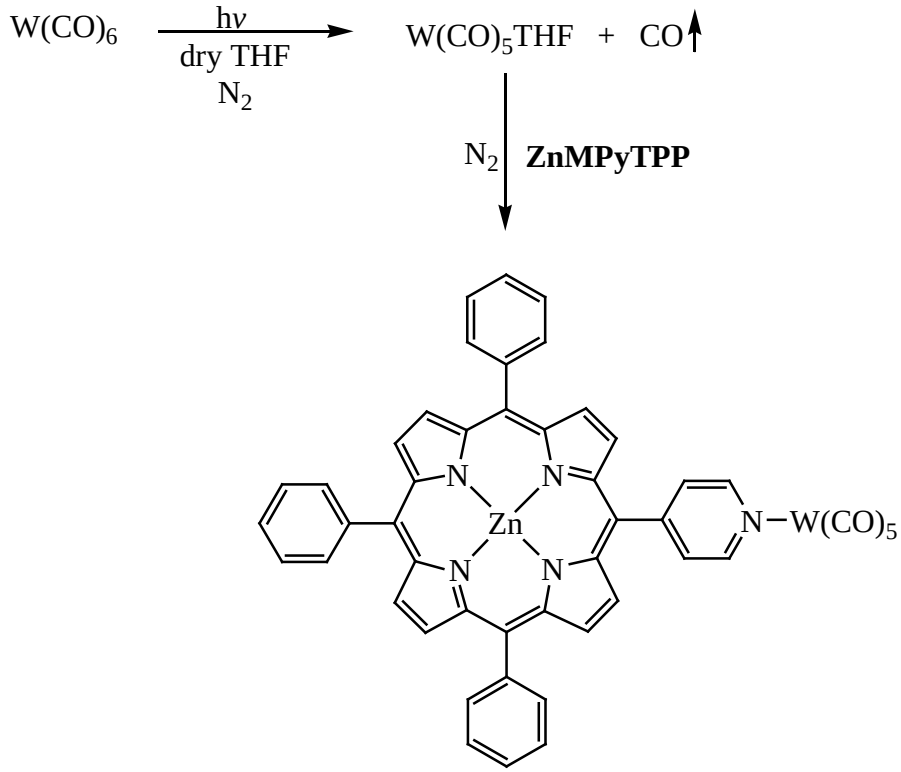

In a similar manner **ZnMPyTPPW(CO)$_5$** was produced. Tungsten hexacarbonyl (0.28 mmol / 100 mg) was dissolved in dry, degassed THF (100 mL) and photolysed while constantly purging with nitrogen. After approximately 30 mins the solution was a yellow colour and the IR spectrum indicated that the $W(CO)_5THF$ adduct had formed. To this solution the zinc porphyrin, **ZnMPyTPP**, (0.074 mmol / 50 mg) was added and allowed to

stir overnight, covered in tinfoil and under an atmosphere of nitrogen. Subsequently the THF was removed and the crude complex was redissolved in chloroform. Purification on a silica gel column using a mobile phase of chloroform/pentane (90:10) initially eluted unreacted hexacarbonyl followed by the porphyrin complex. Any remaining hexacarbonyl was removed by sublimation at reduced pressure and the porphyrin was recrystallised from cold pentane affording the product as pinkish-purple crystals. Spectroscopic data were in good agreement with reported data.[33]

Yield: 0.33 g, 0.032 mmol, 44 %.

^{1}H NMR (400 MHz, $CDCl_3$) δ ppm 9.22(2H,d), 8.86 (8H, m), 8.18 (8H, m), 7.76 (9H, m) ppm.

IR ν_{CO} (CH_2Cl_2): 2071, 1929, 1894 cm^{-1}.

UV-Vis (λ_{max}, CH_2Cl_2): 420, 550, 590 nm.

4.5.12 Copper(II)5-(4-pyridyl)-10,15,20-triphenyl porphyrin chromium pentacarbonyl (CuMPyTPP-$Cr(CO)_5$)

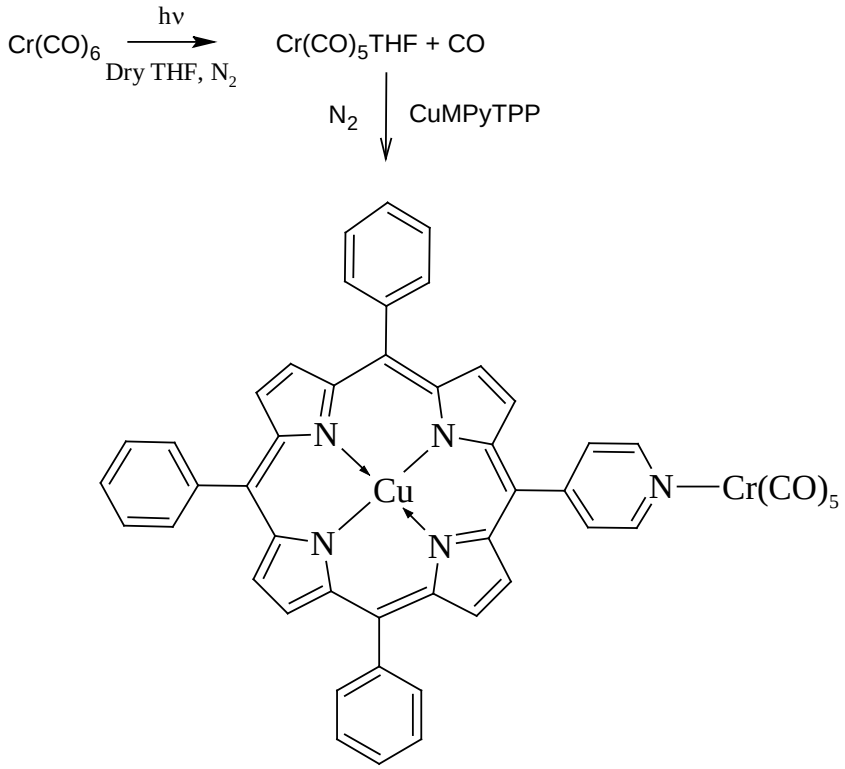

$CuMPyTPPCr(CO)_5$

$CuMPyTPP\text{-}Cr(CO)_5$ was synthesised following the procedure of synthesis of $ZnMPyTPPCr(CO)_5$ affording red crystals. Chromium hexacarbonyl complex (0.40 mmol / 89 mg) was reacted with (0.070 mmol / 47 mg) of CuMPyTPP porphyrin in 100mL THF solution.

Yield: 0.032 g, 0.037 mmol, 50%.

IR ν_{CO} (CH_2Cl_2): 2071, 1927, 1892 cm^{-1}.

UV-Vis (λ_{max}, CH_2Cl_2): 416, 540, 580 nm.

4.5.13 Copper(II)-5-(4-pyridyl)-10,15,20-triphenyl porphyrin tungstun pentacarbonyl [CuMPyTPP-W(CO)$_5$]

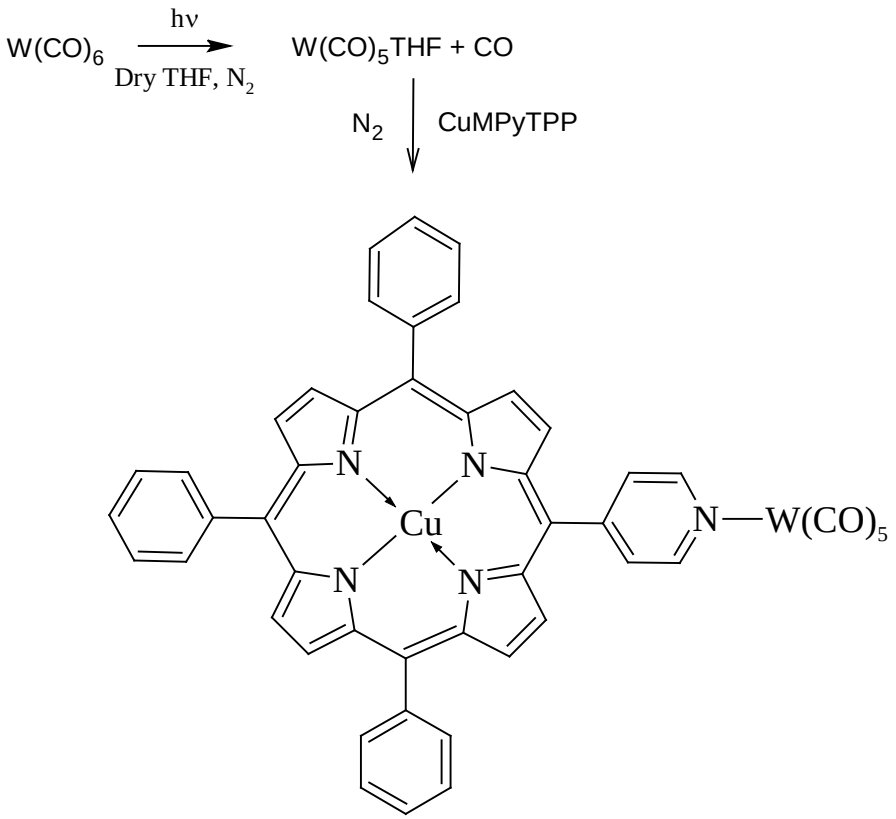

CuMPyTPPW(CO)$_5$

CuMPyTPP-W(CO)$_5$ was synthesised following the procedure of synthesis of ZnMPyTPPW(CO)$_5$ affording red crystals. Tungstun hexacarbonyl complex (0.30 mmol / 107 mg) was reacted with (0.070 mmol / 47 mg) of CuMPyTPP porphyrin in 100mL THF solution.

Yield: 0.37 g, 0.037 mmol, 50%.

IR ν_{CO} (CH_2Cl_2): 2070, 1925, 1893 cm^{-1}.

UV-Vis (λ_{max}, CH_2Cl_2): 418, 542, 582 nm.

4.6 References

1. G. Bottari, O. Trukhina, M. Ince and T. Torres, *Coord. Chem. Rev.*, 2012, **256**, 2453-2477.

2. W. M. Campbell, A. K. Burrell, D. L. Officer and K. W. Jolley, *Coord. Chem. Rev.*, 2004, **248**, 1363-1379.

3. H. E. Toma and K. Araki, *Coord. Chem. Rev.*, 2000, **196**, 307-329.

4. R. W. R. J. N. Gamlln, *Photochem. Photobiol.*, 1999, **70**, 391-475.

5. M. C. DeRosa and R. J. Crutchley, *Coord. Chem. Rev.*, 2002, **234**, 351-371.

6. A. G. Hyslop, M. Orphanide, U. Javed and E. G. Megehee, *Inorg. Chim. Acta*, 2003, **355**, 272-279.

7. R. V. Slone and J. T. Hupp, *Inorg. Chem.*, 1997, **36**, 5422-5423.

8. C. J. Aspley, J. R. Lindsay Smith, R. N. Perutz and D. Pursche, *J. Chem. Soc., Dalton Trans.*, 2002, 170-180.

9. J. Rodriguez, L. McDowell and D. Holten, *Chem. Phys. Lett.*, 1988, **147**, 235-240.

10. J. G. Woller, J. K. Hannestad and B. Albinsson, *J. Am. Chem. Soc.*, 2013, **135**, 2759-2768.

11. J. Y. Lee, H. J. Song, S. M. Lee, J. H. Lee and D. K. Moon, *Eur. Polym. J.*, 2011, **47**, 1686-1693.

12. I. Radivojevic, G. Bazzan, B. P. Burton-Pye, K. Ithisuphalap, R. Saleh, M. F. Durstock, L. C. Francesconi and C. M. Drain, *J. Phys. Chem. C*, 2012, **116**, 15867-15877.

13. N. Boyle, *PhD Thesis*, 2010, Dublin City University

14. K. Kalyanasundaram, *Photochemistry of Polypyridyl and Porphyrin Complexes*, 1992.

15. N. M. Rowley, S. S. Kurek, J.-D. Foulon, T. A. Hamor, C. J. Jones, J. A. McCleverty, S. M. Hubig, E. J. L. McInnes, N. N. Payne and L. J. Yellowlees, *Inorg. Chem.*, 1995, **34**, 4414-4426.

16. C. M. Lemon, E. Karnas, M. G. Bawendi and D. G. Nocera, *Inorg. Chem.*, 2013, **52**, 10394-10406.

17. J. L. Garate-Morales, Y. Reyes-Ortega, C. Alvarez-Toledano, R. Gutierez-Perez, D. Ramarez-Rosales, R. Zamorano-Ulloa, E. Basurto-Uribe, J. Hernandez-Daaz and R. Contreras, *Transition Met. Chem.*, 2002, **27**, 906-917.

18. T. Zoltan, F. Vargas, C. Rivas, V. Lopez, J. Perez and A. Biasutto, *Scientia Pharmaceutica*, 2010, **78**, 767-789.

19. M. S. Wrighton, H. B. Abrahamson and D. L. Morse, *J. Am. Chem. Soc.*, 1976, **98**, 4105-4109.

20. C. Moralejo, C. H. Langford and D. K. Sharma, *Inorg. Chem.*, 1989, **28**, 2205-2209.

21. H. B. A. M.S. Wrighton, D.L. Morse, *J. Am. Chem. Soc*, 1976, **98**, 4105.

22. C. H. L. C. Maralejo, D.K. Sharma, *Inorg Chem.*, 1998, **28**, 2205.

23. P. Glyn, F. P. A. Johnson, M. W. George, A. J. Lees and J. J. Turner, *Inorg. Chem.*, 1991, **30**, 3543-3546.

24. S. Zalis, M. Busby, T. Kotrba, P. Matousek, M. Towrie and A. Vlcek, *Inorg. Chem.*, 2004, **43**, 1723-1734.

25. R. M. Kolodziej and A. J. Lees, *Organometallics*, 1986, **5**, 450-455.

26. J. Zimmermann, J. von Gersdorff, H. Kurreck and B. Röder, *J. Photochem. Photobiol. B: Biol.*, 1997, **40**, 209-217.

27. E. Zenkevich, E. Sagun, V. Knyukshto, A. Shulga, A. Mironov, O. Efremova, R. Bonnett, S. P. Songca and M. Kassem, *J. Photochem. Photobiol. B: Biol.*, 1996, **33**, 171-180.

28. J. Zhang, K. L. Wong, W. K. Wong, N. K. Mak, D. W. J. Kwong and H. L. Tam, *Organic & Biomolecular Chemistry*, 2011, **9**, 6004-6010.

29. J. X. Zhang, J. W. Zhou, C. F. Chan, T. C. K. Lau, D. W. J. Kwong, H. L. Tam, N.-K. Mak, K. L. Wong and W. K. Wong, *Bioconjugate Chem.*, 2012, **23**, 1623-1638.

30. S. Tada-Oikawa, S. Oikawa, J. Hirayama, K. Hirakawa and S. Kawanishi, *Photochemistry & Photobiology*, 2009, **85**, 1391-1399.

31. Y. Kashiwagi, H. Imahori, Y. Araki, O. Ito, K. Yamada, Y. Sakata and S. Fukuzumi, *J. Phys. Chem. A*, 2003, **107**, 5515-5522.

32. K. Hirakawa, T. Hirano, Y. Nishimura, T. Arai and Y. Nosaka, *Photochemistry & Photobiology*, 2011, **87**, 833-839.

33. K. McDonnell, *PhD thesis*, 2004, Dublin City University.

34. J. M. Fernandez, M. D. Bilgin and L. I. Grossweiner, *J. Photochem. Photobiol. B: Biol.*, 1997, **37**, 131-140.

35. R. W. Redmond and J. N. Gamlin, *Photochem. Photobiol.*, 1999, **70**, 391-475.

36. W.-Q. Zhang, A. C. Whitwood, I. J. S. Fairlamb and J. M. Lynam, *Inorg. Chem.*, 2010, **49**, 8941-8952.

37. A. J. Atkin, S. Williams, P. Sawle, R. Motterlini, J. M. Lynam and I. J. S. Fairlamb, *Dalton Trans.*, 2009, 3653-3656.

38. P. C. Kunz, W. Huber, A. Rojas, U. Schatzschneider and B. Spingler, *Eur. J. Inorg. Chem.*, 2009, **2009**, 5358-5366.

39. R. Motterlini, J. E. Clark, R. Foresti, P. Sarathchandra, B. E. Mann and C. J. Green, *Circul. Res.*, 2002, **90**, e17-e24.

40. A. J. Atkin, J. M. Lynam, B. E. Moulton, P. Sawle, R. Motterlini, N. M. Boyle, M. T. Pryce and I. J. S. Fairlamb, *Dalton Trans.*, 2011, **40**, 5755-5761.

41. P. Sawle, R. Foresti, B. E. Mann, T. R. Johnson, C. J. Green and R. Motterlini, *Br. J. Pharmacol.*, 2005, **145**, 800-810.

42. S. Chlopicki, R. Olszanecki, E. Marcinkiewicz, M. Lomnicka and R. Motterlini, *Cardiovasc. Res.*, 2006, **71**, 393-401.

43. P. Sawle, J. Hammad, I. J. S. Fairlamb, B. Moulton, C. T. O'Brien, J. M. Lynam, A. K. Duhme-Klair, R. Foresti and R. Motterlini, *J. Pharmacol. Exp. Ther.*, 2006, **318**, 403-410.

44. C. C. Romao, W. A. Blattler, J. D. Seixas and G. J. L. Bernardes, *Chem. Soc. Rev.*, 2012, **41**, 3571-3583.

45. A. D. Adler, F. R. Longo, J. D. Finarelli, J. Goldmacher, J. Assour and L. Korsakoff, *J. Org. Chem.*, 1967, **32**, 476-476.

46. W. Strohmeier, *Angew. Chem. Int. Ed.*, 1964, **3**, 730-737.

47. Y. Yamamoto and K. Akiba, *J. Organomet. Chem.*, 2000, **611**, 200-209.

48. H. L. Kee, J. Bhaumik, J. R. Diers, P. Mroz, M. R. Hamblin, D. F. Bocian, J. S. Lindsey and D. Holten, *J. Photochem. Photobiol. A: Chem.*, 2008, **200**, 346-355.

49. A. K. Burrell, D. L. Officer, D. C. W. Reid and K. Y. Wild, *Angew. Chem. Int. Ed.*, 1998, **37**, 114-117.

50. G. M. Godziela and H. M. Goff, *J. Am. Chem. Soc.*, 1986, **108**, 2237-2243.

51. U. Eisner and M. J. C. Harding, *J. Chem. Soc. (Res.)*, 1964, 4089-4101.

Chapter 5

Group VI metal carbonyls as CORMs

This chapter deals with the synthesis and characterisation of Group VI (Cr, Mo, W) metal carbonyl complexes using NMR, UV and IR spectroscopic techniques. The compounds were assessed for their ability to act as CO releasing molecules both thermally and photochemically using myoglobin assays.

5.1. Introduction

The use of myoglobin assays to quantify the release of CO from metal carbonyl complexes was first observed by Motterlini *et al*.[1] Transition metal carbonyls act as a perfect source for the delivery of CO as the amount of CO released is easily controlled. Many transition metal based carbonyl complexes especially with Cr, Mo and W have been tested for CO releasing molecules both thermally and photochemically as explained in chapter 1 in detail.[2-4]

The myoglobin assay is based on the fact that if a complex releases CO in solution, deoxymyoglobin (deoxy-Mb) is readily converted to carbomonoxymyoglobin (Mb-CO).

The principle tool for the study is UV-Vis spectroscopy.[5, 6] The change in the Q band region of the heme group present in deoxymyoglobin and Mb-CO is readily visible in the UV-vis spectra. The formation of Mb-CO is measured by monitoring the change in the absorbance value at 540 nm. Factors such as turbidity and extinction coefficient of myoglobin are taken into the calculation for measuring the exact release of CO. The preparation of myoglobin for CO releasing studies of the complexes is carried out using phosphate buffer saline solution at a physiological pH (pH 7.4).[7]

An example of a release profile for a CORM demonstrating the conversion of de-oxy Mb to Mb-CO over time using the Q band region of the heme group is displayed in **Figure 5.1.**[8]

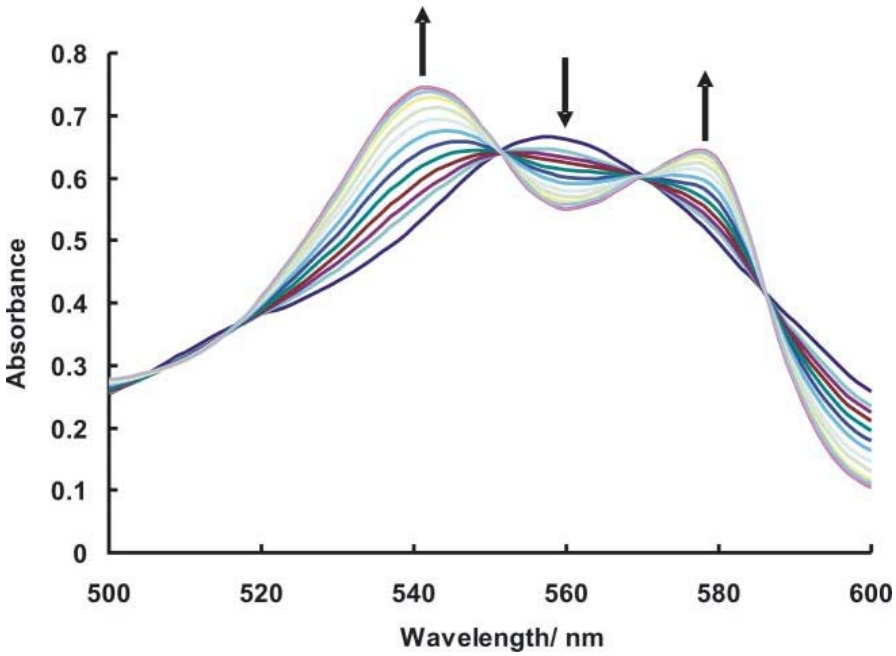

Figure 5.1: *CO release profile for ($[Et_4N][CrI(CO)_5]$, demonstrating the conversion of de-oxy Mb to Mb-CO over time using the Q band region of the heme group.*[8]

It is very effective to study simple metal carbonyl complexes when trying to develop new forms of CO releasing molecules. The biological properties of the complexes are significant in the estimation of their potential use as therapeutic agents.[3] Investigations are in their infancy stage in this field of research with significant improvement required to develop current and future CORMs. The assay should be carried out thermally at physiological temperature (37 ^{o}C) at a pH of 7.4. Also, the metal carbonyl complexes should be synthesised and analysed for their ability to release CO, photochemically, preferably using visible light.[9, 10]

A series of carbon monoxide releasing molecules based on the Cr, Mo and W based pentacarbonyl framework was reported by Lynam and co-workers. The amino esters and amino acids were introduced into the coordination spheres of the Fischer type carbene complexes namely $[M(CO)_5(NH_2CHCO_2R')]$. The rate of CO release from the carbene complexes depended primarily on the specific heteroatom connected to the carbene center. Rapid CO-release is observed in the case of sulphur and methoxy stabilised carbenes

whereas in the case of amino substituted carbenes, release is very slow. This was explained due to the electrophilic character at the carbene carbon atom. The rate of CO release from these complexes varied in order of magnitude increasing in the order Cr > Mo > W. [11]

Another Mo tetracarbonyl complex with an aldehyde group in a peripheral position on the 2,2'-bipyridine (bpy) ligand was coupled (TGF) β-targeting peptide N-terminally functionalised with aminoxy acetic acid. The oxime ligation of an aldehyde with an aminoxy group bound to Mo(CO)4(N-N) was used to assess the CO releasing ability using visible light. Photoactivation at 468 nm with a LED array resulted in a significantly accelerated release of CO from this complex, thus establishing this peptide bio-conjugate as a new photoactivable CO releasing molecule. The half-life for this molecule was found to 44 mins when irradiated at 468 nm using myoglobin assays.[12]

The aim of this chapter was to synthesise transition metal tetra-carbonyls; $M(CO)_4$ and tri-carbonyls; $M(CO)_3$ where M = Mo, Cr, W with the ancillary ligands; 2,2'-dipyridyl, naphthalene, anthracene, 2-methylthionaphthalene (**Figure 5.2**). The synthetic steps for the synthesis of the targeted complexes are known whereby the commercially available metal hexacarbonyls were reacted with an excess of different ligands. Characterisation of the complexes was confirmed using IR, NMR and UV-Vis spectroscopic methods. Next, the CO-releasing ability of the synthesised complexes was assessed thermally as well as photochemically using the myoglobin assay method. All the complexes synthesised in this chapter have been reported before.[13-17]

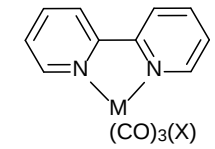

M	X	
Mo	CO	[(bpy)Mo(CO)4] **(1)**
Cr	CO	[(bpy)Cr(CO)4] **(2)**
W	CO	[(bpy)W(CO)4] **(3)**
Mo	PPh_3	[(bpy)Mo(CO)3(PPh3)] **(4)**
Cr	PPh_3	[(bpy)Cr(CO)3(PPh3)] **(5)**
W	PPh_3	[(bpy)W(CO)3(PPh3)] **(6)**

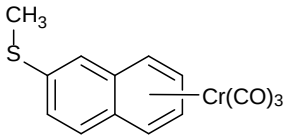

(7)

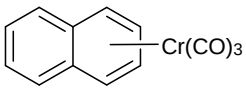

(8)

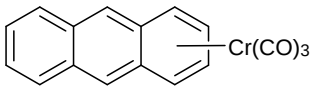

(9)

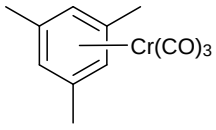

(10)

Figure 5.2: *Structure of bpy based tetra and tricarbonyl complexes of Cr, Mo, W (**1-6**), [η^6-2-MeSnaphthaleneCr(CO)$_3$] (**7**), [η^6-naphthaleneCr(CO)$_3$] (**8**), [η^6-anthraceneCr(CO)$_3$] (**9**) and [η^6-mesityleneCr(CO)$_3$] (**10**).*

5.2 Results and discussion

5.2.1. Infrared Spectroscopy

Formation of [(η^6-arene)Cr(CO)$_3$] complexes such as [(η^6-2-MeSnaphthalene)Cr(CO)$_3$], [(η^6-anthracene)Cr(CO)$_3$], [(η^6-naphthalene)Cr(CO)$_3$] and [(η^6-mesitylene)Cr(CO)$_3$] were confirmed by IR and NMR spectroscopy. The infrared ν(CO) spectra in solution show the usual behaviour of an M(CO)$_3$ group with C_{3v} symmetry: a medium-strong high frequency band (A_1) and a strong, broad (sometimes split) at lower frequency (E). The modes of the Cr(CO)$_3$ units appear as strong bands in the 2000-1800 cm^{-1} region. The spectrum of [(η^6-2-MeSnaphthalene)Cr(CO)$_3$] in **Figure 5.3** clearly shows that the two low frequency bands belong to the two components of the E mode, which is split because of the lower symmetry of the complex. All the IR data presented in this chapter are in agreement with the reported data.[18, 19]

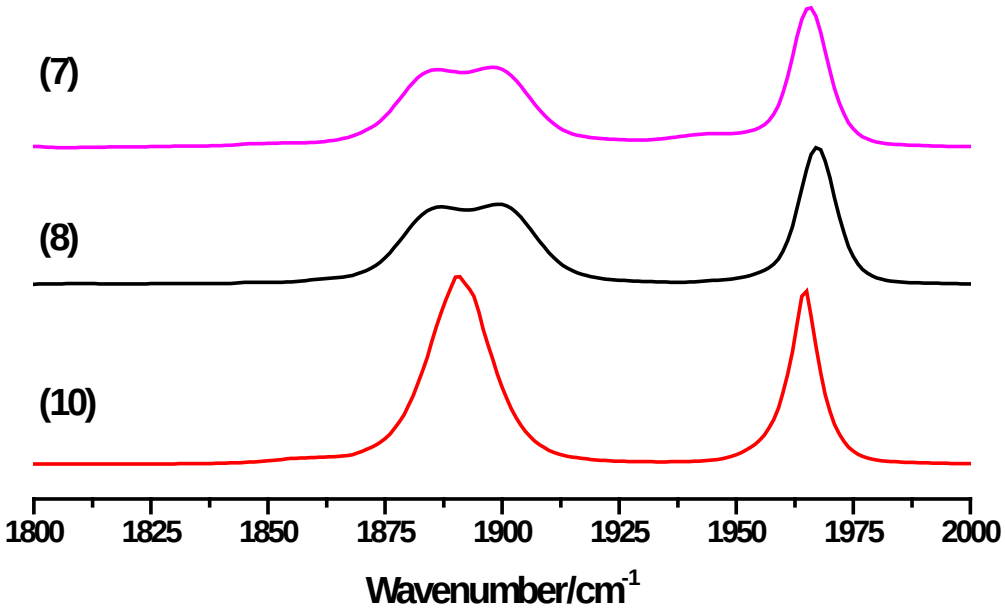

Figure 5.3: *Overlaid IR spectra of [(η^6-2-MeSnaphthalene)Cr(CO)$_3$]* ***(7)****, [(η^6-naphthalene)Cr(CO)$_3$]* ***(8)****, and [(η^6-mesitylene)Cr(CO)$_3$]* ***(10)*** *in hexane.*

IR analysis was performed on each of the synthesised tetracarbonyl complexes using chloroform as a solvent. Since the complexes exhibit C_{2v} symmetry, four C-O stretching modes were observed.[20] All the complexes show four CO stretching bands in the infrared region 2075-1825 cm^{-1} due to 2A1 + B1 + B2 modes as expected for C_{2v} symmetry and in agreement with their *cis*-configuration. The higher frequency Al and B1 bands are assigned to *trans*-carbonyl ligands, while the lower frequency A1 and B2 bands are assigned to *cis*-carbonyl ligands (**Table 5.1**). The spectra are overlaid for comparison (**Figure 5.4**).[21]

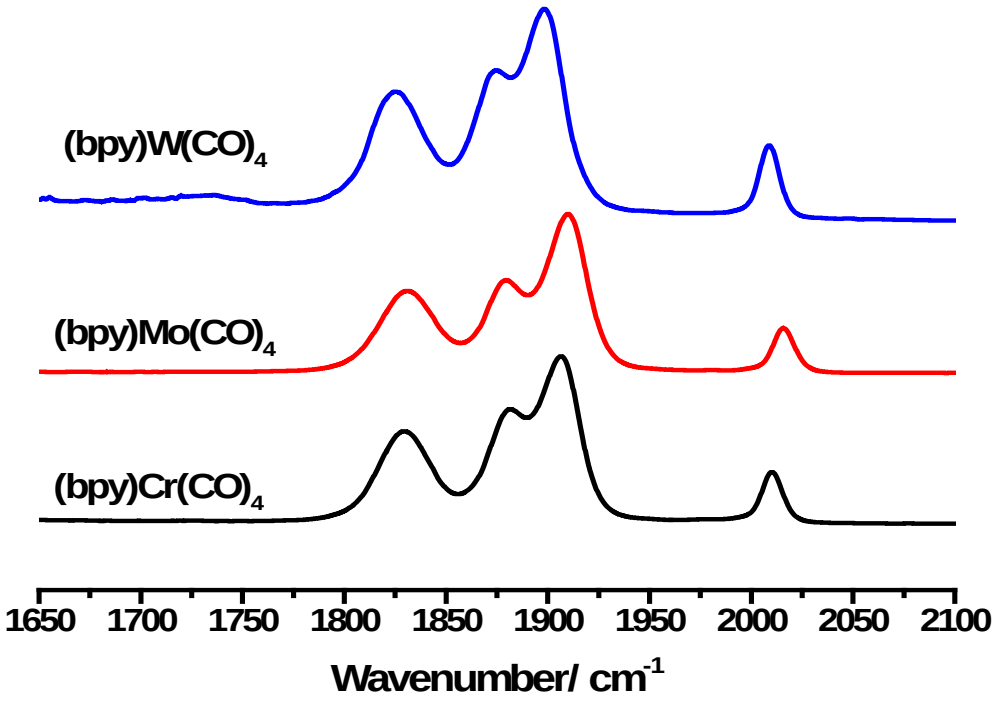

Figure 5.4: *Overlaid IR spectra of [(bpy)Cr(CO)$_4$], [(bpy)Mo(CO)$_4$], and [(bpy)W(CO)$_4$] in chloroform.*

***Table 5.1**: Comparison of the C-O stretching frequencies observed for the tricarbonyl and tetracarbonyl complexes in solution.*

Complexes	**C-O stretching frequencies (cm^{-1})**
[(η^6-2MeSnaphthalene)$Cr(CO)_3$]	1965,1896,1885
[(η^6-anthracene)$Cr(CO)_3$]	1991,1931(br)
[(η^6-naphthalene)$Cr(CO)_3$]	1967,1896,1884
[(η^6-mesitylene)$Cr(CO)_3$]	1965,1895
[(bpy)$Mo(CO)_3(PPh_3)$]	1919,1827,1795
[(bpy)$Cr(CO)_3(PPh_3)$]	1900,1887,1834
[(bpy)$W(CO)_3(PPh_3)$]	1921,1822,1791
[(bpy)$Mo(CO)_4$)]	2018, 1912, 1883, 1835
[(bpy)$Cr(CO)_4$)]	2013, 1910, 1889, 1836
[(bpy)$W(CO)_4$)]	2012, 1903, 1881, 1831

Similarly, IR spectroscopy was also performed on each of the synthesised bipyridyl tricarbonyl complexes (**Figure 5.5**). Generally, there are two characteristic isomers facial (*fac*-) or meridional (*mer*-) in certain groups of metal complexes e.g. $[M(L\text{-}L)(CO)_3X]^{n+}$ where L-L = bidentate ligands (either symmetrical or unsymmetrical) and X = monodentate ligand.[22] *fac*-isomers have two very similar medium peaks in close proximity and a strong peak about a 100 cm^{-1} away (**Figure 5.6**). In comparison, *mer*-isomers demonstrate one distinctive medium peak, one strong peak and one weak peak in the spectrum.

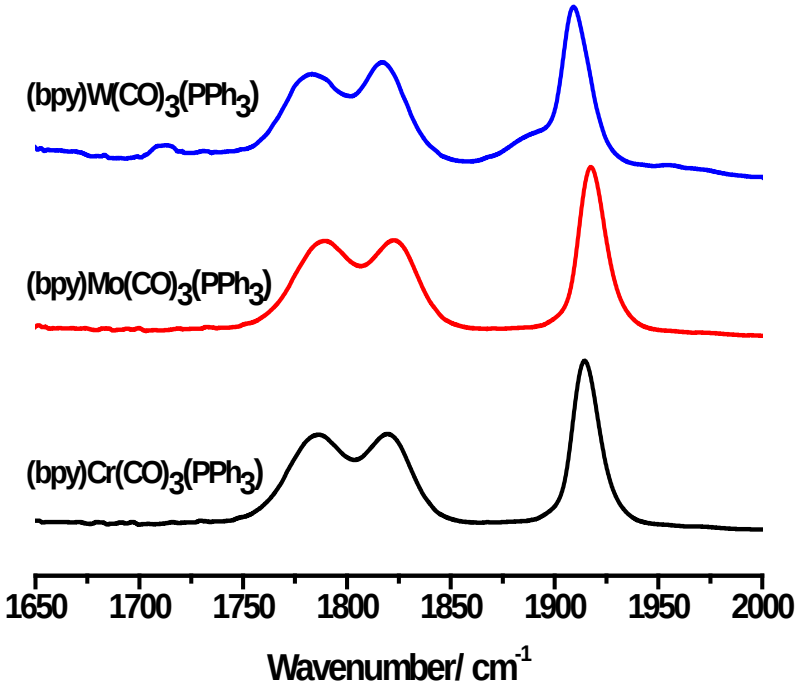

Figure 5.5: *Overlaid IR spectra of $[(bpy)Cr(CO)_3(PPh_3)]$, $[(bpy)Mo(CO)_3(PPh_3)]$ and $[(bpy)W(CO)_3(PPh_3)]$ in chloroform.*

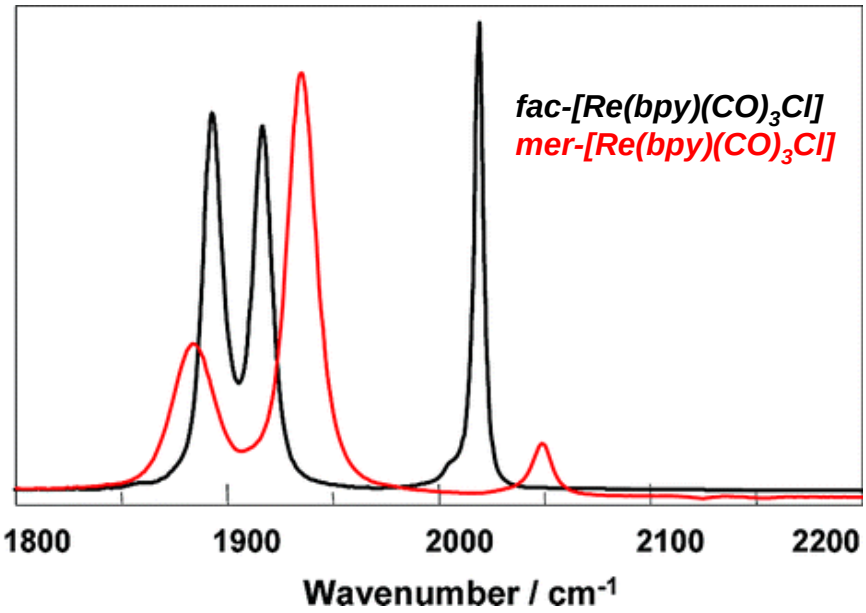

Figure 5.6: *IR spectra of fac-[Re(bpy)(CO)$_3$ Cl] (in black) and mer-[Re(bpy)(CO)$_3$Cl] in THF solution (in red).*[22]

Due to the pattern of the peaks for [(bpy)Mo(CO)$_3$ (PPh$_3$)] , [(bpy)W(CO)$_3$ (PPh$_3$)] and [(bpy)Cr(CO)$_3$ (PPh$_3$)] supported that the facial isomers were produced in all the cases as three M-CO stretching vibrations are observed in the IR spectra.

5.2.2 Absorption Spectroscopy

The UV-Vis spectra of mixed ligand carbonyl derivatives of the type *cis*-M(CO)$_4$L-L (M = Cr, Mo and W and L-L = a bidentate nitrogen ligand) have been extensively studied.[23] The complexes under study exhibit two peaks in the region 290 - 440 nm. These may be attributed to d-π* CO transitions (**Figure 5.7**). A peak of lower intensity in the region of 475 - 520 nm is also observed in these complexes which may be assigned to d-d transition (See **Table 5.2**).

***Table 5.2**: Electronic spectra of cis-[(L-L)M(CO)$_4$] complexes recorded in spectrophotometric grade DCM.*

Complex	λ_{max} (d-π*CO Transition)	λ_{max}(d-d transition)
[(bpy)Cr(CO)$_4$)]	293, 325	519
[(bpy)Mo(CO)$_4$)]	298, 370	474
[(bpy)W(CO)$_4$)]	294, 374	525

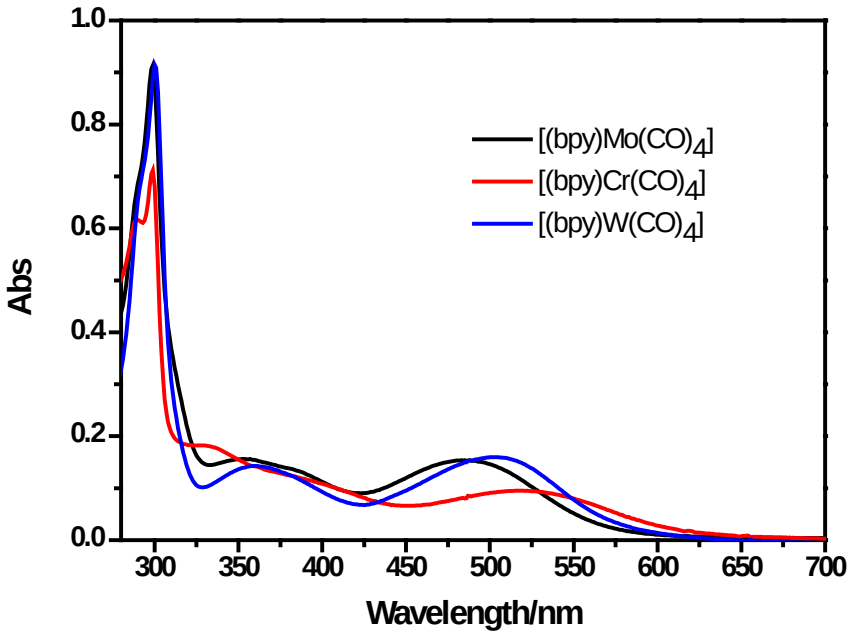

***Figure 5.7:** Overlaid UV-Vis spectra of [(bpy)Mo(CO)$_4$)], [(bpy)Cr(CO)$_4$)] and [(bpy)W(CO)$_4$)] in DCM.*

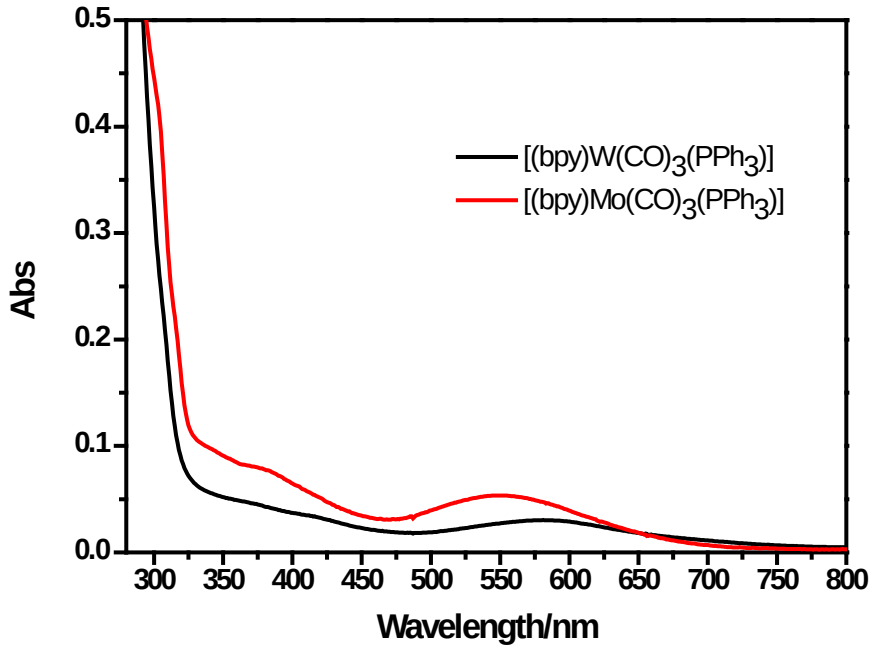

Figure 5.8: *UV-Vis spectra of [(bpy)Mo(CO)$_3$(PPh$_3$)] and [(bpy)W(CO)$_3$(PPh$_3$)] recorded in DCM.*

UV-Vis spectra of substituted tricarbonyl complexes of Cr, Mo and W transition metals exhibit a low absorbance peak in the region 350-440 nm which may be attributed to a d-π* CO transition (see **Figure 5.8**). And another peak in the region of 475-520 nm is also observed in these complexes which may be assigned to a d-d transition (see **Table 5.3**).

***Table 5.3**: Electronic spectra of cis-[$M(CO)_3(L\text{-}L)(PPh_3)$] complexes recorded in spectrophotometric grade DCM*

Complex	λ_{max} (d-π*CO Transition)	λ_{max}(d-d Transition)
[(bpy)$Mo(CO)_3(PPh_3)$]	375	575
[(bpy)$W(CO)_3(PPh_3)$]	378	543
[(bpy)$Cr(CO)_3(PPh_3)$]	365	522

***Table5.4**: Electronic spectra of substituted and unsubstituted [(arene)$Cr(CO)_3$] complexes recorded in spectrophotometric grade hexane.*

Complex	M→π* CO-CT	M→arene CT
[(η^6-naphthalene)$Cr(CO)_3$]	360	445
[(η^6-anthracene)$Cr(CO)_3$]	375	525
[(η^6-2-MeSnaphthalene)$Cr(CO)_3$]	330, 345	446 (very low absorbance)
[(η^6-Mesitylene)$Cr(CO)_3$]	325	absent

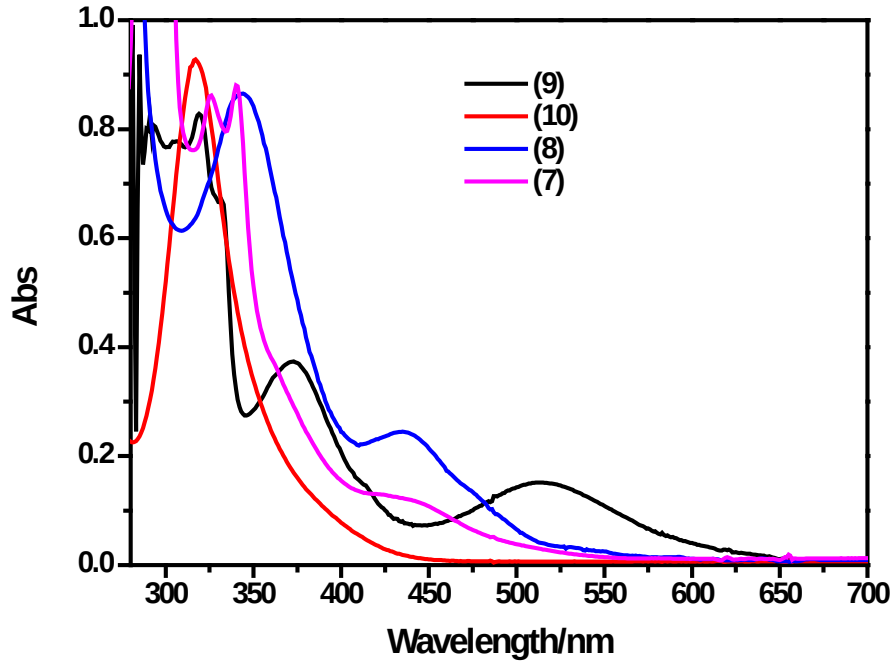

Figure 5.9: *UV-Vis spectra of [(η^6-anthracene)Cr(CO)$_3$] (**9**), [(η^6-mesitylene)Cr(CO)$_3$] (**10**), [(η^6-naphthalene)Cr(CO)$_3$] (**8**) and [(η^6-2-MeSnaphthalene)Cr(CO)$_3$] (**7**) recorded in hexane.*

The electronic structural features of [(η^6-arene)M(CO)$_3$] complexes were studied in detail.[24] In solution spectra of all the unsubstituted [(η^6-arene)Cr(CO)$_3$] complexes in this chapter show a strong absorbance in the near ultraviolet (350 nm) which can be assigned as M→π* CO charge transfer absorption, while a weaker absorption in the lower part of the visible range (445 nm) is assigned as a M→arene charge transfer (see **Figure 5.9**). This lower energy absorption peak is absent in case of [(η^6-mesitylene)Cr(CO)$_3$] and almost negligible in [(η^6-2-MeSnaphthalene)Cr(CO)$_3$] and can be related to ligand field separation effect of Cr d-orbitals. The partial broadness of the peak in the ultraviolet region can be associated to the coordination of the metal. The energy of the onset of absorption in these complexes seems to be related to the energy of the first π→π* energies.

5.2.3 CORMs studies

The majority of the Group-VI metal complexes investigated to date are good CO releasing compounds.[8, 25] For example Peter Ford and co-workers demonstrated photochemical CO releasing properties of water soluble neutral complex of tungsten metal namely $Na_3[W(CO)_5(TPPS)]$ (TPPS is tris(sulfonatophenyl)phosphine).[26] Fisher carbene chromium and molybdenum complexes have been reported as excellent CO releasing molecules.[11] Further Mo complexes with functionalised alkynyl ligands have been studied as effective Photo-CORMs.[12]

The CO-release profile for $[(bpy)Mo(CO)_4]$ (60 μM) is illustrated in **Figure 5.10**. Upon irradiation with monochromatic light (470 nm), spectral changes that are characteristic of CO release were demonstrated in the Q band region. At 0 min, there was one distinct absorption peak characteristic of deoxy-Mb. Over time, the intensity of the Q band at approximately 554 nm slowly decreased while the characteristic peaks of Mb-CO appeared at 546 nm and 578 nm. No spectral changes were observed when the sample was further photolysed after 320 mins. The amount of Mb-CO formation was also measured thermally at body temperature (37 ^{o}C). The temperature of the water bath was held constant for the duration of the experiment. The compounds that were analysed thermally were covered in tin-foil to ensure there were no photochemical effects. In comparison, no CO release was observed for this complex at body temperature as there were no significant changes exhibited in the UV-Vis spectra, up to 24 hours. Only one peak characteristic of deoxy-Mb was observed. Any release observed after this time is insignificant as it could not be therapeutically viable for the compounds to have such a slow release rate. The half-life for the formation of Mb-CO from this complex was found to be 125 mins.

***Table 5.4**: Thermal and photochemical CO release data of tetra and tri carbonyl complexes of Cr, Mo and W, 60 µM represents the concentration of the complexes in solution.*

Name of complex	**Total time required for Thermal CO Release (37 ^{o}C)** (**60 µM**)	**Total time required for Photo CO Release**	
		470 nm (**60 µM**)	**355 nm** **(60 µM)**
[(bpy)Cr(CO)$_4$]	330 mins **($t_{1/2}$ = 155 mins)**	30mins (**$t_{1/2}$ = 12 mins**)	No Release
[(bpy)Mo(CO)$_4$]	No Release	320mins **($t_{1/2}$ = 125 mins)**	No Release
[(bpy)W(CO)$_4$]	No Release	720 mins **($t_{1/2}$ = 335 mins)**	No Release
[(bpy)Mo(CO)$_3$(PPh$_3$)]	No Release	240 mins **($t_{1/2}$ = 102 mins)**	No Release
[(bpy)W(CO)$_3$(PPh$_3$)]	No Release	No Release	No Release
[(bpy)Cr(CO)$_3$(PPh$_3$)]	No Release	No Release	No Release
[(**η^6**-2-Me-S-naphthalene)Cr(CO)$_3$]	170 mins (**$t_{1/2}$ = 50 mins)**	No Release	No Release
[(**η^6**-naphthalene)Cr(CO)$_3$]	180 mins **($t_{1/2}$ = 55 mins)**	No Release	No Release
[(**η^6**-anthracene)Cr(CO)$_3$]	200 mins **($t_{1/2}$ = 60 mins)**	No Release	No Release
[(**η^6**-mesitylene)Cr(CO)$_3$]	330 mins **($t_{1/2}$ = 140 mins)**	No Release	No Release

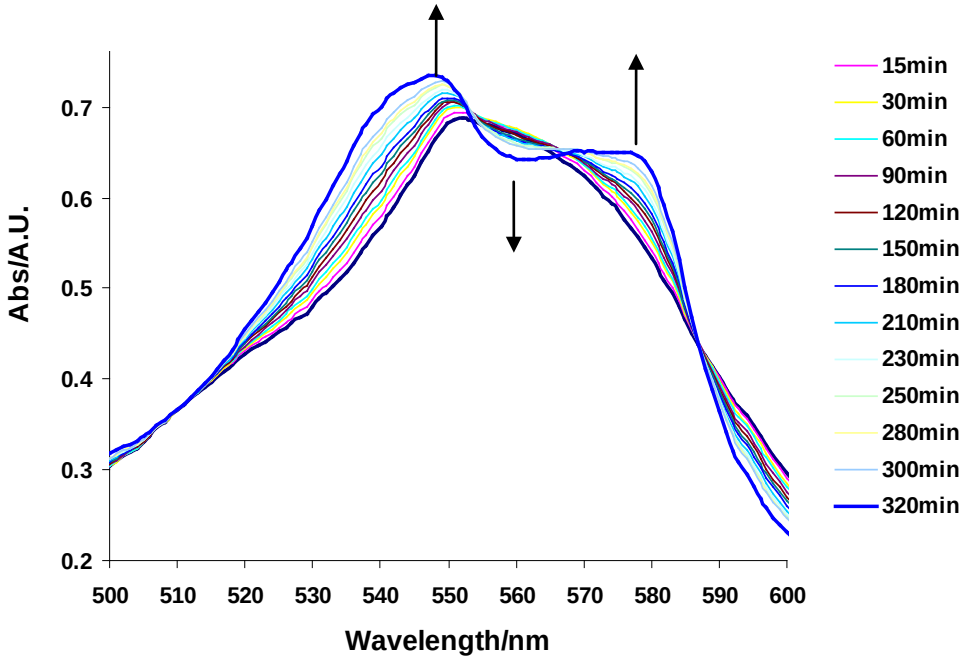

Figure 5.10: *CO-release profile for [(bpy)Mo(CO)$_4$] (60 µM) recorded at 470 nm using deoxymyoglobin solution (66 µM). Legend shows time passed in mins.*

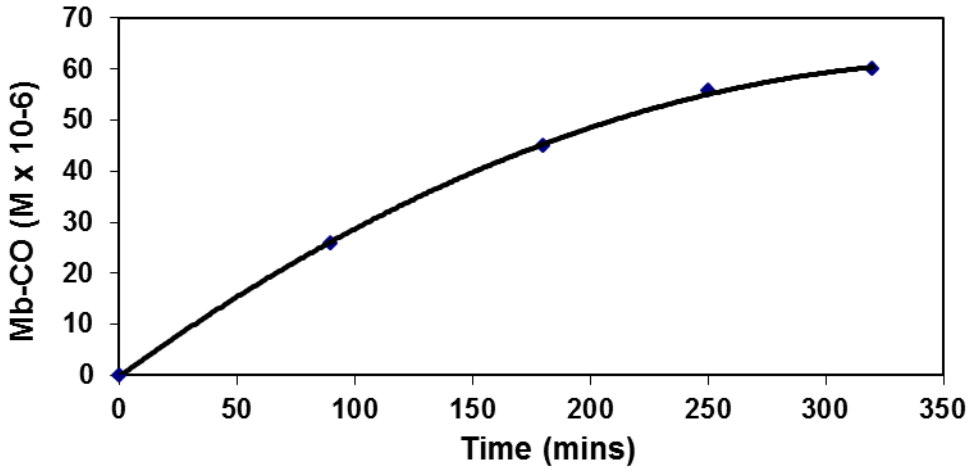

Figure 5.11: *Formation of Mb-CO quantified over time for [(bpy)Mo(CO)$_4$] complex (60 µM) at 470 nm.*

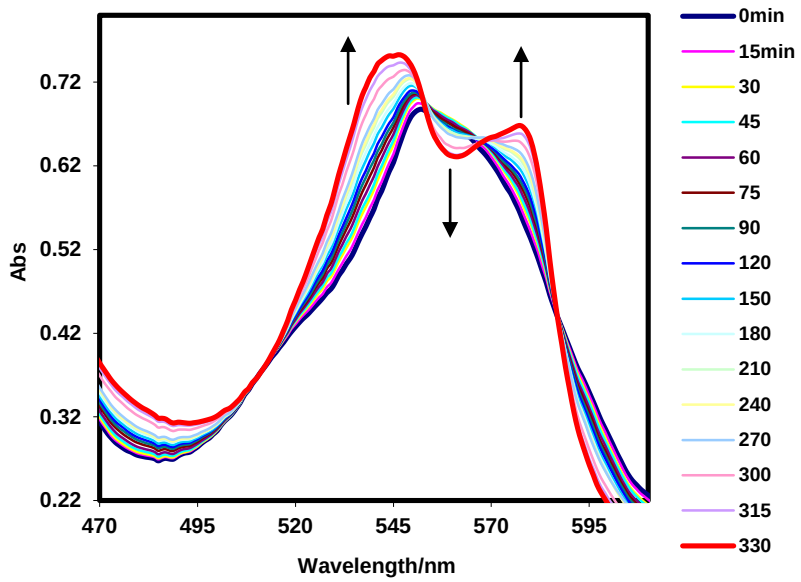

Figure 5.12: *CO-release profile for [(bpy)Cr(CO)$_4$] (60 μM) recorded at 37 ^{o}C using deoxymyoglobin solution (60 μM). Legend shows time passed in mins.*

The CO-release was also measured for [(bpy)Cr(CO)$_4$] thermally at body temperature (37 ^{o}C). Complete CO release was observed for this complex after 330 mins at 37 ^{o}C (see **Figure 5.12**). This is evident as there is a significant difference between the absorption profiles at 0 min compared with the absorption spectrum obtained after 330 mins. The half-life of Mb-CO for this complex was calculated to be 155 mins. The CO generation seen for this compound after 22 hours when measured at room temperature demonstrated a very slow release time.

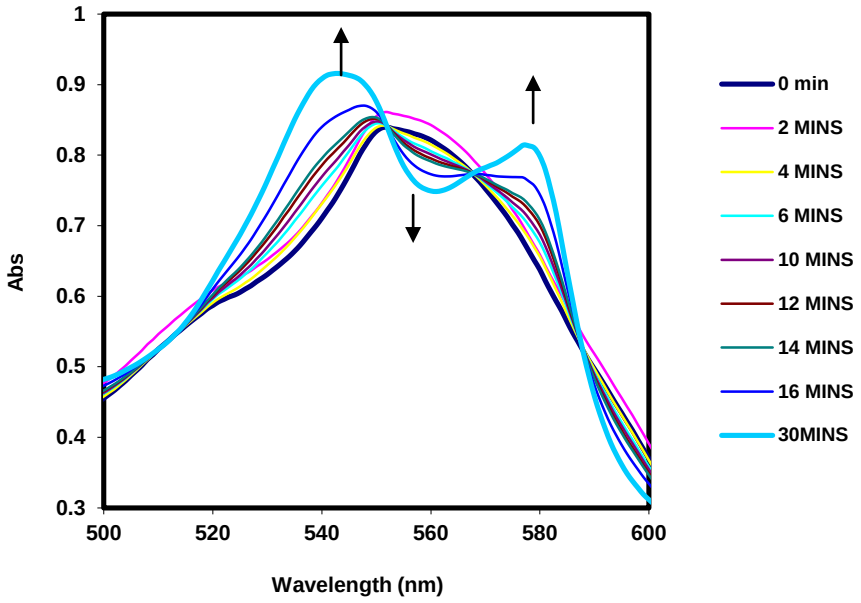

Figure 5.13: *CO-release profile for [(bpy)Cr(CO)$_4$] (60 μM) recorded at 470 nm using deoxymyoglobin solution (60 μM). Legend shows time passed in mins.*

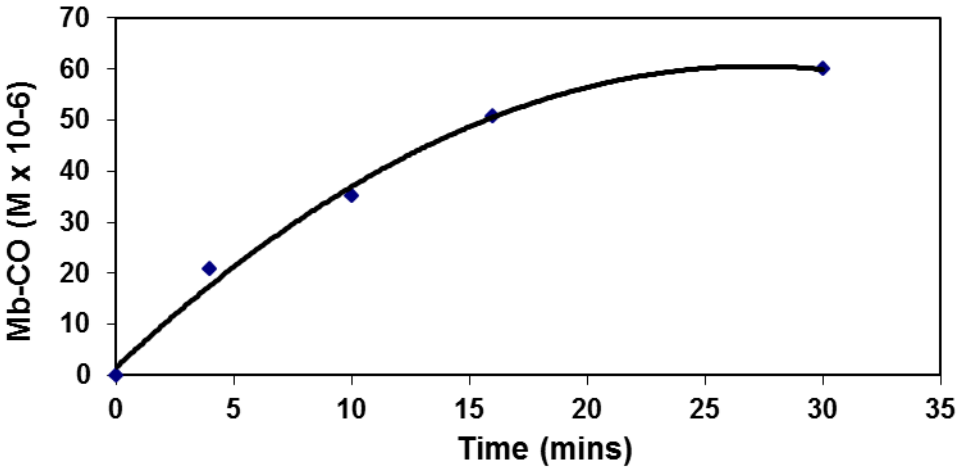

Figure 5.14: *Formation of Mb-CO quantified over time for [(bpy)Cr(CO)$_4$] complex (60 μM) at 470 nm.*

It can be deduced from **Figure 5.13** that after 30 mins photolysis, [(bpy)Cr(CO)$_4$] (60 µM) completely released the maximum amount of CO as there were no further spectral changes observed after this time. This complex is considered as effective thermal CO releasing molecules as half-life ($t_{1/2}$) for the formation of cabomonxymyoglobin was considered to be 12 mins (see **Figure 5.14**). Here light activation (470 nm) was required to initiate the liberation of CO. Again it was demonstrated that over time, the intensity of the Q band at approximately 555 nm slowly decreased while the characteristic peaks of Mb-CO appeared at 540 nm and 577 nm. This is consistent with that reported in literature for the characteristic absorption peaks of deoxy-Mb and Mb-CO.[27]

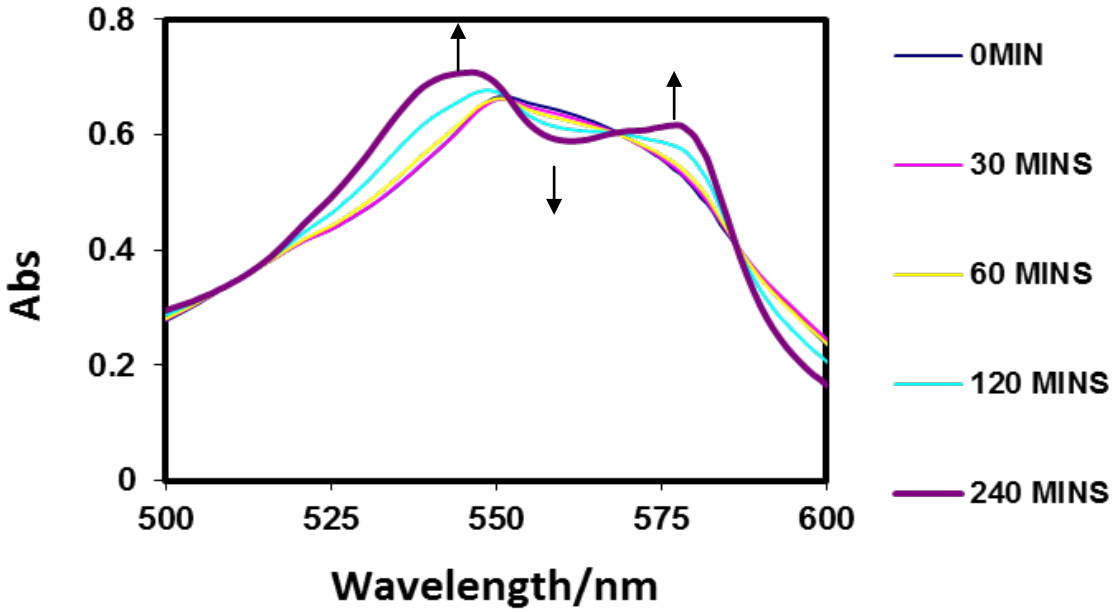

Figure 5.15: *CO-release profile for [(bpy)Mo(CO)$_3$(PPh$_3$)] (60 µM) recorded at 470 nm using myoglobin assay (66 µM). Legend shows time passed in mins.*

Bipyridine based tetracarbonyl complexes have been developed as excellent photo CORMs where it undergoes photoinduced CO release upon excitation above 400nm. For example a new class of photochemical activated CO releasing molecule based on Mn(CO)$_4$(C^N) system (C^N = ortho-metalled 2-phenylpyrdine) was reported by Fairlamb and co workers.

This class of compounds were stable under thermal conditions and found to be fast CO releaser with half-life of 45 mins when the complex (40 μM) was irradiated at 400 nm.[28, 29]

In this work the bipyridine based tetra and tri carbonyl Cr, Mo and W complexes were studied for their CO release efficiency both photochemically and thermally. $[(bpy)Cr(CO)_4]$ complex emerged as an efficient photo CORM. In the case of tetracarbonyl complexes it was observed that the rate of CO release increases in the order Cr > Mo > W which is consistent with the reported data.[11]

The CO release was measured in the same manner for each of the tri-carbonyl complexes; $[(bpy)Mo(CO)_3(PPh_3)]$, $[(bpy)Cr(CO)_3(PPh_3)]$ and $[(bpy)W(CO)_3(PPh_3)]$. Photo-induced CO liberation was only observed for $[(bpy)Mo(CO)_3(PPh_3)]$ after 240 mins when sample was irradiated at 470 nm (**Figure 5.15**). The half-life for the formation of Mb-CO for this complex was found to be 102 min. No appreciable formation of CO was liberated for this complex when analysed by thermal methods both at body temperature and at room temperature. There was no CO release indicated for the other two complexes; $[(bpy)Cr(CO)_3(PPh_3)]$ and $[(bpy)W(CO)_3(PPh_3)]$ either photochemically or thermally. This may be due to increase in electron density in the metal centre from the π electrons that enhance the metal carbonyl bond and hence slows the rate of CO release from these complexes. However, the bipyridine based tricarbonyl complexes were found to be slow CO releasers where only $[(bpy)Mo(CO)_3(PPh_3)]$ released CO photochemically on irradiation at 470 nm. Further in all cases, the CO release from tungsten carbonyl complexes has been sluggish. From the results, it can be said that the corresponding chromium and molybdenum congeners are better CO releasing molecules when compared to tungsten based metal carbonyl complexes.

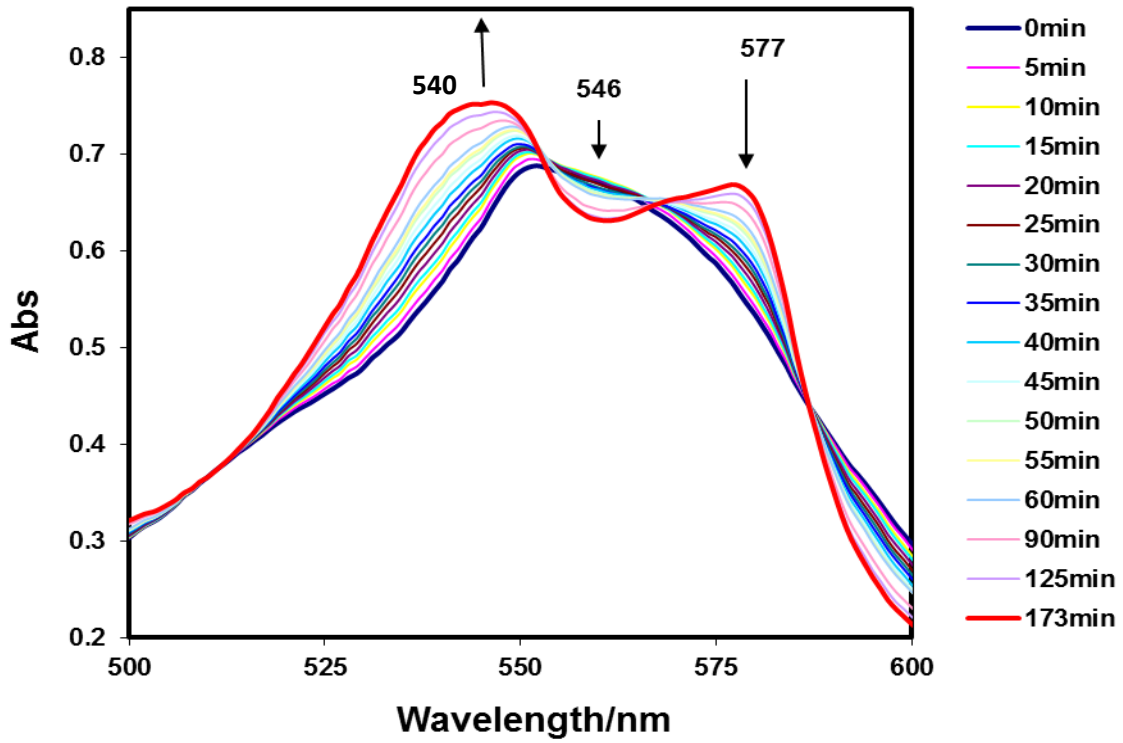

Figure 5.16: *The changes in the UV-Vis spectrum of myoglobin thermally (37 °C) as CO is released from [(η^6-2-methylthionaphthalene)Cr(CO)$_3$] (60 μM) using myoglobin assay (66 μM). Legend shows time passed in mins.*

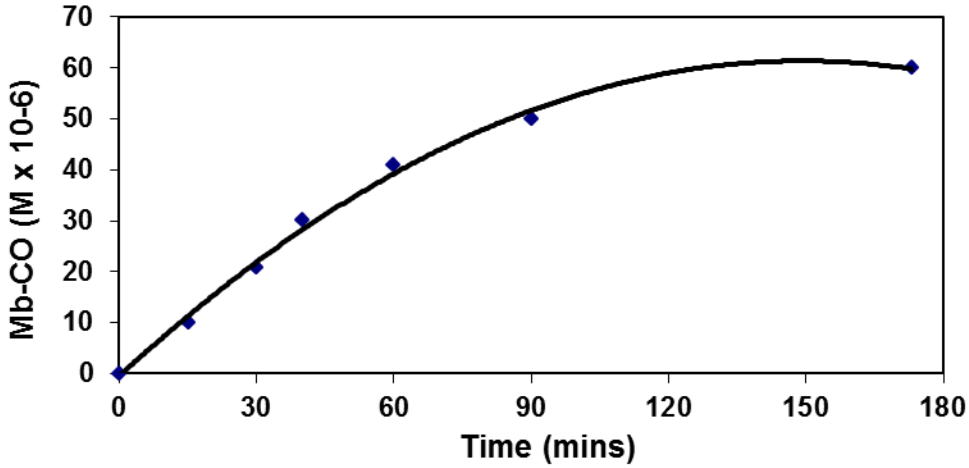

Figure 5.17: *Formation of Mb-CO quantified over time for[(η^6-2-methyl-S-naphthalene)Cr(CO)$_3$] (60 μM) at 37°C.*

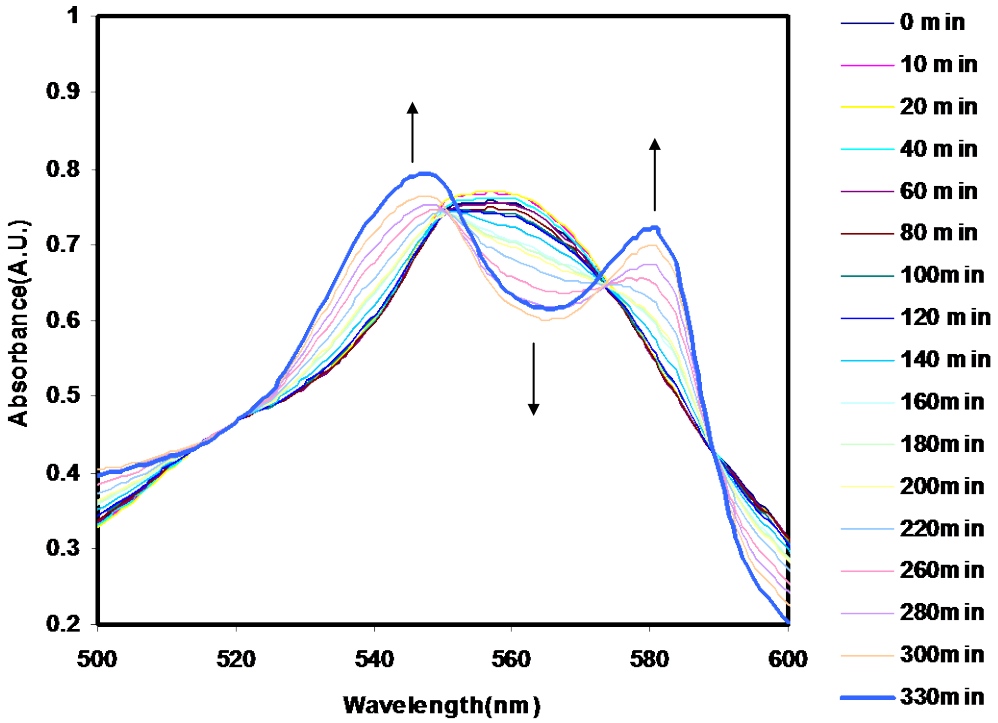

Figure 5.18: *The changes in the UV-Vis spectrum of myoglobin thermally (37 °C) as CO is released from [(η^6-mesitylene)Cr(CO)$_3$] (60 µM) using myoglobin assay (66 µM). Legend shows time passed in mins.*

In the past a large number of arene tricarbonyl complexes with different transition metals were studied for their CO releasing abilities both thermally and photochemically.[30-33] Thus in this study an attempt was made to study the CO releasing properties of the following complexes [(η^6-naphthalene)Cr(CO)$_3$], [(η^6-anthracene)Cr(CO)$_3$], [(η^6-2-MeSnaphthalene)Cr(CO)$_3$] and [(η^6-mesitylene)Cr(CO)$_3$]. It was found that among all the [(η^6-arene)Cr(CO)$_3$] complexes, [(η^6-2Me-S-naphthalene)Cr(CO)$_3$] and [(η^6-mesitylene)Cr(CO)$_3$] (see **Figure 5.16 - 5.18**) were the fastest and slowest thermal CO releaser respectively. Both [(η^6-2-MeSnaphthalene)Cr(CO)$_3$] and [(η^6-naphthalene)Cr(CO)$_3$] can be considered as moderately effective thermal CO releasing molecules as their half-life was calculated to be 50 and 55 mins respectively. [(η^6-mesitylene)Cr(CO)$_3$] released CO thermally after 240 mins as assessed using myoglobin

assays, so the complex is considered to be very slow CO releasing molecule. The half-life for the formation of the Mb-CO was found to be 140 mins.

5.3 Conclusion

Transition metal tetracarbonyl and tricarbonyl compounds based on molybdenum, chromium and tungsten were fully synthesised and characterised by IR, UV-Vis and NMR spectroscopic tools. The release of CO from these compounds was assessed spectrophotometrically by measuring the conversion of deoxymyoglobin to carboxymyoglobin. CO-liberation was monitored by thermal (20 ^{o}C and 37 ^{o}C) and photochemical (470 and 355 nm) means. [(bpy)Cr(CO)$_4$] acted as an excellent photo CO releasing molecule with maximum CO release after 30 mins. [(bpy)Mo(CO)$_4$] and [(bpy)Mo(CO)3(PPh$_3$)] also acted as photo inducible CORMs (photoCORMs). These molybdenum based complexes released the maximum output of CO in the presence of monochromatic light (470 nm) after 320 min and 240 min, respectively.

Also, all the [(η^6-arene)Cr(CO)$_3$] complexes exhibited efficient CO releasing properties with [(η^6-2Me-S-naphthalene)Cr(CO)$_3$] being the fastest, having maximum release of CO in 170 mins. In this study [(η^6-mesitylene)Cr(CO)$_3$] is the only arene chromium complex which released CO very slowly under thermal conditions.

It can be further concluded that among all the synthesised tri and tetracarbonyl complexes of chromium, molybdenum and tungsten here, [bpyCr(CO)$_4$] is the most promising as photoCORM.

5.4 Experimental

5.4.1 Materials

All solvents were supplied by the SigmaAldrich Chemical Company. Chloroform, dichloromethane, pentane, diethyl ether, and hexane were dried over $MgSO_4$ prior to use. All organic reagents were purchased from the SigmaAldrich and used without further purification unless stated otherwise. The hexacarbonyls, $W(CO)_6$, $Mo(CO)_6$ and $Cr(CO)_6$ were used without further purification. All mobile phases for column chromatography were dried over $MgSO_4$ and silica-gel (Merck) was used as received. All syntheses were carried out under an atmosphere of argon or nitrogen using standard Schlenk techniques unless otherwise stated.

5.4.2 Instrumentation

NMR spectra were recorded on a Bruker model AC 400 MHz spectrophotometer and Bruker model ANC 600 MHz spectrophotometer using $CDCl_3$ as solvent. All NMR spectra were calibrated according to the residual solvent peak, i.e. $CDCl_3$ at 7.27 ppm for all ^1H spectra. Chemical shifts (δ) are given in parts per million (ppm). Proton coupling constants (*J*) are given in Hertz (Hz). All UV-Vis spectra were measured on an Agilent Technologies 8453 photodiode array spectrometer using a 1 cm^3 quartz cell. IR spectra were recorded on a Perkin-Elmer 2000 FT-IR spectrophotometer (2 cm^{-1} resolution) in a 0.1 mm sodium chloride liquid solution cell.

5.4.3 Myoglobin assay

This procedure was undertaken in the same manner as reported by Atkin *et al*. and was used for all the complexes in the study.[7] For all the complexes, 12 mM solution of the complex was prepared in a 5 mL volumetric flask using DMSO as solvent. The deoxymyoglobin (deoxy-Mb) standard solution was prepared by weighing 0.0115 g of myoglobin, 0.01 g of sodium dithionite and dissolving them in 10 mL of phosphate-buffer solution (PBS). A UV-Vis spectrum of this standard deoxymyoglobin solution was obtained. The solution was then purged with CO for 30 minsforming carboxymyoglobin (Mb-CO). A UV-Vis spectrum of the standard was then taken. 2 mL of the standard deoxy-Mb, 10 µL of the complex solution and 500 µL of mineral oil were placed into a plastic cuvette. The CO release was monitored by performing UV-Vis analysis at regular interval of time. For thermal studies the samples were kept at 19 or 37 ^{o}C. The solution was allowed to stand wrapped in tin-foil (to prevent light entering) at room temperature (19 ^{o}C) and at body temperature (37 ^{o}C). The CO release was also measured by photochemical means in the same way (the cuvette containing the solution to be measured was placed in front of a LED light source and was placed 10 cm away. A control experiment was also performed. The temperature of the solution placed in front of the LED light was recorded during the experiment to ensure that there was only a photochemical effect and not a thermal effect. In all photochemical experiments the temperature was confirmed to remain constant at 19 ^{o}C. The procedure described here was used for all the complexes tetra and tricarbonyl chromium, molybdenum and tungsten complexes studied in this chapter

5.5 Synthesis

5.5.1 [(bpy)Mo(CO)$_4$]

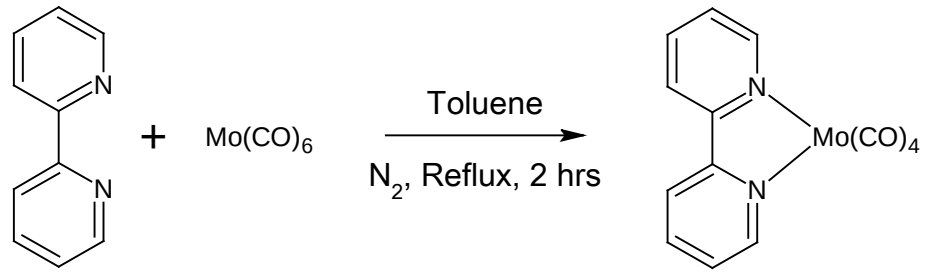

Molybdenum hexacarbonyl (9.98 mmol/0.261 g) and (7.5 mmol/1.175 g) of 2, 2'-dipyridyl (bpy) were added to the reaction flask containing 20 mL of toluene. The reaction mixture was purged with nitrogen for 15 mins. The reaction mixture was refluxed for 2 hours under a nitrogen atmosphere. During refluxing the solution went from colourless to deep red. The reaction mixture was allowed to cool to room temperature. 4 mL of ice-cold petroleum ether 60-80 ^{o}C was added to the reaction flask. The reaction flask was placed in an ice bath to promote further precipitation. The precipitate was filtered on a Hirsch funnel and was washed with ice cold pentane. The purple coloured complex was dried under vacuum. Spectroscopic data analysed were in agreement with the reported data.[13]

Yield: 3.319 g, 9.11mmol, 93 %.

^{1}H NMR (400 MHz, $CDCl_3$) δ ppm: 9.09 (d, 2H), 8.05 (d, 2H), 7.86 (td, 2H), 7.32 (td, 2H).

IR ν_{CO} ($CHCl_3$)**:** 2018, 1912, 1883, 1835 cm^{-1}.

UV-Vis (λ_{max}, $CHCl_3$): 298, 474 nm.

5.4.2. [(bpy)Cr(CO)$_4$]

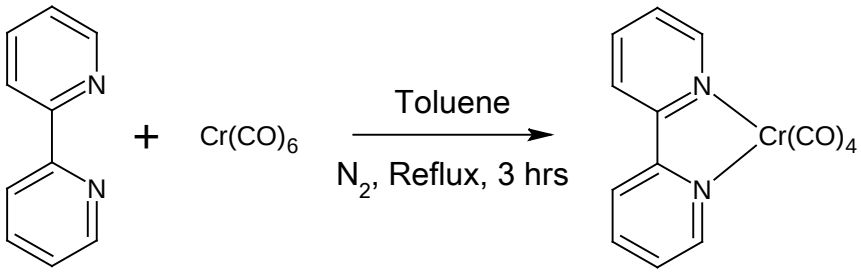

The synthetic procedure used for [(bpy)Mo(CO)$_4$] was followed for this complex. Chromium hexacarbonyl (1.847 mmol/0.406 g) and (9.114 mmol/1.423 g) of 2, 2'-dipyridyl were used. The reaction mixture was allowed to reflux under nitrogen atmosphere for 3 hours to produce a deep orange / red coloured product. Spectroscopic data analysed were in agreement with the reported data.[14, 34]

Yield: 1.152 g, 3.6 mmol, 40 %.

^{1}H NMR (400 MHz, $CDCl_3$) δ ppm: 8.62 (d,2H), 8.33 (d,2H); 8.02 (td ,2H); 7.78 (td, 2H).

IR ν_{CO} ($CHCl_3$): 2013, 1910, 1889, 1836 cm^{-1}.

UV-Vis (λ_{max}, $CHCl_3$): 293nm, 519 nm.

5.4.3 [(bpy)W(CO)$_4$]

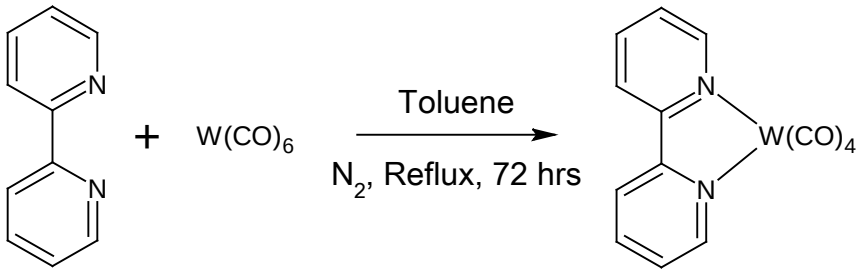

The synthetic procedure used for [(bpy)Mo(CO)$_4$] was followed for this complex. Tungsten hexacarbonyl (5.67 mmol/0.4019 g) and (5.681 mmol/0.887g) of 2, 2'-dipyridyl were used. The reaction mixture was refluxed for 72 hours under nitrogen atmosphere to yield a deep orange coloured product formed. Spectroscopic data were in agreement with the reported data.[13]

Yield: 0.718 g, 1.58 mmol, 28 %.

^{1}H-NMR (400MHz; $CDCl_3$) δ ppm 9.20 (d, 2H); 8.08 (d, 2H); 7.90 (td, 2H); 7.34 (td, 2H).

IR ν_{CO} ($CHCl_3$): 2012, 1903, 1881, 1831 cm^{-1}.

UV-Vis (λ_{max} ,$CHCL_3$) : 299, 498 nm.

5.4.4 [(bpy)Mo(CO)$_3$(PPh$_3$)]

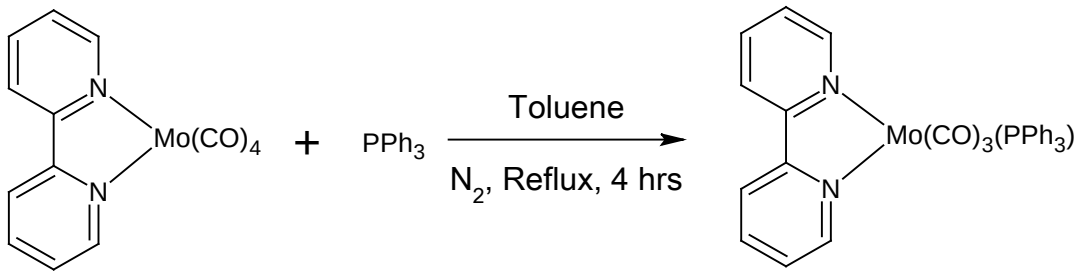

2, 2'-bipyridyl molybdenum tetracarbonyl (0.203 mmol/0.0741 g) was placed in a 3-necked 50 mL round bottom flask. 3-4 anti-bumping chips and (0.412 mmol/0.108 g) of triphenylphosphine was placed in the reaction flask containing 10 mL of toluene. The reaction mixture was purged with nitrogen for 15 mins and the reaction mixture was refluxed for 4 hours under a nitrogen atmosphere. Solution became dark purple / black solution in colour. The reaction mixture was allowed to cool to room temperature. The solution containing the product was filtered and dried under vacuum, yielding a deep purple / black powder. The crude product was purified using silica gel and ethyl acetate / pentane (8:2) as mobile phase. Therefore, the product was washed with this solution while under vacuum filtration. The product remained in the filtrate (intense deep purple colour). The solvent from the filtrate was evaporated under vacuum. A dark purple product was obtained. Spectroscopic data analysed were in agreement with the reported data.[35]

Yield: 0.0582 g, 0.097 mmol, 48 %.

^{1}H-NMR (400MHz; $CDCl_3$) δ ppm 8.75 (d, 2H); 7.69 (d, 2H); 7.58 (td, 2H); 7.24 (m, 15H); 6.91 (td, 2H).

IR ν_{CO} ($CHCl_3$): 1919, 1827, 1795 cm^{-1} .

UV-Vis (λ_{max} , $CHCl_3$): 252, 543 nm.

5.4.5 [(bpy)Cr(CO)$_3$(PPh$_3$)]

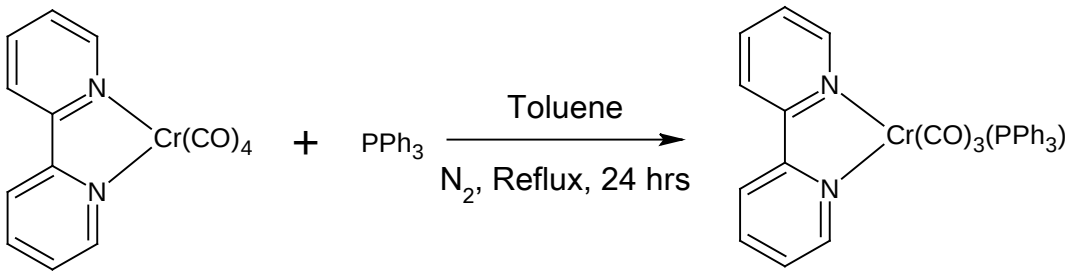

The synthetic procedure used for [(bpy)Mo(CO)$_3$(PPh$_3$)] was followed for this complex. 2, 2'-bipyridyl chromium tetracarbonyl (0.178 mmol/0.057 g) and (0.315 mmol/0.082 g) of triphenylphosphine were used. The Schlenk technique was used to ensure air and moisture were eliminated from the reaction. The reaction mixture was allowed to reflux for 24 hours under nitrogen atmosphere. A brown coloured solid powder was obtained as product. Spectroscopic data analysed were in agreement with the reported data.[15]

Yield: 0.0137 g, 0.025 mmol, 14 %.

^{1}H-NMR (400MHz; $CDCl_3$) δ ppm 8.75 (d, 2H); 7.69 (d, 2H); 7.58 (td, 2H); 7.24 (m, 15H); 6.91 (td, 2H).

IR ν_{CO} ($CHCl_3$): 2015, 1900, 1887, 1834 cm^{-1}.

UV-Vis (λ_{max}, $CHCl_3$) : 257, 570 nm.

5.4.6 [(bpy)W(CO)$_3$(PPh$_3$)]

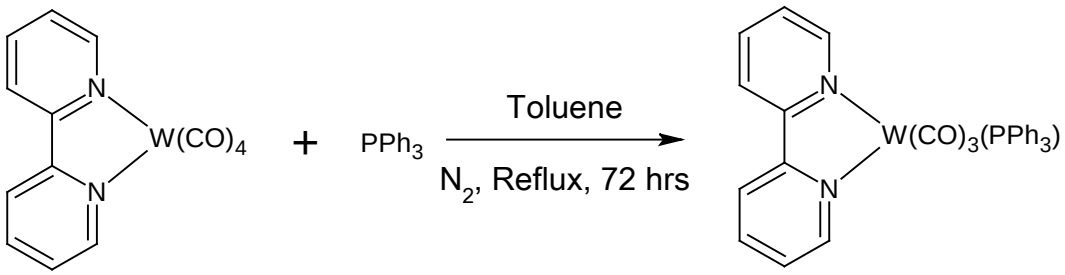

The synthetic procedure employed for [(bpy)W(CO)$_3$(PPh$_3$)] was followed. 2, 2'-bipyridyl tungsten tetracarbonyl (0.099 mmol/0.045 g) and (2.2 mmol/0.058 g) of triphenylphosphine were used. The reaction mixture was brought to reflux temperature for 72 hours under nitrogen atmosphere. Once the flask had cooled, the solution was filtered through a glass centred crucible containing celite and charcoal. The product was washed further using chloroform. The filtrate was evaporated using the high vacuum pump. Spectroscopic data analysed were in agreement with the reported data.[35]

Yield: 0. 010 g, 0.013mmol, 14 %.

^{1}H NMR (400 MHz, CHLOROFORM-*d*) δ ppm 9.21 (d, 2H); 8.62 (d, 2H); 8.33 (td, 2H); 7.94 (td, 2H); 7.53 (m, 15H).

IR ν_{CO} ($CHCl_3$): 1912, 1822, 1791 cm^{-1} .

UV-Vis (λ_{max} , $CHCl_3$): 261, 522 nm.

5.4.7 [(η^6-2-MeSnapthalene)Cr(CO)$_3$]

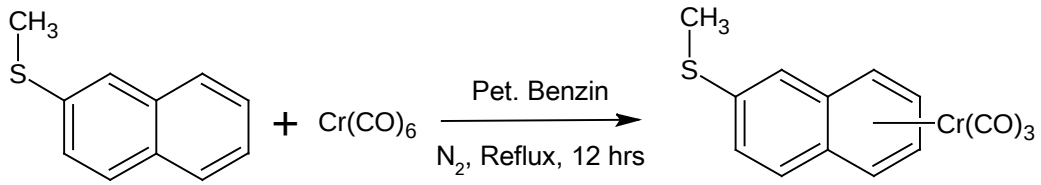

Chromium hexacarbonyl (5.68 mmol/1.25 g) and 2methylthionaphthalene (1.24 mmol /0.216 g) were added to the reaction flask containing 40 mL of petroleum-benzin. The reaction mixture was purged with nitrogen for 15 mins and the reaction mixture was brought to reflux temperature overnight under a nitrogen atmosphere. Solvent was removed under vacuum and column chromatography was performed using petroleum ether as an eluent. Recrystallisation was carried out using petroleum ether. An orange coloured product was obtained. Spectroscopic data analysed were in agreement with the reported data.[16]

Yield: 0.934 g, 3.01 mmol, 53 %.

^{1}H NMR (400 MHz, $CDCl_3$) δ ppm 0-7.3 (m, 4H); 6.3 (d, 2H); 5.4 (d, 2H); 5.32 (s, 1H); 3.1(s, 3H).

IR ν_{CO} (Hexane): 2018, 1965, 1895 cm^{-1}

UV-Vis (λ_{max}, Hexane) : 320, 416 nm.

5.4.8 [(η^6-napthalene)$Cr(CO)_3$]

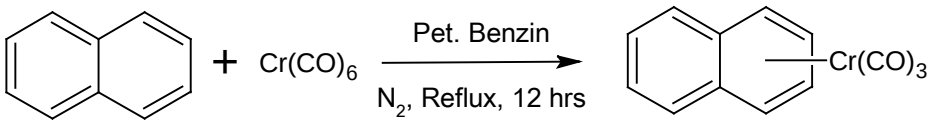

The synthetic procedure employed to synthesise 2 methyl thionaphthalene chromium tricarbonyl was followed. Naphthalene (1.24 mmol/0.158 g) and (5.68 mmol/1.25 g) of chromium hexacarbonyl are used for the synthesis. Spectroscopic data analysed were in agreement with the reported data.[17]

Yield: 0.900 g, 3.4 mmol, 60 %.

^{1}H NMR (400 MHz, $CDCl_3$) δ ppm 7.0-7.4 (m, 4H); 6.1 (d, 2H); 5.46 (d, 2H); 5.32 (s, 1H); 3.1(s, 3H).

IR ν_{CO} (Hexane): 2018, 1967, 1896 cm^{-1}.

UV-Vis (λ_{max}, Hexane) : 341, 436 nm.

5.4.9 [(η^6-anthracene)Cr(CO)$_3$]

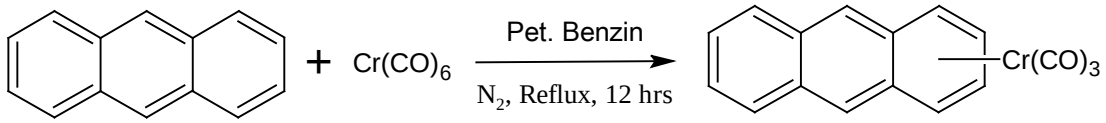

The synthetic procedure employed to synthesise 2 methyl thionaphthalene chromium tricarbonyl was followed. Anthracene (1.24 mmol/0.221 g) and (5.68 mmol/1.25 g) of chromium hexacarbonyl are used for the synthesis. Spectroscopic data analysed were in agreement with the reported data.[17]

Yield: 0.945 g, 3.01mmol, 60 %

IR ν_{CO} (Hexane) : 2018, 1991, 1931 cm^{-1}.

UV-Vis (λ_{max}, Hexane) : 376, 571 nm

5.4.10 [(η^6-mesitylene)Cr(CO)$_3$]

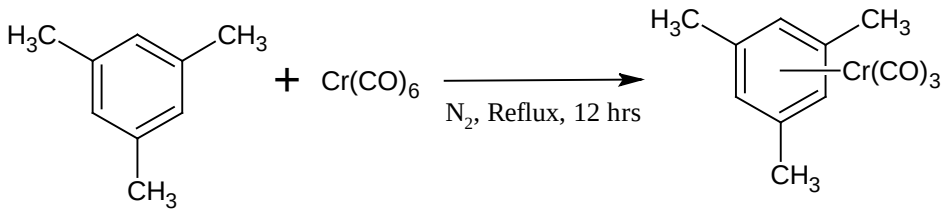

The Synthetic procedure employed to synthesise 2 methyl thionaphthalene chromium tricarbonyl was followed. Mesitylene (0.286 mol/40 mL) and (4.6 mmol/1.02 g) of chromium hexacarbonyl are used for the synthesis. Spectroscopic data analysed were in agreement with the reported data.[17]

Yield: 0.824 g, 3.22mmol, 70 %.

IR ν_{CO} (Hexane): 2018, 1965 cm^{-1}.

UV-Vis (λ_{max}, Hexane) : 320 nm.

5.6 References

1. R. Motterlini, J. E. Clark, R. Foresti, P. Sarathchandra, B. E. Mann and C. J. Green, *Circul. Res.*, 2002, **90**, e17-e24.

2. C. G. Hartinger and P. J. Dyson, *Chem. Soc. Rev.*, 2009, **38**, 391-401.

3. R. Alberto and R. Motterlini, *Dalton Trans.*, 2007, 1651-1660.

4. S. Chlopicki, R. Olszanecki, E. Marcinkiewicz, M. Lomnicka and R. Motterlini, *Cardiovasc. Res.*, 2006, **71**, 393-401.

5. J. C. Obirai, S. Hamadi, A. Ithurbide, C. Wartelle, T. Nyokong, J. Zagal, S. Top and F. Bedioui, *Electroanalysis*, 2006, **18**, 1689-1695.

6. A. J. Atkin, J. M. Lynam, B. E. Moulton, P. Sawle, R. Motterlini, N. M. Boyle, M. T. Pryce and I. J. S. Fairlamb, *Dalton Trans.*, 2011, **40**, 5755-5761.

7. A. J. Atkin, S. Williams, P. Sawle, R. Motterlini, J. M. Lynam and I. J. S. Fairlamb, *Dalton Trans.*, 2009, 3653-3656.

8. W.-Q. Zhang, A. J. Atkin, R. J. Thatcher, A. C. Whitwood, I. J. S. Fairlamb and J. M. Lynam, *Dalton Trans.*, 2009, 4351-4358.

9. U. Schatzschneider, *Inorg. Chim. Acta*, 2011, **374**, 19-23.

10. P. Govender, S. Pai, U. Schatzschneider and G. S. Smith, *Inorg. Chem.*, 2013, **52**, 5470-5478.

11. W.-Q. Zhang, A. C. Whitwood, I. J. S. Fairlamb and J. M. Lynam, *Inorg. Chem.*, 2010, **49**, 8941-8952.

12. H. Pfeiffer, T. Sowik and U. Schatzschneider, *J. Organomet. Chem.*, 2013, **734**, 17-24.

13. M. H. B. Stiddard, *J. Chem. Soc. (Res.)*, 1962, **0**, 4712-4715.

14. C. S. Kraihanzel and F. A. Cotton, *Inorg. Chem.*, 1963, **2**, 533-540.

15. R. J. Angelici and J. R. Graham, *J. Am. Chem. Soc.*, 1965, **87**, 5586-5590.

16. A. Ãysul, N. S. Bykkidan, B. BÃkkidan and O. Akmak, *Turkish J. Chem*, 2006, **30**, 235-241.

17. J. A. Morley and N. F. Woolsey, *J. Org. Chem.*, 1992, **57**, 6487-6495.

18. J. A. Connor and C. Overton, *J. Chem. Soc., Dalton Trans.*, 1982, 2397-2402.

19. D. M. Adams and A. Squire, *J. Chem. Soc., Dalton Trans.*, 1974, 558-565.

20. F. A. Cotton and C. S. Kraihanzel, *J. Am. Chem. Soc.*, 1962, **84**, 4432-4438.

21. M. H. B. Stiddard, *J. Chem. Soc. (Res.)*, 1962, 4712-4715.

22. S. Sato, T. Morimoto and O. Ishitani, *Inorg. Chem.*, 2007, **46**, 9051-9053.

23. P. G. Sennikov, V. A. Kuznetsov, A. N. Egorochkin, N. I. Sirotkin, R. G. Nazarova and G. A. Razuvaev, *J. Organomet. Chem.*, 1980, **190**, 167-176.

24. H. Saito, Fujita, Junnosuke, *Bull. Chem. Soc. Jpn.*, 1968, **41**, 359-364.

25. W.-Q. Zhang, A. J. Atkin, I. J. S. Fairlamb, A. C. Whitwood and J. M. Lynam, *Organometallics*, 2011, **30**, 4643-4654.

26. R. D. Rimmer, H. Richter and P. C. Ford, *Inorg. Chem.*, 2010, **49**, 1180-1185.

27. G. DoÌˆrdelmann, H. Pfeiffer, A. Birkner and U. Schatzschneider, *Inorg. Chem.*, 2011, **50**, 4362-4367.

28. M. A. Gonzalez, M. A. Yim, S. Cheng, A. Moyes, A. J. Hobbs and P. K. Mascharak, *Inorg. Chem.*, 2012, **51**, 601-608.

29. P. Rudolf, F. Kanal, J. Knorr, C. Nagel, J. Niesel, T. Brixner, U. Schatzschneider and P. Nuernberger, *J. Phys. Chem. Lett.*, 2013, **4**, 596-602.

30. M. J. Rose and P. K. Mascharak, *Coord. Chem. Rev.*, 2008, **252**, 2093-2114.

31. N. E. Brückmann, M. Wahl, G. J. Reiß, M. Kohns, W. Wätjen and P. C. Kunz, *Eur. J. Inorg. Chem.*, 2011, **2011**, 4571-4577.

32. J. S. Ward, J. M. Lynam, J. W. B. Moir, D. E. Sanin, A. P. Mountford and I. J. S. Fairlamb, *Dalton Trans.*, 2012, **41**, 10514-10517.

33. P. C. Kunz, W. Huber, A. Rojas, U. Schatzschneider and B. Spingler, *Eur. J. Inorg. Chem.*, 2009, **2009**, 5358-5366.

34. M.H.B.Stiddard, *J. Chem. Soc., Dalton Trans.*, 1962, 4712.

35. J. R. Graham and R. J. Angelici, *J. Am. Chem. Soc.*, 1965, **87**, 5590-5597.

Chapter 6

Future Work

This chapter outlines the future work, based on the results presented in this thesis.

Chapter 2 describes different dipyrrin based rhenium tricarbonyl and tetracarbonyl complexes, their synthetic procedures, characterisations, photophysical properties, picosecond time resolved infrared spectroscopy and CO releasing properties. Future work will involve carrying out the electrochemical studies on the complexes. The ps-TRIR study of 5-mesityl and 5-phenyl dipyrrin Re tetracarbonyl complexes allowed the identification of an IL (π-π^*) dipyrrin based excited state following excitation at 520 nm and 470 nm respectively. Wavelength dependent TRIR studies using these rhenium tetracarbonyl complexes should be carried out at higher energy values (400 nm, 320 nm). In addition pyrene based dipyrrin rhenium tetracarbonyl complex was found to be fastest CO releasing molecule. To make these molecules water soluble, one of the carbonyl ligands present in the complexes can be substituted with tris(hyroxymethyl)phosphine $P(CH_2OH)_3$ ligand and study the CO releasing properties under thermal and photochemical conditions.

Chapter 3 reports the synthesis of mononuclear bisbpy based rhenium and manganese tricarbonyl complexes and dinuclear Ru/Re and Ru/Mn complexes. These complexes are characterised with different spectroscopic tools. Further ps-TRIR spectroscopic study of $[Ru(bpy)_2(bisbpy)Re(CO)_3Cl](PF_6)_2$ at λ_{exc} = 450 nm in acetonitrile solution resulted in formation of a long lived Ru(II) to bisbpy bridging ligand based MLCT excited state whereas the time resolved infrared spectroscopic study of $[(bisbpy)Re(CO)_3Cl]$ at λ_{exc} = 320 nm led to the shifting of IR bands to higher energy than their ground state counterparts which correspond to a Re to bisbpy based MLCT excited state. Future work should focus on low temperature emission and room temperature lifetime studies on these complexes. Also, from the CO release study it was observed that only manganese based tri carbonyl complexes released CO under photochemical conditions. Toxicological tests should be investigated for these complexes as part of the future work.

Chapter 4 discusses the synthesis of free base and metallated porphyrins tethered to chromium and tungsten based pentacarbonyl moieties and their characterisation by NMR, UV and IR spectroscopy. Electrochemical and time resolved infrared studies should be carried out on Pd based freebase porphyrin (PdMPyTPP) and Cu tethered to $MpyTPPW(CO)_5$ and $MpyTPPCr(CO)_5$ compounds. Further emission and singlet lifetime studies can be carried out on these porphyrin macrocycles.

Chapter 5 describes the synthesis of a series of arene based chromium, molybdenum and tungsten based tricarbonyl and tetracarbonyl complexes and further their CO releasing properties were studied using myoglobin assays. Time resolved infrared spectroscopic studies can be carried out on bpy based chromium, molybdenum and tungstun tricarbonyl complexes with an aim to see CO loss from these complexes. [2-Me-S-naphthaleneCr$(CO)_3$], [naphthaleneCr$(CO)_3$]and [bpyCr$(CO)_4$] complexes were found to be efficient CO releasing molecules under thermal conditions. Hence, toxicological studies should be carried on these complexes to test their toxicity against the strains of bacteria such as *Pseudomonas putida* (CP1) and *E. coli*.

APPENDIX

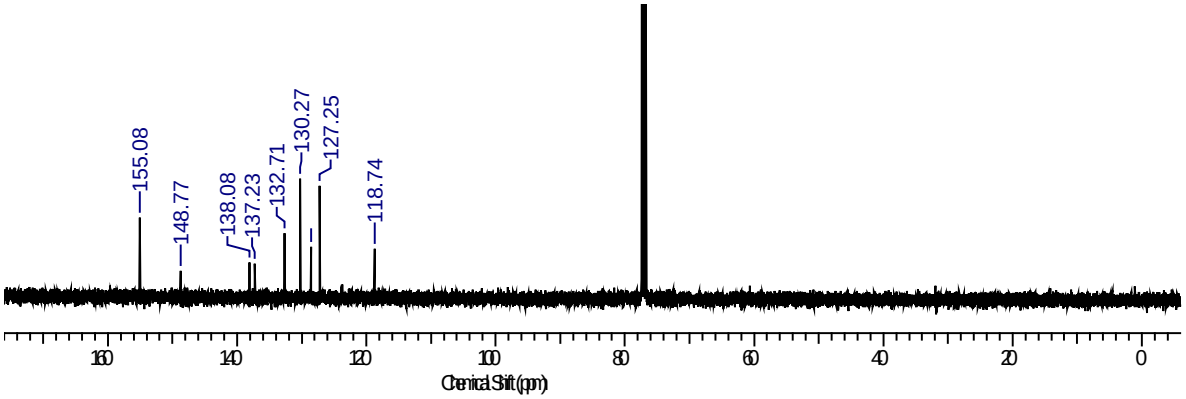

^{13}C NMR ($CDCl_3$, 400 MHz) of [(5-phenyl-4,6-dipyrrinato)$Re(CO)_4$]

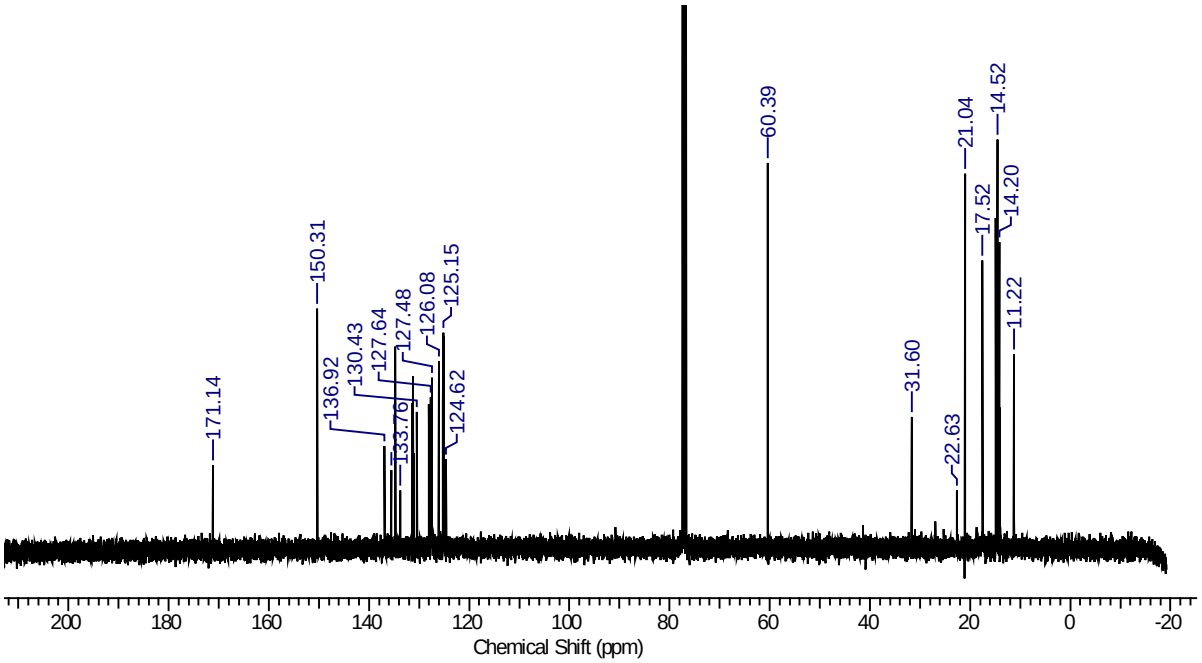

^{13}C NMR ($CDCl_3$, 400 MHz) of [(5-pyrenyl-4,6-dipyrrinato)$Re(CO)_4$]

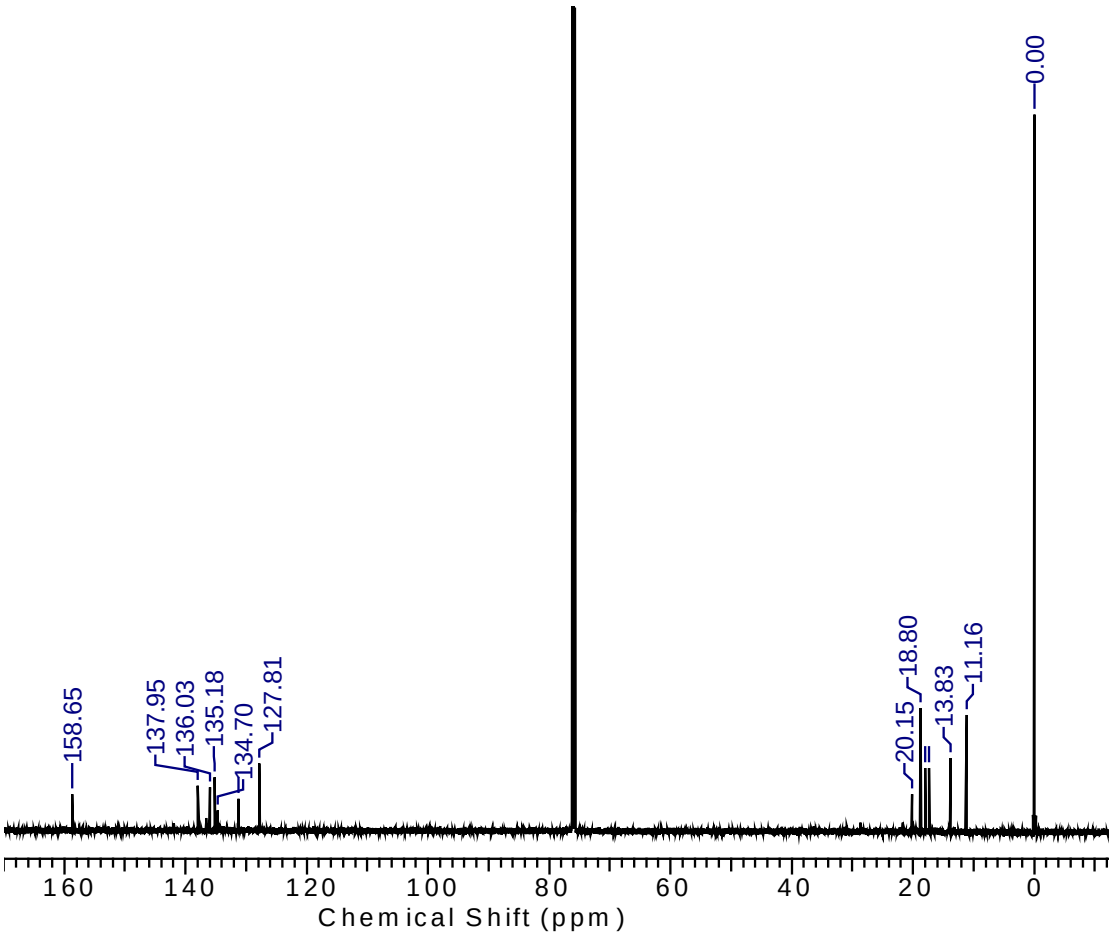

^{13}C NMR ($CDCl_3$, 400 MHz) of [(5-mesityl-4,6-dipyrrinato)$Re(CO)_4$]

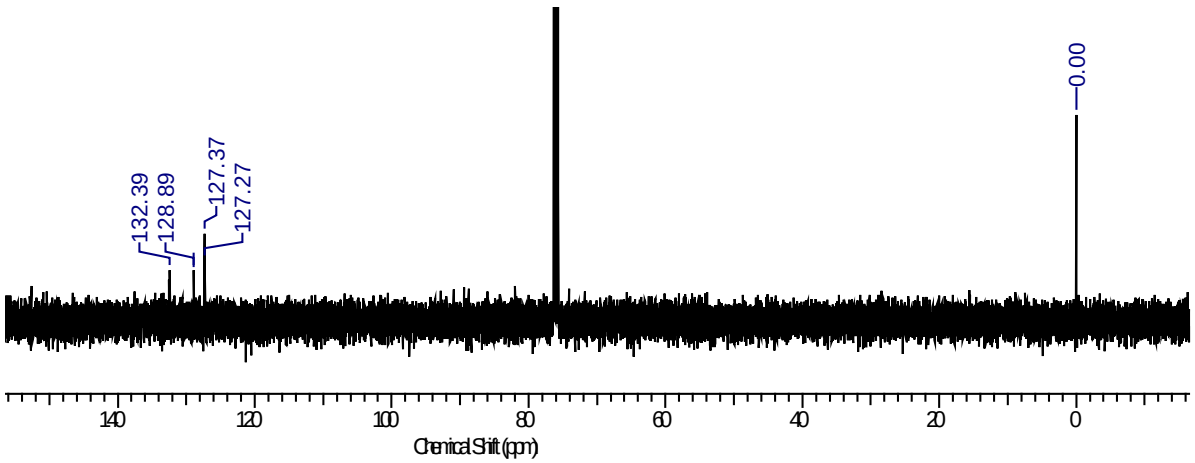

^{13}C NMR ($CDCl_3$, 400 MHz) of [(5-phenyl-4,6-dipyrrinato)$Re(CO)_3PPh_3$]

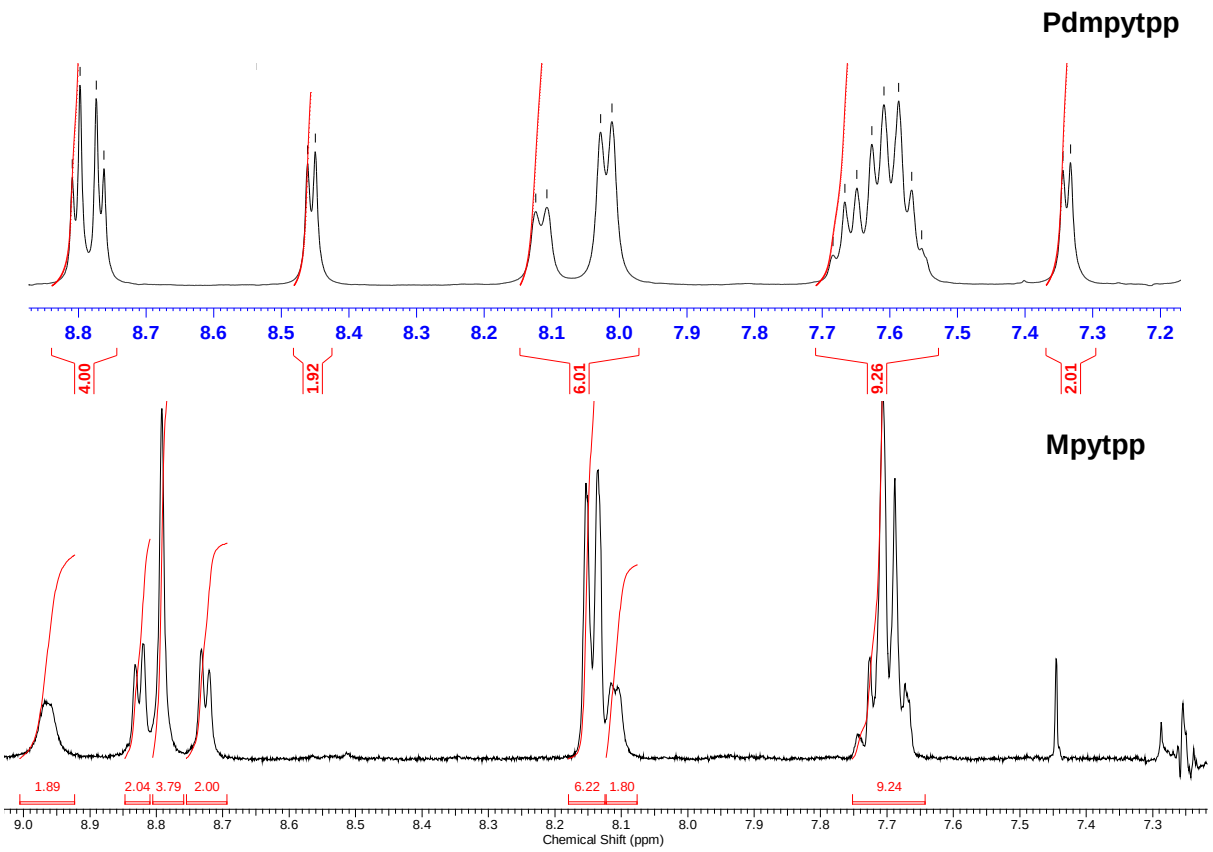

^{1}H NMR spectra of MPyTPP and PdMPyTPP porphyrin compounds in $CDCl_3$

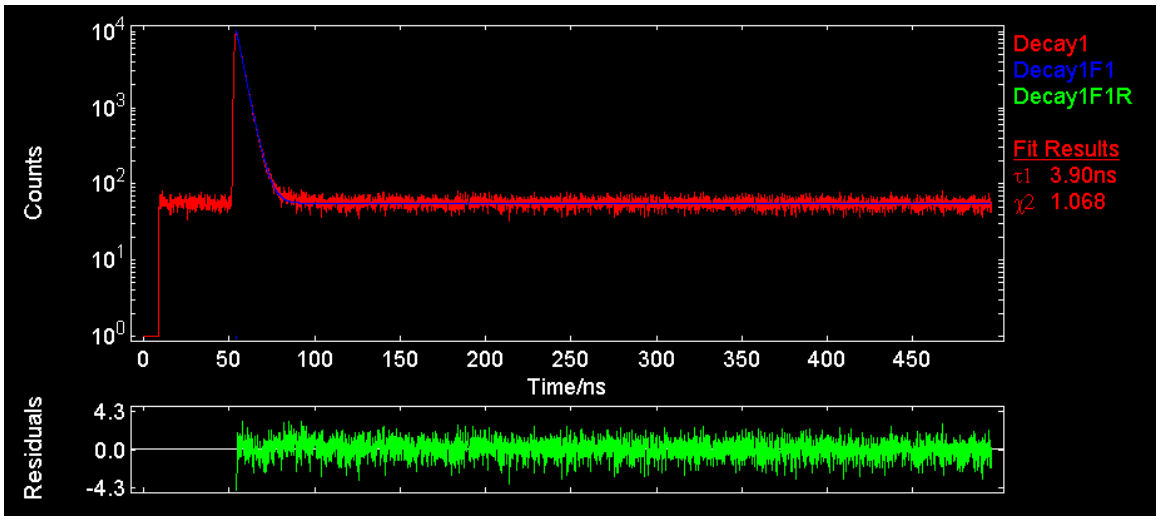

Room temperature fluorescence decay of [(5-pyrenyl-4,6-dipyrrinato)Re(CO)$_4$]

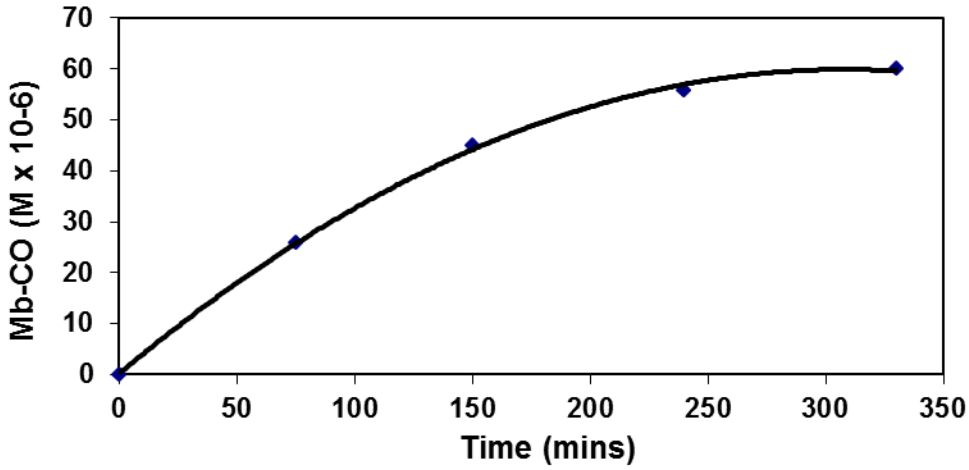

Formation of MbCO quantified for [(bpy)Cr(CO)$_4$] (60 µM) at 37 ^{o}C

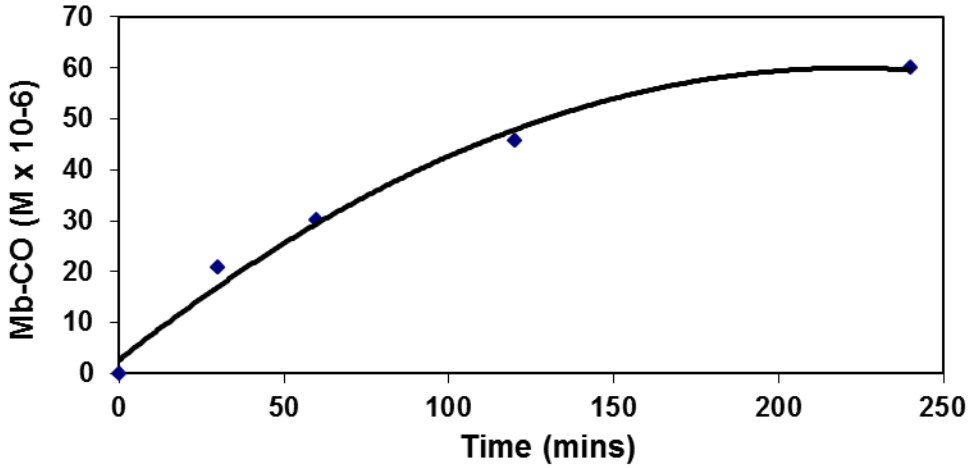

.

Formation of MbCO quantified for [(bpy)Cr(CO)$_3$PPh$_3$] (60 µM) at 470 nm

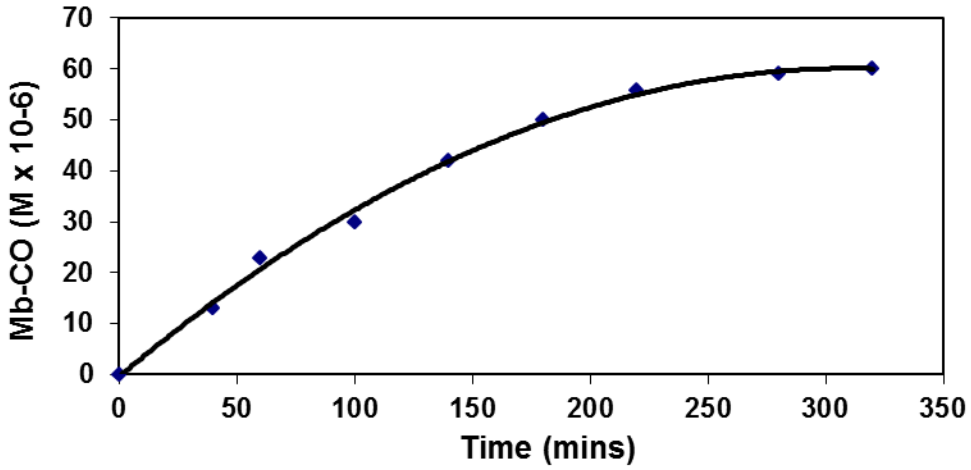

Formation of MbCO quantified for [(η^6-mesitylene))$Cr(CO)_3$] (60 µM) at 37 ^oC

POSTER 1 (Kavli Royal Society International Centre, Buckinghamshire, UK, June 2012)

Porphyrins as Potential Photodynamic Therapeutic Agents

Nivedita Das,[1] Nicola Boyle,[2] Wesley R. Brown,[2] Mary T. Pryce[1]

[1]*School of Chemical Sciences, Dublin City University, Dublin-9, Ireland.*

[2]*Stratingh Institute for Chemistry, Faculty of Mathematics and Natural Sciences, University of Groningen, Nijenborgh 4, 9747 AG Groningen, The Netherlands.*

Email id: nivedita.das2@mail.dcu.ie

Introduction

Photo dynamic therapy (PDT), a new form of cancer therapy has gained much attention due to the promise of selectivity for diseased tissue.[1] PDT requires a combination of three components; a photosensitiser, visible light and oxygen to produce lethal agents which inactivate the tumour cells. It is widely agreed that the generation of cytotoxic singlet oxygen is the primary agent responsible for the photo-degradation of malignant cells. The mechanism of PDT arises from the preferential accumulation of the photosensitiser in the affected tissue and the ability to confine activation of the photosensitiser by illumination of the tumour region only. Hence, it destructs the tumour cells without effecting normal healthy cells. The role of porphyrins for the cancer photodynamic therapy has become undoubtly its most relevant application. The usefulness of porphyrins in cancer therapy originates from their ability for the generation of singlet oxygen, in the photodegradation of malignant cells. Numerous porphyrins with different structures and substitution patterns have been reported which produce singlet oxygen in high quantum yields.[2,3] In this poster we will present and discuss the raman spectra and singlet oxygen quantum yields for a range of unsymmetrically substituted porphyrins.

Synthesis & Characterisation

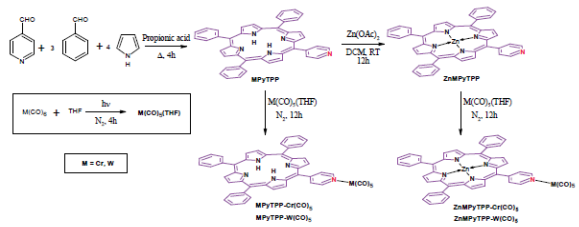

Scheme1: Synthesis of metal pentacarbonyl porphyrin complexes

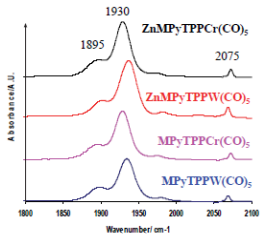

Fig. 1: FTIR spectra

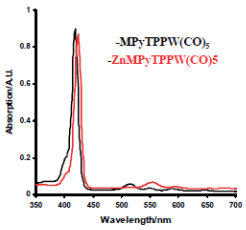

Fig. 2: UV-Vis spectra

Results

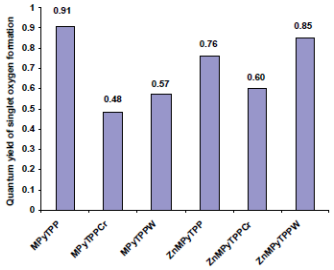

Fig. 3: Comparison of singlet oxygen quantum yields of the synthesized porphrin complexes.(All the measurements were made in toluene solutions with TPP taken as reference)

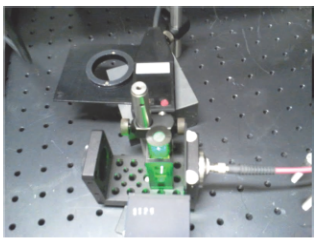

Fig. 4: Experimental setup for the singlet oxygen measurements at 532nm using DPSS CW laser (25 mW, Cobalt lasers)

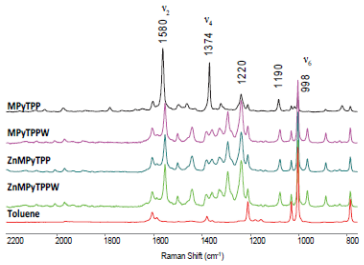

Fig. 5: Resonance Raman spectra of the Porphyrin complexes recorded in toulene as a solvent at λ_{exc} = 400 nm

Discussion & Conclusion

This work describes a comparison of the singlet-oxygen quantum yields in solution (toluene) by means of luminescence techniques. From the analysis of the singlet oxygen quantum yields a first observation can be made: similar or even higher values of singlet oxygen quantum yields were found for MPyTPP, ZnMPyTPP, ZnMPyTPPCr and ZnMPyTPPW compounds in comparison to those of the reference TPP(ϕ_Δ = 0.68). We conclude that the substitution of the phenyl ring by a pyridine ring in TPP increases the intersystem crossing rate to yield the triplet state and this state lives long enough to sensitise singlet oxygen with increase in the quantum yield. However, the attachment of W/Cr pentacarbonyl to the freebase mono pyridyl porphrin decreases the quantum yield of the singlet oxygen formation compared to the parent mono pyridyl porphyrin. Further, Zinc metallated W pentacarbonyl to porphyrin complex increases the singlet oxygen quantum yield efficiency compared to Cr pentacarbonyl when attached to Zn metallated porphyrin. The molecules synthesised in this study have the photochemical properties required for a good PDT sensitiser.From the resonance raman spectra it can be concluded that the bands observed at 1580, 1374 and 998 cm^{-1} are assigned to ν_6, ν_4 and ν_2 vibrational levels. The oscillations due to pyridyl groups are observed at 1220 and 1190 cm^{-1}. There are no raman bands observed in the region of 1800 to 2100 cm^{-1}, which suggests the metal-carbonyl stretching frequencies are not raman active.

Acknowledgement

We acknowledge and thank Faculty of Science and Health, Dublin City University for Daniel O' Hare postgraduate scholarship.

References

(1) Chatterjee, D. K.; Fong, L. S.; Zhang, Y. *Adv. Drug Delivery Rev.* **2008**, *60*, 1627-1637.

(2) Oliveira, A. S.; Licsandru, D.; Boscencu, R.; Socoteanu, R.; Nacea, V.; Vieira Ferreira, L. F. *Int. J. Photoenergy* **2009**, *2009*. 1-10.

(3) Redmond, R. W.; Gamlin, J. N. *Photochem. Photobiol.* **1999**, *70*, 391-475.

POSTER 2 (2nd Best Poster Prize, Dalton 2014, Warwick University, UK, April 2014)

A Time Resolved IR Study of Mono-nuclear Re(I) and Bi-nuclear Ru(II)-Re(I) Complexes and their ability to reduce CO_2

Nivedita Das,[1] Saeed Amirjalayer,[2] Avishek Paul,[1] Suzanne Mc Mahon,[1] Conor Long,[1] Wybren J. Buma,[2] Mary T. Pryce[1]

[1]School of Chemical Sciences, Dublin City University, Dublin-9, Ireland
[2] Van't hoff School of Molecular Sciences, University of Amsterdam, Amsterdam, Netherlands

Email: nivedita.das2@mail.dcu.ie

Abstract: The sufficient and sustainable energy supply of a growing world population is one of the largest challenges facing us in the 21st century.[1,2] Due to the release of large amounts of carbon dioxide to the atmosphere, the need for renewable and sustainable energy sources is paramount. At present there is much incentive to convert the sun's energy into solar fuels e.g. H_2 as well reduce CO_2 to C1- synthons such as methane, methanol or formate.[3] Hence, suitable catalysts or photochemical molecular devices (PMDs) are necessary to drive the redox processes for the conversion of CO_2 into useful products. A huge number of cyclometallated complexes of Re, Ru Co, and Ir have been successfully used as PMDs to date for the reduction of CO_2 and the generation of H_2 gas.[4,5] In this poster we will present our TRIR studies on novel mononuclear Re and binuclear Ru-Re tricarbonyl complexes as potential photocatalysts for the reduction of CO_2.

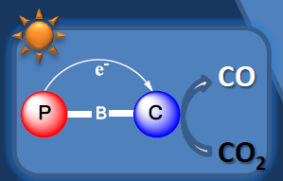

P= Photosensitiser
B= Bridging ligand
C= Catalyst

Photocatalysts

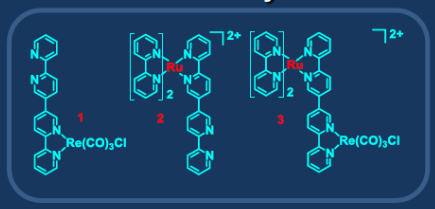

Introduction:

The best known photocatalyst to date for CO_2 reduction is bpyRe(CO)$_3$Cl but one of the major drwabacks with this system is the use of UV light. In the Ru-Re bimetallic catalyst presented here we have tuned the absorption spectrum to enable the use of visible light as the excitation source. Despite the fact that numerous systems have been reported for CO_2 reduction studies, few studies have published the reaction pathway. In this presentation ultrafast time resolved infrared spectroscopy is applied to study the excited states of mononuclear [Re(bisbpy)(CO)$_3$Cl] and the binuclear [Ru(bpy)$_2$(bisbpy)Re(CO)$_3$Cl](PF$_6$)$_2$ complex. The Ru-Re bimetallic polypyridyl complex was further investigated for photocatalytic intramolecular CO_2 reduction. The absorption spectra for the complexes are shown in Figure 1. The TRIR spectra of the complexes monitored from 1-1000ps are shown in Figure 2 and 3.

Absorption spectra

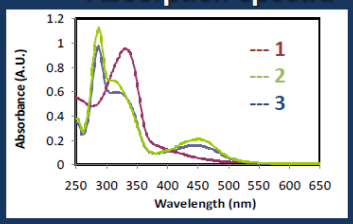

Figure 1: UV-vis spectra

Table 1

	TRIR bands (cm^{-1})	
	Parent bands	Transient bands
1	2010, 1905, 1890	2055, 1978, 1947
3	2013, 1909, 1890	2010, 1875

FTIR & TRIR spectroscopy

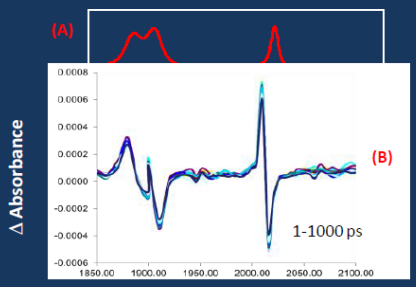

Figure 2: (A) FTIR *and* (B) Time resolved infra-red difference spectra following laper photolysis (λ_{exc} = 450 nm) for *[Ru(bpy)$_2$(bisbpy)Re(CO)$_3$Cl](PF$_6$)$_2$* complex in acetonitrile (10^{-5} M).

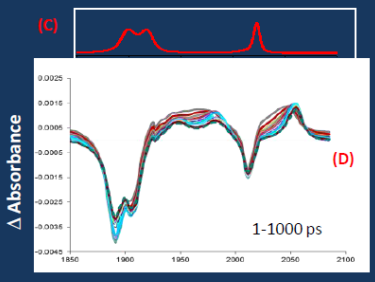

Figure 3: (C) FTIR *and* (D) Time resolved infra-red difference spectra following laser photolysis (λ_{exc} = 320 nm) for *[(bisbpy)Re(CO)$_3$Cl]* complex in acetonitrile (10^{-5} M).

Discussion and Conclusion:

Picosecond time resolved infrared studies carried out on [Ru(bpy)$_2$(bisbpy)Re(CO)$_3$Cl](PF$_6$)$_2$ at λ_{exc} = 450 nm in acetonitrile solution resulted in depletion of the parent bands at 2013, 1909, 1890 cm^{-1} with the growth of new IR bands at 2010 and 1910 cm^{-1} within the laser pulse (Figure 2). Shifting of these bands to lower frequencies compared to parent bands indicates an increase in electron density at the Re metal, leading to an increase in π-back bonding. Thus, it can be concluded that the excitation at 450 nm led to formation of a relaxed Ru(II) to bisbpy bridging ligand based MLCT excited state ([(bpy)$_2$Ru^{III}(bisbpy)Re^{I}(CO)$_3$Cl]$^{2+}$).[6] The TRIR spectra of the [(bisbpy)Re(CO)$_3$Cl] complex shown in Figure 3 are similar to other rhenium tricarbonyl complexes as reported in the literature.[7] The shifting of IR bands to higher energy than their ground state counterparts correspond to a Re to bisbpy based MLCT excited state. Furthermore, the [Ru(bpy)$_2$(bisbpy)Re(CO)$_3$Cl](PF$_6$)$_2$ complex was used for intramolecular photocatalytic reduction of CO_2 (conditions: 5:1 MeCN/TEOA + 0.1 M BNAH using 470 nm irradiation). CO was observed with a TON of 190. Studies are ongoing to elucidate the exact mechanism for this reaction.

Acknowledgements: The authors would like to thank SFI/TIDA/E2763, Daniel O' Hare scholarship and EU access LLAMS-1961 grant for financial support.

References: 1. T. Muckerman James and E. Fujita, in *Chemical Evolution II: From the Origins of Life to Modern Society*, American Chemical Society, Editon edn., 2009, vol. 1025, pp. 283-312. 2. H. Takeda and O. Ishitani, *Coord. Chem. Rev.*, 2009, 254, 346-354. 3. Y. Amao, *ChemCatChem*, 3, 2005, 458-474. 4. H. Takeda, O. Ishitani and S. Inagaki, *Inorg. Chem.*, 2010, 49, 4554-4559. 5. M. Schulz, M. Karnahl, M. Schwalbe and J. G. Vos, *Coord. Chem. Rev.*, 2012, 256, 1682-1705. 6. A. Gabrielsson and R. N. Perutz, *J. Am. Chem. Soc.*, 2006, 128, 4253-4266. 7. J. R. Schoonover, A. P. Shreve, M. D. Ward and C. A. Bignozzi, *Inorg. Chem.*, 1998, 37, 2598-2601.

POSTER 3 (ISACS 13, Dublin, Ireland, July 2014)

A Time Resolved IR Study of Macrocyclic Re(I) Complexes and Their Use as Photosensitisers/Photocatalysts for the Reduction of CO_2

Nivedita Das,[1] Saeed Amirjalayer,[2] Finn Connoughton,[1] Conor Long,[1] Wybren J. Buma,[2] Johannes G. Vos,[1] Mary T. Pryce[1]

[1] School of Chemical Sciences, Dublin City University, Dublin-9, Ireland
[2] Van't hoff School of Molecular Sciences, University of Amsterdam, Amsterdam, Netherlands

Email: nivedita.das2@mail.dcu.ie

Abstract: Rising atmospheric levels of carbon dioxide and depleting fossil fuel reserves raise serious concerns about ensuing effects on the global climate change and future energy supply. Utilizing the abundant solar energy to convert CO_2 into fuels such as methane or methanol could solve both problems simultaneously as well as provide a sustainable energy source.[1,2] Hence, suitable catalysts or photochemical molecular devices (PMDs) are necessary to drive the redox processes for the conversion of CO_2 into useful products. A huge number of cyclometallated complexes of Re, Ru Co, and Ir have been successfully used as PMDs to date for the reduction of CO_2 and the generation of H_2 gas but very few studies published the reaction pathway.[4,5] TRIR spectroscopic technique is a valuable tool in understanding the properties of the excited states of the transition metal complexes containing ligands such as CO or CN.[6] In this poster we will present our TRIR investigations to study the excited states of the novel dipyrrin based Re(I) macrocyclic tetracarbonyl complexes and hence their potential application as photocatalysts for the reduction of CO_2.

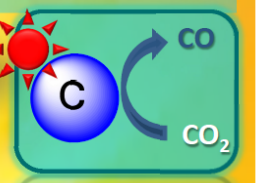

C= Catalyst

Photocatalysts

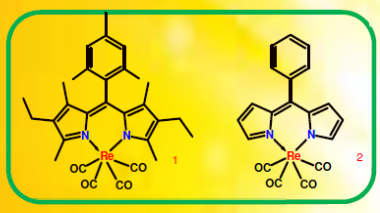

Introduction:

The best known photocatalyst to date for CO_2 reduction is [bpyRe(CO)$_3$Cl] but one of the major drawbacks with this system is the use of UV light. In the Re(I) dipyrrin based tetracarbonyl complexes presented here we have tuned the absorption spectrum to enable the use of visible light as the excitation source. Despite the fact that numerous systems have been reported for CO_2 reduction studies, few studies have published the reaction pathway. In this presentation ultrafast time resolved infrared spectroscopy is applied to study the excited states of Re(I) macrocyclic complexes such as [5-mesityl-4,6-dipyrrinatoRe(CO)$_4$] and [5-phenyl-4,6-dipyrrinatoRe(CO)$_4$]. The absorption spectra for the complexes are shown in Figure 1. The TRIR spectra of the complexes monitored from 1-1000 ps are shown in Figure 2 and 3. The 5-phenyldipyrrin based Re(I) tetracarbonyl complex was further investigated for photocatalytic intramolecular CO_2 reduction. The absorption spectra for the complexes are shown in Figure 1.

Absorption spectra

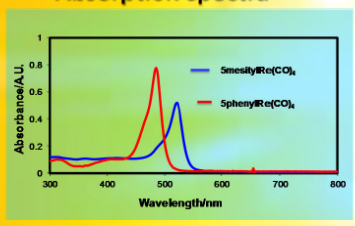

Figure 1: UV-vis spectra

Table 1

	TRIR bands (cm^{-1})	
	Parent bands	Transient bands
1	2095, 1990, 1972, 1930	2081, 1981, 1965, 1959
2	2098, 2006, 2001, 1979	2086, 1985, 1989

FTIR & TRIR spectroscopy

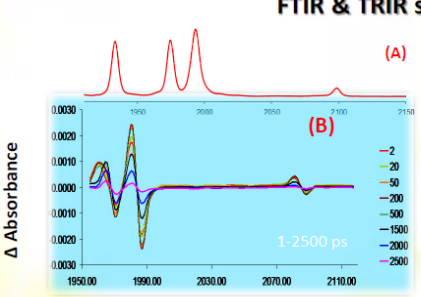

Figure 2: (A) FTIR *and* (B) Time resolved infra-red difference spectra following laser photolysis (λ_{exc} = 520 nm) for *[5-mesityl-4,6-dipyrrrinatoRe(CO)$_4$]* complex in pentane (10^{-5} M).

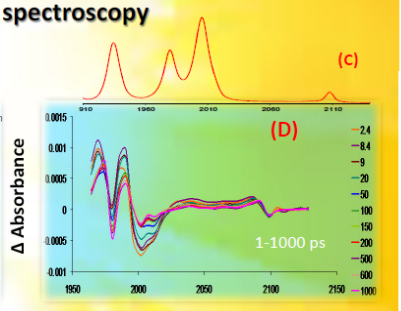

Figure 3: (C) FTIR *and* (D) Time resolved infra-red difference spectra following laser photolysis (λ_{exc} = 470 nm) for *[5-phenyl-4,6-dipyrrinatoRe(CO)$_4$]* complex in heptane (10^{-5} M).

Discussion and Conclusion:

Picosecond time resolved infrared studies carried out on [5-mesityl-4,6-dipyrrinatoRe(CO)$_4$] at λ_{exc} = 520 nm in pentane solution resulted in depletion of the parent bands at 2095, 1990, 1972 and 1930 cm^{-1} with the growth of new IR bands at 2081, 1981, 1965 and 1959 cm^{-1} within the laser pulse (Figure 2). Shifting of these bands to lower frequencies compared to the parent bands indicates an increase in electron density at the Re metal, leading to an increase in π-back bonding. Thus, it can be concluded that excitation at 520 nm led to formation of a IL π-π* dipyrrin based excited state. Further, it was noted that even after 50 ps the band at 1959 cm^{-1} shifted to 1965 cm^{-1} with a lifetime of 200 ps. This observation may indicate interconversion of an IL π-π* states localised on pyrrolic and mesityl group of the dipyrrin ligand.[7] The TRIR spectrum of the [5-phenyl-4,6-dipyrrinatoRe(CO)$_4$] complex shown in Figure 3 is very similar. Furthermore, the [5-phenyl4,6-dipyrrinatoRe(CO)$_4$] complex was used for intramolecular photocatalytic reduction of CO_2 (conditions: 5:1 MeCN/TEOA + 0.1 M BNAH using 470 nm irradiation) and from GC analysis only CO was observed in the head space . Preliminary studies are ongoing to replicate the results obtained.

Acknowledgement: The authors would like to thank SFI/TIDA/E2763, Daniel O' Hare scholarship and EU access program LLAMS-1961 grant for financial support.

References: 1. T. Muckerman James and E. Fujita, in *Chemical Evolution II: From the Origins of Life to Modern Society*, American Chemical Society, Editon edn., **2009**, vol. 1025, pp. 283-312. 2. H. Takeda and O. Ishitani, *Coord. Chem. Rev.*, **2009**, 254, 346-354. 3. Y. Amao, *ChemCatChem*, 3, **2005**, 458-474. 4. H. Takeda, O. Ishitani and S. Inagaki, *Inorg. Chem.*, **2010**, 49, 4554-4559. 5. M. Schulz, M. Schwalbe and J. G. Vos, *Coord. Chem. Rev.*, **2012**, 256, 1682-1705. 6. J.N. Butler, M.W. George, J.R. Schoonover, D. M. Dattelbaum and T. J. Meyer, *Coord. Chem. Rev.*, **2007**, 251, 492-514. 7. J. Dyer, W. J. Blau, M. W. George, S. Hudson, J. M. Kelly, P. Matousek,A. W. Parker, M. Towrie, J. A. Weinstein, *Photochemical & Photobiological Sciences* **2003**, *2*, 542.